
Electronic Thesis and Dissertation Repository

4-10-2014 12:00 AM

Study of Virus Dynamics by Mathematical Models

Xiulan Lai

The University of Western Ontario

Supervisor

Xingfu Zou

The University of Western Ontario

Graduate Program in Applied Mathematics

A thesis submitted in partial fulfillment of the requirements for the degree in Doctor of
Philosophy

© Xiulan Lai 2014

Follow this and additional works at: <https://ir.lib.uwo.ca/etd>



Part of the [Dynamic Systems Commons](#), [Immunology of Infectious Disease Commons](#), [Non-linear Dynamics Commons](#), [Numerical Analysis and Computation Commons](#), [Ordinary Differential Equations and Applied Dynamics Commons](#), [Partial Differential Equations Commons](#), and the [Virology Commons](#)

Recommended Citation

Lai, Xiulan, "Study of Virus Dynamics by Mathematical Models" (2014). *Electronic Thesis and Dissertation Repository*. 1978.

<https://ir.lib.uwo.ca/etd/1978>

This Dissertation/Thesis is brought to you for free and open access by Scholarship@Western. It has been accepted for inclusion in Electronic Thesis and Dissertation Repository by an authorized administrator of Scholarship@Western. For more information, please contact wlsadmin@uwo.ca.

STUDY OF VIRUS DYNAMICS BY MATHEMATICAL MODELS
(Thesis format: Integrated Article)

by

Xiulan Lai

Graduate Program in Applied Mathematics

A thesis submitted in partial fulfillment
of the requirements for the degree of
Doctor of Philosophy

The School of Graduate and Postdoctoral Studies
The University of Western Ontario
London, Ontario, Canada

© Xiulan Lai 2014

Abstract

This thesis studies within-host virus dynamics by mathematical models, and topics discussed include viral release strategies, viral spreading mechanism, and interaction of virus with the immune system.

Firstly, we propose a delay differential equation model with distributed delay to investigate the evolutionary competition between budding and lytic viral release strategies. We find that when an antibody is not established, the dynamics of competition depends on the respective basic reproduction numbers of the two viruses. If the basic reproductive ratio of budding virus is greater than that of lytic virus and one, budding virus can survive. When an antibody is established for both strains but the neutralization capacities are the same for both strains, consequence of the competition also depends only on the basic reproduction numbers of the budding and lytic viruses. Using two concrete forms of the viral production functions, we are also able to conclude that budding virus will outcompete if the rates of viral production, death rates of infected cells and neutralizing capacities of the antibodies are the same for budding and lytic viruses. In this case, budding strategy would have evolutionary advantage. However, if the antibody neutralization capacity for the budding virus is larger than that for the lytic virus, lytic virus can outcompete provided that its reproductive ratio is very high. An explicit threshold is derived.

Secondly, we consider model containing two modes for viral infection and spread, one is the diffusion-limited free virus transmission and the other is the direct cell-to-cell transfer of viral particles. By incorporating infection age, a rigorous analysis of the model shows that the model demonstrates a global threshold dynamics, fully described by the basic reproduction number, which is identified explicitly. The formula for the basic reproduction number of our model reveals the effects of various model parameters including the transmission rates of the two modes, and the impact of the infection age. We show that the basic reproduction number is underestimated in the existing models that only consider the cell-free virus transmission, or the cell-to-cell infection, ignoring the other. Assuming logistic growth for target cells, we find that if the basic reproduction number is greater than one, the infection can persist and Hopf bifurcation can occur from the positive equilibrium within certain parameter ranges.

Thirdly, the repulsion effect of superinfecting virion by infected cells is studied by a reaction diffusion equation model for virus infection dynamics. In this model, the diffusion of virus depends not only on its concentration gradient but also on the concentration of infected

cells. The basic reproduction number, linear stability of steady states, spreading speed, and existence of traveling wave solutions for the model are discussed. It is shown that viruses spread more rapidly with the repulsion effect of infected cells on superinfecting virions, than with random diffusion only. For our model, the spreading speed of free virus is not consistent with the minimal traveling wave speed. With our general model, numerical computations of the spreading speed shows that the repulsion of superinfecting virion promotes the spread of virus, which confirms, not only qualitatively but also quantitatively, some recent experimental results.

Finally, the effect of chemotactic movement of $CD8^+$ cytotoxic T lymphocytes (CTLs) on HIV-1 infection dynamics is studied by a reaction diffusion model with chemotaxis. Choosing a typical chemosensitive function, we find that chemoattractive movement of CTLs due to HIV infection does not change stability of the positive steady state of the model. However, chemorepulsion movement of CTLs destabilizes the positive steady state as the strength of the chemotactic sensitivity increases. In this case, Turing instability occurs, which can be Hopf bifurcation or steady state bifurcation, and spatial heterogeneous patterns may form.

Keywords: Mathematical modeling, basic reproduction number, virus dynamics, viral release strategy, cell-to-cell infection, repulsion of superinfecting virion, viral infection-induced CTL-chemotaxis.

Co-Authorship Statement

This thesis has been prepared in accordance with the regulations for an Integrated-Article format thesis stipulated by the School of Graduate and Postdoctoral Studies at the University of Western Ontario. Chapter 2-6 of this thesis consist of the following papers:

Chapter 2: Xiulan Lai and Xingfu Zou, The dynamics of evolutionary competition between budding and lytic viral release strategies, submitted.

Chapter 3: Xiulan Lai and Xingfu Zou, Modeling virus-to-cell and cell-to-cell spread of HIV-1, SIAM J. Appl. Math., revised.

Chapter 4: Xiulan Lai and Xingfu Zou, Modeling cell-to-cell spread of HIV-1 with logistic target cell growth, in preparation.

Chapter 5: Xiulan Lai and Xingfu Zou, Repulsion effect on superinfecting virions by infected cells, submitted.

Chapter 6: Xiulan Lai and Xingfu Zou, A Reaction diffusion system modeling virus dynamics and CTL response with chemotaxis, in preparation.

The formation of the models, mathematical analysis and numerical simulations were performed by the author under the supervision of Dr. Xingfu Zou. The original drafts of the above papers were prepared by the author. Subsequent revisions were completed by the author and Dr. Xingfu Zou.

Acknowledgements

First and foremost, I would like to express my genuine gratitude to my supervisor Dr. Xingfu Zou, for his support and excellent intellectual guidance, continued support, encouragement and patience throughout the years. He provided plenty of valuable advices and offered a motivational push of my work. His limitless enthusiasm and curiosity for research has allowed me to pursue my research interest, while exploring various interesting projects. His devotion to research, caring attitude and his supportive help will serve me greatly in the future. The opportunity to attend and present at various conferences, summer schools and workshops as well as preparing and finishing manuscripts gave me the invaluable technical and communication skills. Thank him for not only improving my skills as a researcher, but also offering me help and support during my life at London, and for his positive outlook which kept me motivated during difficult times. Moreover, I would like to thank his family for their hospitality in each of the Christmas, which I enjoyed so much.

Next I would like to thank my advisory committee members, Dr. Lindi Wahl, Dr. Geoff Wild and Dr. Pei Yu for providing me with valuable feedback, recommendations, and insights into my projects. I would like to also thank all members of Bio-math group and Dynamical Systems group. They were an invaluable source of advice and ideas, and responsible for shaping an enjoyable working environment. Thanks to Audrey Kager and Cinthia MacLean for their help and assistance in these four years as well.

I am grateful for the funding I received from China Scholarship Council, Department of Applied Mathematics, Graduate Teaching Assistants' Union, and Society of Graduate Students.

Finally, I would like to thank all of my family and friends for their consistent encouragement and support. Special thanks goes to my mother. As my greatest inspiration, my mother provided me with endless love and unconditional support. Her inner strength inspires and pushes me to constantly do better. I could never thank her enough for all of the sacrifices she has made for me over the years.

Contents

Abstract	ii
Co-Authorship Statement	iv
Acknowledgements	v
List of Figures	viii
List of Tables	x
1 Introduction	1
1.1 Virus-induced diseases	1
1.2 Viral life cycle and immune responses against viral infections	3
1.3 Mathematical modeling of virus dynamics	5
1.4 Thesis motivations and outlines	14
2 Dynamics of evolutionary competition between budding and lytic viral release strategies	24
2.1 Introduction	24
2.2 Model formulation	26
2.3 Positivity and boundedness of solutions	28
2.4 Equilibria and their stability	29
2.5 Influence of antibody effect on the evolutionary competition between budding and lytic strategies	42
2.6 Discussion and Conclusion	48
3 Modeling HIV-1 virus dynamics with both virus-to-cell infection and cell-to-cell transmission	52
3.1 Introduction	52
3.2 Positivity and boundedness of solutions	56
3.3 Local stability of equilibria and the basic reproduction number	58

3.4	Persistence of infection	63
3.5	Global stability of equilibria	67
3.6	Conclusion and discussion	70
4	Modeling cell-to-cell spread of HIV-1 with logistic target cell growth	79
4.1	Introduction	79
4.2	Nonnegativity and boundedness of solutions	82
4.3	Stability of the infection-free equilibrium	84
4.4	Uniform persistence of infection	86
4.5	Stability of the positive equilibrium \bar{E} and Hopf bifurcation	89
4.6	Numerical simulation	91
4.7	Conclusion and discussion	102
5	Repulsion effect on superinfecting virions by infected cells	106
5.1	Introduction	106
5.2	In a bounded domain	109
5.3	Spreading speed in the case $\Omega = \mathbb{R}$	119
5.4	Existence of traveling wave solutions in the case $\Omega = \mathbb{R}$	123
5.5	Conclusion and discussion	130
6	A reaction diffusion system modeling HIV-1 infection dynamics with CTL-chemotaxis	136
6.1	Introduction	136
6.2	Global existence of solutions	138
6.3	Linear stability analysis	141
6.4	Turing instability and pattern formation	145
6.5	Numerical simulation	148
6.6	Conclusion and discussion	154
7	Conclusion and future work	158
7.1	Conclusion	158
7.2	Future work	160
	Bibliography	162
	Curriculum Vitae	162

List of Figures

1.1	Overview of main types of viral infection and the most notable species involved	2
1.2	Leading infectious killers in 1998 and 2007	3
1.3	A typical virus replication cycle	4
1.4	Schematic diagram of the basic model (1.1)	7
1.5	Release of viruses	15
1.6	Chemoattraction and chemorepulsion.	17
2.1	The stability regions of equilibria, when $\eta_B > \eta_L$	39
2.2	The stability regions of equilibria, when $\eta_B < \eta_L$	41
2.3	The stability regions of equilibria, when $\eta_B = \eta_L$	41
2.4	$\gamma(a)$ function given by (2.23) under the constraint (2.26)	43
2.5	$\gamma(a)$ function given by (2.27) under the constraint (2.28)	44
2.6	Burst size $K(\tau)$	45
2.7	The death rate function $d_{T^*}(a)$	45
2.8	The burst size $K(\tau)$ with age dependent death rate (2.31) and $\tau_0 = 5$	46
2.9	The burst size $K(\tau)$ with age dependent death rate (2.31) and $\tau_0 = 10$	46
4.1	The surface of $F(\rho_1, \rho_2)$	92
4.2	The function $F(\rho_1)$	93
4.3	Trajectories of system (4.5), when $\rho_1 = 20$	95
4.4	Trajectories of system (4.5), when $\rho_1 = 70$	96
4.5	Trajectories of system (4.5), when $\rho_1 = 80$	97
4.6	The function $F(\rho_2)$	98
4.7	Trajectories of system (4.5), when $\rho_2 = 1$	100
4.8	Trajectories of system (4.5), when $\rho_2 = 25$	101
5.1	The basic reproduction number \mathcal{R}_0 as functions of D_0 and D_T	116
5.2	The basic reproduction number \mathcal{R}_0 as a function of γ	116
5.3	The diffusion function of virus $D_V(I) = D_0 + aI/(b + I)$	120
5.4	The evolution of $V(t, x)$ from an initial distribution $V_0(x)$	121

5.5	The evolution of $V(t, x)$ from another initial distribution $V_0(x)$	122
5.6	Impact of $D(0)$ on c^*	127
5.7	Wave profiles of $u(s)$ and $w(s)$ when $a = 0$	129
5.8	Wave profiles of $v(s)$ when $a = 0$	130
5.9	No traveling wave solution for $c = 5$	130
5.10	A traveling wave solution exists when $c = 14$	131
6.1	Temporal and spatial evolution of cell populations, when $D_T = 0$	149
6.2	Graphs of $\phi_e(s, \chi) = 0$ and $\phi_d(s, \chi) = 0$, when $D_T = 0$	149
6.3	Curves of $\phi_e(s, \chi) = 0$ and $\phi_d(s, \chi) = 0$ for different sets of $D_E, D_T > 0$	150
6.4	Determination of bifurcation threshold values for the case in Figure 6.3(a)	150
6.5	Stable positive steady state	151
6.6	Hopf bifurcation and pattern formation for the case in Figure 6.3(a)	151
6.7	Periodic solutions for the case in Figure 6.3(a)	152
6.8	Steady state bifurcation and pattern formation for the case in Figure 6.3(a)	152
6.9	Determination of threshold values for the case in Figure 6.3(b)	153
6.10	Steady state bifurcation and pattern formation for the case in Figure 6.3(b)	153

List of Tables

2.1	The conditions for the existence and stability of the equilibria	39
2.2	Stability regions of the equilibria corresponding to Figure 2.1(a)	40
2.3	Stability regions of the equilibria corresponding to Figure 2.1(b)	41

Chapter 1

Introduction

A virus is a small infectious agent that is only able to replicate inside the living cells of an organism. Viruses are found in almost every ecosystem on Earth and known to infect most types of organisms, including bacteria, fungi, plants, insects, vertebrates and so on. A vast number of viruses cause diseases in humans, domestic animals or crop plants.

1.1 Virus-induced diseases

The common human diseases such as the common cold, influenza, chickenpox and cold sores are caused by viruses. There are currently 21 families of viruses known to cause diseases in humans. Figure 1.1 displays the main human diseases caused by different viruses. Some of these diseases are very serious infectious diseases, such as acquired immune deficiency syndrome (AIDS), Hepatitis, Herpes Simplex, Measles, avian influenza and SARS and so on [47], and they are a major component of infectious diseases and continue to plague humans. The leading infectious diseases as causes of death in 1998 and 2007 are shown in Figure 1.2. About 3.5 million and 4.4 million deaths occurred as a result of acute respiratory diseases in 1998 and 2007 respectively, much of which are due to viruses. AIDS has killed 2.3 million and 1 million people worldwide in 1998 and 2007 respectively, and measles is still a significant killer in developing countries. Some viruses cause major epidemics, for instance, HIV and AIDS, Influenza, Insect-Borne Diseases, Yellow fever and Dengue. According to the World Health Organization report on global situation and trends of HIV/AIDS, almost 70 million people have been infected with the HIV virus and about 35 million people have died of AIDS since the beginning of the epidemic. Although the burden of the epidemic varies considerably between countries and regions, the epidemic continues and at the end of 2011, 34.0 million (31.4 - 35.9 million) people and 0.8% of adults aged 15-49 years worldwide were estimated to

be living with HIV.

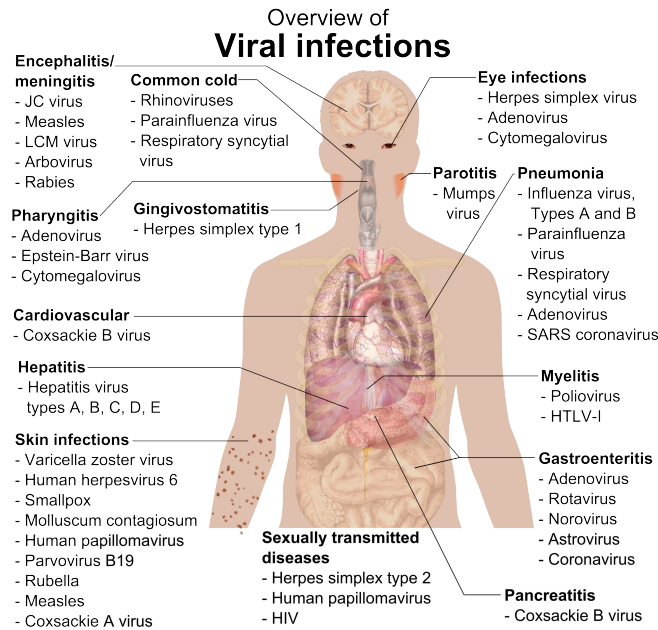


Figure 1.1: Overview of main types of viral infection and the most notable species involved (Wikipedia: <http://en.wikipedia.org/wiki/Virus>).

Most of dangerous viruses have been controlled effectively by the introduction of vaccine. There are useful vaccines for some virus induced diseases, for example, Smallpox, measles, Rubella, Mumps, Varicella-Zoster, Hepatitis A and Hepatitis B. The incidences of some diseases, such as measles, have been dramatically reduced in some developed countries through the use of vaccines. However, they are still leading diseases in many developing countries. Moreover, for most serious virus-induced diseases such as Hepatitis C, Hepatitis D and HIV, there are still no vaccines available.

Viruses have different mechanisms in causing diseases in an organism, which depends largely on the viral species. Viruses can usually cause damage in the host via cell lysis, production of toxic substances and cell transformation [3]. When a virus enters a cell and completes its normal replication cycle, the host cell may undergo lysis due to a physical internal pressure exerted by the multiplying virus or immune response. Furthermore, during the course of virus replication, many cytotoxic viral components as well as by-products of viral replication accumulate in the cell. Cell lysis and cytotoxic components cause death of the cell. In multicellular organisms, if enough cells die, the whole organism will start to suffer the effects. Some viruses can cause lifelong or chronic infections, where the viruses continue to replicate in the body

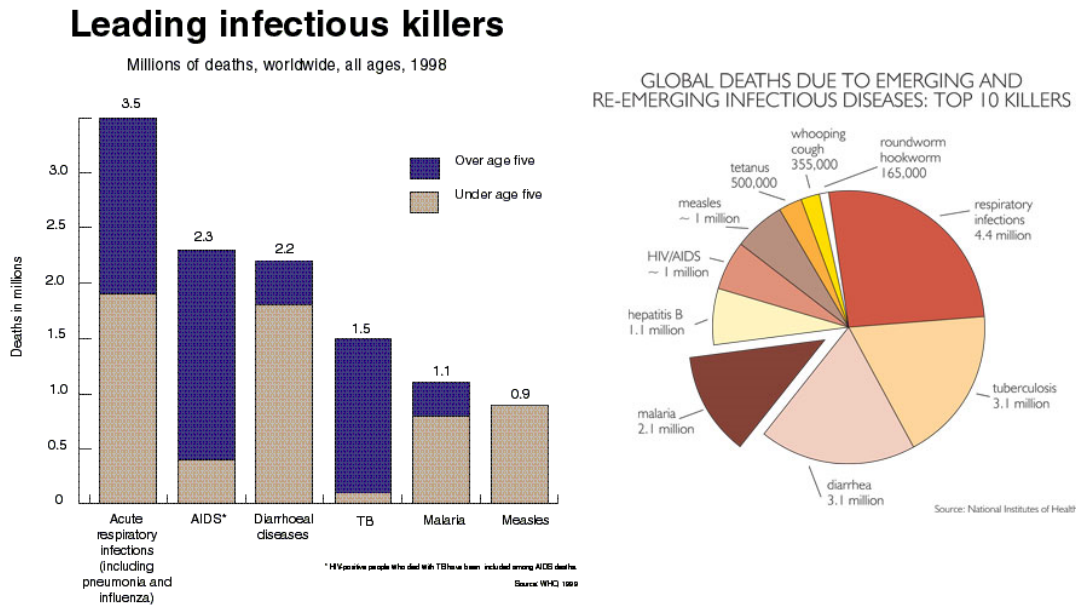


Figure 1.2: Leading infectious killers in 1998 and 2007.

<http://www.who.int/infectious-disease-report/pages/graph5.html>

<https://www.research.olemiss.edu/UMQuest/2007/Winter/ThePowerOfPartnerships.html>

despite the host's defence mechanisms. This is common in Hepatitis B virus and Hepatitis C virus infections.

1.2 Viral life cycle and immune responses against viral infections

A virus is made up of a core of genetic material, either DNA or RNA, surrounded by a protective protein coat called a capsid or nucleocapsid. For some viruses, the capsid is surrounded by an additional lipid coat called the envelope [3]. Viral populations produce multiple copies of themselves in a host cell utilizing the machinery and metabolism of the cell. The life cycle of viruses differs greatly between species, but there are five basic stages in the life cycle of viruses (see Figure 1.3): attachment, penetration/entry, uncoating, replication and release.

A viral replication cycle begins with binding of free virus to host cell through interaction between specific viral capsid/surface proteins and cellular receptors. Following attachment, the virus (or at least its nucleic acid) enters the host cell through receptor-mediated endocytosis or membrane fusion. For some viruses, the genome is completely released from the capsid during or after penetration, which is known as "uncoating". Viral capsid is degraded by viral enzymes or host enzymes. In the viral replication cycle, viral genetic materials and viral

proteins are processed in the host cell. The mechanisms of this phase depend on the type and family of viruses. Once new viral genomes and proteins have been produced, they are assembled into new virions. In the case of non-enveloped viruses, these newly formed virions accumulate in the cell and are released by cell lysis, a process that kills the cell by bursting its membrane and cell wall if present. Enveloped viruses (e.g., HIV) are often released from the host cell by budding. During the budding process, a virus acquires the phospholipid envelope containing the embedded viral glycoproteins. These particles can then go through additional maturation events to give rise to infectious virus.

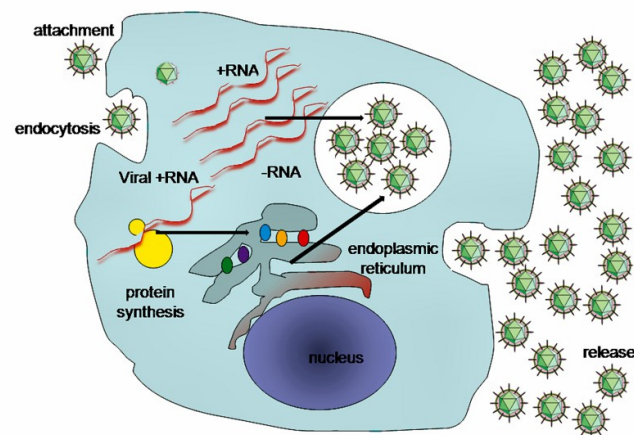


Figure 1.3: A typical virus replication cycle (<http://en.wikipedia.org/wiki/Virus>).

Within the life cycle, viruses have a relatively short extracellular period, prior to infecting the cells, and a longer intracellular period during which they undergo replication. In most viral infections, the immune system has mechanisms which can attack the virus in both of these phases of its life cycle. During the protein production or viral assembling phase, antigens that appear in the membrane of the infected cell can activate the immune response which targets infected cells. Different mechanisms of innate (non-specific) and adaptive (specific) immunity are used against viral infections.

The most effective mechanisms of the innate response against viral infections are mediated by interferon and by the activation of natural killer (NK) cells. These mechanisms are mainly aimed against infected cells. Viral infection of cells directly stimulates the production of interferons from macrophages or lymphocytes. Interferon is a cytokine which has strong anti-viral actions, such as inhibition of both viral replication and cell proliferation, and enhancement of the ability of natural killer cells to lyse virally infected cells. Naturally activated natural killer

cells can recognize and lyse virally infected cells. On the other hand, the alternative pathway of complement activation also has the effect of very effectively activating the destruction of the viral particle [31].

Viruses are strongly immunogenic inducing both types of adaptive immune responses, humoral and cellular immune responses, which are essential for antiviral defense. The contribution of each immune response varies, depending on the virus and the host. Antibodies generally bind to virus particles in the blood and at mucosal surfaces, thereby blocking the spread of infection. In contrast, effector T cells recognize and kill infected cells. Adaptive immunity acts against both viral particles and infected cells.

Humoral response is responsible for blocking the infectivity of the virus. The viral capsid is made of proteins and very antigenic. It induces the production of a large number of antibodies that can have different actions against the virus. The most effective type of antiviral antibody is “neutralizing” antibody, the antibody which binds to the virus, usually to the viral envelope or capsid proteins, and which blocks the virus from binding to and entering into the host cell. Neutralizing antibody is an effective form of protective immunity against viral infections, and used for many successful viral vaccine, which work by stimulating virus-neutralizing antibody responses.

In contrast, the cellular immune response kills the virus-infected cells expressing viral proteins on their surfaces. The principal effector cells involved in clearing established viral infections are the virus specific $CD8^+$ cytotoxic T lymphocytes (CTL). These cells recognize viral antigens which have been synthesized within cell’s nucleus or cytosol, and which have been degraded. Recognition of these antigens by an antigen-specific CTL usually results in the destruction of the infected cell. Cells infected by viruses can express on their membranes viral antigens long before the viral assembling takes place. Thus, their destruction is a very effective mechanism for avoiding the production of more viruses. The cytotoxicity mechanisms mediated by $CD8^+$ lymphocytes is one of the most effective mechanisms against viral infections [31].

1.3 Mathematical modeling of virus dynamics

Mathematical modeling in epidemiology provides understanding of the underlying mechanisms that influence the spread of disease and, in the process, it suggests control strategies. For within-host virus dynamics, mathematical models based on understanding of biological interactions, can also provide nonintuitive insights into the dynamics of host response to viruses and can suggest new avenues for experimentation. In HIV infection, for example, mathematical models have been devised to describe the slow decline in the number of $CD4^+$ T cells over

many years, the interaction between HIV and other opportunistic infections, the emergence of drug-resistant viruses, and the consequences of antigenic diversity and viral evolution during single infections [34, 35, 39, 40, 46]. In HIV and Hepatitis B virus (HBV) infection, mathematical models of drug treatment dynamics have provided estimates for the turnover rates of infected cells and free virus [13, 38].

Basic reproduction number The basic reproduction number (sometimes called basic reproduction rate or basic reproductive ratio, denoted as \mathcal{R}_0) is used to measure the transmission potential of a disease. It is thought of as the number of secondary infections produced by a typical case of infection in a population that is totally susceptible. It can therefore be measured by counting the number of secondary cases following the introduction of an infection into a totally susceptible population [9, 11, 23, 29, 48, 52]. The basic reproduction number is affected by several factors: (1) the rate of contacts in the host population; (2) the probability of infection being transmitted during contact; (3) the duration of infectiousness. In general, for an epidemic to occur in a susceptible population, \mathcal{R}_0 must be greater than 1, so that the number of cases is increasing. If $\mathcal{R}_0 < 1$, the number of cases decreases, for example, if a new vaccine has been introduced.

Basic model A general mathematical model for the basic dynamics of virus-host cell interaction was developed [34, 38, 39, 46]. The basic principles that underly models of virus dynamics are as follows (Figure 1.4). Susceptible uninfected cells, $x(t)$, are infected when they meet free viruses, $v(t)$. Infected cells, $y(t)$, produce new virus particles that leave the cell and find other susceptible target cells. Repeated rounds of infection result in the growth of the virus population. Growth is limited by the availability of target cells.

$$\begin{aligned}\frac{dx}{dt} &= \lambda - dx - \beta xv, \\ \frac{dy}{dt} &= \beta xv - (d + \alpha)y, \\ \frac{dv}{dt} &= ky - uv.\end{aligned}\tag{1.1}$$

Uninfected target cells are produced at a constant rate, λ , from a pool of precursor cells and die at a rate dx . When these susceptible cells encounter with free virus articles, they become infected at a rate βxv . The infected cells die at an additional rate αy , which is the viral caused cell death (cytopathicity or cytotoxicity). Infected cells produce new virus particles with a rate ky , and the free virus particles that have been released from the cells decay with a rate uv . Thus, the average lifetime of an infected cell is $1/(d + \alpha)$; the average lifetime of a free virus particle is $1/u$; the total number of virus particles produced from one infected cell is $k/(d + \alpha)$.

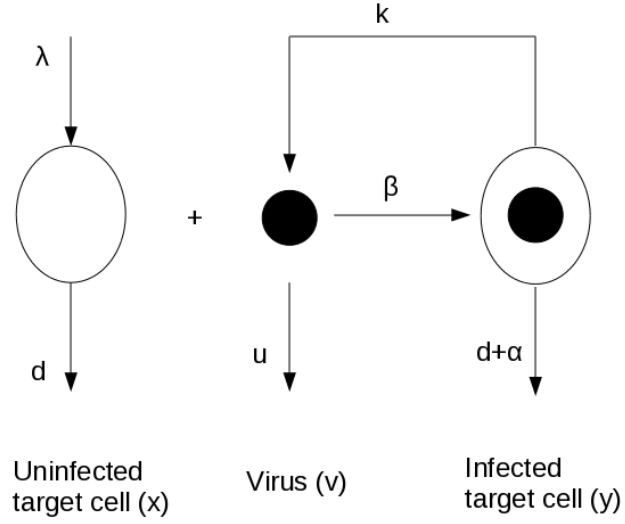


Figure 1.4: Schematic diagram of the basic model (1.1)

The outcome is determined by the basic reproduction number of the virus [22], which is the average number of newly infected cells produced by a single infected cell when almost all cells are still uninfected. For the system (1.1), the basic reproduction number of the virus is given by

$$\mathcal{R}_0 = \frac{\lambda\beta k}{du(d + \alpha)}.$$

If $\mathcal{R}_0 < 1$, the infection-free equilibrium $E_0 = (\lambda/d, 0, 0)$ is stable. If $\mathcal{R}_0 > 1$, E_0 is unstable and there exists a stable positive equilibrium $E^* = (x^*, y^*, v^*)$, where

$$x^* = \frac{\lambda}{d\mathcal{R}_0}, \quad y^* = \frac{\lambda}{d + \alpha} \left(1 - \frac{1}{\mathcal{R}_0}\right), \quad v^* = \frac{k}{u}y^*.$$

When $\mathcal{R}_0 < 1$, one cell on average produces less than one newly infected cell, and the virus population fails to spread and goes extinct, thus the system converges to the infection-free equilibrium E_0 . However, when $\mathcal{R}_0 > 1$, one cell on average gives rise to more than one newly infected cell, and the infection can spread, the system will converge to the positive equilibrium E^* . We see that the outcome is determined not only by viral, but also by host parameters.

In this model, the absorption of free virus particles by infection is ignored. Considering the loss of free virus particles, the virus population equation reads [21, 24]

$$\frac{dv}{dt} = ky - uv - \beta xv.$$

The basic model has been derived to model in vivo dynamics of HIV-1, HBV and some other viruses infection. The further developments of the model are given as follows.

Logistic growth If new target cells are not created at a constant rate, but created by proliferation of existing cells, and the proliferation is described as a logistic function, we have the following equation for susceptible cell population

$$\frac{dx}{dt} = rx \left(1 - \frac{x}{K}\right) - \beta xv.$$

Here r is the proliferation rate and K is the maximum capacity of cell proliferation, that is the density at which cell proliferation shuts off. If new target cells are created not only from sources within the body at a constant rate λ , but also by proliferation of existing cells, the susceptible cell population follows [40]

$$\frac{dx}{dt} = \lambda - dx + rx \left(1 - \frac{x}{K}\right) - \beta xv.$$

Considering that the total concentration of cells is $x + y$, the models can be changed to the following equations [7, 26, 50]

$$\frac{dx}{dt} = rx \left(1 - \frac{x+y}{K}\right) - \beta xv, \quad \text{or} \quad \frac{dx}{dt} = \lambda - dx + rx \left(1 - \frac{x+y}{K}\right) - \beta xv.$$

The logistic term can destabilize the positive equilibrium, and Hopf bifurcation is expected.

Immune responses The infected cells and free virus particles can be cleared by immune responses with CTLs and some neutralizing antibodies respectively. The basic model is extended to consider immune responses. Let z denote the magnitude of CTL response, that is, the abundance of virus-specific CTLs. One of CTL response dynamics is given by the following equation [34]

$$\frac{dz}{dt} = cyz - bz,$$

where CTLs proliferate in response to antigenic stimulation with a rate cyz . In the absence of stimulation, CTLs decay at rate b . The parameter c denotes the CTL responsiveness, that is, the growth rate of specific CTLs after encountering infected cells. In this model, there is a minimum level of infected cells y necessary to stimulate a CTL response. That is, the CTL response will increase only if $cy > b$. This simple model of CTL dynamics can be modified to consider the saturation of CTL expansion as the number of CTLs grows to relatively high numbers, which is expressed by the following equation [54]

$$\frac{dz}{dt} = \frac{cyz}{1 + \epsilon z} - bz.$$

The variable ϵ represents the saturation level. This model has similar dynamical properties as the previous simple model. The difference is the steady state levels of virus load and cells. If

the saturation occurs at lower level of CTLs (high value of ϵ), this model is verified to a simple one given by [5]

$$\frac{dz}{dt} = cy - bz.$$

Here, the rate of CTL expansion is simply proportional to the amount of antigen, but not the rate of CTLs. In this model, the CTL response never goes extinct provided there are antigens.

By a lytic mechanisms, CTL is assumed to kill infected cells, which is expressed by [54, 55]

$$\frac{dy}{dt} = \beta xv - (d + \alpha)y - pyz.$$

Infected cells are killed by CTL at a rate pyz . The parameter p specifies the rate at which CTL kills infected cells. The CTL response also functions by nonlytic mechanisms. CTL decreases the rate at which uninfected target cells become infected, which is expressed by the following equations [54, 56, 57]

$$\begin{aligned} \frac{dx}{dt} &= \lambda - dx - \frac{\beta}{1 + qz}xv, \\ \frac{dy}{dt} &= \frac{\beta}{1 + qz}xv - (d + \alpha)y. \end{aligned} \tag{1.2}$$

The term qz represents the suppression/inhibition of CTL on the viral infection. Similarly, the immune response may also reduce the rate of viral production [54],

$$\begin{aligned} \frac{dy}{dt} &= \beta xv - \left(d + \frac{\alpha}{1 + qz} \right) y, \\ \frac{dv}{dt} &= \frac{k}{1 + qz}y - uv. \end{aligned} \tag{1.3}$$

In this case, the CTL immune response follows the equation [54]

$$\frac{dz}{dt} = \frac{cyz}{(1 + qz)(1 + \epsilon z)} - bz.$$

Another important immune response in controlling virus infection is the antibody response. The antibody response is modeled in a similar way as the CTL response. The main difference is that antibody secreting B cells are activated by antigen specific $CD4^+$ T cells which recognize viral antigen on the surface of antigen presenting cells (APCs) such as macrophages or some dendritic cells. Since the amount of antigen presentation by the APCs is proportional to the abundance of free virus particles, the growth of this immune response must be proportional to v rather than y . Denoting the antibody response by z , the model for z is given as

$$\frac{dz}{dt} = \frac{cvz}{1 + \epsilon z} - bz,$$

Once the antibody response has developed, it removes free virus particles, which is given by equation [18]

$$\frac{dv}{dt} = ky - uv - pvz.$$

Here, antibody response removes free virus particles at a rate pvz .

Antiviral drugs For retroviruses, such as HIV-1, the efficacy of antiviral drugs is estimated by mathematical modeling. Let ϵ_{RT} and ϵ_{PI} denote the efficacy of the therapy with reverse transcriptase (RT) inhibitors and protease inhibitors, respectively ($0 \leq \epsilon_{RT}, \epsilon_{PI} < 1$). The newly produced virus particles are divided into two classes, infectious virions with concentration $v_I(t)$ and noninfectious viral particles with concentration $v_{NI}(t)$, to study the effect of protease inhibitor. The virus dynamics is reformed to the following system [28],

$$\begin{aligned}\frac{dx}{dt} &= \lambda - dx - (1 - \epsilon_{RT})\beta xv_I, \\ \frac{dy}{dt} &= (1 - \epsilon_{RT})\beta xv - ay, \\ \frac{dv_I}{dt} &= (1 - \epsilon_{PI})ky - uv_I, \\ \frac{dv_{NI}}{dt} &= \epsilon_{PI}ky - uv_{NI}.\end{aligned}$$

The equation of noninfectious virions v_{NI} is decoupled from the other first three equations. The dynamics of the first three equations is similar to the basic model. The difference is that the effects of drug is incorporated in the model and the basic reproduction number is changed to

$$\mathcal{R}_0 = \frac{(1 - \epsilon_{RT})(1 - \epsilon_{PI})\lambda\beta k}{dua}.$$

Time delays A time delay exists in the processes of viral infection, immune control and drug therapy. There is an intracellular time delay between infection of a cell and production of new virus particles. Let τ be the time delay from the time of initial infection until the production of new virions. For the basic model, incorporating this delay, the equation of infected cell population reads [13]

$$\frac{dy}{dt} = e^{-m\tau}\beta x(t - \tau)v(t - \tau) - (d + \alpha)y,$$

where τ is a constant, or

$$\frac{dy}{dt} = \int_0^\infty f(\tau)e^{-m\tau}\beta x(t - \tau)v(t - \tau)d\tau - (d + \alpha)y,$$

where τ is distributed according a distribution function $f(\tau)$ [32]. The recruitment of virus-producing cells at time t is given by the number of cells that were newly infected at time $t - \tau$

and are still alive at time t . With the assumption of a constant death rate m for infected but not yet virus-producing cells, the probability of surviving the time period from $t - \tau$ to t is $e^{-m\tau}$. For the constant delay model, the basic reproduction number for this model is

$$\mathcal{R}_0 = \frac{k\lambda\beta e^{-m\tau}}{du(d + \alpha)}.$$

If $\mathcal{R}_0 < 1$, the infection-free equilibrium is globally asymptotically stable. If $\mathcal{R}_0 > 1$, the infection-free equilibrium is unstable, and all positive solutions converge to the positive equilibrium with all $\tau > 0$ [25]. However, when both logistic growth of uninfected cells and this time delay are considered, Hopf bifurcation occurs from the positive equilibrium as the delay τ exceeds some threshold [60].

There are also a delay for activation of CD8⁺ T cell response. Considering this time delay, the equation of immune response is given by [5, 37]

$$\frac{dz}{dt} = cy(t - \tau), \quad \text{or} \quad \frac{dz}{dt} = cy(t - \tau)z(t - \tau).$$

With drug therapy, time delays of viral productive infection and viral reproduction are considered by [32, 51]

$$\frac{dy}{dt} = (1 - \epsilon_{RT})\beta \int_0^\infty f(\tau)x(t - \tau)v(t - \tau)d\tau - (d + a)y,$$

where $f(\tau)$ accounts for the probability of cells infected at time $t - \tau$ becoming productive at time t .

Infection age More precisely than a discrete fixed delay, the infection age of infected cells is considered in some models. The infected cells structure by the infection age, that is, the time that has elapsed since an HIV virion has penetrated the cell. Let $y(a, t)$ denotes the concentration of infected cells of infection age a at time t . Then the population of infected cells evolves by [12, 33]

$$\frac{\partial}{\partial t}y(a, t) + \frac{\partial}{\partial a}y(a, t) = -\delta(a)y(a, t),$$

where $\delta(a)$ is the age-dependent per capita death rate of infected cells. Infected cells of age zero are created by infection, that is,

$$y(0, t) = \beta x(t)v(t).$$

The concentration of infectious virus at time t , $v(t)$ evolves by

$$\frac{d}{dt}v(t) = \int_0^\infty P(a)y(a, t)da - uv,$$

where $P(a)$ is the viral production rate of an infected cell with age a . The functional form of viral production kernel, $P(a)$, and the death rate of infected cells, $\delta(a)$, need to be determined experimentally. Two possible functions for $P(a)$ are considered [33]. The first one is a delayed exponential function

$$P(a) = \begin{cases} P_{max}(1 - e^{-\theta(a-a_1)}) & \text{if } a \geq a_1, \\ 0 & \text{else,} \end{cases}$$

where θ controls how rapidly the saturation level P_{max} is reached. a_1 represents a delay in virus production, that is, it takes time a_1 after initial infection for the first virus particles to be produced. The second one is a Hill type function

$$P(a) = P_{max} \frac{a^n}{K_a^n + a^n},$$

where K_a is the half-saturation level and n is a constant called the Hill coefficient. This function allows for quick growth to a maximal level, depending upon the value of K_a , but can also approximate the delayed effect seen in the previous function. One possible choice of $\delta(a)$ is given by

$$\delta(a) = \begin{cases} \delta_0 & \text{if } a < a_2, \\ \delta_0 + \delta_m(1 - e^{-\gamma(a-a_2)}) & \text{if } a \geq a_2, \end{cases}$$

where $\delta_0 + \delta_m$ is the maximal death rate, γ controls the time to reach saturation level and a_2 is the delay between infection and the onset of cell-mediated killing. The term δ_0 represents a background death rate.

Age-structured models have also been developed to study the antiviral drug efficacy for HIV infection [41]. The class of infected cells, $y(a, t)$, is divided into two subclasses: $y_1(a, t)$ and $y_2(a, t)$, where $y_1(a, t)$ represents the density of cells that have been infected by an HIV virion but in which reverse transcription has not been completed at infection age a , called preRT cell; $y_2(a, t)$ represents the density of infected cells that have completed reverse transcription at infection age a , called postRT cell. The densities of the preRT and postRT cells are given by

$$y_1(a, t) = \gamma(a)y(a, t), \quad y_2(a, t) = (1 - \gamma(a))y(a, t),$$

where $\gamma(a)$ describes the proportion of infected cells those have not completed reverse transcription at age a , which is a non-increasing function with the following properties: $\gamma(a) \in L^1[0, \infty]$; $0 \leq \gamma(a) \leq 1$; $\gamma(0) = 1$; $\gamma(a) = 0$ for $a \geq a_1$; $\gamma'(a) \leq 0$ a.e. Let $\eta(\epsilon_{RT})$ denote the rate at which preRT cells revert to the uninfected stage due to the failure of reverse transcription.

Then the model reads [41]

$$\begin{aligned}\frac{dx}{dt} &= \lambda - dx - \beta xv_I + \int_0^\infty \eta(\epsilon_{RT})y_1(a, t)da, \\ \frac{\partial}{\partial t}y(a, t) + \frac{\partial}{\partial a}y(a, t) &= -\delta(a)y(a, t) - \int_0^\infty \eta(\epsilon_{RT})y_1(a, t)da, \\ y(0, t) &= kv_Ix, \\ \frac{dv_I}{dt} &= \int_0^\infty (1 - \epsilon_{PI})p(a)y_2(a, t)da - uv_I, \\ \frac{dv_{NI}}{dt} &= \int_0^\infty \epsilon_{PI}p(a)y_2(a, t)da - uv_{NI}.\end{aligned}$$

The limiting system of this model was considered, and then the basic reproduction number (ignoring the v_{NI} equation) is given by

$$\mathcal{R}_0 = \frac{\lambda\beta K}{du},$$

where K is the infectious virus burst size, and

$$K = \int_0^\infty (1 - \epsilon_{PI})(1 - \gamma(a))p(a)e^{-\int_0^a (\delta(s) + \eta(\epsilon_{RT})\gamma(s))ds} da.$$

The model with entry and protease inhibitors is given by

$$\begin{aligned}\frac{dx}{dt} &= \lambda - dx - (1 - \epsilon_{EI})\beta xv_I, \\ \frac{\partial}{\partial t}y(a, t) + \frac{\partial}{\partial a}y(a, t) &= -\delta(a)y(a, t), \\ y(0, t) &= (1 - \epsilon_{EI})kv_Ix, \\ \frac{dv_I}{dt} &= \int_0^\infty (1 - \epsilon_{PI})p(a)y_2(a, t)da - uv_I, \\ \frac{dv_{NI}}{dt} &= \int_0^\infty \epsilon_{PI}p(a)y_2(a, t)da - uv_{NI}.\end{aligned}$$

Similarly to the previous model, considering the limiting system of this model, the basic reproduction number (ignoring the v_{NI} equation) is given by

$$\mathcal{R}_0 = \frac{\lambda(1 - \epsilon_{EI})\beta K}{du},$$

where K is the infectious virus burst size, and

$$K = \int_0^\infty (1 - \epsilon_{PI})(1 - \gamma(a))p(a)e^{-\int_0^a \delta(s)ds} da.$$

These two systems have similar dynamical properties. Each of them has two equilibria respectively, an infection-free equilibrium and a positive equilibrium. The infection-free equilibrium is locally asymptotically stable if $\mathcal{R}_0 < 1$ and it is unstable if $\mathcal{R}_0 > 1$. The positive equilibrium is locally asymptotically stable if $\mathcal{R}_0 > 1$ [41].

1.4 Thesis motivations and outlines

Newly formed viruses are released to the outside environment either upon lysis (lytic virus) or by budding through the plasma membrane of the host cell (budding virus). Why some virus choose the former while the others choose the latter? We study the evolutionary competition of these two modes of viral release strategies in Chapter 2. Lytic viruses accumulate inside the host cell and exit in a burst killing the host cell (see figure 1.5(a)), while budding virus are produced and released from the host cell gradually (see Figure 1.5(b) and 1.5(c)). Most naked viruses are released by lysis, when infected cells breaks open (cell lysis/destruction) due to the activity of viral enzymes. Poliovirus is an example of a lytic virus. Budding is a typical feature of enveloped viruses. Enveloped viruses often obtain their envelopes from host cell membranes by budding. Budding occurs either at the outer cytoplasmic membrane, the nuclear membrane, or at the membranes of the Golgi apparatus. Viruses obtaining their envelope from the cytoplasmic membrane are released during the budding process. Viruses obtaining their envelopes from the membranes of the nucleus, the endoplasmic reticulum, or the Golgi apparatus are then released by exocytosis via transport vesicles. The examples of budding virus are retroviruses, togaviruses, orthomyxoviruses, paramyxoviruses, bunyaviruses, coronaviruses, rhabdoviruses and hepadnaviruses. We derive a mathematical model to study the evolutionary competitiveness of this two types of viruses by focusing on the infection age and release strategy. More specifically, we propose a mathematical model described by differential equations with distributed delay accounting for infection age. We first discuss the conditions for the existence and stability of equilibria of the model. Then we choose two explicit forms of the viral production function to investigate the effect of antibody on evolutionary competition of budding and lytic strategies.

Virus infection and spread is generally believed to be a recursive process of the binding of free virions to permissive target cells followed by entry, replication, making multiple copies of themselves and releasing them to extracellular environment, and then moving to infect adjacent target cells. New research and findings have challenged this classical view of how viruses infect and spread, suggesting that both cell-free virus infection and cell-to-cell transfer of HIV-1 are important mechanisms in virus spread. In the classical mode of infection (cell-free virus

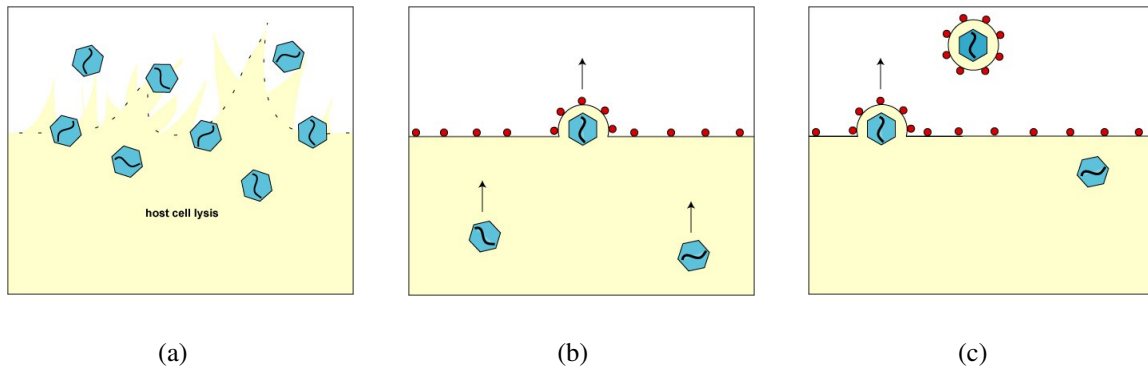


Figure 1.5: Release of viruses. (a) Release of naked viruses by host cell lysis. (b)-(c) Release of an enveloped virus by host cell budding (<http://me-you-and-virus.blogspot.ca/>).

infection), the virions spread around the body through freely circulating particles by the movement between cells and tissues of the body via fluid-phase diffusion. This route of infection is undoubtedly important. However, many viruses that are pathogenic for humans can also spread between cells without diffusing through the extracellular environment by exploiting preexisting mechanisms of physiological communication between cells [42, 43]. For example, HIV-1, herpes simplex virus and measles can be transported from one cell to adjacent cells without being released. Recent studies have advanced our understanding about the mechanism of cell-to-cell spread for some viruses [2, 16, 30, 44]. The dominant form of cell-to-cell spread for HIV-1 is likely to be spread via virological synapse, a structure that arises between a productively HIV-1-infected cell such as $CD4^+$ T cell or a macrophage and an uninfected permissive target cell [4, 8]. A stable adhesive junction is formed between two cells in a virological synapse. In the HIV-1 virological synapse, viral assembly and budding are polarized towards the synapse, and virus is released into the synaptic cleft before fusing with the target cell plasma membrane. An infected cell can polarize viral budding towards the receptor-expressing target cell in a virological synapse. Virions bud from the infected cell into a synaptic cleft, from which they fuse with target-cell plasma membrane. Cell-to-cell spread not only facilitates rapid viral dissemination, but may also promote immune evasion, escape from drug therapy and influence disease [27].

We consider both cell-to-cell infection mechanism and virus-to-cell infection mode by mathematical modeling. In Chapter 3, we incorporate an infinite intracellular delay which reflects the fact that an infected cell may remain latent forever, corresponding to various stages during the complicated process of virus replication and the survival rate of infected cells before they become productive. First, we identify the basic reproduction number of the model, in terms of which we discuss local stability of the infection-free equilibrium and the positive

equilibrium. Then we prove the persistence of infection, and further explore the global stability of the two equilibria. Our theoretical results show that the virus dynamics of the model are fully determined by the basic reproduction number. In Chapter 4, we further consider logistic cell growth ignoring the delay effect. We study the stability of the infection-free equilibrium and positive equilibrium, uniform persistence of the infection. Hopf bifurcation is discussed and illustrated numerically.

In the classical mode of virus infection and spread, the speed at which a virus can spread within a host would be limited by how quickly it can reproduce in each cell. New research [10, 6] have challenged the classical view of how viruses spread, indicating that some viruses could spread much faster than previously thought. Using live video microscopy, the researchers from Imperial College London discovered that vaccinia virus, the vaccine used to eradicate smallpox, could spread four times quicker than previously thought possible, based on the rate at which it replicates. They disclosed the underlying mechanism for the faster spread. Videos of virus-infected cells revealed that the virus spreads by surfing from cell to cell, using a mechanism that allows it to bounce past the adjacent infected cells and reach uninfected cells as quickly as possible. This can be called as viral ping-pong. The researchers believe that other viruses also employ rapid spreading mechanisms. For instance, herpes simplex virus (HSV-1), which causes cold sores, spreads at a faster rate than should be possible given its replication rate. Thus, this phenomenon discovered with vaccinia may be a common feature of some viruses. The discovery may ultimately enable scientists to create new antiviral drugs that target this spreading mechanism.

In Chapter 5, we study this ping-pong effect by a reaction diffusion equation model where the diffusion of virus population depends not only on its concentration but also on the concentration of infected cells. The well-posedness of the model, the basic reproduction number of the model is obtained. For spatial heterogeneous case (some parameters depend on space location), the basic reproduction number for the model is derived to be a spectral radius of the linear next generation operator. We compute it numerically by orthogonal projection method. When all the parameters do not depend on space location, we show the linear stability of steady states of model. With a one dimensional domain, we estimate the spread rate of virus numerically and discuss the effect of repulsion of superinfecting virions. With a one dimensional infinite space, we analyzed the minimal traveling wave speed and existence of traveling wave solution numerically, when the diffusion of target cell and infected cell is ignored.

In Chapter 6, we study the effect of CTL-chemotaxis response on HIV-1 infection dynamics. Many motile cells and organisms, such as somatic cells, bacteria, and other single-cell

or multicellular organisms, direct their movements according to certain chemicals in their environment. This oriented movement is called chemotaxis. In the experimental community, chemotaxis or chemoattraction describes a directed movement of organisms up a concentration gradient of chemotactic agents (called chemoattractant, see Figure 1.6). Conversely, chemorepulsion or fugetaxis is defined as a directed movement of organisms down a concentration gradient of chemotactic agents (called chemorepellent) [49, 17]. However, in mathematical literature, chemotaxis has a broader meaning of the directed movements of organisms toward or away from the chemotactic agents [15]. Positive chemotaxis means chemoattraction, while negative chemotaxis denotes chemorepulsion.

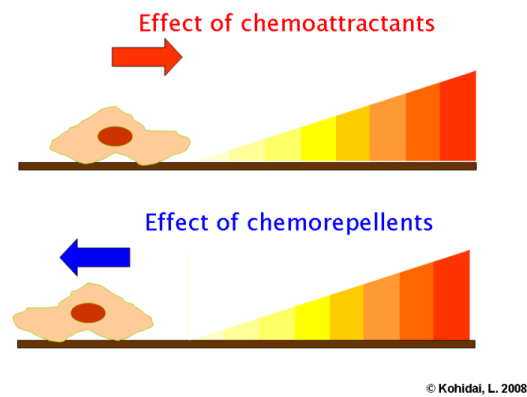


Figure 1.6: Chemoattraction and chemorepulsion (<http://en.wikipedia.org/wiki/Chemotaxis>).

Cell-mediated immunity depends in part on appropriate migration and localization of CTLs. This process is regulated by chemokines and adhesion molecules [20]. Many viruses encode chemotactically active proteins. The envelope protein gp120 of HIV-1 has been shown to act as a T-cell chemoattractant via binding to the chemokine receptor and HIV-1 coreceptor CXCR4. Some studies [1, 19] showed that high concentrations of the viral protein CXCR4-binding HIV-1 gp120 repels HIV-specific CTLs, while low concentration of gp120 attracts CTLs with specific interaction with CXCR4. In HIV-1 infection dynamics, if we assume virus population is at a quasi-steady state, the virus load is proportional to the concentration of infected cells $I(x, t)$. Furthermore, the concentration of gp120 is proportional to the infected cells, and chemotaxis flux of CTLs, $E(x, t)$, is given by $\mathbf{J} = E\Psi(E, I)\nabla I$, where $\Psi(E, I)$ is the chemotactic response function. Negative $\Psi(E, I)$ indicates chemoattraction, while positive $\Psi(E, I)$ represents chemorepulsion. Incorporating this chemotaxis term into the HIV-1 infection model, we derive a reaction diffusion-chemotaxis model.

A challenging problem for chemotaxis models is the blow-up of solutions in finite time. That means the whole population concentrate in a single point in a finite time. To avoid a

blow up, various mechanisms are introduced [14, 15, 53, 58]. One mechanism is to consider the volume-filling effect [36, 59], which means only a finite number of cells can be accommodated at any site. If the chemotactic response function is assumed to be of the form $\Psi(u, v) := q(u)\chi(v)$, the volume-filling effect can be described by $q(u)$ satisfying $q(U_{max}) = 0$, and $q(u) \geq 0$ for all $0 \leq u < U_{max}$, where U_{max} denotes the maximum number of cells those can be accommodated at any site. For example, a simple form, $q(u) = 1 - \frac{u}{U_{max}}$. The function $q(u)$ is considered as the probability of the cell finding a space at its neighboring location depends upon the availability of space.

Considering the volume-filling effect, we show the global existence and well-posedness of solutions. Linear stability of the steady states and the conditions for Turing instability and pattern formation are analyzed. Assuming a constant chemotactic sensitivity function, we show the stability of positive steady state, steady state bifurcation, Hopf bifurcation and pattern formation numerically under different conditions.

The thesis ends up with a conclusion in Chapter 7, where we summarize the main results of the thesis, and point out some possible topics for future work.

Bibliography

- [1] Brainard D.M. et al., Migration of antigen-specific T cells away from CXCR4-binding Human Immunodeficiency Virus type 1 gp120, *J. Virol.*, Vol. 78 No. 10 (2004) 5184-5193.
- [2] Burckhard C.J. and Greber U.F., Virus movements on the plasma membrane support infection and transmission between cells, *PLoS Pathogens*, Vol. 5 Issue 11 (2009) 1-9.
- [3] Carter J.B. and Saunders V.A., *Virology: principles and applications*. Hoboken, NJ, John Wiley & Sons, 2007.
- [4] Chen K.B., T cell virological synapses and HIV-1 pathogenesis, *Immunol. Res.*, 54 (2012) 133-139.
- [5] Ciupe M.S., Bivort B.L., Bortz D.M. and Nelson P.W., Estimating kinetic parameters from HIV primary infection data through the eyes of three different mathematical models, *Math. Biosci.*, 200 (2006) 1-27.
- [6] Condit R.C., Surf and Turf: mechanism of enhanced virus spread during poxvirus infection, *Viruses*, 2 (2010) 1050-1054.
- [7] Culshaw R.V. and Ruan S., A delay-differential equation model of HIV infection of CD4⁺ T-cells, *Math. Biosci.*, 165 (2000) 27-39.
- [8] Dale B.M., Alvarez R.A. and Chen B.K., Mechanisms of enhanced HIV spread through T-cell virological synapses, *Immuno. Reviews*, 251 (2013) 113-124.
- [9] Diekmann O., Heesterbeek J.A.P. and Metz J.A.J., On the definition and computation of the basic reproduction ratio R_0 in models for infectious diseases in heterogeneous populations, *J. Math. Biol.*, 28 (1990) 365-382.
- [10] Doceul V. et al., Repulsion of superinfecting virions: a mechanism for rapid virus spread, *Science*, 327 (2010) 873-876.

- [11] Driessche P. van den and Watmough J., Reproduction number and sub-threshold endemic equilibria for compartmental models of disease transmission, *Math. Biosci.*, 180 (2002) 29-48.
- [12] Gilchrist M.A., Coombs D. and Perelson A.S., Optimizing within-host viral fitness: infected cell lifespan and virion production rate, *J. Theor. Biol.*, 229 (2004) 281-288.
- [13] Herz A.V.M., Bonhoeffer S., Anderson R.M., May R.M. and Nowak M.A., Viral dynamics in vivo: Limitations on estimates of intracellular delay and virus decay, *Proc. Natl. Acad. Sci. USA*, 93 (1996) 7247-7251.
- [14] Hillen T. and Painter K., Global existence for a parabolic chemotaxis model with prevention of overcrowding, *Advances in Appl. Math.*, 26 (2001) 280-301.
- [15] Hillen T. and Painter K.J., A users' guide to PDE models for chemotaxis, *J. Math. Biol.*, 58 (2009) 183-217.
- [16] Hübner W., McNerney G.P., Chen P., Dale B.M., Gordan R.E., Chuang F.Y.S., Li X.D., Asmuth D.M., Huser T. and Chen B.K., Quantitative 3D video microscopy of HIV transfer across T cell virological synapses, *Science*, 323 (2009) 1743-1747.
- [17] Huttenlocher A. and Poznansky M.C., Reverse leukocyte migration can be attractive or repulsive, *Trends Cell Biol.*, Vol. 8 No. 16 (2008) 298-306.
- [18] Inoue T., Kajiwara T. and Sasaki T., Global stability of models of humoral immunity against multiple viral strains, *J. Biol. Dyn.*, Vol. 4 No. 3 (2010) 282-295.
- [19] Iyengar S., Schwartz D.H. and Hildreth J.E.K., T cell-tropic HIV gp120 mediates CD4 and CD8 cell chemotaxis through CXCR4 independent of CD4: implications for HIV pathogenesis, *J. Immunology*, 162 (1999) 6263-6267.
- [20] Jin T., Xu X. and Hereld D., Chemotaxis, chemokine receptors and human disease, *Cytokine*, 44 (2008) 1-8.
- [21] Kajiwara T. and Sasaki T., Global stability of pathogen-immune dynamics with absorption, *J. Biol. Dyn.*, Vol. 4 No. 3 (2010) 258-269.
- [22] Korobeinikov A., Global properties of basic virus dynamics models, *Bull. Math. Biol.*, 66 (2004) 879-883.
- [23] Krkošek M. and Lewis M., An R_0 theory for source-sink dynamics with application to *Dreissena* competition, *Theor. Ecol.*, 3 (2010) 25-43.

- [24] Leenheer P.D. and Smith H.L., Virus dynamics: a global analysis, *SIAM J. Appl. Math.*, Vol. 63 No. 4 (2003) 1313-1327.
- [25] Li M.Y. and Shu H., Global dynamics of an in-host viral model with intracellular delay, *Bull. Math. Biol.*, 72 (2010) 1492-1505.
- [26] Li J., Wang K. and Yang Y., Dynamical behaviors of an HBV infection model with logistic hepatocyte growth, *Mathematical and Computer Modelling*, 54 (2011) 704-711.
- [27] Martin N. and Sattentau Q., Cell-to-cell HIV-1 spread and its implications for immune evasion, *Curr. Opin. HIV AIDS*, 4 (2009) 143-149.
- [28] Di Mascio M., Ribeiro R.M., Markowitz M., Ho D.D. and Perelson A.S., Modeling the longterm control of viremia in HIV-1 infected patients treated with antiretroviral therapy, *Math. Biosci.*, 188 (2004) 47-62.
- [29] Mckenzie H.W., Jin Y., Jacobsen J. and Lewis M.A., R_0 analysis of a spatiotemporal model for a stream population, *SIAM J. Appl. Dyn. Sys.*, Vol. 11 No. 2 (2012) 567-596.
- [30] Mothes W., Sherer N.M., Jin J., Zhong P., Virus cell-to-cell transmission, *J. Virol.*, Vol. 84 No. 17 (2010) 8360-8368.
- [31] Muphy K., with acknowledgment to Travers P., Walport M., with contributions by Mowat A., Weaver. C.T., *Janeway's immunobiology*, London, New York: Garland Science, c2012.
- [32] Nelson P.W. and Perelson A.S., Mathematical analysis of delay differential equation models of HIV-1 infection, *Math. Biosci.*, 179 (2002) 73-94.
- [33] Nelson P.W., Gilchrist M.A., Coombs D., Hyman J.M. and Perelson A.S., An age-structured model of HIV infection that allows for variations in the production rate of viral particles and the death rate of productively infected cells, *Math. Biosci. Eng.*, Vol. 1 No. 2 (2004) 267-288.
- [34] Nowak M.A. and Bangham C.R.M., Population dynamics of immune responses to persistent viruses, *Science*, 272 (1996) 74-79.
- [35] Nowak M.A. and May R.M., *Virus dynamics: mathematical principles of immunology and virology*, New York, Oxford University Press, 2000.

- [36] Painter K.J. and Hillen T., Volume-filling and quorum-sensing in modeling for chemosensitive movement, *Canadian Appl. Math. Quarterly*, Vol. 10 No. 4 (2002) 501-543.
- [37] Pawelek K.A., Liu S., Pahlevani F. and Rong L., A model of HIV-1 infection with two time-delays: Mathematical analysis and comparison with patient data, *Math. Biosci.*, Vol. 235 No. 1 (2012) 98-109.
- [38] Payne R.J.H., Nowak M. A. and Blumberg B., The dynamics of hepatitis B virus infection, *Proc. Natl. Acad. Sci. USA*, 93 (1996) 6542-6546.
- [39] Perelson A.S., Neumann A.U., Markowitz M., Leonard J.M. and Ho D.D., HIV-1 dynamics in vivo: virion clearance rate, infected cell life-span, and viral generation time, *Science*, 271 (196) 1582-1586.
- [40] Perelson A.S. and Nelson P.W., Mathematical analysis of HIV-1 dynamics in vivo, *SIAM Review*, Vol. 41 No 1 (1999) 3-44.
- [41] Rong L., Feng Z. and Perelson A.S., Mathematical analysis of age-structured HIV-1 dynamics with combination antiretroviral therapy, *SIAM J. Appl. Math.*, Vol. 67 No. 3 (2007) 731-756.
- [42] Sattentau Q., Avoiding the void: cell-to-cell spread of human viruses, *Nat. Rev. Microbiol.*, 6 (2008) 28-41.
- [43] Sattentau Q., The direct passage of animal viruses between cells, *Current Opinion in Virology*, 1 (2011) 396-402.
- [44] Sherer N.M., Lehmann M.J., Jimenez-Soto L.F., Horensavitz C., Pypaert M. and Mothes W., Retroviruses can establish filopodial bridges for efficient cell-to-cell transmission, *Nat. Cell Biol.*, 9 (2007) 310-315.
- [45] Shors T., *Understanding viruses*, Burlington, MA: Jones & Bartlett Learning, 2013.
- [46] Stafford M.A., Corey L., Cao Y., Daar E.S., Ho D.D. and Perelson A.S., Modeling plasma virus concentration during primary HIV infection, *J. theor. Biol.*, 203 (2000) 285-301.
- [47] Strauss J.H. and Strauss E.G., *Viruses and human disease*, Boston, Elsevier Academic Press, 2008.

- [48] Thieme H.R., Spectral bound and reproduction number for infinite-dimensional population structure and time heterogeneity, *SIAM J. Appl. Math.*, Vol. 70 No. 1 (2009) 188-211.
- [49] Vianello F. and Olszak T.I., Fugetaxis: active movement of leukocytes away from a chemokinetic agent, *J. Mol. Med.*, 83 (2005) 752-763.
- [50] Wang L. and Li M.Y., Mathematical analysis of the global dynamics of a model for HIV infection of CD4⁺ T cells, 200 (2006) 44-57.
- [51] Wang J., Huang G. and Takeuchi Y., Global asymptotic stability for HIV-1 dynamics with two distributed delays, *Math. Med. Biol.*, Vol. 29 No. 3 (2012) 283-300.
- [52] Wesley C.L. and Allen L.J.S., The basic reproduction number in epidemic models with periodic demographics, *J. Biol. Dyn.*, Vol. 3 No. 2 (2009) 116-129.
- [53] Winkler M., Absence of collapse in a parabolic chemotaxis system with signal-dependent sensitivity, *Math. Nachr.*, Vol. 283 No. 11 (2010) 1664-1673.
- [54] Wodarz D. and Nowak M.A., Immune responses and viral phenotype: do replication rate and cytopathogenicity influence virus load, *J. Theor. Med.*, 2 (2000) 113-127.
- [55] Wodarz D. and Krakauer D.C., Defining CTL-induced pathology: implications for HIV, *Virology*, 274 (2000) 94-104.
- [56] Wodarz D., Christensen J.P. and Thomsen A.R., The importance of lytic and nonlytic immune responses in viral infections, *TRENDS Immun.*, Vol. 23 No. 4 (2002) 191-200.
- [57] Wodarz D., Mathematical models of immune effector responses to viral infections: Virus control versus the development of pathology, *J. Comput. Appl. Math.*, 184 (2005) 301-319.
- [58] Wrzosek D., Global attractor for a chemotaxis model with prevention of overcrowding, *Nonlinear Analysis*, 59 (2004) 1293-1310.
- [59] Wrzosek D., Volume filling effect in modeling chemotaxis, *Math. Model. Nat. Phenom.*, Vol. 5 No. 1 (2010) 123-147.
- [60] Zhou X., Song X. and Shi X., Analysis of stability and Hopf bifurcation for an HIV infection model with time delay, *Appl. Math. Comput.*, 199 (2008) 23-38.

Chapter 2

Dynamics of evolutionary competition between budding and lytic viral release strategies

2.1 Introduction

In the real world, there are mainly two types of viral release strategies: lytic and budding. Viruses can be released from the host cell by lysis, a process that kills the cell by bursting its membrane, after a period of accumulation of new virions inside the host cell. This is a feature of many bacterial and animal naked viruses, such as many types of phages, rhinoviruses and picornaviruses [2]. Many viruses do not lyse their host cells; instead, progeny virions are released from the cells over a period of time by gradually budding. Enveloped viruses, such as HIV and influenza, are typically released from host cells by this strategy (see [5], [9]). During this process a virus acquires its envelope from cell surface membrane.

A typical viral production process consists of viral attachment (to the host cells), penetration, uncoating, replication and release. However, lytic and budding viral strains have different life cycles. A lytic virus has a lytic cycle during which the new virions are produced and accumulated inside the host cell, and released by a burst (lysis) when the number of viruses inside becomes too large for the cell to hold. A budding virus reproduces inside and escapes the host cell by constantly budding throughout the lifespan of the infected cell.

There is some research on the kinetics of viral production. Coombs [4] examined the optimal virus production schedules by considering the trade-off between viral replication and cell death rate. Burst size, defined as the expected number of virions produced over the lifetime of an infected cell, was considered as viral reproductive fitness. It was found that if viral

production rate and cell mortality rate are linked, replicating at the maximal rate so that the burst size is maximized, may not be the optimal strategy for virus, even if natural selection favors viral strains whose virion production rate maximizes viral burst size. The optimal viral production rate may be lower than the maximum viral production rate, or may not be a constant, meaning that it may vary with the time or the age of the infected cell, depending on the trade-off between cell mortality and viral production. In a subsequent work, Gilchrist *et al.* [6] used an age-structured model of virus dynamics to study the optimal viral fitness. It was shown that trade-offs between virion production and immune system clearance of infected cells could lead natural selection to favor production rates lower than the one that maximizes burst size. Nelson *et al.* [10] also used an age structured model to study the influence of different profiles of nonconstant viral production rate and nonconstant infected cell death rate on HIV infection dynamics. As for lytic virus, Wang *et al.* (see [13],[14]) studied the optimal lysis time and phage fitness. It was found that a delay in lysis time can lead to production of more progeny per infected host. Therefore, there is a trade-off between a present immediate linear gain by extending the vegetative cycle of phage and a future uncertain exponential gain derived from lysing the current host and releasing the progeny virion.

Komarova [8] studied the evolutionary competition between budding and lytic strategies. It was concluded that if all the parameters, such as the rate of viral production, cell lifespan and neutralizing capacity of antibodies, were the same for the lytic and budding viruses, the budding life-strategy would have a large evolutionary advantage because it is advantageous for an organism to reproduce earlier in life rather than later, given that the offspring is the same in both cases. However when the antibody effect is considered, the difference in removal capacity of the antibodies against budding and lytic virions could make lytic virus evolutionarily more competitive. Newly produced virions of a budding virus exit the host cell gradually and are immediately attacked by antibodies, while that of a lytic strain exit all at once, in a burst, and if there are sufficiently many of them, they can "flood" the immune system making it less effective.

Komarova [8] used the Euler-Lotka equation for the host cell population and reaction diffusion equations for antibody flooding effect. The disadvantage of the Euler-Lotka model is that it only models a steady state of viral spread, when the uninfected host cells are freely available. In this chapter, we aim at providing an alternative perspective by focusing on the infection age and release strategy. More specifically, we propose a mathematical model described by ordinary differential equations with distributed delay accounting for infection age. By analyzing this structured model system, we study the evolutionary competition between these two viral productive strategies.

The rest of this chapter is organized as follows. In Section 2, we present an age structured

model and its simplified form with distributed delay. In Section 3, we prove that all the solutions of our model are positive and bounded. In Section 4, the equilibria of the model and their stability are discussed. In Section 5, we give two explicit forms of the viral production function and investigate the effect of antibody on evolutionary competition of budding and lytic strategies. The chapter is ended by Section 6, where in addition to conclusion, some discussion is also presented.

2.2 Model formulation

Age structured models have been used to study the within-host dynamics for HIV (see [10], [6], [11]). We use an age structured model for the infected cell population. The infection age, a , is the time lapsed since a cell was infected by a virus. Suppose that $T(t)$ is the density of uninfected target cells at time t ; $V_B(t)$ is the density of virus produced by the budding strategy at time t (we call it budding virus); $V_L(t)$ is the density of virus produced by the lytic strategy at time t (we call it lytic virus); $T_B^*(t, a)$ is the density of infected cells at infection age a at time t , which are infected by budding virus; $T_L^*(t, a)$ is the density of infected cells at infection age a and at time t , which are infected by lytic virus; $A(t)$ is the density of antibody at time t . By infection, budding virus and lytic virus compete for uninfected target cells. Assuming mass action infection mechanism, we propose the following system of differential equations to describe the competition dynamics of budding and lytic viruses:

$$\left\{ \begin{array}{l} \frac{dT(t)}{dt} = H - d_T T(t) - \beta_B T(t) V_B(t) - \beta_L T(t) V_L(t), \\ \frac{\partial T_B^*(t, a)}{\partial t} + \frac{\partial T_B^*(t, a)}{\partial a} = -d_{T_B^*}(a) T_B^*(t, a), \\ \frac{\partial T_L^*(t, a)}{\partial t} + \frac{\partial T_L^*(t, a)}{\partial a} = -d_{T_L^*}(a) T_L^*(t, a), \\ \frac{dV_B(t)}{dt} = \int_{\tau_B}^{\tau^*} \gamma_B(a) T_B^*(t, a) da - d_V V_B(t) - \eta_B V_B(t) A(t), \\ \frac{dV_L(t)}{dt} = \int_{\tau_L}^{\tau^*} \gamma_L(a) T_L^*(t, a) da - d_V V_L(t) - \eta_L V_L(t) A(t), \\ \frac{dA(t)}{dt} = p(V_B(t) + V_L(t)) A(t) - d_A A(t) - \eta_B V_B(t) A(t) - \eta_L V_L(t) A(t). \end{array} \right. \quad (2.1)$$

Here, β_B and β_L represent the infection rates of budding virus and lytic virus respectively. $\gamma_B(a)$ and $\gamma_L(a)$ are the virion production rates from infected cells with an infection age a by budding strategy and by lytic strategy respectively. τ_B and τ_L denote the ages when the infected cells begin to release new virions by budding and lysis respectively. p is the activation rate of antibodies. η_B and η_L are the neutralization rates of antibodies for budding virus and lytic virus

respectively.

We assume that viruses are introduced at time $t = 0$, meaning that there is neither virus nor infection for $t \in [-\tau^*, 0)$, and infection occurs at $t = 0$ immediately after introduction of viruses. Accordingly

$$T_B^*(0, a) = 0, \quad T_L^*(0, a) = 0, \quad \text{for all } a > 0.$$

The infected cells of age zero come from the new infections, that is

$$T_B^*(t, 0) = \beta_B T(t) V_B(t), \quad T_L^*(t, 0) = \beta_L T(t) V_L(t).$$

Now, for the budding virus, the dynamics are determined by the following initial-boundary value problem:

$$\begin{cases} \frac{\partial T_B^*(t, a)}{\partial t} + \frac{\partial T_B^*(t, a)}{\partial a} = -d_{T_B^*}(a) T_B^*(t, a), \\ T_B^*(t, 0) = \beta_B T(t) V_B(t), \\ T_B^*(0, a) = 0, \forall a > 0. \end{cases} \quad (2.2)$$

Solving this problem by the method of characteristics, we obtain

$$T_B^*(t, a) = \begin{cases} \beta_B T(t - a) V_B(t - a) e^{-\int_0^a d_{T_B^*}(\xi) d\xi}, & t \geq a, \\ 0, & t < a. \end{cases}$$

Similarly, we have

$$T_L^*(t, a) = \begin{cases} \beta_L T(t - a) V_L(t - a) e^{-\int_0^a d_{T_L^*}(\xi) d\xi}, & t \geq a, \\ 0, & t < a. \end{cases}$$

Substituting the above formulas for $T_B^*(t, a)$ and $T_L^*(t, a)$ into V_B and V_L equations in (6.1), and by our assumptions that $V_B(\theta) = 0$, $V_L(\theta) = 0$, for all $\theta \in [-\tau^*, 0)$, we obtain the following model system:

$$\begin{cases} \frac{dT(t)}{dt} = H - d_T T(t) - \beta_B T(t) V_B(t) - \beta_L T(t) V_L(t), \\ \frac{dV_B(t)}{dt} = \int_{\tau_B}^{\tau^*} \gamma_B(a) e^{-\int_0^a d_{T_B^*}(\xi) d\xi} \beta_B T(t - a) V_B(t - a) da - d_V V_B(t) - \eta_B V_B(t) A(t), \\ \frac{dV_L(t)}{dt} = \int_{\tau_L}^{\tau^*} \gamma_L(a) e^{-\int_0^a d_{T_L^*}(\xi) d\xi} \beta_L T(t - a) V_L(t - a) da - d_V V_L(t) - \eta_L V_L(t) A(t), \\ \frac{dA(t)}{dt} = p(V_B(t) + V_L(t)) A(t) - d_A A(t) - \eta_B V_B(t) A(t) - \eta_L V_L(t) A(t). \end{cases} \quad (2.3)$$

In the rest of the chapter, we shall investigate the dynamics of this system.

2.3 Positivity and boundedness of solutions

Let $\mathbb{X} = C([- \tau^*, 0], \mathbb{R}^4)$ be the Banach space of continuous functions with supremum norm. By the fundamental theory of FDEs [7], we know that there is a unique solution $(T(t), V_B(t), V_L(t), A(t))$ to the system with given initial conditions $(T(\theta), V_B(\theta), V_L(\theta), A(\theta)) \in \mathbb{X}$. Due to the biological meanings of the unknown functions, we need to further assume that the initial functions $T(\theta)$, $V_B(\theta)$, $V_L(\theta)$, and $A(\theta)$ satisfy

$$\begin{cases} T(\theta) \geq 0, V_B(\theta) = 0, V_L(\theta) = 0, A(\theta) \geq 0, \text{ for all } \theta \in [-\tau^*, 0), \\ T(0) > 0, V_B(0) > 0, V_L(0) > 0, A(0) > 0. \end{cases} \quad (2.4)$$

The following theorem addresses the well-posedness of the model (2.3).

Theorem 2.3.1 *Let $(T(t), V_B(t), V_L(t), A(t))$ be a solution of the system (2.3) satisfying (2.4). Then $T(t)$, $V_B(t)$, $V_L(t)$ and $A(t)$ are non-negative and bounded for all $t \geq 0$.*

Proof From the first and last equations of the system (2.3), we have

$$\begin{aligned} T(t) &= T(0)e^{-\int_0^t (d_T + \beta_B V_B(\xi) + \beta_L V_L(\xi)) d\xi} + \int_0^t H e^{-\int_\eta^t (d_T + \beta_B V_B(\xi) + \beta_L V_L(\xi)) d\xi} d\eta > 0, \\ A(t) &= A(0)e^{\int_0^t [pV_B(\xi) + pV_L(\xi) - d_A - \eta_B V_B(\xi) - \eta_L V_L(\xi)] d\xi} > 0. \end{aligned}$$

Next, we show that $V_B(t) > 0$ for all $t \in (0, \infty)$. Otherwise, there exists a first time $t_1 > 0$ such that $V_B(t_1) = 0$ and $V_B(t) > 0$ for $t \in [0, t_1)$. This would lead to

$$\frac{dV_B(t_1)}{\partial t} = \int_{\tau_B}^{\tau^*} \gamma_B(a) e^{-\int_0^a d_{T_B^*}(\xi) d\xi} \beta_B T(t_1 - a) V_B(t_1 - a) da > 0.$$

This implies $V_B(t)$ is negative in a small left neighborhood of t_1 , a contradiction. Therefore, $V_B(t) > 0$ for all $t > 0$. Similarly, we can prove $V_L(t) > 0$ for all $t > 0$.

To prove the boundedness, let $\bar{\gamma}_B = \max_{a \in [\tau_B, \tau^*]} \gamma_B(a)$, $\bar{\gamma}_L = \max_{a \in [\tau_L, \tau^*]} \gamma_L(a)$, $\bar{\gamma} = \max\{\bar{\gamma}_B, \bar{\gamma}_L\}$, $d_{T^*} = \min\{\min_{\tau_B \leq a \leq \tau^*} d_{T_B^*}(a), \min_{\tau_L \leq a \leq \tau^*} d_{T_L^*}(a)\}$ and $\eta = \min\{\eta_B, \eta_L\}$. Define

$$G(t) = \bar{\gamma} \int_{\tau_B}^{\tau^*} e^{-d_{T^*} a} T(t - a) da + V_B(t) + V_L(t) + \frac{\eta}{p} A(t).$$

By the nonnegativity of solutions, it follows that

$$\begin{aligned}
\frac{dG(t)}{dt} &= H\bar{\gamma} \int_{\tau_B}^{\tau^*} e^{-d_T a} da - d_T \bar{\gamma} \int_{\tau_B}^{\tau^*} e^{-d_T a} T(t-a) da \\
&\quad - \bar{\gamma} \int_{\tau_B}^{\tau^*} e^{-d_T a} [\beta_B T(t-a) V_B(t-a) + \beta_L T(t-a) V_L(t-a)] da \\
&\quad + \int_{\tau_B}^{\tau^*} \gamma_B(a) e^{-\int_0^a d_{T_B^*}(\xi) d\xi} \beta_B T(t-a) V_B(t-a) da - d_V V_B(t) - \eta_B V_B(t) A(t), \\
&\quad + \int_{\tau_L}^{\tau^*} \gamma_L(a) e^{-\int_0^a d_{T_L^*}(\xi) d\xi} \beta_L T(t-a) V_L(t-a) da - d_V V_L(t) - \eta_L V_L(t) A(t) \\
&\quad + \eta(V_B(t) + V_L(t)) A(t) - \frac{d_A \eta}{p} A(t) - \frac{\eta \eta_B}{p} V_B(t) A(t) - \frac{\eta \eta_L}{p} V_L(t) A(t) \\
&\leq H\bar{\gamma} \int_{\tau_B}^{\tau^*} e^{-d_T a} da - d_T \bar{\gamma} \int_{\tau_B}^{\tau^*} e^{-d_T a} T(t-a) da - d_V V_B(t) - d_V V_L(t) - d_A \frac{\eta}{p} A(t) \\
&\leq Q - dG(t),
\end{aligned}$$

where $Q = H\bar{\gamma} \int_{\tau_B}^{\tau^*} e^{-d_T a} da > 0$ and $d = \min\{d_T, d_V, d_A\} > 0$. Therefore, $\limsup_{t \rightarrow \infty} G(t) \leq Q/d$, implying that $G(t)$ is bounded, and so are $T(t)$, $V_B(t)$, $V_L(t)$ and $A(t)$. \blacksquare

2.4 Equilibria and their stability

Let

$$\begin{aligned}
R_B^{(0)} &= \frac{\beta_B H K_B}{d_V d_T}, \quad R_L^{(0)} = \frac{\beta_L H K_L}{d_V d_T}, \\
R_B^{(1)} &= R_B^{(0)} - \sigma_B, \quad R_L^{(1)} = R_L^{(0)} - \sigma_L.
\end{aligned}$$

where

$$\begin{aligned}
K_B &= \int_{\tau_B}^{\tau^*} \gamma_B(a) e^{-\int_0^a d_{T_B^*}(\xi) d\xi} da, \quad K_L = \int_{\tau_L}^{\tau^*} \gamma_L(a) e^{-\int_0^a d_{T_L^*}(\xi) d\xi} da, \\
\sigma_B &= \frac{\beta_B d_A}{d_T(p - \eta_B)}, \quad \sigma_L = \frac{\beta_L d_A}{d_T(p - \eta_L)}.
\end{aligned}$$

Here, $e^{-\int_0^a d_{T_B^*}(\xi) d\xi}$ denotes the age-specific survival probability of an infected cell infected by budding virus, i.e., the probability of an infected cell remaining alive at infection age a . Thus, K_B is the total number of new virions produced by one infected cell, infected by budding virus, over its whole lifespan. We call K_B the burst size of budding virus. Similarly, K_L is the burst size of lytic virus. Notice that $1/d_V$ is the life span of budding virus in the absence of antibody, H/d_T is the cell density without infection, and β_B is the infection rate. Hence, one budding virus, once inoculated into an environment containing H/d_T uninfected cells, can lead to $\beta_B H/(d_T d_V)$ infected cells. These infected cells then produce the amount $\beta_B H K_B/(d_T d_V)$ of

new virions. Therefore, $R_B^{(0)}$ gives the reproductive ratio of the budding virus in the absence of antibody (also referred to as the basic reproductive number). In parallel, $R_L^{(0)}$ is the reproductive ratio of the lytic virus in the absence of antibody. Note that σ_B accounts for the clearance rate of antibody for budding virus. Thus, $R_B^{(1)}$ is the reproductive ratio of budding virus when the antibody for budding virus is established. Similarly, $R_L^{(1)}$ is the reproductive ratio of lytic virus when the antibody for lytic virus is established.

For system (2.3), there always exists an infection free equilibrium $E_0 = (T^{(0)}, 0, 0, 0)$, where $T^{(0)} = H/d_T$. Other possible equilibria are summarized below:

(I) If $R_B^{(0)} > 1$, there exists an equilibrium $E_{10} = (T^{(10)}, V_B^{(10)}, 0, 0)$, where

$$T^{(10)} = \frac{d_V}{K_B \beta_B}, \quad V_B^{(10)} = \frac{d_T}{\beta_B} (R_B^{(0)} - 1).$$

(II) If $R_L^{(0)} > 1$, there exists an equilibrium $E_{01} = (T^{(01)}, 0, V_L^{(01)}, 0)$, where

$$T^{(01)} = \frac{d_V}{K_L \beta_L}, \quad V_L^{(01)} = \frac{d_T}{\beta_L} (R_L^{(0)} - 1).$$

(III) If $R_B^{(0)} = R_L^{(0)} > 1$, there are infinitely many equilibria of the form $\hat{E} = (\hat{T}, \hat{V}_B, \hat{V}_L, 0)$, where

$$\hat{T} = \frac{d_V}{K_B \beta_B}, \quad \beta_B \hat{V}_B + \beta_L \hat{V}_L = d_T (R_B^{(0)} - 1).$$

(IV) If $p > \eta_B$ and $R_B^{(1)} > 1$, there exists an equilibrium $E_{20} = (T^{(20)}, V_B^{(20)}, 0, A^{(20)})$, where

$$T^{(20)} = \frac{H}{d_T(1 + \sigma_B)}, \quad V_B^{(20)} = \frac{d_A}{p - \eta_B}, \quad A^{(20)} = \frac{d_V}{\eta_B(1 + \sigma_B)} (R_B^{(1)} - 1).$$

(V) If $p > \eta_L$ and $R_L^{(1)} > 1$, there exists an equilibrium $E_{02} = (T^{(02)}, 0, V_L^{(02)}, A^{(02)})$, where

$$T^{(02)} = \frac{H}{d_T(1 + \sigma_L)}, \quad V_L^{(02)} = \frac{d_A}{p - \eta_L}, \quad A^{(02)} = \frac{d_V}{\eta_L(1 + \sigma_L)} (R_L^{(1)} - 1).$$

(VI) The positive equilibrium $E_{22} = (T^{(22)}, V_B^{(22)}, V_L^{(22)}, A^{(22)})$, where

$$\begin{aligned} T^{(22)} &= \frac{H(\eta_L - \eta_B)}{d_T (R_B^{(0)} \eta_L - R_L^{(0)} \eta_B)}, \quad A^{(22)} = \frac{d_V (R_L^{(0)} - R_B^{(0)})}{R_B^{(0)} \eta_L - R_L^{(0)} \eta_B}, \\ V_B^{(22)} &= \frac{d_T (\frac{H}{T^{(22)} d_T} - 1 - \sigma_L) \sigma_B}{\beta_B (\sigma_B - \sigma_L)}, \quad V_L^{(22)} = \frac{d_T (\frac{H}{T^{(22)} d_T} - 1 - \sigma_B) \sigma_L}{\beta_L (\sigma_L - \sigma_B)}, \end{aligned}$$

exists in any of the following cases:

(VI-1) $\sigma_B > \sigma_L, \eta_L > \eta_B, R_L^{(0)} > R_B^{(0)}$, and

$$R_B^{(0)} \frac{\eta_L}{\eta_B} + (1 + \sigma_L) \left(1 - \frac{\eta_L}{\eta_B}\right) > R_L^{(0)} > R_B^{(0)} \frac{\eta_L}{\eta_B} + (1 + \sigma_B) \left(1 - \frac{\eta_L}{\eta_B}\right).$$

(VI-2) $\sigma_B > \sigma_L, \eta_L < \eta_B, R_L^{(0)} < R_B^{(0)}$, and

$$R_B^{(0)} \frac{\eta_L}{\eta_B} + (1 + \sigma_B) \left(1 - \frac{\eta_L}{\eta_B}\right) > R_L^{(0)} > R_B^{(0)} \frac{\eta_L}{\eta_B} + (1 + \sigma_L) \left(1 - \frac{\eta_L}{\eta_B}\right).$$

(VI-3) $\sigma_B < \sigma_L, \eta_L > \eta_B, R_L^{(0)} > R_B^{(0)}$, and

$$R_B^{(0)} \frac{\eta_L}{\eta_B} + (1 + \sigma_B) \left(1 - \frac{\eta_L}{\eta_B}\right) > R_L^{(0)} > R_B^{(0)} \frac{\eta_L}{\eta_B} + (1 + \sigma_L) \left(1 - \frac{\eta_L}{\eta_B}\right).$$

(VI-4) $\sigma_B < \sigma_L, \eta_L < \eta_B, R_L^{(0)} < R_B^{(0)}$, and

$$R_B^{(0)} \frac{\eta_L}{\eta_B} + (1 + \sigma_L) \left(1 - \frac{\eta_L}{\eta_B}\right) > R_L^{(0)} > R_B^{(0)} \frac{\eta_L}{\eta_B} + (1 + \sigma_B) \left(1 - \frac{\eta_L}{\eta_B}\right).$$

We now consider the stability of some equilibria. The following result suggests that if the basic reproductive ratios of both budding virus and lytic virus are less than one, then the population sizes of both budding virus and lytic virus will approach zero as $t \rightarrow \infty$ and the antibody cannot be established.

Theorem 2.4.1 *The equilibrium $E_0 = (H/d_T, 0, 0, 0)$ is globally asymptotically stable if $R_B^{(0)} < 1$ and $R_L^{(0)} < 1$.*

Proof First we consider local stability of the equilibrium E_0 . Linearizing the system (2.3) at equilibrium E_0 leads to

$$\begin{cases} \frac{du_1(t)}{dt} = -d_T u_1(t) - \beta_B \frac{H}{d_T} u_2(t) - \beta_L \frac{H}{d_T} u_3(t), \\ \frac{du_2(t)}{dt} = \int_{\tau_B}^{\tau^*} \gamma_B(a) e^{-\int_0^a d_{T_B}(\xi) d\xi} \beta_B \frac{H}{d_T} u_2(t-a) da - d_V u_2(t), \\ \frac{du_3(t)}{dt} = \int_{\tau_L}^{\tau^*} \gamma_L(a) e^{-\int_0^a d_{T_L}(\xi) d\xi} \beta_L \frac{H}{d_T} u_3(t-a) da - d_V u_3(t), \\ \frac{du_4(t)}{dt} = -d_A u_4(t). \end{cases} \quad (2.5)$$

The characteristic equation of this linear system is

$$J_0(\lambda) = \begin{vmatrix} \lambda + d_T & \beta_B \frac{H}{d_T} & \beta_L \frac{H}{d_T} & 0 \\ 0 & \lambda + d_V - \beta_B \frac{H}{d_T} \bar{K}_B(\lambda) & 0 & 0 \\ 0 & 0 & \lambda + d_V - \beta_L \frac{H}{d_T} \bar{K}_L(\lambda) & 0 \\ 0 & 0 & 0 & \lambda + d_A \end{vmatrix} = 0,$$

where

$$\bar{K}_B(\lambda) = \int_{\tau_B}^{\tau^*} \gamma_B(a) e^{-\left(\int_0^a d_{T_B^*}(\xi) d\xi + \lambda a\right)} da, \quad \bar{K}_L(\lambda) = \int_{\tau_L}^{\tau^*} \gamma_L(a) e^{-\left(\int_0^a d_{T_L^*}(\xi) d\xi + \lambda a\right)} da.$$

It is obvious that $\lambda_1 = -d_T < 0$ and $\lambda_2 = -d_A < 0$ are two eigenvalues and the other eigenvalues are determined by

$$\lambda + d_V = \beta_B \frac{H}{d_T} \bar{K}_B(\lambda),$$

and

$$\lambda + d_V = \beta_L \frac{H}{d_T} \bar{K}_L(\lambda),$$

which are equivalent respectively to

$$\frac{\lambda}{d_V} + 1 = R_B^{(0)} \frac{\bar{K}_B(\lambda)}{K_B}, \quad (2.6)$$

and

$$\frac{\lambda}{d_V} + 1 = R_L^{(0)} \frac{\bar{K}_L(\lambda)}{K_L}. \quad (2.7)$$

We need to show that under the conditions of the theorem, all roots of (2.6) and (2.7) have negative real parts. Let $\lambda = x + iy$ be a root of (2.6). We show that $x < 0$. Otherwise, $x \geq 0$ implies

$$|\bar{K}_B(\lambda)| \leq \int_{\tau_B}^{\tau^*} \gamma_B(a) \left| e^{-\left(\int_0^a d_{T_B^*}(\xi) d\xi + \lambda a\right)} \right| da \leq \int_{\tau_B}^{\tau^*} \gamma_B(a) e^{-\int_0^a d_{T_B^*}(\xi) d\xi} da = K_B.$$

Thus, if $R_B^{(0)} < 1$, then

$$\left| \frac{\lambda}{d_V} + 1 \right| \geq 1, \quad \left| R_B^{(0)} \frac{\bar{K}_B(\lambda)}{K_B} \right| < 1,$$

a contradiction to (2.6). Therefore, $x < 0$ under $R_B^{(0)} < 1$, implying that all roots of (2.6) have negative real parts if $R_B^{(0)} < 1$. Similarly, if $R_L^{(0)} < 1$, then all roots of (2.7) also have negative real parts. It follows from [7], that the equilibrium E_0 is locally asymptotically stable if $R_B^{(0)} < 1$ and $R_L^{(0)} < 1$.

To show that E_0 is globally asymptotically stable, it is sufficient to show that E_0 is globally attractive. By the positivity of solutions, we have

$$\begin{aligned} \frac{dT(t)}{dt} &= H - d_T T(t) - \beta_B T(t) V_B(t) - \beta_L T(t) V_L(t), \\ &\leq H - d_T T(t). \end{aligned}$$

This implies

$$\limsup_{t \rightarrow \infty} T(t) \leq \frac{H}{d_T}. \quad (2.8)$$

Denote

$$R_B^{(0)}(\varepsilon) = \frac{\beta_B(H + \varepsilon)K_B}{d_V d_T}, \quad R_L^{(0)}(\varepsilon) = \frac{\beta_L(H + \varepsilon)K_L}{d_V d_T}.$$

Let $\varepsilon > 0$ be sufficiently small such that $R_B^{(0)}(\varepsilon) < 1$ and $R_L^{(0)}(\varepsilon) < 1$. For such an $\varepsilon > 0$, by (2.8), there exists a $t^* > 0$ such that

$$T(t) \leq \frac{H + \varepsilon}{d_T}, \quad \text{for } t \geq t^*.$$

Thus,

$$\begin{aligned} \frac{dV_B(t)}{dt} &\leq \frac{H + \varepsilon}{d_T} \int_{\tau_B}^{t^*} \gamma_B(a) e^{-\int_0^a d_{T_B^*}(\xi) d\xi} \beta_B V_B(t - a) da - d_V V_B(t), \\ \frac{dV_L(t)}{dt} &\leq \frac{H + \varepsilon}{d_T} \int_{\tau_L}^{t^*} \gamma_L(a) e^{-\int_0^a d_{T_L^*}(\xi) d\xi} \beta_L V_L(t - a) da - d_V V_L(t). \end{aligned}$$

We consider the following auxiliary linear system

$$\begin{cases} \frac{dw_2(t)}{dt} = \frac{H + \varepsilon}{d_T} \int_{\tau_B}^{t^*} \gamma_B(a) e^{-\int_0^a d_{T_B^*}(\xi) d\xi} \beta_B w_2(t - a) da - d_V w_2(t), \\ \frac{dw_3(t)}{dt} = \frac{H + \varepsilon}{d_T} \int_{\tau_L}^{t^*} \gamma_L(a) e^{-\int_0^a d_{T_L^*}(\xi) d\xi} \beta_L w_3(t - a) da - d_V w_3(t). \end{cases} \quad (2.9)$$

Notice that the two equations in (2.9) are the same as the second and third equations in (2.5) except that H is replaced by $H + \varepsilon$. Thus, the characteristic equation of (2.9) is the product of two equations of the form (2.6) and (2.7) with H replaced by $H + \varepsilon$. Thus, $R_B^{(0)}(\varepsilon) < 1$ and $R_L^{(0)}(\varepsilon) < 1$ ensure that all eigenvalues of (2.9) have negative real parts, and hence, the trivial solution of (2.9) is globally (since (2.9) is linear) asymptotically stable, meaning that every solution $(w_2(t), w_3(t)) \rightarrow (0, 0)$ as $t \rightarrow \infty$. Notice that (2.9) is a co-operative delay system. By the comparison theorem ([12]), we conclude that $\lim_{t \rightarrow \infty} (V_B(t), V_L(t))^T = (0, 0)$.

Finally, the first and the last equations of (2.3) form a system which has the following autonomous system as the limit system.

$$\begin{cases} \frac{dw_1(t)}{dt} = H - d_T w_1(t), \\ \frac{dw_4(t)}{dt} = -d_A w_4(t). \end{cases}$$

Obviously, every solution of this system approaches $(H/d_T, 0)$. By the theory of asymptotically autonomous systems (see, e.g., [3]), for any positive solution $(T(t), V_B(t), V_L(t), A(t))$ of (2.3), $T(t) \rightarrow H/d_T$ and $A(t) \rightarrow 0$ as $t \rightarrow \infty$, and therefore, $(T(t), V_B(t), V_L(t), A(t)) \rightarrow (H/d_T, 0, 0, 0)$ as $t \rightarrow \infty$. That is, E_0 is globally attractive, completing the proof. \blacksquare

The following result indicates that if the basic reproductive ratio for the budding virus are greater than one and exceeds the basic reproductive ratio for the lytic virus, then the budding virus can survive when the antibody effect is not established.

Theorem 2.4.2 *Assume that $R_B^{(0)} > 1$ and $R_B^{(0)} > R_L^{(0)}$. If either (i) $p \leq \eta_B$; or (ii) $p > \eta_B$ and $R_B^{(1)} < 1$, then the equilibrium E_{10} is locally asymptotically stable. If $R_B^{(0)} < R_L^{(0)}$, or $p > \eta_B$ and $R_B^{(1)} > 1$, then this equilibrium is unstable.*

Proof Linearizing system (2.3) at equilibrium E_{10} gives

$$\begin{cases} \frac{du_1(t)}{dt} = -d_T u_1(t) - \beta_B V_B^{(10)} u_1(t) - \beta_B T^{(10)} u_2(t) - \beta_L T^{(10)} u_3(t), \\ \frac{du_2(t)}{dt} = \int_{\tau_B}^{\tau^*} \gamma_B(a) e^{-\int_0^a d_{T_B^*}(\xi) d\xi} [\beta_B V_B^{(10)} u_1(t-a) + \beta_B T^{(10)} u_2(t-a)] da - d_V u_2(t) - \eta_B V_B^{(10)} u_4(t), \\ \frac{du_3(t)}{dt} = \int_{\tau_L}^{\tau^*} \gamma_L(a) e^{-\int_0^a d_{T_L^*}(\xi) d\xi} \beta_L T^{(10)} u_3(t-a) da - d_V u_3(t), \\ \frac{du_4(t)}{dt} = (p - \eta_B) V_B^{(10)} u_4(t) - d_A u_4(t). \end{cases}$$

The characteristic equation of this linear system is

$$\begin{vmatrix} \lambda + d_T + \beta_B V_B^{(10)} & \beta_B T^{(10)} & \beta_L T^{(10)} & 0 \\ -\beta_B V_B^{(10)} \bar{K}_B(\lambda) & \lambda + d_V - \beta_B T^{(10)} \bar{K}_B(\lambda) & 0 & \eta_B V_B^{(10)} \\ 0 & 0 & \lambda + d_V - \beta_L T^{(10)} \bar{K}_L(\lambda) & 0 \\ 0 & 0 & 0 & \lambda + d_A - (p - \eta_B) V_B^{(10)} \end{vmatrix} = 0.$$

One eigenvalue is

$$\lambda_1 = -d_A + (p - \eta_B) V_B^{(10)} = \frac{d_A}{\sigma_B} (R_B^{(1)} - 1).$$

It is clear that if $p \leq \eta_B$, then $\lambda_1 < 0$. If $p > \eta_B$ but $R_B^{(1)} < 1$, we also have $\lambda_1 < 0$; and if $R_B^{(1)} > 1$, then $\lambda_1 > 0$.

The other eigenvalues are determined by

$$\lambda + d_V = \beta_L T^{(10)} \bar{K}_L(\lambda), \quad (2.10)$$

and

$$(\lambda + d_T)(\lambda + d_V) + (\lambda + d_V) \beta_B V_B^{(10)} - (\lambda + d_T) \beta_B T^{(10)} \bar{K}_B(\lambda) = 0. \quad (2.11)$$

Equation (2.10) is equivalent to

$$\frac{\lambda}{d_V} + 1 = \frac{R_L^{(0)} \bar{K}_L(\lambda)}{R_B^{(0)} K_L}. \quad (2.12)$$

By a similar argument to that in analyzing (2.6), we conclude that all roots of (2.10) have negative real parts if $R_B^{(0)} > R_L^{(0)}$. Equation (2.11) is equivalent to

$$(\lambda + d_T)(\lambda + d_V) + (\lambda + d_V)d_T(R_B^{(0)} - 1) - (\lambda + d_T)d_V \frac{\bar{K}_B(\lambda)}{K_B} = 0,$$

which can be further rewritten as

$$(\lambda + d_T R_B^{(0)}) \left(\frac{\lambda}{d_V} + 1 \right) = (\lambda + d_T) \frac{\bar{K}_B(\lambda)}{K_B}. \quad (2.13)$$

Let $\lambda = x + iy$ be a root of (2.13). If $x \geq 0$, then by $R_B^{(0)} > 1$, we have

$$|\lambda + d_T R_B^{(0)}| > |\lambda + d_T|, \quad \left| \frac{\lambda}{d_V} + 1 \right| \geq 1, \quad \left| \frac{\bar{K}_B(\lambda)}{K_B} \right| \leq 1.$$

Therefore,

$$\left| (\lambda + d_T R_B^{(0)}) \left(\frac{\lambda}{d_V} + 1 \right) \right| > \left| (\lambda + d_T) \frac{\bar{K}_B(\lambda)}{K_B} \right|.$$

This is a contradiction to equation (2.13). Therefore, if $R_B^{(0)} > 1$, then $x < 0$ for equation (2.13), implying that all roots of (2.13) have negative real parts.

In summary, we have shown that under the assumption that $R_B^{(0)} > 1$ and $R_B^{(0)} > R_L^{(0)}$, if either (i) $p < \eta_B$, or (ii) $p > \eta_B$ and $R_B^{(1)} < 1$, then all roots of the characteristic equation have negative real parts and hence equilibrium E_{10} is locally asymptotically stable.

If $p > \eta_B$ and $R_B^{(1)} > 1$, then $\lambda_1 > 0$ implying that E_{10} is unstable. For case that $R_B^{(0)} < R_L^{(0)}$, let

$$\psi(\lambda) = \frac{\lambda}{d_V} + 1 - \frac{R_L^{(0)} \bar{K}_L(\lambda)}{R_B^{(0)} K_L}.$$

Then

$$\psi(0) = 1 - \frac{R_L^{(0)}}{R_B^{(0)}} < 0.$$

On the other hand, $\psi(\lambda) \rightarrow +\infty$, as $\lambda \rightarrow +\infty$. Thus, there exists a $\lambda^* > 0$ such that $\psi(\lambda^*) = 0$, that is, (5.9) has a positive root, implying that E_{10} is unstable. The proof is completed. ■

Parallel to Theorem 3.3.2, we have the following conclusion about the lytic virus when the antibody effect against lytic virus is not established.

Theorem 2.4.3 *Assume that $R_L^{(0)} > 1$ and $R_L^{(0)} > R_B^{(0)}$. If (i) $p < \eta_L$; or (ii) $p > \eta_L$ and $R_L^{(1)} < 1$, then the equilibrium E_{01} is locally asymptotically stable. If $R_L^{(0)} < R_B^{(0)}$ or $p > \eta_L$ and $R_L^{(1)} > 1$, then this equilibrium is unstable.*

Assume that $R_B^{(0)} > 1$ and $p > \eta_B$. Then when $R_B^{(1)}$ passes the value 1, E_{10} loses its stability, giving rise to the equilibrium E_{20} . The following theorem describes the stability of E_{20} , characterizing the conditions under which the budding virus will persist in the presence of established antibody.

Theorem 2.4.4 Assume that $p > \eta_B$ and $R_B^{(1)} > 1$. If

$$R_L^{(0)} < 1 + \sigma_B + \frac{\eta_L}{\eta_B} (R_B^{(1)} - 1), \quad (2.14)$$

the equilibrium E_{20} is locally asymptotically stable; if

$$R_L^{(0)} > 1 + \sigma_B + \frac{\eta_L}{\eta_B} (R_B^{(1)} - 1), \quad (2.15)$$

this equilibrium is unstable.

Proof Firstly, note that $p > \eta_B$ and $R_B^{(1)} > 1$ imply $R_B^{(0)} > 1$. Linearizing the system (2.3) at E_{20} leads to

$$\left\{ \begin{array}{l} \frac{du_1(t)}{dt} = -d_T u_1(t) - \beta_B V_B^{(20)} u_1(t) - \beta_B T^{(20)} u_2(t) - \beta_L T^{(20)} u_3(t), \\ \frac{du_2(t)}{dt} = \int_{\tau_B}^{\tau^*} \gamma_B(a) e^{-\int_0^a d_{T_B^*}(\xi) d\xi} [\beta_B V_B^{(20)} u_1(t-a) + \beta_B T^{(20)} u_2(t-a)] da - d_V u_2(t) \\ \quad - \eta_B A^{(20)} u_2(t) - \eta_B V_B^{(20)} u_4(t), \\ \frac{du_3(t)}{dt} = \int_{\tau_L}^{\tau^*} \gamma_L(a) e^{-\int_0^a d_{T_L^*}(\xi) d\xi} \beta_L T^{(20)} u_3(t-a) da - d_V u_3(t) - \eta_L A^{(20)} u_3(t), \\ \frac{du_4(t)}{dt} = (p - \eta_B) A^{(20)} u_2(t) + (p - \eta_L) A^{(20)} u_3(t) + (p - \eta_B) V_B^{(20)} u_4(t) - d_A u_4(t). \end{array} \right.$$

The characteristic equation of this linear system is

$$J_{20}(\lambda) = \begin{vmatrix} \lambda + d_T + \beta_B V_B^{(20)} & & & \beta_B T^{(20)} \\ -\beta_B V_B^{(20)} \bar{K}_B(\lambda) & \lambda + d_V + \eta_B A^{(20)} - \beta_B T^{(20)} \bar{K}_B(\lambda) & & \\ 0 & & 0 & \\ 0 & & & -(p - \eta_B) A^{(20)} \\ & \beta_L T^{(20)} & & 0 \\ & 0 & & \eta_B V_B^{(20)} \\ \lambda + d_V + \eta_L A^{(20)} - \beta_L T^{(20)} \bar{K}_L(\lambda) & & 0 & \\ -(p - \eta_L) A^{(20)} & & \lambda + d_A - (p - \eta_B) V_B^{(20)} & \end{vmatrix} = 0.$$

The roots of this equation are determined by

$$\lambda + d_V + \eta_L A^{(20)} - \beta_L T^{(20)} \bar{K}_L(\lambda) = 0, \quad (2.16)$$

and

$$\begin{vmatrix} \lambda + d_T + \beta_B V_B^{(20)} & \beta_B T^{(20)} & 0 \\ -\beta_B V_B^{(20)} \bar{K}_B(\lambda) & \lambda + d_V + \eta_B A^{(20)} - \beta_B T^{(20)} \bar{K}_B(\lambda) & \eta_B V_B^{(20)} \\ 0 & -(p - \eta_B) A^{(20)} & \lambda + d_A - (p - \eta_B) V_B^{(20)} \end{vmatrix} = 0. \quad (2.17)$$

Equation (2.16) is equivalent to

$$\lambda + d_V + \frac{\eta_L}{\eta_B} \frac{d_V}{1 + \sigma_B} (R_B^{(1)} - 1) = R_L^{(0)} \frac{d_V}{1 + \sigma_B} \frac{\bar{K}_L(\lambda)}{K_L},$$

which can be further rewritten as

$$\frac{1 + \sigma_B}{d_V} \lambda + 1 + \sigma_B + \frac{\eta_L}{\eta_B} (R_B^{(1)} - 1) = R_L^{(0)} \frac{\bar{K}_L(\lambda)}{K_L}. \quad (2.18)$$

Let $\lambda = x + iy$ be a root of (2.18). If $x \geq 0$, then the left hand side of the equation (2.18) satisfies

$$\left| \frac{1 + \sigma_B}{d_V} \lambda + 1 + \sigma_B + \frac{\eta_L}{\eta_B} (R_B^{(1)} - 1) \right| \geq 1 + \sigma_B + \frac{\eta_L}{\eta_B} (R_B^{(1)} - 1),$$

and the right hand side of the equation satisfies

$$\left| R_L^{(0)} \frac{\bar{K}_L(\lambda)}{K_L} \right| \leq R_L^{(0)}.$$

Therefore, if (2.14) holds, then the above two inequalities contradict to each other. Thus $x < 0$ if (2.14) holds, implying that all roots of (2.18) have negative real parts.

Equation (2.17) is equivalent to

$$\begin{aligned} & \lambda \left[(\lambda + d_T) (\lambda + d_V + \eta_B A^{(20)}) + \beta_B V_B^{(20)} (\lambda + d_V + \eta_B A^{(20)}) - \beta_B T^{(20)} \bar{K}_B(\lambda) (\lambda + d_T) \right] \\ & + \eta_B V_B^{(20)} (p - \eta_B) A^{(20)} (\lambda + d_T + \beta_B V_B^{(20)}) = 0, \end{aligned}$$

which is further equivalent to

$$\left(1 + \frac{\sigma_B}{\frac{\lambda}{d_T} + 1} \right) \left(\frac{1 + \sigma_B}{d_V R_B^{(0)}} \lambda + 1 \right) + \frac{d_A}{\lambda} \left(1 - \frac{1}{R_B^{(0)}} \right) \left(1 + \frac{\sigma_B}{\frac{\lambda}{d_T} + 1} \right) = \frac{\bar{K}_B(\lambda)}{K_B}. \quad (2.19)$$

Let $\lambda = x + iy$ be a root of (2.19). If $x \geq 0$, by $R_B^{(0)} > 1$, the right hand side of the equation (2.19) satisfies

$$\left| \frac{\bar{K}_B(\lambda)}{K_B} \right| \leq 1,$$

and the left hand side of the equation satisfies

$$\begin{aligned} & \left| \left(1 + \frac{\sigma_B}{\frac{\lambda}{d_T} + 1} \right) \left(\frac{1 + \sigma_B}{d_V R_B^{(0)}} \lambda + 1 \right) + \frac{d_E}{\lambda} \left(1 - \frac{1}{R_B^{(0)}} \right) \left(1 + \frac{\sigma_B}{\frac{\lambda}{d_T} + 1} \right) \right| \\ & > \left| \left(1 + \frac{\sigma_B}{\frac{\lambda}{d_T} + 1} \right) \left(\frac{1 + \sigma_B}{d_V R_B^{(0)}} \lambda + 1 \right) \right| \\ & > 1, \end{aligned}$$

leading to a contradiction to (2.19). Thus $x < 0$, implying that all roots of (2.19) have negative real parts.

In summary, we conclude that if (2.14) holds, then the equilibrium E_{20} is locally asymptotically stable.

Let

$$\psi(\lambda) = \frac{1 + \sigma_B}{d_V} \lambda + 1 + \sigma_B + \frac{\eta_L}{\eta_B} (R_B^{(1)} - 1) - R_L^{(0)} \frac{\bar{K}_L(\lambda)}{K_L}.$$

Then $\psi(\lambda) \rightarrow \infty$ as $\lambda \rightarrow \infty$. On the other hand

$$\psi(0) = 1 + \sigma_B + \frac{\eta_L}{\eta_B} (R_B^{(1)} - 1) - R_L^{(0)} < 0,$$

provided that (2.15) holds. Therefore, there exists a $\lambda^* > 0$, such that $\psi(\lambda^*) = 0$. This means the equation (2.18) has at least one positive eigenvalue, implying that the equilibrium E_{20} is unstable. The proof of the theorem is completed. ■

Similarly, for lytic virus we have the following result when the antibody effect is established.

Theorem 2.4.5 *Assume that $p > \eta_L$ and $R_L^{(1)} > 1$. If*

$$R_B^{(0)} < 1 + \sigma_L + \frac{\eta_B}{\eta_L} (R_L^{(1)} - 1), \quad (2.20)$$

the equilibrium E_{02} is locally asymptotically stable; if

$$R_B^{(0)} > 1 + \sigma_L + \frac{\eta_B}{\eta_L} (R_L^{(1)} - 1), \quad (2.21)$$

this equilibrium is unstable.

The conditions for the existence and stability of some equilibria are summarized in Table 2.1. We see that if $p < \eta_B$ and $p < \eta_L$, there may only be three equilibria E_0 , E_{01} , and E_{10} (except the equilibrium line \hat{E}), whose stability are determined by basic reproductive ratios $R_B^{(0)}$ and $R_L^{(0)}$. If $R_B^{(0)} > 1$ and $R_B^{(0)} > R_L^{(0)}$, E_{10} is locally asymptotically stable. If $R_L^{(0)} > 1$ and $R_L^{(0)} > R_B^{(0)}$, E_{01} is locally asymptotically stable. In this case, the antibody does not play a role

in the long-term virus dynamics, this is because when p is too small ($p < \eta_B$ and $p < \eta_L$), activation of new antibodies cannot satisfy the demand on antibodies involved in neutralization of the virus for both strains. In the following discussion, we always assume that $p > \eta_B$ or $p > \eta_L$.

Table 2.1: The conditions for the existence and stability of the equilibria

Equilibrium	existence	L.A.S.
E_0	Always	$R_B^{(0)} < 1$ and $R_L^{(0)} < 1$
E_{10}	$R_B^{(0)} > 1$	$R_B^{(0)} > R_L^{(0)}$ and $\{p < \eta_B, \text{ or } p > \eta_B \text{ and } R_B^{(1)} < 1\}$
E_{01}	$R_L^{(0)} > 1$	$R_L^{(0)} > R_B^{(0)}$ and $\{p < \eta_L, \text{ or } p > \eta_L \text{ and } R_L^{(1)} < 1\}$
E_{20}	$p > \eta_B, R_B^{(1)} > 1$	$R_L^{(0)} < R_B^{(0)} \frac{\eta_L}{\eta_B} + (1 + \sigma_B)(1 - \frac{\eta_L}{\eta_B})$
E_{02}	$p > \eta_L, R_L^{(1)} > 1$	$R_L^{(0)} > R_B^{(0)} \frac{\eta_L}{\eta_B} + (1 + \sigma_L)(1 - \frac{\eta_L}{\eta_B})$

The bifurcation diagrams in different cases are given by figures from Figure 2.1 to Figure 2.3, representing the three cases $\eta_B > \eta_L$, $\eta_B = \eta_L$, $\eta_B < \eta_L$ respectively.

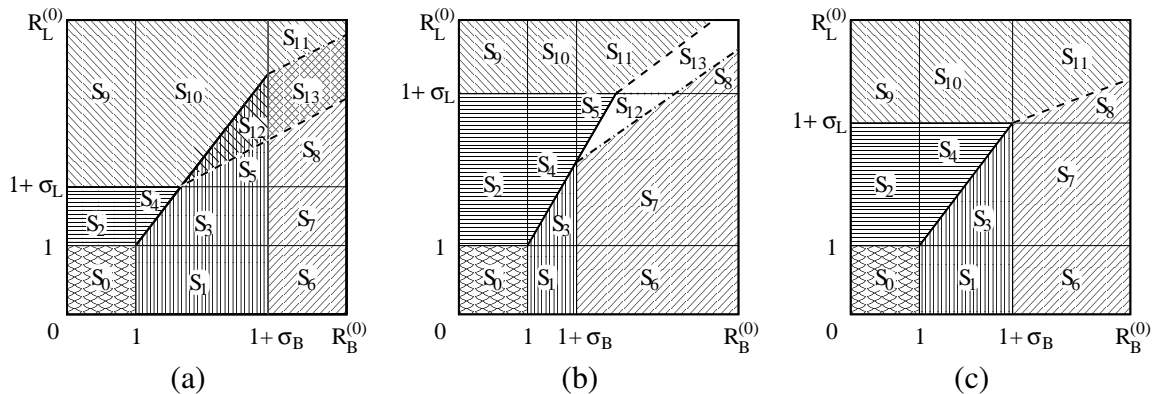


Figure 2.1: The stability regions (S_i ; $i = 1, \dots, 13$) of equilibria (E_{ij} ; $i, j = 0, 1, 2$) with respect to $R_B^{(0)}$ and $R_L^{(0)}$, when $\eta_B > \eta_L$: (a) $\sigma_B > \sigma_L$, (b) $\sigma_B < \sigma_L$, (c) $\sigma_B = \sigma_L$.

For the case $\eta_B > \eta_L$, the bifurcation diagram is shown in Figure 2.1, in which, the first quadrant of $R_B^{(0)} - R_L^{(0)}$ plane is divided into sub-regions with appropriate shadings, representing the stability of the different equilibria. The shadings are given in such a way that regions with the same shading pattern share the same stable equilibrium. For example, in Figure 2.1(a) where $\sigma_B > \sigma_L$, the stability regions of equilibria E_{ij} ($i, j = 0, 1, 2$) with respect to $R_B^{(0)}$ and $R_L^{(0)}$ are denoted by S_i ; $i = 1, \dots, 13$. Here the *solid diagonal line* is $R_L^{(0)} = R_B^{(0)}$; the *dash-dot line* is $R_L^{(0)} = R_B^{(0)} \frac{\eta_L}{\eta_B} + (1 + \sigma_B)(1 - \frac{\eta_L}{\eta_B})$; and the *dashed line* is $R_L^{(0)} = R_B^{(0)} \frac{\eta_L}{\eta_B} + (1 + \sigma_L)(1 - \frac{\eta_L}{\eta_B})$. In the regions shaded with *vertical lines* (S_1, S_3 and S_5), E_{10} is locally asymptotically; in regions shaded with *southwest-northeast lines* (S_6, S_7 and S_8), E_{20} is locally asymptotically stable. In these six regions, budding virus outcompetes. Similarly, in the regions shaded with

horizontal lines (i.e., S_2 and S_4), E_{01} is locally asymptotically stable; in the regions shaded with northwest-southeast lines (i.e., S_9 , S_{10} and S_{11}), E_{02} is locally asymptotically stable. In these five regions, lytic virus outcompetes. In the regions with overlap shadings, there are two locally asymptotically stable equilibria. For instance, in S_{13} both E_{20} and E_{02} are locally asymptotically stable; and in S_{12} , both E_{10} and E_{01} are locally asymptotically stable. In these two regions with overlap shadings (S_{12} and S_{13}), in addition to the two locally stable boundary equilibria (E_{10} and E_{01} , or E_{20} and E_{02}) there is also a positive equilibrium E_{22} whose stability is undetermined. In the region S_0 , the disease-free equilibrium E_0 is locally asymptotically stable. Table 2.2 summarizes the situations in these regions.

In Figure 2.1(b), $\sigma_B > \sigma_L$. As is shown in this figure, existence and stability of equilibria are the same as Figure 2.1(a) in all regions other than S_5 , S_{12} and S_{13} , the situation of which is shown in Table 2.3: in both regions S_{12} and S_{13} there is no stable equilibrium except the positive equilibrium E_{22} whose stability is undetermined. Figure 2.1(c) covers the case $\sigma_B = \sigma_L$. Comparing Figure 2.1(c) with Figure 2.1(a) and Figure 2.1(b), there is no region S_5 , S_{12} and S_{13} . The existence and stability of equilibria in all other regions remain the same as Figure 2.1(a) and Figure 2.1(b).

Table 2.2: Stability regions of the equilibria corresponding to Figure 2.1(a)

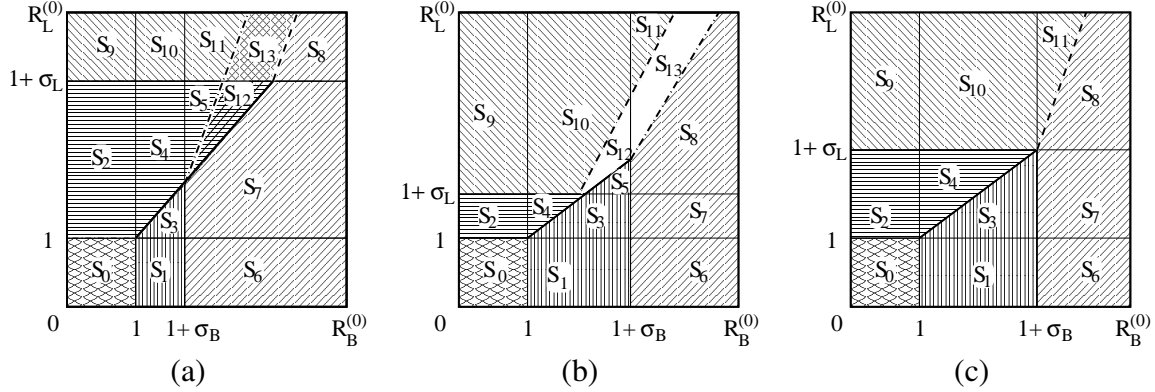
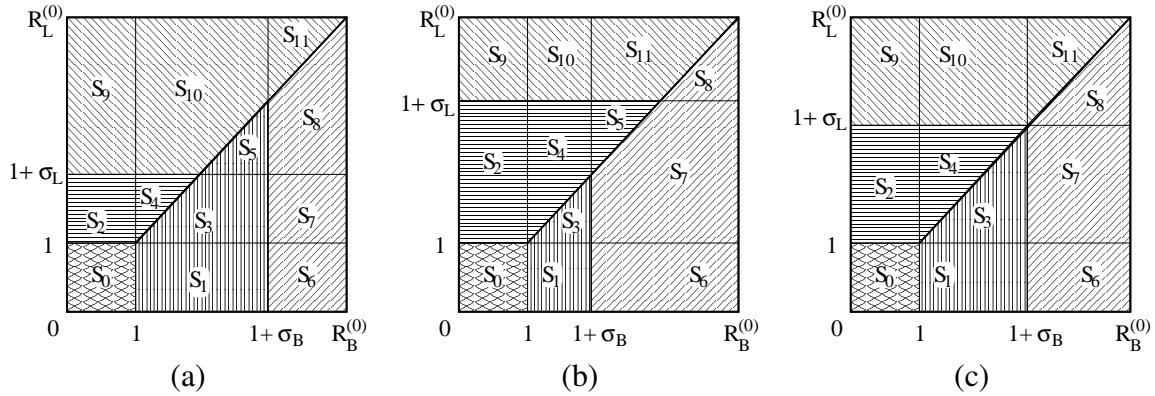
Region	existence	L.A.S.	Possibly S.
S_0	E_0	E_0	–
S_1	E_0, E_{10}	E_{10}	–
S_2	E_0, E_{01}	E_{01}	–
S_3	E_0, E_{10}, E_{01}	E_{10}	–
S_4	E_0, E_{01}, E_{10}	E_{01}	–
S_5	$E_0, E_{01}, E_{10}, E_{02}$	E_{10}	–
S_6	E_0, E_{10}, E_{20}	E_{20}	–
S_7	$E_0, E_{10}, E_{01}, E_{20}$	E_{20}	–
S_8	$E_0, E_{10}, E_{01}, E_{20}, E_{02}$	E_{20}	–
S_9	E_0, E_{01}, E_{02}	E_{02}	–
S_{10}	$E_0, E_{01}, E_{10}, E_{02}$	E_{02}	–
S_{11}	$E_0, E_{01}, E_{10}, E_{02}, E_{20}$	E_{02}	–
S_{12}	$E_0, E_{01}, E_{10}, E_{02}, E_{22}$	E_{10}, E_{02}	E_{22}
S_{13}	$E_0, E_{10}, E_{01}, E_{20}, E_{02}, E_{22}$	E_{20}, E_{02}	E_{22}

By symmetry, we have Figure 2.2 for the case $\eta_B < \eta_L$ which is parallel to Figure 2.1. Tables parallel to Table 2.2 and Table 2.3 can be drawn but are omitted here.

If $\eta_B = \eta_L$, the positive equilibrium E_{22} does not exist. Furthermore, there are no regions S_{12} and S_{13} . The properties of equilibria in all other regions are same as Figure 2.1(a) for Figure 2.3(a), Figure 2.1(b) for Figure 2.3(b), Figure 2.1(c) for Figure 2.3(c).

Table 2.3: Stability regions of the equilibria corresponding to Figure 2.1(b)

Region	existence	L.A.S.	Possibly S.
S_5	$E_0, E_{01}, E_{10}, E_{20}$	E_{01}	–
S_{12}	$E_0, E_{01}, E_{10}, E_{20}, E_{22}$	–	E_{22}
S_{13}	$E_0, E_{10}, E_{01}, E_{20}, E_{02}, E_{22}$	–	E_{22}

Figure 2.2: The stability regions of equilibria with respect to $R_B^{(0)}$ and $R_L^{(0)}$, when $\eta_B < \eta_L$: (a) $\sigma_B < \sigma_L$, (b) $\sigma_B > \sigma_L$, (c) $\sigma_B = \sigma_L$.Figure 2.3: The stability regions of equilibria with respect to $R_B^{(0)}$ and $R_L^{(0)}$, when $\eta_B = \eta_L$: (a) $\sigma_B > \sigma_L$, (b) $\sigma_B < \sigma_L$, (c) $\sigma_B = \sigma_L$.

From the above analysis, we know that if $p < \min\{\eta_B, \eta_L\}$, the antibody cannot establish and the dynamics of the model (2.3) are determined by basic reproductive ratios $R_B^{(0)}$ and $R_L^{(0)}$. If $R_B^{(0)} > \max\{1, R_L^{(0)}\}$, the budding strategy is advantageous over the lytic strategy; if $R_L^{(0)} > \max\{1, R_B^{(0)}\}$, the lytic strategy is advantageous. If $\max\{R_B^{(0)}, R_L^{(0)}\} < 1$, neither strategy will succeed since both strains will eventually go to extinction.

If $p > \eta_B$ or $p > \eta_L$, antibody may have effect on the dynamics, depending on the antibody mediated reproductive ratios $R_B^{(1)}$ and $R_L^{(1)}$. If $p > \max\{\eta_B, \eta_L\}$ and $\max\{R_B^{(1)}, R_L^{(1)}\} < 1$, the dynamical behavior of the model also only depends on the basic reproductive ratios $R_B^{(0)}$ and $R_L^{(0)}$. If $R_B^{(1)} > 1$ or $R_L^{(1)} > 1$, antibody will affect the dynamics, since there exists the stable equilibrium E_{20} or E_{02} or E_{22} .

We also see from Figure 2.3 that if the neutralizing capacities of the antibodies for budding and lytic viruses are the same (i.e., $\eta_B = \eta_L$), the evolutionary dominance of budding or lytic virus is also determined by the basic reproductive ratios $R_B^{(0)}$ and $R_L^{(0)}$, regardless of $p < \min\{\eta_B, \eta_L\}$ or $p > \min\{\eta_B, \eta_L\}$, in the sense that when $R_B^{(0)} > \max\{1, R_L^{(0)}\}$, then E_{10} or E_{20} is locally asymptotically stable, implying that budding virus can survive. Similarly, if $R_L^{(0)} > \max\{1, R_B^{(0)}\}$, then E_{01} or E_{02} is locally asymptotically stable.

2.5 Influence of antibody effect on the evolutionary competition between budding and lytic strategies

From the above results on the dynamics of the model (2.3), we see that the impact of the production/release strategies for new virions is reflected by the dependence of the reproductive ratios on K_B and K_L , the burst sizes of budding virus and lysis virus under the respective production/release strategies represented by $\gamma_B(a)$ and $\gamma_L(a)$ and the initial releasing time τ_B and τ_L . In this section, we consider two particular forms for the release strategy functions $\gamma_B(a)$ and $\gamma_L(a)$, by which we hope to obtain more information on the impact of antibody and the release strategy. To this end, we assume that the total number of virions replicated from an infected cell without considering cell death is the same for all strategies, that is,

$$\int_{\tau_B}^{\tau^*} \gamma_B(a) da = \int_{\tau_L}^{\tau^*} \gamma_L(a) da = N \quad (\text{a constant}). \quad (2.22)$$

The first possible candidate for the viral production kernel function is the one used in [10] which has the form

$$\gamma(a) = \begin{cases} m_1 (1 - e^{-m_2(a-\tau)}) & \text{if } a \geq \tau, \\ 0 & \text{if } a < \tau. \end{cases} \quad (2.23)$$

Here m_2 controls how rapidly the saturation level m_1 is reached, while $\tau \geq 0$ is the initial releasing time. For this production kernel, the constraint equation

$$\int_{\tau}^{\tau^*} \gamma(a) da \equiv N, \quad (2.24)$$

defines a trade-off relation of τ , m_1 and m_2 , which is

$$m_1 \left(\tau^* - \tau + \frac{1}{m_2} (e^{-m_2(\tau^*-\tau)} - 1) \right) = N, \quad (2.25)$$

or equivalently,

$$m_1 = \frac{Nm_2}{m_2(\tau^* - \tau) + (e^{-m_2(\tau^* - \tau)} - 1)}. \quad (2.26)$$

Figure 2.4 demonstrates the strategy function $\gamma(a)$ with $N = 100$ and $\tau = 30$ fixed and m_1 determined by the trade-off equation (2.26) for some values of m_2 and τ . As is shown in Figure 2.4, larger m_2 will make $\gamma(a)$ to approach the saturation level m_1 faster. Smaller τ represents the budding strategy and larger τ accounts for lytic strategy.

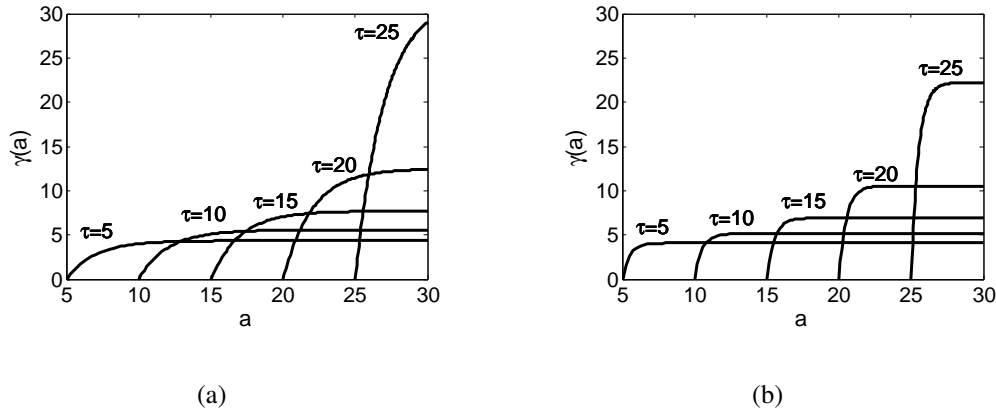


Figure 2.4: $\gamma(a)$ function given by (2.23) under the constraint (2.26), with $N = 100$, $\tau^* = 30$. $m_2 = 0.5$ in (a) and $m_2 = 2$ in (b); different curves correspond to different values of τ : $\tau = 5, 10, 15, 20, 25$. Smaller τ represents the budding virus and large τ accounts for lytic virus.

Another candidate for $\gamma(a)$ has the following form which was used in [1]:

$$\gamma(a) = \begin{cases} \frac{k_1(a - \tau)}{k_2 + (a - \tau)^2} & \text{if } a \geq \tau, \\ 0 & \text{if } a < \tau, \end{cases} \quad (2.27)$$

This function is not monotone, and it has the maximum $k_1/(2\sqrt{k_2})$ at $a = \tau + \sqrt{k_2}$. Here k_2 determines how rapidly the maximum is reached. For this function, the calculation gives

$$\int_{\tau}^{\tau^*} \gamma(a) da = \frac{k_1}{2} \ln \left(1 + \frac{(\tau^* - \tau)^2}{k_2} \right),$$

thus, the constraint (2.24) reads

$$k_1 = \frac{2N}{\ln \left(1 + \frac{(\tau^* - \tau)^2}{k_2} \right)}. \quad (2.28)$$

Similarly, Figure 2.5 shows the behavior of $\gamma(a)$ given by (2.27) for some values of the parameters. As is in Figure 2.4, we also fix $N = 100$ and $\tau = 30$. k_2 is fixed at $k_2 = 2$ in Figure 2.5(a) and at $k_2 = 20$ in Figure 2.5(b), the plots are for $\tau = 5, 10, 15, 20, 25$ respectively

with k_1 determined by (2.28). We can see from Figure 2.5 that with small k_2 , $\gamma(a)$ reaches the maximum rapidly. Furthermore, for small τ , there is a small surge in viral production with a subsequent long period of low level viral production; in contrast, for large τ , there is a big surge in viral production. Again, small τ accounts for the scenario of budding strategy while large τ explains lytic strategy.

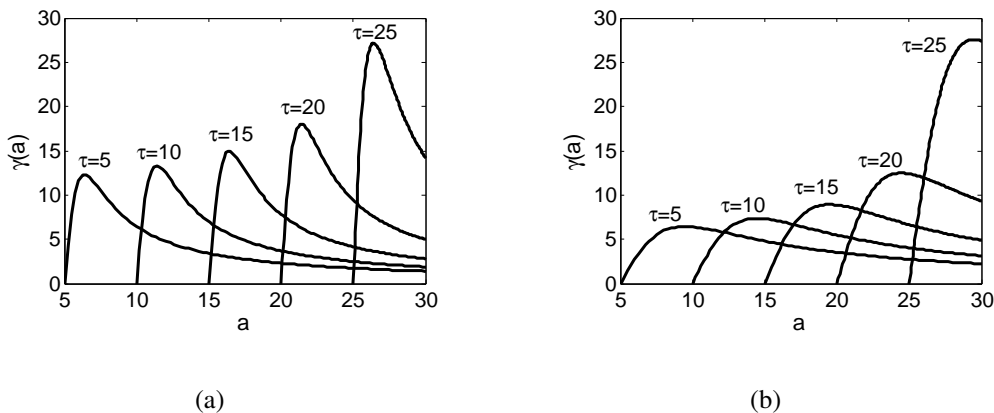


Figure 2.5: $\gamma(a)$ function given by (2.27) under the constraint (2.28) with $N = 100$ and $\tau^* = 30$ fixed. $k_2 = 2$ in (a) and $k_2 = 20$ in (b); different curves correspond to values of $\tau = 5, 10, 15, 20, 25$ respectively. Small τ accounts for budding strategy and large τ explains lytic strategy.

For the above two concrete forms of $\gamma(a)$, if we further assume that the death rate of infected cells is constant: $d_{T^*}(a) = d_{T^*}$, we can calculate the total number of new virions produced/released by an infected cell under the strategy $\gamma(a)$ as

$$K(\tau) = \frac{Nm_2 \left[m_2 \left(e^{-d_{T^*}\tau} - e^{-d_{T^*}\tau^*} \right) - d_{T^*} e^{-d_{T^*}\tau^*} + d_{T^*} e^{-m_2(\tau^*-\tau) - d_{T^*}\tau^*} \right]}{d_{T^*}(m_2 + d_{T^*}) \left[m_2(\tau^* - \tau) + e^{-m_2(\tau^*-\tau)} - 1 \right]}, \quad (2.29)$$

for $\gamma(a)$ given by (2.23), and

$$K(\tau) = \frac{2Ne^{-d_{T^*}\tau} \int_0^{\tau^*-\tau} \frac{a}{k_2+a^2} e^{-d_{T^*}a} da}{\ln \left(1 + \frac{(\tau^*-\tau)^2}{k_2} \right)}, \quad (2.30)$$

for $\gamma(a)$ given by (2.27). One can explore the dependence of $K(\tau)$ on τ , as well as on m_2 and k_1 , to obtain more information. For example, numeric plotting shows that these two functions are both decreasing in τ (see Figure 2.6).

When $d_{T^*}(a)$ is not constant, it is generally difficult to obtain an explicit formula for K , but numerical calculation can still give some information. To illustrate this, we consider the

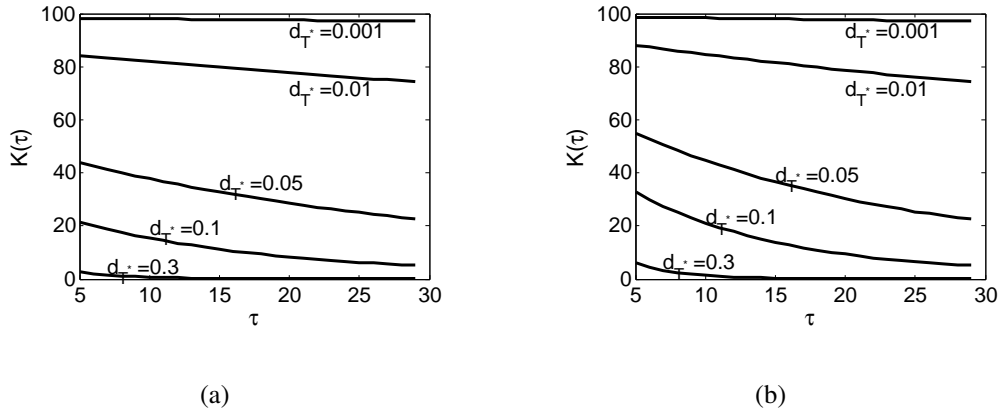


Figure 2.6: Burst size $K(\tau)$, with viral production kernel $\gamma(a)$ given by (2.23) in (a) and $\gamma(a)$ given by (2.27) in (b). $N = 100$, $\tau^* = 30$, $k_2 = 2$ and $m_2 = 2$ are fixed and d_{T^*} taking different values.

following death rate function proposed in [10]:

$$d_{T^*}(a) = \begin{cases} \delta_0 & a < \tau_0, \\ \delta_0 + \delta_1 (1 - e^{-\delta_2(a-\tau_0)}) & a \geq \tau_0, \end{cases} \quad (2.31)$$

where δ_0 is the background death rate, τ_0 is the delay between infection and the onset of cell-mediated killing or the beginning of cell death due to the viral cytopathic effects, $\delta_0 + \delta_1$ is the maximal death rate and δ_2 controls how quickly it approaches the saturation level. Figure 2.7 shows some plots of this function for some parameter values.

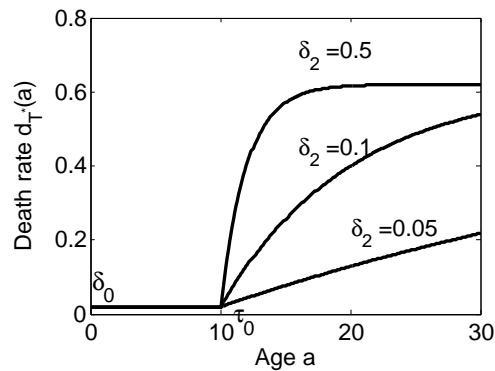


Figure 2.7: The death rate function $d_{T^*}(a)$ of infected cells when $\delta_0 = 0.02$, $\delta_1 = 0.6$, and $\tau_0 = 5$ are fixed and δ_2 taking 0.02, 0.1 and 0.5 respectively.

For this death function, if $\tau_0 \leq \tau$, the burst size reads

$$K(\tau) := \int_{\tau}^{\tau^*} \gamma(a) e^{-\int_0^a d_{T^*}(\xi) d\xi} da = e^{\delta_1 \tau_0 + \frac{\delta_1}{\delta_2}} \int_{\tau}^{\tau^*} \gamma(a) e^{-\left[(\delta_0 + \delta_1)a + \frac{\delta_1}{\delta_2} e^{-\delta_2(a-\tau_0)}\right]} da; \quad (2.32)$$

if $\tau_0 > \tau$,

$$K(\tau) = \int_{\tau}^{\tau_0} \gamma(a) e^{-\delta_0 a} da + e^{\delta_1 \tau_0 + \frac{\delta_1}{\delta_2}} \int_{\tau_0}^{\tau^*} \gamma(a) e^{-\left[(\delta_0 + \delta_1)a + \frac{\delta_1}{\delta_2} e^{-\delta_2(a-\tau_0)}\right]} da. \quad (2.33)$$

Numeric plots in Figure 2.8 and Figure 2.9 also show how the values of τ and δ_2 affect $K(\tau)$, e.g., $K(\tau)$ is indeed decreasing in both τ and δ_2 .

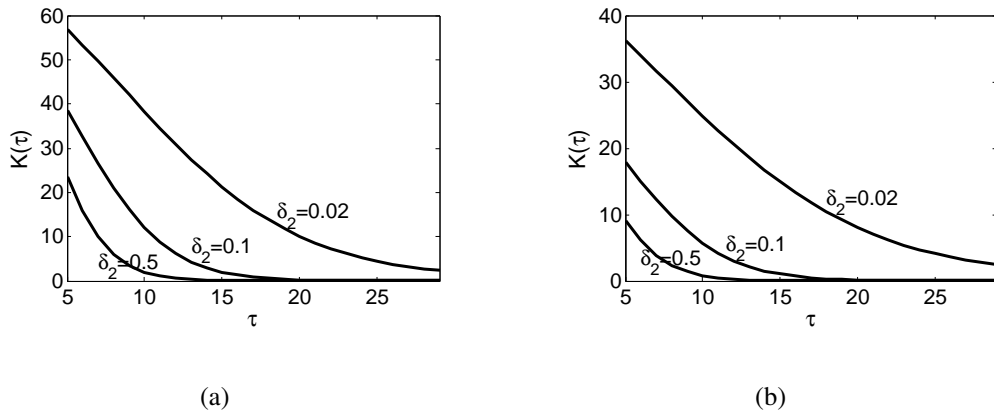


Figure 2.8: The burst size $K(\tau)$ when death rate function is given by (2.31): (a) with viral production kernel (2.23); (b) with viral production kernel (2.27). $N = 100$, $\tau^* = 30$, $k_2 = 2$ and $\tau_0 = 5$.

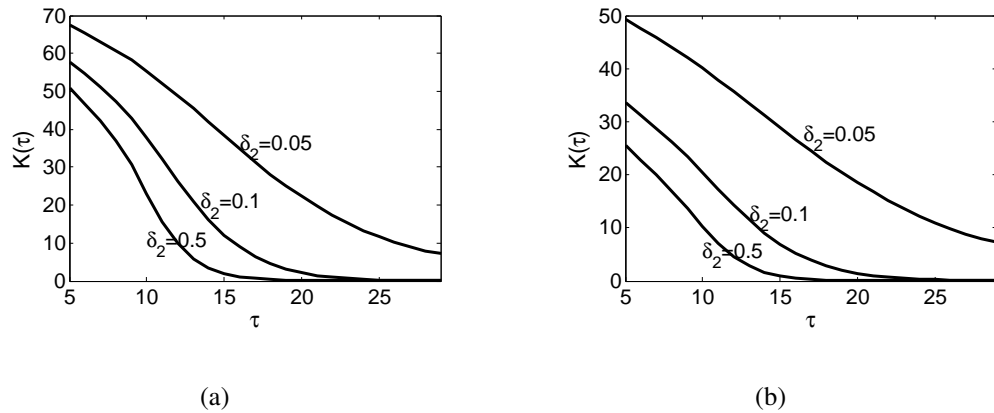


Figure 2.9: The burst sizes, $K(\tau)$, with (a) viral production kernel (2.23), (b) viral production kernel (2.27), are decreasing functions of τ . When $N = 100$, $\tau^* = 30$, $k_2 = 2$, $\tau_0 = 10$. and death rate function (2.31).

The above framework enables us to compare the burst sizes K_B and K_L when the strategies $\gamma_B(a)$ and $\gamma_L(a)$ have the same form of either (2.23) or (2.27). For example, suppose

$$\gamma_B(a) = \begin{cases} m_1 (1 - e^{-m_2(a-\tau_B)}) & \text{if } a \geq \tau_B, \\ 0 & \text{if } a < \tau_B; \end{cases} \quad \gamma_L(a) = \begin{cases} m_1 (1 - e^{-m_2(a-\tau_L)}) & \text{if } a \geq \tau_L, \\ 0 & \text{if } a < \tau_L, \end{cases} \quad (2.34)$$

where $\tau_B < \tau_L$. If the infected cells have the same death rate for both virus, i.e., $d_{T_B^*}(a) = d_{T_L^*}(a)$, then

$$\int_{\tau_B}^{\tau^*} \gamma_B(a) e^{-\int_0^a d_{T_B^*}(\xi) d\xi} da > \int_{\tau_L}^{\tau^*} \gamma_L(a) e^{-\int_0^a d_{T_L^*}(\xi) d\xi} da \quad (2.35)$$

that is, $K_B > K_L$. If we further assume that the budding virus and lytic virus have the same infection rate, $\beta_B = \beta_L$, then $R_B^{(0)} > R_L^{(0)}$ holds, implying that the budding strategy would have evolutionary advantage and would be favored. If the neutralization capacity of the antibodies against budding virus is larger than that of lytic virus, $\eta_B > \eta_L$, then $\sigma_B > \sigma_L$ assuming also that $\beta_B = \beta_L$.

From the bifurcation diagram Figure 2.1 and Table 2.2, we see that lytic virus can survive if the basic reproductive ratio satisfies

$$R_L^{(0)} > \max \left\{ 1, \min \left\{ R_B^{(0)}, R_B^{(0)} \frac{\eta_L}{\eta_B} + (1 + \sigma_B) \left(1 - \frac{\eta_L}{\eta_B} \right) \right\} \right\}.$$

Similarly, budding virus can survive if

$$R_B^{(0)} > \max \left\{ 1, \min \left\{ R_L^{(0)}, R_L^{(0)} \frac{\eta_B}{\eta_L} + (1 + \sigma_L) \left(1 - \frac{\eta_B}{\eta_L} \right) \right\} \right\}.$$

Both viruses can survive, if $R_L^{(0)} < R_B^{(0)}$ and

$$R_B^{(0)} \frac{\eta_L}{\eta_B} + (1 + \sigma_L) \left(1 - \frac{\eta_L}{\eta_B} \right) < R_L^{(0)} < R_B^{(0)} \frac{\eta_L}{\eta_B} + (1 + \sigma_B) \left(1 - \frac{\eta_L}{\eta_B} \right).$$

With the assumption that $d_{T_B^*} = d_{T_L^*}$ and (2.22), we also have (2.35) and further, $R_B^{(0)} > R_L^{(0)}$ if $\beta_B = \beta_L$. Moreover, from Figure 2.1, we see that lytic virus should have very high basic reproductive ratio in order to survive, say $R_L^{(0)} > (1 + \sigma_B) \left(1 + \frac{\eta_L}{\eta_B} \right) + \frac{\eta_L}{\eta_B} R_B^{(0)}$ (the equilibrium E_{02} is stable, in region S_{11} where $R_B^{(0)} > R_L^{(0)}$). From Figure 2.2, we know that if $\eta_L > \eta_B$, the lytic virus cannot survive, since $R_B^{(0)} > R_L^{(0)}$ (both E_{10}, E_{20} are unstable).

We see that if the neutralization capacities of antibodies against budding and lytic virus are different, the dynamical behavior is not only determined by the basic reproductive ratios $R_B^{(0)}$ and $R_L^{(0)}$, but also by other parameters measuring antibody effects, such as η_B, η_L, σ_B and σ_L .

2.6 Discussion and Conclusion

In this chapter, proposed and analyzed is a mathematical model with distributed delays that describes the competition of budding and lytic virus within a host. Budding virus is featured by a longer release period of new virions, while lytic virus is characterized by a long accumulation period but a shorter release period of new virions. These motivate us to use the infection age a and an age structured model to govern the populations of the target cell and virus. Two viral release strategies are distinguished by two beginning ages of viral release, τ_B for budding and τ_L for lytic, as well as by two viral production functions, γ_B and γ_L .

We have analyzed the dynamical behavior of the model (2.3). More specifically, we studied the global asymptotical stability of the infection free equilibrium E_0 ; and we have also established local asymptotical stability of E_{01} , E_{10} , E_{02} and E_{20} which accounting for a scenario that among the two viruses, only one can survive within the host. The local stability depends on $R_B^{(0)}$ and $R_L^{(0)}$, the respective basic reproductive ratios in the absence of antibody, and on $R_B^{(1)}$ and $R_L^{(1)}$ which are the respective reproductive ratios in the presence of antibody. If $p < \eta_B$ and $p < \eta_L$, there are only three equilibrium E_0 , E_{01} , and E_{10} (except the equilibrium line \hat{E}), whose stability are determined by basic reproductive ratios $R_B^{(0)}$ and $R_L^{(0)}$. If $R_B^{(0)} < 1$ and $R_L^{(0)} < 1$, E_0 is locally asymptotically stable; if $R_B^{(0)} > 1$ and $R_B^{(0)} > R_L^{(0)}$, E_{10} is locally asymptotically stable; if $R_L^{(0)} > 1$ and $R_L^{(0)} > R_B^{(0)}$, E_{01} is locally asymptotically stable. In this case, the antibody does not have any effect on the long-term dynamics. However, when $p > \eta_B$ and/or $p > \eta_L$, the antibody will have effect on the dynamical behavior of the model. If $\eta_B = \eta_L$, that is, the neutralization capacity of antibody is the same for both budding and lytic viruses, then, whether the budding virus or the lytic virus can survive depends on the basic reproductive ratios $R_B^{(0)}$ and $R_L^{(0)}$ (see Figure 2.3). Yet, if $\eta_B > \eta_L$ or $\eta_B < \eta_L$, the positive equilibrium occurs in some regions in the $R_B^{(0)}$ - $R_L^{(0)}$ plane. Bistability may arise in these regions. For example, in Figure 2.1, in region S_{12} , both E_{10} and E_{02} are locally stable; and in region S_{13} , both E_{02} and E_{20} are locally stable.

We have considered two concrete forms of functions for the viral production kernel, as a function of the infection age. To study the evolutionary competition of budding and lysis strategies, we assume that the total amount of virions replicated during the lifespan of infected cell is the same for both strains, without considering the release procedure and cell death. Under such a circumstance, the burst size of the budding virus is greater than that of the lytic virus (i.e., $K_B > K_L$) provided that $d_{T_B^*} = d_{T_L^*}$. If the budding virus and lytic virus have a same infection rate, $\beta_B = \beta_L$, then $R_B^{(0)} > R_L^{(0)}$ always holds. This means that if the rate of viral production, the infected cell lifespan and neutralizing capacity of the antibodies were the same for the budding and lytic viruses, the budding virus would outcompete the lytic virus. In this case, budding strategy would have evolutionary advantage. If the neutralization capacities of

the antibodies against the budding virus and lytic virus are different, then the lytic virus can survive as long as the reproductive ratio $R_L^{(0)}$ is very high.

Using a diffusion model for virus and antibody, Komarova [8] observed that if the production rate of the virions and the efficacy of the antibodies were the *same* for a budding and a lytic virus, the lytic virus would always be significantly less efficient in spreading, and thus the lytic strategy would be evolutionary disadvantageous. Lytic virus can be competitive against budding virus if the antibodies are less effective against lytic virions than they are against budding virions. This is because the effect of *antibody flooding* increases the rate of spread of lytic virions. In this work, we do not consider the diffusion effect of antibodies; instead, we use an ordinary differential equation model with distributed delays accounting for the release strategies. Our model can also predict a possibility that lytic virus may have evolutionary advantage when the efficacies of antibodies are different for the two viruses. Thus this work offers an alternative view point for the scenario that a lytic virus can also outcompete budding virus under certain circumstances.

Bibliography

- [1] Brännström A. and Sumpter D.J.T., The role of competition and clustering in population dynamics, *Proc. R. Soc. B.*, 272 (2005) 2065-2072.
- [2] Carter J. and Saunders V., *Virology: principles and application*, John Wiley and Sons, Ltd, 2007.
- [3] Castillo-Chaves C. and Thieme H. R., Asymptotically autonomous epidemic models, In: *Mathematical population dynamics: analysis of heterogeneity, I. Theory of epidemics* (eds. Arino O. *et al.*), Wuerz, Winnipeg, 1995, pp 33-50.
- [4] Coombs D., Optimal viral production, *Bull. Math. Biol.*, 65 (2003) 1003-1023.
- [5] Garoff H., Hewson R. and Opstelten D., Virus maturation by budding, *Microbiology and Molecular Biology Reviews*, Vol.62 No.4 (1998) 1171-1190.
- [6] Gilchrist M.A., Coombs D. and Perelson A.S., Optimizing within-host viral fitness: infected cell lifespan and virion production rate, *J. Theor. Biol.*, 229 (2004) 281-288.
- [7] Hale J.K. and Verduyn Lunel S.M., *Introduction to functional differential equations*, Springer-Verlag, New York, 1993.
- [8] Komarava N.L., Viral reproductive strategies: how can lytic viruses be evolutionarily competitive? *J. Theor. Biol.*, 249 (2007) 766-784.
- [9] Nayak D.P., Assembly and budding of influenza virus, *Virus Research*, 106 (2004) 147-165.
- [10] Nelson P.W., Gilchrist M.A., Coombs D., Hyman J.M. and Perelson A.S., An age-structured model of HIV infection that allows for variation in the production rate of viral particles and the death rate of productively infected cells, *Math. Biosci. Eng.*, Vol.1 No.2 (2004) 267-288.

- [11] Rong L., Feng Z. and Perelson A.S., Mathematical analysis of age-structured HIV-1 dynamics with combination antiretroviral therapy, *J. Appl. Math.*, Vol.67 No.3 (2007) 731-756.
- [12] Smith, H.L., *Monotone dynamical systems—An introduction to the theory of competitive and cooperative systems*, Vol. 41, AMS, Providence, 1995.
- [13] Wang I.N., Dykhuizen D.E. and Slobodkin, L.B., The evolution of phage lysis timing, *Evolutionary Ecology*, 10 (1996) 545-558.
- [14] Wang I.N., Lysis timing and bacteriophage fitness, *Genetics*, 172 (2006) 17-26.

Chapter 3

Modeling HIV-1 virus dynamics with both virus-to-cell infection and cell-to-cell transmission

3.1 Introduction

It is known that the primary target cell for Human Immunodeficiency Virus Type 1 (HIV-1) infection is the CD4⁺T cell. For decades it was believed that the spreading of HIV-1 within a host was mainly through free circulation of the viral particles, with a repeated process consisting of attachment of viruses to T cells, fusion of viruses into the T cells, replication and assembling of viruses inside the infected T cells, release of newly produced viral particles from the infected cells, and diffusion of the released viral particles to catch other T cells. However, recent studies have revealed that a large amount of viral particles can also be transferred from infected cells to uninfected cells through the formation of virally induced structures termed virological synapses [14].

Indeed, the direct cell-to-cell transmission of HIV-1 is found to be a more potent and efficient means of virus propagation than the virus-to-cell infection mechanism. Cell-to-cell spread not only facilitates rapid viral dissemination, but may also promote immune invasion and thereby, influence the disease [24]. Cell-to-cell spread of HIV-1 may reduce the effectiveness of neutralizing antibodies and viral inhibitors. However, it is unclear whether this mechanism of HIV-1 viral spread is susceptible or resistant to inhibition (by neutralizing antibodies) and to entry inhibition, causing some controversies in this field of studies [3, 25]. Despite these controversies, it is commonly agreed that the high efficiency of infection by large numbers of virions is likely to result in a transfer of multiple virions to a target cell [7, 15]. In particular, a

recent study published in Nature [39] shows that cell-to-cell spread of HIV-1 does reduce the efficacy of *antiretroviral therapy*, because cell-to-cell infection can cause multiple infections of target cells, which can in turn reduce the sensitivity to the antiretroviral drugs.

While HIV-1 can pass directly from an infected T cell to an uninfected and receptor-bearing T cell via virological synapses or membrane nanotubes, many other viruses also have some mechanisms to support their cell-to-cell transmissions [35, 36, 37]. For example, murine leukemia virus (MLV) moves between fibroblasts either by polarized assembly and budding at intact intercellular junctions [28] or by crossing adhesive bridges formed by filopodia [38]. Herpes simplex virus type-1 (HSV-1) can spread between a fibroblast and a T cell via a virological synapse while it can also move between fibroblasts by assembly and budding at basolateral intercellular junctions [37]. In fact, the cell-to-cell spread mode has been adopted by a variety of animal virus families, including *Asfar*, *Flavi*, *Herpes*, *Paramyxo*, *Pox*, *Rhabdo*, and *Retroviridae*.

To compare the two transmission modes, Dimitrov *et al.* [8] studied the kinetics of HIV-1 accumulation in cell culture supernatants during multiple rounds of infections by viral production models. They found that the infection rate constant is the critical parameter that affects the kinetics of HIV-1 infection, and furthermore the infectivity of HIV-1 during cell-to-cell transmission is greater than the infectivity of cell-free viruses. Dixit and Perelson [9] studied the kinetics of HIV-1 infection by exploring the mechanisms of multiple infections. They found that multiple infections can be caused by both cell-free infection mode and cell-to-cell transmission mode. In cell-to-cell transfer mode, by contact of a target cell, an infectious cell can transfer multiple virions or genomes. However, in cell-free mode, multiple genomes are acquired one by one in a series of infectious contacts of a target cell with free virions.

Dynamical system models have been widely and effectively used to model viral infection dynamics. Most existing models only considered virus-to-cell infection mechanism. Among such models is the following classic and basic model proposed in [1, 30, 31, 32] which describes the virus dynamics within a host by a system of ordinary differential equations:

$$\begin{cases} \frac{dT(t)}{dt} = h - d_T T(t) - \beta V(t)T(t), \\ \frac{dT^*(t)}{dt} = \beta V(t)T(t) - \delta T^*(t), \\ \frac{dV(t)}{dt} = bT^*(t) - cV(t), \end{cases} \quad (3.1)$$

where $T(t)$, $T^*(t)$ and $V(t)$ are the concentrations of uninfected T cells, infected T cells, and free viral particles at time t respectively. The model assumes that uninfected T cells are produced at a constant rate h , infected by free virions at a rate $\beta V(t)T(t)$. The free virions are produced from the infected cells at a rate $bT^*(t)$. Uninfected T cells, infected T cells and free virions

are lost at rates $d_T T(t)$, $\delta T^*(t)$ and $cV(t)$ respectively. For this model, the virus dynamics are fully determined by an important parameter, called the basic reproduction number and given by $\mathcal{R}_0 = \beta hb/c\delta d_T$, in the following sense: if $\mathcal{R}_0 < 1$, then $V(t) \rightarrow 0$ and $T^*(t) \rightarrow 0$ as $t \rightarrow \infty$ implying infection cannot persist; while if $\mathcal{R}_0 > 1$ the virus will persist in the host [22].

Based on (3.1), there have been a variety of modifications/generalizations of (3.1) resulted from incorporating into (3.1) various factors/effects, such as immune responses (CTLs), non-linear infection rate, latencies in virus infection and replications, and drug therapies etc. For details see, e.g., [17, 29, 41, 42, 43, 44, 45] and the references cited therein. Among these generalizations is the following model proposed and studied by Nelson and Perelson [29]:

$$\begin{cases} \frac{dT}{dt} = h - d_T T - (1 - n_{rt})\beta V_I T, \\ \frac{dT^*}{dt} = \int_0^\infty f(s)e^{-\mu s}(1 - n_{rt})\beta V_I(t-s)T(t-s)d\tau - \delta T^*, \\ \frac{dV_I}{dt} = (1 - n_p)N\delta T^* - cV_I, \\ \frac{dV_{NI}}{dt} = n_p N\delta T^* - cV_{NI}, \end{cases} \quad (3.2)$$

where n_{rt} and n_p are the efficacy of reverse transcriptase (RT) inhibitor and protease inhibitor respectively, and V_I and V_{NI} are the populations of infectious and non-infectious virions respectively. Here, a time delay, s , from the time of initial infection until the production of new virions, is considered, and assumed to vary according to a probability distribution $f(s)$. The term e^{-ms} accounts for the survive rates of cells that are infected at time t and becoming productively infected s time units later. Note that the V_{NI} equation in (3.2) is decoupled from the other three equations which, by renaming the parameters, constitute the model system of the form investigated in Zhu and Zou[44]. We point out that, as in (3.1), all those variations in [17, 29, 41, 42, 43, 44, 45] have assumed that uninfected T cells can only be infected by the attachment of free virions, while the mechanism of cell-to-cell transmission has been neglected.

As far as cell-to-cell infection is concerned, much less has been done in mathematical modeling. Culshaw *et al.* [4] studied the cell-to-cell spread of HIV-1 by the model

$$\begin{cases} \frac{dT}{dt} = rT(t)\left(1 - \frac{T(t)+T^*(t)}{K}\right) - \beta T(t)T^*(t), \\ \frac{dT^*}{dt} = \beta' \int_{-\infty}^t T(s)T^*(s)f(t-s)e^{-ms}ds - \delta T^*(t). \end{cases} \quad (3.3)$$

Here, a logistic growth for the uninfected cells is assumed with r being the intrinsic growth rate of uninfected cells, and K being the effective carrying capacity of the host. Assuming that $f(u)$ is a probability distribution, the integral in (3.3) reflects the variance of productivity of virions by infected cells at different infection ages. We see that in this model, only cell-

to-cell infection is considered (at rate $\beta T(t)T^*(t)$), while virus-to-cell infection mechanism is neglected, in contrast to (3.1) and its variations/modifications.

Recently, Komarova *et al.* [18] studied the relative contribution of free-virus and synaptic transmission to the spread of HIV-1 using a dynamical system model. With data fitting they determined that the two transmission pathways contribute approximately equally to the growth of the virus population. Komarova *et al.* [19, 20] further investigated the effect of synaptic transmission on virus dynamics and viral fitness in HIV infection. More specifically, using dynamical system models, they discussed the cell-to-cell transmission in different contexts such as multiple infection and different viral synaptic strategies, and explored the effect of different strategies of the virus on the basic reproductive ratio of the virus. In a more recent chapter [21], using a virus infection dynamical model with multiple infections, Komarova *et al.* explored the role of synaptic transmission in susceptibility of HIV infection to antiretroviral drugs. They found that multiple infection via synapses does not simply reduce susceptibility to treatment, which depends on the relative probability of individual virions to infect a cell during cell-free virus and synaptic transmission.

In this chapter, we propose a dynamical system model that incorporates both cell-to-cell infection mechanism and virus-to-cell infection mode. As in [4, 29, 44], we also consider infection age. But we will adopt the simpler production mechanism for uninfected cells as in (3.1) and (3.2). We also consider a well-mixed situation and no multiple infection for both modes of transmission. All these considerations lead to the following model:

$$\begin{cases} \frac{dT(t)}{dt} = h - d_T T(t) - \beta_1 T(t)V(t) - \beta_2 T(t)T^*(t), \\ \frac{dT^*(t)}{dt} = \int_0^\infty [\beta_1 T(t-s)V(t-s) + \beta_2 T(t-s)T^*(t-s)]e^{-\mu s} f(s) ds - \delta T^*(t), \\ \frac{dV(t)}{dt} = bT^*(t) - cV(t), \end{cases} \quad (3.4)$$

where β_1 is the infection rate of free virus, β_2 is the infection rate of productively infected cells. The infected cells may die or be cleared at rate μ before becoming productively infected, and thus, after a time period of length s , only a proportion $e^{-\mu s}$ survives. The time for infected cells to become productively infected may vary from individuals to individuals, and hence, a distribution function $f(s)$ is introduced to account such variance. For mathematical tractability, yet without losing the major biological feature, we assume that $f : [0, \infty) \rightarrow [0, \infty)$ has compact support, $f(s) \geq 0$ and $\int_0^\infty f(s) ds = 1$. Other parameters in (3.4) are as in (3.1) and are self-explanatory.

In the rest of this chapter, we will analyze the model (3.4). In Section 2, we address the well-posedness of (3.4) by verifying the positivity and boundedness of solutions of system (3.4) with reasonable initial data. In Section 3, we identify the basic reproduction number \mathcal{R}_0

of the model, in terms of which we discuss local stability of the infection-free equilibrium and the positive equilibrium. In Section 4, we prove the persistence of infection under $\mathcal{R}_0 > 1$, and in Section 5, we further explore the global stability of the two equilibria. Our theoretical results show that the virus dynamics governed by (3.4) are fully determined by \mathcal{R}_0 . Thus, the dependence of \mathcal{R}_0 on the model's parameters may reveal some insights on the virus spread in the presence of both infection modes, and we discuss this in Section 5.

We conclude this introduction by pointing out the main difference of this work from [18, 19, 20, 21]. The dynamical system models in [18, 19, 20, 21] are all given by ordinary differential equations. Such ODE models have neglected the effect of infection ages which correspond to various stages during the complicated process of virus replication (see, e.g., [4, 29, 44]), and the survival rate of infected cells before they become productive. Our model (3.4) incorporates not only both cell-to-cell infection mechanism and virus-to-cell infection mode, but also an infinite intracellular delay which reflects the fact that an infected cell may remain latent forever. Moreover, in this work, in addition to the derivation of the basic reproduction number, the global dynamics of the model are completely and analytically obtained.

3.2 Positivity and boundedness of solutions

The model (3.4) is a system of integro-differential equations with infinite delays. For such a system, the phase space needs to be equipped with some norm that accounts for fading memory. In other words, we need to specify a continuous and non-decreasing function $g : (-\infty, 0) \rightarrow [1, \infty)$ satisfying (i) $g(0) = 1$; (ii) $g(s+t)/g(s) \rightarrow 1$ uniformly on $(-\infty, 0]$ as $t \rightarrow 0^-$; and (iii) $g(s) \rightarrow \infty$ as $s \rightarrow -\infty$. For details on this topic, see, e.g., [10, 13, 23]. For the purpose of this chapter, we choose $g(s) = e^{-\Delta s}$ with $\Delta \in (0, \mu/2)$. Accordingly, the phase space is given by

$$C_\Delta := \left\{ \phi \in C((-\infty, 0], \mathbb{R}) : \begin{array}{l} \phi(\theta)e^{\Delta\theta} \text{ is uniformly continuous on } (-\infty, 0] \\ \text{and } \sup_{\theta \leq 0} \{|\phi(\theta)|e^{\Delta\theta}\} < \infty \end{array} \right\}, \quad (3.5)$$

equipped with the norm $\|\phi\| = \sup_{\theta \leq 0} \{|\phi(\theta)|e^{\Delta\theta}\}$.

For a given function $u(t) = (x(t), y(t), z(t)) : (\infty, \tau] \rightarrow \mathbb{R}^3$ ($\tau > 0$), we follow the standard notation to define $u_t \in C_\Delta \times C_\Delta \times C_\Delta$ by $u_t(\theta) = (x_t(\theta), y_t(\theta), z_t(\theta)) = u(t + \theta) = (x(t + \theta), y(t + \theta), z(t + \theta))$ respectively for $\theta \in (-\infty, 0]$. By the fundamental theory of functional differential equations [10, 13, 23], we know that for any initial function $\phi \in C_\Delta \times C_\Delta \times C_\Delta$, (3.4) has a unique solution $(T(t), T^*(t), V(t))$ satisfying $(T_0, T_0^*, V_0) = \phi$.

The fact that all unknown variables in the model are populations suggests that we only need to consider non-negative initial functions, i.e, initial functions taken from the natural positive

cone of this phase space given by $X := C_{\Delta}^+ \times C_{\Delta}^+ \times C_{\Delta}^+$ where $C_{\Delta}^+ = \{\phi \in C_{\Delta} : \phi(\theta) \geq 0, \text{ for } \theta \in (-\infty, 0]\}$.

For an initial function $\phi = (\phi_1, \phi_2, \phi_3) \in X$, if $\phi_2(\theta) = 0 = \phi_3(\theta)$ for all $\theta \in (-\infty, 0]$, (i.e, there is no initial inoculation/invasion of both viruses and infectious cells), one easily sees (e.g., by uniqueness of solution) that the $T^*(t)$ and $V(t)$ components of the corresponding solution remain zero for all $t \geq 0$. However if either $\phi_2(\theta) > 0$ or $\phi_3(\theta) > 0$ for some $\theta \in (-\infty, 0]$, these two components of the corresponding solution should remain positive for all $t > 0$. It is also reasonable to expect that a solution should remain bounded. The following theorem establishes these properties of well-posedness for the model (3.4).

Theorem 3.2.1 *Let $(T(t), T^*(t), V(t))$ be the solution of the system (3.4) with initial conditions*

$$\phi \in X^0 := \{\phi = (\phi_1, \phi_2, \phi_3) \in X : \text{either } \phi_2(\theta) > 0 \text{ or } \phi_3(\theta) > 0 \text{ for some } \theta \in (-\infty, 0]\}. \quad (3.6)$$

Then $T(t)$, $T^(t)$ and $V(t)$ are all positive and bounded for $t > 0$.*

Proof. Let $a(t) = d_T + \beta_1 T^*(t) + \beta_2 V(t)$. From the first equation in (3.4), we then have

$$T(t) = e^{\int_0^t a(\xi) d\xi} T(0) + \int_0^t e^{\int_{\xi}^t a(\theta) d\theta} h d\xi > 0 \text{ for } t \geq 0.$$

Next, we prove the positivity of $T^*(t)$ and $V(t)$. Denote by $r(t)$ the integral term in the second equation of (3.4). From the second and the third equations in (3.4), one obtains

$$T^*(t) = e^{-\delta t} T^*(0) + \int_0^t e^{-\delta(t-\xi)} r(\xi) d\xi, \quad V(t) = e^{-ct} V(0) + \int_0^t e^{-c(t-\xi)} b T^*(\xi) d\xi,$$

which together with $\phi \in X^0$ implies that $T^*(t) > 0$ and $V(t) > 0$ for small $t > 0$. We now show $T^*(t) > 0$ and $V(t) > 0$ for all $t > 0$. Otherwise, there exists $t_2 > 0$ such that $\min\{T(t_2), V(t_2)\} = 0$ for the first time. If $T^*(t_2) = 0$, $T^*(t) > 0$ for $0 \leq t < t_2$, and $V(t) > 0$ for $0 \leq t \leq t_2$, then

$$\frac{dT^*(t_2)}{dt} = \int_0^{\infty} [\beta_1 T(t_2 - s)V(t_2 - s) + \beta_2 T(t_2 - s)T^*(t_2 - s)] e^{-\mu s} f(s) ds > 0,$$

which is a contradiction with $T^*(t_2) = 0$, $T^*(t) > 0$ for $0 \leq t < t_2$. If $V(t_2) = 0$, $V(t) > 0$ for $0 \leq t < t_2$, and $T^*(t) > 0$ for $0 \leq t \leq t_2$, then

$$\frac{dV(t_2)}{dt} = b T^*(t_2) > 0,$$

which is also a contradiction. Therefore, $T^*(t) > 0$ and $V(t) > 0$ for all $t > 0$.

To prove boundedness, firstly by the positivity of solutions we have

$$\frac{dT(t)}{dt} < h - d_T T(t).$$

It follows that $\limsup_{t \rightarrow \infty} T(t) \leq h/d_T$, implying $T(t)$ is bounded.

Next, we prove the boundedness of $T^*(t)$ and $V(t)$. To this end, we define

$$G(t) = \int_0^\infty e^{-\mu s} f(s) T(t-s) ds + T^*(t) + \frac{\delta}{2b} V(t).$$

Since $T(t)$ is bounded and $\int_0^\infty f(s) ds$ is convergent, the integral in $G(t)$ is well-defined and differentiable with respect to t . Moreover, when taking time derivative of $G(t)$, the order of the differentiation and integration can be switched. Thus, we have

$$\begin{aligned} \frac{dG(t)}{dt} &= h \int_0^\infty e^{-\mu s} f(s) ds - d_T \int_0^\infty e^{-\mu s} f(s) T(t-s) ds \\ &\quad - \int_0^\infty e^{-\mu s} f(s) [\beta_1 T(t-s) V(t-s) + \beta_2 T(t-s) T^*(t-s)] ds \\ &\quad + \int_0^\infty e^{-\mu s} f(s) [\beta_1 T(t-s) V(t-s) + \beta_2 T(t-s) T^*(t-s)] ds - \delta T^*(t) \\ &\quad + \frac{\delta}{2} T^*(t) - c \frac{\delta}{2b} V(t) \\ &= h \int_0^\infty e^{-\mu s} f(s) ds - d_T \int_0^\infty e^{-\mu s} f(s) T(t-s) ds - \frac{\delta}{2} T^*(t) - c \frac{\delta}{2b} V(t) \\ &\leq h\eta - dG(t), \end{aligned}$$

where

$$\eta = \int_0^\infty e^{-\mu s} f(s) ds, \quad d = \min \left\{ d_T, \frac{\delta}{2}, c \right\} > 0. \quad (3.7)$$

Therefore, $\limsup_{t \rightarrow \infty} G(t) \leq h\eta/d$, implying that $\limsup_{t \rightarrow \infty} T^*(t) \leq h\eta/d$ and $\limsup_{t \rightarrow \infty} V(t) \leq 2bh\eta/\delta d$. Hence $T^*(t)$ and $V(t)$ are also bounded. \blacksquare

3.3 Local stability of equilibria and the basic reproduction number

System (3.4) has the infection-free equilibrium $E_0 = (h/d_T, 0, 0)$. In order to determine the stability of E_0 , we consider the linearization of (3.4) at E_0 :

$$\begin{aligned} \frac{du_1(t)}{dt} &= -d_T u_1(t) - \beta_1 \frac{h}{d_T} u_3(t) - \beta_2 \frac{h}{d_T} u_2(t), \\ \frac{du_2(t)}{dt} &= \int_0^\infty \left[\beta_1 \frac{h}{d_T} u_3(t-s) + \beta_2 \frac{h}{d_T} u_2(t-s) \right] e^{-\mu s} f(s) ds - \delta u_2(t), \\ \frac{du_3(t)}{dt} &= bu_2(t) - cu_3(t). \end{aligned} \quad (3.8)$$

The characteristic equation of this linear system is given by

$$\begin{vmatrix} \lambda + d_T & \beta_2 h/d_T & \beta_1 h/d_T \\ 0 & \lambda + \delta - \bar{\eta}(\lambda)\beta_2 h/d_T & -\bar{\eta}(\lambda)\beta_1 h/d_T \\ 0 & -b & \lambda + c \end{vmatrix} = 0, \quad (3.9)$$

where

$$\bar{\eta}(\lambda) = \int_0^\infty e^{-(\mu+\lambda)s} f(s) ds.$$

We see that (3.9) has an eigenvalue $\lambda_1 = -d_T < 0$, and other eigenvalues are determined by

$$[\lambda + \delta - \bar{\eta}(\lambda)\beta_2 h/d_T](\lambda + c) - \bar{\eta}(\lambda)\beta_1 b h/d_T = 0.$$

That is

$$\begin{aligned} (\lambda + \delta)(\lambda + c) &= (\lambda + c)\bar{\eta}(\lambda)\beta_2 h/d_T + \bar{\eta}(\lambda)\beta_1 b h/d_T \\ &= \bar{\eta}(\lambda) \left(\lambda \frac{h\beta_2}{d_T} + \mathcal{R}_0 \frac{c\delta}{\eta} \right) = \frac{\delta \bar{\eta}(\lambda)}{\eta} (\lambda \mathcal{R}_{02} + c \mathcal{R}_0), \end{aligned}$$

or

$$\left(\frac{\lambda}{\delta} + 1 \right) (\lambda + c) = \mathcal{R}_0 \frac{\bar{\eta}(\lambda)}{\eta} \left(\frac{\mathcal{R}_{02}}{\mathcal{R}_0} \lambda + c \right), \quad (3.10)$$

where $\eta = \bar{\eta}(0)$ and

$$\mathcal{R}_{01} = \frac{h\eta\beta_1 b}{d_T \delta c}, \quad \mathcal{R}_{02} = \frac{h\eta\beta_2}{d_T \delta}, \quad \mathcal{R}_0 = \mathcal{R}_{01} + \mathcal{R}_{02}. \quad (3.11)$$

We first consider the case $\mathcal{R}_0 < 1$. We show that if $\lambda = x + iy$ is a solution of (3.10), then $x < 0$. Otherwise, $x \geq 0$ would imply

$$\left| \frac{\lambda}{\delta} + 1 \right| \geq 1, \quad |\lambda + c| > \left| \frac{\mathcal{R}_{02}}{\mathcal{R}_0} \lambda + c \right|, \quad \left| \frac{\bar{\eta}(\lambda)}{\eta} \right| \leq 1,$$

and thus

$$\left| \left(\frac{\lambda}{\delta} + 1 \right) (\lambda + c) \right| > \left| \mathcal{R}_0 \frac{\bar{\eta}(\lambda)}{\eta} \left(\frac{\mathcal{R}_{02}}{\mathcal{R}_0} \lambda + c \right) \right|,$$

a contradiction to (3.10). Therefore, all roots of (3.10) have negative real parts when $\mathcal{R}_0 < 1$, implying that E_0 is locally asymptotically stable.

Next we consider the case $\mathcal{R}_0 > 1$. Let

$$\psi(\lambda) := \left(\frac{\lambda}{\delta} + 1 \right) (\lambda + c) - \mathcal{R}_0 \frac{\bar{\eta}(\lambda)}{\eta} \left(\frac{\mathcal{R}_{02}}{\mathcal{R}_0} \lambda + c \right).$$

Then $\psi(0) = c(1 - \mathcal{R}_0) < 0$. On the other hand, note that

$$\bar{\eta}(\lambda) = \int_0^\infty e^{-(\mu+\lambda)s} f(s) ds \leq \int_0^\infty f(s) ds = 1,$$

Thus,

$$\begin{aligned}\psi(\lambda) &\geq \left(\frac{\lambda}{d_{T^*}} + 1\right)(\lambda + c) - \mathcal{R}_0 \frac{1}{\eta} \left(\frac{\mathcal{R}_{02}}{\mathcal{R}_0} \lambda + c\right) \\ &= \frac{1}{d_{T^*}} \lambda^2 + \left(\frac{c}{d_{T^*}} + 1 - \frac{\mathcal{R}_{02}}{\eta}\right) \lambda - \frac{\mathcal{R}_0 c}{\eta} \rightarrow \infty \text{ as } \lambda \rightarrow \infty,\end{aligned}$$

implying $\lim_{\lambda \rightarrow +\infty} \psi(\lambda) = +\infty$. Therefore, there exists a positive (real) number λ^* such that $\psi(\lambda^*) = 0$. This means, if $\mathcal{R}_0 > 1$, (3.10) has a positive eigenvalue, and hence E_0 is unstable.

Summarizing the above analysis, we have proven the following theorem on the local stability/instability of E_0 .

Theorem 3.3.1 *Let \mathcal{R}_0 be as in (3.11). If $\mathcal{R}_0 < 1$, the infection-free equilibrium E_0 is locally asymptotically stable; if $\mathcal{R}_0 > 1$, E_0 is unstable.*

When $\mathcal{R}_0 > 1$, model system (3.4) has a unique positive equilibrium $\bar{E} = (\bar{T}, \bar{T}^*, \bar{V})$ given by

$$\bar{T} = \frac{\delta c}{\eta(\beta_1 b + \beta_2 c)} = \frac{h}{d_T} \frac{1}{\mathcal{R}_0}, \quad \bar{T}^* = \frac{d_T c}{\beta_1 b + \beta_2 c} (\mathcal{R}_0 - 1), \quad \bar{V} = \frac{b}{c} \bar{T}^* = \frac{b d_T}{\beta_1 b + \beta_2 c} (\mathcal{R}_0 - 1). \quad (3.12)$$

Linearizing (3.4) at \bar{E} yields

$$\begin{aligned}\frac{du_1(t)}{dt} &= -d_T u_1(t) - \beta_1 \bar{V} u_1(t) - \beta_1 \bar{T} u_3(t) - \beta_2 \bar{T}^* u_1(t) - \beta_2 \bar{T} u_2(t), \\ \frac{du_2(t)}{dt} &= \int_0^\infty \left[\beta_1 \bar{T} u_3(t-s) + \beta_1 \bar{V} u_1(t-s) + \beta_2 \bar{T} u_2(t-s) + \beta_2 \bar{T}^* u_1(t-s) \right] e^{-\mu s} f(s) ds \\ &\quad - \delta u_2(t), \\ \frac{du_3(t)}{dt} &= b u_2(t) - c u_3(t).\end{aligned}$$

The characteristic equation of this linear system is given by

$$\bar{J}(\lambda) = \begin{vmatrix} \lambda + d_T + \beta_1 \bar{V} + \beta_2 \bar{T}^* & \beta_2 \bar{T} & \beta_1 \bar{T} \\ -\bar{\eta}(\lambda)(\beta_1 \bar{V} + \beta_2 \bar{T}^*) & \lambda + \delta - \bar{\eta}(\lambda) \beta_2 \bar{T} & -\bar{\eta}(\lambda) \beta_1 \bar{T} \\ 0 & -b & \lambda + c \end{vmatrix} = 0.$$

Noticing that $d_T + \beta_1 \bar{V} + \beta_2 \bar{T}^* = d_T \mathcal{R}_0$, we have

$$\bar{J}(\lambda) = \begin{vmatrix} \lambda + d_T \mathcal{R}_0 & \beta_2 \bar{T} & \beta_1 \bar{T} \\ \bar{\eta}(\lambda)(\lambda + d_T) & \lambda + \delta & 0 \\ 0 & -b & \lambda + c \end{vmatrix} = 0,$$

or

$$(\lambda + d_T \mathcal{R}_0)(\lambda + \delta)(\lambda + c) - b\beta_1 \bar{T} \bar{\eta}(\lambda)(\lambda + d_T) - \beta_2 \bar{T} \bar{\eta}(\lambda)(\lambda + d_T)(\lambda + c) = 0.$$

This equation is equivalent to

$$\begin{aligned} (\lambda + d_T \mathcal{R}_0)(\lambda + \delta)(\lambda + c) &= b\beta_1 \bar{T} \bar{\eta}(\lambda)(\lambda + d_T) + \beta_2 \bar{T} \bar{\eta}(\lambda)(\lambda + d_T)(\lambda + c) \\ &= (\lambda + d_T) \bar{\eta}(\lambda) \bar{T} [b\beta_1 + \beta_2(\lambda + c)] \\ &= (\lambda + d_T) \bar{\eta}(\lambda) \left(\lambda \frac{h\beta_2}{d_T \mathcal{R}_0} + \frac{c\delta}{\eta} \right) \\ &= (\lambda + d_T) \frac{\delta \bar{\eta}(\lambda)}{\eta} \left(\lambda \frac{\mathcal{R}_{02}}{\mathcal{R}_0} + c \right), \end{aligned}$$

that is

$$(\lambda + d_T \mathcal{R}_0) \left(\frac{\lambda}{\delta} + 1 \right) (\lambda + c) = (\lambda + d_T) \frac{\bar{\eta}(\lambda)}{\eta} \left(\lambda \frac{\mathcal{R}_{02}}{\mathcal{R}_0} + c \right). \quad (3.13)$$

Assume $\lambda = x + iy$ is a solution of (3.13). We show that $x < 0$ if $\mathcal{R}_0 > 1$. Otherwise, $x \geq 0$ would imply

$$|\lambda + d_T \mathcal{R}_0| > |\lambda + d_T|, \quad \left| \frac{\lambda}{\delta} + 1 \right| \geq 1, \quad |\lambda + c| > \left| \lambda \frac{\mathcal{R}_{02}}{\mathcal{R}_0} + c \right|, \quad \left| \frac{\bar{\eta}(\lambda)}{\eta} \right| \leq 1,$$

and thus

$$\left| (\lambda + d_T \mathcal{R}_0) \left(\frac{\lambda}{\delta} + 1 \right) (\lambda + c) \right| > \left| (\lambda + d_T) \frac{\bar{\eta}(\lambda)}{\eta} \left(\lambda \frac{\mathcal{R}_{02}}{\mathcal{R}_0} + c \right) \right|.$$

This is a contradiction to (3.13). Therefore, if $\mathcal{R}_0 > 1$, then all roots of (3.13) have negative real parts, implying that \bar{E} is locally asymptotically stable. Thus, we have proven the following theorem.

Theorem 3.3.2 *Let \mathcal{R}_0 be as in (3.11). If $\mathcal{R}_0 > 1$, model system (3.4) has a positive equilibrium \bar{E} given by (3.12) which is locally asymptotically stable.*

Theorem 6.2.2 and Theorem 3.3.2 show that \mathcal{R}_0 defined by (3.11) determines whether or not an infection caused by a small inoculation/invasion of virus can persist. Indeed, \mathcal{R}_0 is the basic reproduction number of the model (3.4).

We can justify \mathcal{R}_{01} and \mathcal{R}_{02} in (3.11) from biological point of view. \mathcal{R}_{01} can be rewritten as

$$\mathcal{R}_{01} = \beta_1 \frac{h}{d_T} \cdot \frac{1}{\delta} \cdot \eta \cdot \frac{b}{c},$$

where h/d_T is the total number of uninfected cells when all cells are uninfected; β_1 is the infection rate by free viruses; $1/\delta$ is the life span of infected cells; η is the total survive rate of infected cells at all ages; b is the burst size of viruses; $1/c$ is the virus clearance rate;

b/c represents the total amount of virus particles produced efficiently from one infected cell. Therefore, \mathcal{R}_{01} means the total number of newly infected cells that arise from any one infected cell when almost all cells are uninfected, where the infection occurs by free virus infection of cells, that is the basic reproduction number corresponding to virus-to-cell infection mode. Similarly rewriting \mathcal{R}_{02} as

$$\mathcal{R}_{02} = \beta_2 \frac{h}{d_T} \cdot \frac{1}{\delta} \cdot \eta$$

where β_2 is the infection rate by the cell-to-cell transfer; $1/\delta$ is the life span of infected cells; η is the total survival rate of infected cells at all ages. Therefore, \mathcal{R}_{02} means the total number of newly infected cells that arise from any one infected cell when almost all cells are uninfected, where the infection occurs by virus-to-cell transfer, that is the basic reproduction number corresponding to cell-to-cell infection mode.

To see this mathematically, we just need to look at the linearization of (3.4) at the infection free equilibrium E_0 , that is, system (3.8), which carries all information of virus dynamics when the virus population is very small. Note that variables $u_2(t)$ and $u_3(t)$ correspond to $T^*(t)$ and $V(t)$, and at low densities these two variables are governed only by the last two equations (decoupled from the first one). Let $u(t) = (u_2(t), u_3(t))^T$, then the equations of u_2 and u_3 in (3.8) can be rewritten as

$$\frac{d}{dt}u(t) = \int_0^\infty Bu(t-s)e^{-\mu s}f(s)ds - Cu(t),$$

where

$$B = \begin{bmatrix} \beta_2 \frac{h}{d_T} & \beta_1 \frac{h}{d_T} \\ 0 & 0 \end{bmatrix}, \quad C = \begin{bmatrix} \delta & 0 \\ -b & c \end{bmatrix}.$$

We assume the initial distributions of $u_2(t)$ and $u_3(t)$ are $\psi(\theta) = (\psi_2(\theta), \psi_3(\theta))$, then without new infection these populations evolve as

$$S_0(t)\psi := e^{-Ct}\psi.$$

If new infection occurs at time $t = 0$, since there is a time delay s , from the time of initial infection until becoming productively infectious, the total distributions of the new infection

populations are

$$\begin{aligned}
L\psi &:= \int_0^\infty \int_s^\infty B e^{-C(t-s)} \psi e^{-\mu s} f(s) dt ds \\
&= \int_0^\infty B \int_s^\infty e^{-C(t-s)} dt \cdot \psi e^{-\mu s} f(s) ds \\
&= \int_0^\infty BC^{-1} \psi e^{-\mu s} f(s) ds \\
&= BC^{-1} \psi \int_0^\infty e^{-\mu s} f(s) ds \\
&= BC^{-1} \eta \psi.
\end{aligned}$$

Notice that

$$C^{-1} = \frac{1}{c\delta} \begin{bmatrix} c & 0 \\ b & \delta \end{bmatrix}, \quad BC^{-1} = \frac{1}{c\delta} \begin{bmatrix} c\beta_2 \frac{h}{d_T} + b\beta_1 \frac{h}{d_T} & \beta_1 \delta \frac{h}{d_T} \\ 0 & 0 \end{bmatrix}.$$

Therefore,

$$\mathcal{R}_0 = \rho(L) = \rho(BC^{-1})\eta = \frac{1}{c\delta} \left[\beta_2 c \frac{h}{d_T} + \beta_1 b \frac{h}{d_T} \right] = \frac{\beta_1 h b \eta}{d_T c \delta} + \frac{\beta_2 h \eta}{d_T \delta}.$$

Making use of the result and procedure on basic reproduction number for structured models (here there is the structure in infection age) in [40], we confirm that \mathcal{R}_0 is the basic reproduction number.

3.4 Persistence of infection

In this section, we will show that the model system is persistent when $\mathcal{R}_0 > 1$. Such a property itself is of some biological significance, in addition, it will be used in constructing Lyapunov functional in Section 5 to prove the global stability of the positive equilibrium.

Due to the infinite delay in the model, the solution semi-flow of (3.4)-(3.6) may not be compact, and this brings in some mathematical challenge. In the following, just as in Röst and Wu [34], we will apply a theorem in Hale and Watman [11] to achieve our goal. To this end, let $S(t)$, $t > 0$, be the solution semi-flow of model system (3.4)-(3.6). Then, we shall make use of the following theorem to the semi-flow $S(t)$ on X , which does not require $S(t)$ to be compact.

Theorem 3.4.1 (Hale and Watman [11, Theorem 4.2]) *Suppose we have the following:*

- (i) X^0 is an open and dense set in X with $X^0 \cup X_0 = X$ and $X^0 \cap X_0 = \emptyset$;
- (ii) $S(t)$ satisfies $S(t)X^0 \subset X^0$ and $S(t)X_0 \subset X_0$ for $t > 0$;

- (iii) $S(t)$ is point dissipative in X ;
- (iv) $\gamma^+(U)$ is bounded in X if U is bounded in X ;
- (v) $S(t)$ is asymptotically smooth;
- (vi) $\mathcal{A} = \cup_{x \in A_b} \omega(x)$ is isolated and has an acyclic covering $Q = \cup_{i=1}^k Q_i$, where A_b is the global attractor of $S(t)$ restricted to X_0 ;
- (vii) For each $Q_i \in Q$, $W^s(Q_i) \cap X^0 = \emptyset$, where W^s refers to the stable set.

Then $S(t)$ is uniformly persistent, that is, there is a $\sigma > 0$ such that for any $x \in X^0$,

$$\liminf_{t \rightarrow \infty} d(S(t)x, X_0) \geq \sigma.$$

Applying the above theorem, we can prove the following persistence result for (3.4)-(3.6).

Theorem 3.4.2 *For system (3.4), if $\mathcal{R}_0 > 1$, then the solution semi-flow $S(t)$ is uniformly persistent, that is, there exists a $\sigma > 0$ such that any solution of (3.4)-(3.6) satisfies*

$$\liminf_{t \rightarrow \infty} T(t) \geq \sigma, \quad \liminf_{t \rightarrow \infty} T^*(t) \geq \sigma, \quad \liminf_{t \rightarrow \infty} V(t) \geq \sigma.$$

Proof Let X^0 be as in (3.6) and

$$X_0 = \{\phi = (\phi_1, \phi_2, \phi_3) \in X : \phi_2(\theta) = \phi_3(\theta) = 0 \text{ for all } \theta \in (-\infty, 0]\}.$$

We just need to verify the conditions in Theorem 3.4.1. (i) is obvious and (ii) has been confirmed in Section 2. We now prove (iii), that is, the solutions of (3.4)-(3.6) are ultimately bounded. By $\limsup_{t \rightarrow \infty} T(t) \leq h/d_T$, we know that, there exists an $N_1 > 0$ such that $T(t) \leq h/d_T + 1$ for all $t > N_1$. Let M_1 be the maximum of $T(t)$ on $[0, N_1]$. Then for any $0 < t \leq N_1$, we have

$$\begin{aligned} \|T_t\| &= \sup_{-\infty < \theta \leq 0} |T_t(\theta)|e^{\Delta\theta} = \sup_{-\infty < s \leq t} |T(s)|e^{\Delta s}e^{-\Delta t} \\ &\leq \max\{\|\phi_1\|e^{-\Delta t}, M_1e^{\Delta t}e^{-\Delta t}\} \leq \max\{\|\phi_1\|, M_1\}, \end{aligned}$$

and for $t > N_1$, we obtain

$$\|T_t\| = \sup_{-\infty < \theta \leq 0} |T_t(\theta)|e^{\Delta\theta} = \sup_{-\infty < s \leq t} |T(s)|e^{\Delta s}e^{-\Delta t} \leq \max\{\|\phi_1\|e^{-\Delta t}, M_1e^{\Delta N_1}e^{-\Delta t}, h/d_T + 1\}.$$

Thus, there is an $N_2 > N_1$ such that

$$\|\phi_1\|e^{-\Delta t} \leq h/d_T + 1 \quad \text{and} \quad M_1e^{\Delta N_1}e^{-\Delta t} \leq h/d_T + 1, \quad \text{for } t \geq N_2,$$

and therefore,

$$\|T_t\| \leq h/d_T + 1 =: T_M \text{ for } t \geq N_2. \quad (3.14)$$

Similarly, from $\limsup_{t \rightarrow \infty} T^*(t) \leq h\eta/d$ and $\limsup_{t \rightarrow \infty} V(t) \leq 2bh\eta/\delta d$ (see proof of Theorem 6.2.1), we know that there exist $N_3 > 0$ and $N_4 > 0$ such that

$$\|T_t^*\| \leq h\eta/d + 1 =: T_M^* \text{ for } t \geq N_3 \quad (3.15)$$

$$\|V_t\| \leq 2bh\eta/\delta d + 1 =: V_M \text{ for } t \geq N_4. \quad (3.16)$$

Thus, the solution $(T(t), T^*(t), V(t))$ is ultimately bounded, that is, $S(t)$ is point dissipative in X , proving (iii).

Noticing that the three bounds in (3.14), (3.15) and (3.16) are all independent of initial functions, condition (iv) is verified.

Next we verify condition (v): $S(t)$ is asymptotically smooth, that is, for any bounded subset U of X , for which $S(t)U \subset U$ for $t \geq 0$, there exists a compact set \mathcal{M} such that $d(S(t)U, \mathcal{M}) \rightarrow 0$ as $t \rightarrow \infty$. Let U be an arbitrarily given bounded set in X , and (T_t, T_t^*, V_t) be the segment of solution with initial condition $(\phi_1, \phi_2, \phi_3) \in U$. Set

$$\mathcal{M}_1 = \left\{ \phi \in C_{\Delta}^+ : \sup_{\theta \leq 0} \phi(\theta) e^{\frac{\delta}{2}\theta} \leq T_M \right\},$$

$$\mathcal{M}_2 = \left\{ \phi \in C_{\Delta}^+ : \sup_{\theta \leq 0} \phi(\theta) e^{\frac{\delta}{2}\theta} \leq T_M^* \right\},$$

$$\mathcal{M}_3 = \left\{ \phi \in C_{\Delta}^+ : \sup_{\theta \leq 0} \phi(\theta) e^{\frac{\delta}{2}\theta} \leq V_M \right\},$$

and let $\mathcal{M} = \mathcal{M}_1 \times \mathcal{M}_2 \times \mathcal{M}_3$. It follows from Lemma 3.2 in Burton and Hutson [6] that \mathcal{M} is compact in X . Then, by using exactly the same argument in proving $\lim_{t \rightarrow \infty} d(E_t, \mathcal{M}) = 0$ in the proof of Theorem 6.1 in Röst and Wu [34], we conclude that

$$\lim_{t \rightarrow \infty} d(T_t, \mathcal{M}_1) = 0, \quad \lim_{t \rightarrow \infty} d(T_t^*, \mathcal{M}_2) = 0, \quad \lim_{t \rightarrow \infty} d(V_t, \mathcal{M}_3) = 0.$$

Therefore, $S(t)$ is asymptotically smooth, proving (v).

For condition (vi), it is obvious that $\mathcal{A} = \{E_0\}$ and it is isolated, where $E_0 = (h/d_T, 0, 0)$. Thus the covering \mathcal{Q} is simply $\mathcal{Q} = \{E_0\}$, which is acyclic because there is no orbit connecting E_0 to itself in X_0 .

Finally, we verify (vii). To show $W^s(E_0) \cap X^0 = \emptyset$, we suppose the opposite, that is there exists a solution $u_t \in X^0$ such that

$$\lim_{t \rightarrow \infty} T(t) = \frac{h}{d_T}, \quad \lim_{t \rightarrow \infty} T^*(t) = 0, \quad \lim_{t \rightarrow \infty} V(t) = 0.$$

Note that $\mathcal{R}_0 > 1$ is equivalent to

$$\frac{h}{d_T} \left(\frac{\beta_1 b}{c} + \beta_2 \right) \int_0^\infty e^{-\mu s} f(s) ds > \delta.$$

Choose $\varepsilon > 0$ be sufficiently small such that

$$\left(\frac{h}{d_T} - \varepsilon \right) \left(\frac{\beta_1 b}{c} + \beta_2 \right) \int_0^\infty e^{-\mu s} f(s) ds > \delta. \quad (3.17)$$

For this ε , there exists a $\tau_0 > 0$ such that $T(t) > h/d_T - \varepsilon$ for all $t > \tau_0$. Truncating the integral in (3.17), there is another $\tau_1 > 0$ such that

$$\left(\frac{h}{d_T} - \varepsilon \right) \left(\frac{\beta_1 b}{c} + \beta_2 \right) \int_0^{\tau_1} e^{-\mu s} f(s) ds > \delta. \quad (3.18)$$

Let $\tau_2 = \tau_0 + \tau_1$. Then for $t \geq \tau_2$, we have

$$\begin{aligned} \frac{dT^*}{dt} &\geq \int_0^{\tau_1} [\beta_1 T(t-s)V(t-s) + \beta_2 T(t-s)T^*(t-s)] e^{-\mu s} f(s) ds - \delta T^*(t) \\ &= \int_{t-\tau_1}^t [\beta_1 T(\xi)V(\xi) + \beta_2 T(\xi)T^*(\xi)] e^{-\mu(t-\xi)} f(t-\xi) d\xi - \delta T^*(t) \\ &\geq \left(\frac{h}{d_T} - \varepsilon \right) \int_{t-\tau_1}^t [\beta_1 V(\xi) + \beta_2 T^*(\xi)] e^{-\mu(t-\xi)} f(t-\xi) d\xi - \delta T^*(t) \\ &= \left(\frac{h}{d_T} - \varepsilon \right) \int_0^{\tau_1} [\beta_1 V(t-s) + \beta_2 T^*(t-s)] e^{-\mu s} f(s) ds - \delta T^*(t). \end{aligned} \quad (3.19)$$

This suggests the following comparison system for $(T^*(t), V(t))$,

$$\begin{cases} n'_1(t) = \left(\frac{h}{d_T} - \varepsilon \right) \int_0^{\tau_1} [\beta_1 n_2(t-s) + \beta_2 n_1(t-s)] e^{-\mu s} f(s) ds - \delta n_1(t), \\ n'_2(t) = bn_1(t) - cn_2(t), \end{cases} \quad \text{for } t \geq \tau_2. \quad (3.20)$$

Notice that this is a monotone system, and hence, by the comparison theorem and the limit $\lim_{t \rightarrow \infty} T^*(t) = 0$ and $\lim_{t \rightarrow \infty} V(t) = 0$, one should have $\lim_{t \rightarrow \infty} (n_1(t), n_2(t)) = (0, 0)$. On the other hand, the two equations for $n_1(t)$ and $n_2(t)$ are in the same forms of the second and third equations in (3.8) except the upper limit ∞ in the integral is replaced by τ_1 and the h/d_T is perturbed to $h/d_T - \varepsilon$. Repeating the same argument for proving the instability of E_0 in Theorem 6.2.2 and replacing the condition $\mathcal{R}_0 > 1$ by (3.18), we conclude that the characteristic equation of (3.20) has a positive real eigenvalue, a contradiction to $\lim_{t \rightarrow \infty} (n_1(t), n_2(t)) = (0, 0)$. Thus, we have $W^s(E_0) \cap X^0 = \emptyset$, confirming condition (vii).

Now, by Theorem 3.4.1, there exists a $\sigma_1 > 0$ such that $\liminf_{t \rightarrow \infty} d(S(t)\phi, X_0) \geq \sigma_1$ for every $\phi \in X^0$, implying that the T^* and V components of the solution with initial function $\phi \in X^0$ satisfy

$$\liminf_{t \rightarrow \infty} \|T_t^*\| \geq \sigma_1 \quad \text{and} \quad \liminf_{t \rightarrow \infty} \|V_t\| \geq \sigma_1.$$

By similar estimates as in the proof of Theorem 2.1, we obtain

$$\liminf_{t \rightarrow \infty} T^*(t) > \sigma_1 \quad \text{and} \quad \liminf_{t \rightarrow \infty} V(t) > \sigma_1. \quad (3.21)$$

It remains to show the persistence of $T(t)$. From (3.14) and (3.15), we have

$$\frac{dT(t)}{dt} > h - (d_T + \beta_1 T_M + \beta_2 T_M^*)T(t) \quad \text{for } t \geq N_5,$$

where $N_5 = \max\{N_3, N_4\}$. This means that whenever $T(t) < \sigma_2 := h/(d_T + \beta_1 T_M + \beta_2 T_M^*)$ with $t \geq N_5$, $T(t)$ will be increasing, which implies that $\liminf_{t \rightarrow \infty} T(t) > \sigma_2/2$. Taking $\sigma = \min\{\sigma_1, \sigma_2/2\}$, the proof of the theorem is completed.

3.5 Global stability of equilibria

In this section, we prove that E_0 is actually *globally* asymptotically stable when $\mathcal{R}_0 < 1$, and so is \bar{E} provided that $\mathcal{R}_0 > 1$. Therefore, the model (3.4) demonstrates global threshold dynamics. We shall achieve our goal by constructing an appropriate Lyapunov functional. The form of our Lyapunov functional is motivated by the Lyapunov function in [16], and similar functionals have recently been applied to many other models, including some with infinite delays, see e.g., [26, 27] and the references therein.

We first deal with the global asymptotic stability of E_0 under $\mathcal{R}_0 < 1$.

Theorem 3.5.1 *If $\mathcal{R}_0 < 1$, the infection-free steady state E_0 is indeed globally asymptotically stable.*

Proof. Let $T_0 = h/d_T$, and $(T(t), T^*(t), V(t))$ be a solution of system (3.4)-(3.6) satisfying $T(t) > 0$. Let

$$\Psi_{01}(T, T^*, V)(t) = T(t) - T_0 \ln \frac{T(t)}{T_0} + \frac{1}{\eta} T^*(t) + \frac{h\beta_1}{cd_T} V(t).$$

Calculating the time derivative of Ψ_{01} along (3.4), we have

$$\begin{aligned}
\frac{d}{dt}\Psi_{01}(t) &= \left(1 - \frac{T_0}{T(t)}\right)[h - d_T T(t) - \beta_1 T(t)V(t) - \beta_2 T(t)T^*(t)] \\
&\quad + \frac{1}{\eta} \left[\int_0^\infty [\beta_1 T(t-s)V(t-s) + \beta_2 T(t-s)T^*(t-s)]e^{-\mu s} f(s) ds - \delta T^*(t) \right] \\
&\quad + \frac{h\beta_1}{d_T c} [bT^*(t) - cV(t)] \\
&= d_T T_0 \left(2 - \frac{T_0}{T(t)} - \frac{T(t)}{T_0}\right) - \beta_1 T(t)V(t) - \beta_2 T(t)T^*(t) + \beta_1 T_0 V(t) + \beta_2 T_0 T^*(t) \\
&\quad + \frac{1}{\eta} \int_0^\infty [\beta_1 T(t-s)V(t-s) + \beta_2 T(t-s)T^*(t-s)]e^{-\mu s} f(s) ds - \frac{\delta}{\eta} T^*(t) \\
&\quad + \frac{h\beta_1}{d_T c} [bT^*(t) - cV(t)] \\
&= d_T T_0 \left(2 - \frac{T_0}{T(t)} - \frac{T(t)}{T_0}\right) + \beta_1 T_0 V(t) + \beta_2 T_0 T^*(t) - \frac{\delta}{\eta} T^*(t) \\
&\quad + \frac{h\beta_1}{d_T c} [bT^*(t) - cV(t)] - \frac{1}{\eta} \int_0^\infty f(s)e^{-\mu s} [\beta_1 T(t)V(t) + \beta_2 T(t)T^*(t) \\
&\quad - \beta_1 T(t-s)V(t-s) - \beta_2 T(t-s)T^*(t-s)] ds \\
&= d_T T_0 \left(2 - \frac{T_0}{T(t)} - \frac{T(t)}{T_0}\right) + \frac{\delta}{\eta} (\mathcal{R}_0 - 1) T^*(t) - \frac{1}{\eta} \int_0^\infty f(s)e^{-\mu s} [\beta_1 T(t)V(t) \\
&\quad + \beta_2 T(t)T^*(t) - \beta_1 T(t-s)V(t-s) - \beta_2 T(t-s)T^*(t-s)] ds. \tag{3.22}
\end{aligned}$$

In light of the integral term in (3.22), we define

$$\Psi_{02}(T, T^*, V)(t) = \int_0^\infty f(s)e^{-\mu s} \int_{t-s}^t [\beta_1 T(\tau)V(\tau) + \beta_2 T(\tau)T^*(\tau)] d\tau ds.$$

Then,

$$\frac{d}{dt}\Psi_{02}(t) = \int_0^\infty f(s)e^{-\mu s} [\beta_1 T(t)V(t) + \beta_2 T(t)T^*(t) - \beta_1 T(t-s)V(t-s) - \beta_2 T(t-s)T^*(t-s)] ds.$$

Using $\Psi_{01}(t)$ and $\Psi_{02}(t)$, we define the following functional

$$\Psi_0(t) = \Psi_{01}(t) + \frac{1}{\eta}\Psi_{02}(t).$$

Then

$$\frac{d}{dt}\Psi_0(t) = d_T T_0 \left(2 - \frac{T_0}{T(t)} - \frac{T(t)}{T_0}\right) + \frac{\delta}{\eta} (\mathcal{R}_0 - 1) T^*(t). \tag{3.23}$$

Notice that

$$2 - \frac{T_0}{T(t)} - \frac{T(t)}{T_0} \leq 0,$$

for all $T(t) > 0$, and the equality holds if and only if $T(t) = T_0$. Hence if $\mathcal{R}_0 < 1$, then $\Psi'_0(t) \leq 0$. Let $E = \{(T(t), T^*(t), V(t)) : \Psi'_0(t) = 0\}$ and M be the largest invariant set in E . By

the LaSalle invariance principle (e.g., [12, Theorem 5.3.1], or [23, Theorem 2.5.3]), all non-negative solutions tend to M . Note that $\Psi'_0(t) = 0$ if and only if $T(t) = T_0$ and $T^*(t) = 0$. Using this and the invariance of M , we easily see that M is indeed the singleton $M = \{E_0\}$, showing that every non-negative solution with $T(t) > 0$ indeed approaches E_0 . Hence E_0 is globally attractive under $\mathcal{R}_0 < 1$, which, together with local stability of E_0 established in Section 3, confirms the global asymptotic stability of E_0 under $\mathcal{R}_0 < 1$. ■

For \bar{E} , we also have

Theorem 3.5.2 *If $\mathcal{R}_0 > 1$, then any solution $u(t) = (T_t, T_t^*, V_t)$ of (3.4)-(3.6) converges to the positive equilibrium \bar{E} , that is,*

$$\lim_{t \rightarrow \infty} (T(t), T^*(t), V(t)) = (\bar{T}, \bar{T}^*, \bar{V}).$$

Proof. For convenience of notations, we denote $P(x) = x - 1 - \ln x$ and let

$$\begin{aligned} \Psi_1(T, T^*, V)(t) &= T(t) - \bar{T} \ln \frac{T}{\bar{T}} + \frac{1}{\eta} \left[T^*(t) - \bar{T}^* \ln \frac{T^*(t)}{\bar{T}^*} \right] + \frac{\beta_1 \bar{T} \bar{V}}{\bar{T}^* b} \left[V(t) - \bar{V} \ln \frac{V(t)}{\bar{V}} \right], \\ \Psi_{11}(T, V)(t) &= \int_0^\infty e^{-\mu s} f(s) \int_{t-s}^t P\left(\frac{T(\tau)V(\tau)}{\bar{T}\bar{V}}\right) d\tau ds, \\ \Psi_{12}(T, T^*)(t) &= \int_0^\infty e^{-\mu s} f(s) \int_{t-s}^t P\left(\frac{T(\tau)T^*(\tau)}{\bar{T}\bar{T}^*}\right) d\tau ds. \end{aligned}$$

By the boundedness and persistence of solutions established in Sections 2 and 4, and the assumption that $f(s)$ has compact support, we know that the above functions are well defined for large t . Let

$$\Psi_2(t) = \Psi_1(t) + \frac{\beta_1 \bar{T} \bar{V}}{\eta} \Psi_{11}(t) + \frac{\beta_2 \bar{T} \bar{T}^*}{\eta} \Psi_{12}(t).$$

Taking derivative of $\Psi_2(t)$ and making use of the equations defining the positive equilibrium \bar{E} , we obtain, after simplifications, the following:

$$\begin{aligned} \frac{d}{dt} \Psi_2(t) &= \frac{dT}{dt} \left(2 - \frac{\bar{T}}{T(t)} - \frac{T(t)}{\bar{T}} \right) + \frac{\beta_1 \bar{T} \bar{V}}{\eta} \int_0^\infty e^{-\mu s} f(s) \left[3 - \frac{\bar{T}}{T(t)} \right. \\ &\quad \left. - \frac{\bar{T}^* T(t-s)V(t-s)}{T^*(t)\bar{T}\bar{V}} - \frac{T^*(t)\bar{V}}{\bar{T}^* V(t)} + \ln \frac{T(t-s)V(t-s)}{T(t)V(t)} \right] ds \\ &\quad + \frac{\beta_2 \bar{T} \bar{T}^*}{\eta} \int_0^\infty \left[2 - \frac{\bar{T}}{T(t)} - \frac{T(t-s)T^*(t-s)}{\bar{T}\bar{T}^*(t)} + \ln \frac{T(t-s)T^*(t-s)}{T(t)T^*(t)} \right] ds. \end{aligned} \quad (3.24)$$

Notice that

$$2 - \frac{\bar{T}}{T(t)} - \frac{T(t)}{\bar{T}} \leq 0. \quad (3.25)$$

Also note that $P(x) \geq 0$ for all $x \in (0, \infty)$ and $P(x) = 0$ if and only if $x = 1$. Making use of this function $P(x)$, we have

$$\begin{aligned} & 3 - \frac{\bar{T}}{T(t)} - \frac{\bar{T}^* T(t-s)V(t-s)}{T^*(t)\bar{T}\bar{V}} - \frac{T^*(t)\bar{V}}{\bar{T}^* V(t)} + \ln \frac{T(t-s)V(t-s)}{T(t)V(t)} \\ = & -P\left(\frac{\bar{T}}{T(t)}\right) - P\left(\frac{\bar{T}^* T(t-s)V(t-s)}{T^*(t)\bar{T}\bar{V}}\right) - P\left(\frac{T^*(t)\bar{V}}{\bar{T}^* V(t)}\right) \leq 0, \end{aligned} \quad (3.26)$$

and

$$\begin{aligned} & 2 - \frac{\bar{T}}{T(t)} - \frac{T(t-s)T^*(t-s)}{\bar{T}T^*(t)} + \ln \frac{T(t-s)T^*(t-s)}{T(t)T^*(t)} \\ = & -P\left(\frac{\bar{T}}{T(t)}\right) - P\left(\frac{T(t-s)T^*(t-s)}{\bar{T}T^*(t)}\right) \leq 0, \end{aligned} \quad (3.27)$$

for all $T(t), T^*(t), V(t) > 0$. Thus $\Psi'_2(t) \leq 0$. Let $E = \{(T(t), T^*(t), V(t)) : \Psi'_2(t) = 0\}$ and let M be the largest invariant set in E . By the LaSalle invariance principle (e.g., [12, Theorem 5.3.1], or [23, Theorem 2.5.3]) and Theorem 6.2.1, every positive solution tends to M .

It remains to show that $M = \{\bar{E}\}$. From (3.25), (3.26) and (3.27), we know that

$$\begin{aligned} & \frac{d}{dt}\Psi_2(t) = 0 \\ \Leftrightarrow & \begin{cases} T(t) = \bar{T}, & \bar{T}^* T(t-s)V(t-s) = T^*(t)\bar{T}\bar{V}, & T^*(t)\bar{V} = \bar{T}^* V(t), \\ T(t-s)V(t-s) = T(t)V(t), & T(t-s)T^*(t-s) = \bar{T}T^*(t), \\ T(t-s)T^*(t-s) = T(t)T^*(t). \end{cases} \\ \Leftrightarrow & \begin{cases} T(t) = \bar{T}, & T^*(t)\bar{V} = \bar{T}^* V(t), \\ T(t-s)V(t-s) = \bar{T}V(t), & T(t-s)T^*(t-s) = \bar{T}T^*(t). \end{cases} \end{aligned}$$

Applying $T^*(t)\bar{V} = \bar{T}^* V(t)$ to the third equation in (3.4), we have $\frac{dV(t)}{dt} = 0$, meaning that $V(t)$ is a constant; this in turn implies that T^* is also a constant. Since $T(t) = \bar{T}$, by the uniqueness of the positive equilibrium, we then conclude that $T^*(t) = \bar{T}^*$, $V(t) = \bar{V}$. Therefore, $M = \{\bar{E}\}$, that is, \bar{E} is globally attractive for all positive solutions. The global attractivity and the local stability of \bar{E} proved under $\mathcal{R}_0 > 1$ lead to the global asymptotic stability of \bar{E} , completing the proof. ■

3.6 Conclusion and discussion

HIV-1 has two predominant infection modes: the classical virus-to-cell infection and cell-to-cell spread. In the classical virus-to-cell infection, viruses released from infected cells randomly move around to find a new target cell to infect. Recently, it was revealed that HIV-1

infection may also occur by the transfer of viruses through direct contact between infected cells and uninfected cells via certain structures, for example membrane nanotubes or macromolecular adhesive contacts termed virological synapses [37]. During this cell-to-cell transmission, many viral particles can be simultaneously transferred from infected to uninfected CD4⁺ T cells.

In this chapter, we have considered a mathematical model to describe presence of both of these two transmission modes. By a rigorous analysis, we have shown that the model has a threshold dynamics. Such a threshold dynamics is fully determined by the basic reproduction number \mathcal{R}_0 in the sense that the infection-free equilibrium E_0 is globally asymptotically stable if $\mathcal{R}_0 < 1$, and when $\mathcal{R}_0 > 1$, E_0 yields to a globally asymptotically stable positive equilibrium \bar{E} implying the infection will persist.

Examining the formula for the basic reproduction number \mathcal{R}_0 , we found that it is larger than that given in existing models that only considered one infection mode. Indeed, note that when $\beta_1 = 0$, meaning that infection is exclusively through cell-to-cell transmission, which is the scenario of the work in [4], the basic reproduction number \mathcal{R}_0 reduces to \mathcal{R}_{02} . This would be the basic reproduction number of the corresponding model that ignores the virus-to-cell infection mode. Similarly, when $\beta_2 = 0$, \mathcal{R}_0 reduces to \mathcal{R}_{01} which is exactly the basic reproduction number for the corresponding model that neglects the cell-to-cell transmission mechanism. Therefore, we see that our model not only reveals that the basic reproduction number of the model that neglects either the cell-to-cell spread or virus-to-cell infection is under-evaluated, but also tells precisely by how much it is under-evaluated, reflected by the relation $\mathcal{R}_0 = \mathcal{R}_{01} + \mathcal{R}_{02}$ and the formulas for \mathcal{R}_{01} and \mathcal{R}_{02} in (3.11). This formula also reflects the impact of the infection age through the distribution function $f(s)$.

When applying models only considering cell-to-cell transmission or infection by cell-free viruses to experimental data, parameters are always estimated to be an average of the effect of both modes of transmission. Thus, the estimate of \mathcal{R}_0 based on a model neglecting cell-to-cell transmission is not the exact basic reproductive number of the model with infection by cell-free mode, but an average of both modes of infections.

Cell-to-cell spread not only facilitates rapid viral dissemination, but may also promote immune invasion and influence disease [24]. Cell-to-cell spread of HIV-1 may also reduce the effectiveness of neutralizing antibodies and viral inhibitors. However, it is unclear whether this mode of viral spread is susceptible or resistant to inhibition by neutralizing antibodies and entry inhibition. There are ongoing controversies in this field of study [3, 25]. Considering the antiretroviral therapy of reverse transcriptase (RT) inhibitor and incorporating the efficacy

of the RT inhibitor in same way as in [29] (see (3.2)), our model (3.4) now reads

$$\begin{cases} \frac{dT(t)}{dt} = h - d_T T(t) - (1 - n_1)\beta_1 V(t)T(t) - (1 - n_2)\beta_2 T(t)T^*(t), \\ \frac{dT^*(t)}{dt} = \int_0^\infty f(s)e^{-\mu s} [(1 - n_1)\beta_1 T(t-s)V(t-s), \\ \quad + (1 - n_2)\beta_2 T(t-s)T^*(t-s)] ds - \delta T^*(t), \\ \frac{dV(t)}{dt} = bT^*(t) - cV(t), \end{cases} \quad (3.28)$$

where n_1 denotes the efficacy of the RT inhibitor inhibiting the virus-to-cell infection; n_2 represents the efficacy of the RT inhibitor with respect to the cell-to-cell channel. Comparing (3.28) to (3.4), we see that the basic reproduction number for (3.28) is

$$\hat{\mathcal{R}}_0 = \frac{(1 - n_1)\beta_1 \eta h b}{d_T \delta c} + \frac{(1 - n_2)\beta_2 \eta h}{d_T \delta} =: \hat{\mathcal{R}}_{01} + \hat{\mathcal{R}}_{02}.$$

It follows that if the RT inhibitor is very effective for inhibition of virus-to-cell infection, then large n_1 would make $\hat{\mathcal{R}}_{01}$ less than one, meaning that the virus would be eliminated by the therapy in the absence of cell-to-cell transmission ($\beta_2 = 0$). However, if cell-to-cell transmission co-exists ($\beta_2 > 0$) and is less sensitive to the RT inhibitor, then n_2 could be small, such that $\hat{\mathcal{R}}_{02} > 1$. Thus $\hat{\mathcal{R}}_0 > 1$, meaning the virus would persist. The virus can be cleared if and only if the RT inhibitor is effective for both modes of infections, such that $\hat{\mathcal{R}}_0 < 1$.

In our model, we do not consider multiple infection per cell which may occur by synaptic transmission. However, the high efficiency of infection by large numbers of virions is likely to result in a transfer of multiple virions to a target cell [7, 15]. Komarova *et al.* [19, 20] considered multiple infection during the cell-to-cell transmission by mathematical modeling and explored the effect of different strategies of the virus (that is, the number of viruses passed per synapse) on the basic reproductive ratio of the virus. They showed that the strategy of single virus transmission per synapse maximizes the reproductive ratio if the synapses can be formed quickly and the process of infection is independent of the number of resident viruses, while strategies with intermediate numbers of viruses transferred correspond to the highest values of the basic reproductive number if the synapse formation is slow or if the multiplicity of infection strongly influences the kinetic of virus production. Multiple infection of the same cell may waste a large number of viruses that could otherwise enter uninfected target cells, hence fewer newly infected cells are generated and the infection eventually cannot be maintained for larger numbers of transferred viruses.

Multiple infections may reduce the sensitivity to antiretroviral therapies. Sigal *et al.* [39] showed that cell-to-cell spread of HIV-1 is sufficient to reduce the efficacy of antiretroviral therapy. A possible explanation is that the cell-to-cell transmission may play a significant role for multiple infection per target cell which reduced sensitivity to drugs. They found that

virus-to-cell infection was efficiently prevented by *tenofovir* and *efavirenz*. In the presence of tenofovir, virus-to-cell infection declined thirty-fold. But once infection became established, cell-to-cell transfer through direct contact between cells become possible (likely dominant), the infection is much less affected by the presence of drugs. Sigal *et al.* [39] attempted to explain why highly potent regimens that target several different steps in the HIV-1 life cycle cannot shut down replication, despite reducing HIV-1 replication to very low levels, which could be due to cell-to-cell transfer of multiple virions and the drugs' inability to inhibit replication when virus levels are high.

However, Permanyer *et al.* [33] argued that the results of Sigal *et al.* depend on their particular experimental conditions and that the results therefore might not be correct. Permanyer *et al.* also pointed out that the conclusion of drug resistant of cell-to-cell transfer by Sigal *et al.* was obtained under the incorrect assumption that each virus transferred will lead to a productive infection. They found that antiretroviral drugs, such as the reverse transcriptase inhibitors *zidovudine* and *tenofovir*, and the attachment inhibitor IgGb120, are able to block virus replication with similar efficacy to cell-free virus infections. That indicates that cell-to-cell transmission may not allow for ongoing virus replication in the presence of antiretroviral therapy.

Komarova *et al.* [21] explored the role of synaptic transmission in susceptibility of HIV-1 infection to antiretroviral drugs, using a virus infection dynamical model with multiple infections. They found that multiple infection via synapses does not simply reduce susceptibility to treatment, which depends on the relative probability of individual virions to infect a cell during cell-free virus and cell-to-cell virus transmission. If this probability is higher for cell-free virus transmission, then susceptibility to antiretroviral drugs is lowest when a single virus is transferred per synapse, which maximizes the release of free virus. On the other hand, if the infection probability is higher for synaptic transmission, then they found that the susceptibility to antiretroviral drugs is minimized for an intermediate number of virions transferred per synapse. It needs further experimental investigations to determine whether the virus persist by synaptic transmission during antiretroviral therapy.

HIV-1 infection can be very effectively suppressed with antiretroviral therapy, a combination of drugs that block various steps in the HIV-1 lifecycle such as the ability of the virus to reversely transcribe its RNA genome to DNA (RT-inhibitor), integrate DNA into the cell genome, or make viable new virions by the cleavage of viral protein precursors (protease inhibitor). However, these antiretroviral therapies cannot completely eliminate HIV-1 infection, and the infection can re-establish itself within weeks after therapy interruption. The main reason is the existence of reservoir of infected cells that are insensitive to drugs, which could be latently infected cells consisting of those that are quiescent in the genomically integrated form,

long-lived infected cells, or those on ongoing transmission cycles called ongoing replication. It is believed that the reservoir of infected cells is enough to cause a huge rebound in viral load within weeks after stopping an antiretroviral treatment. Considering an antiretroviral therapy in the presence of both cell-free and cell-to-cell transmissions seems to be an interesting yet worthy project.

In our model (3.4), we have assumed that target cells $T(t)$ are produced at a constant rate h and has a constant death rate d_T . It would be more reasonable to consider density dependent production rate. One possibility is to assume a logistic growth for the healthy cells in the absence of infection, as in [5]. We leave this as a future project.

Bibliography

- [1] Bonhoeffer S., May R.M., Shaw G.M. and Nowak M.A., Virus dynamics and drug therapy, Proc. Natl. Acad. Sci. USA, 94 (1997) 6971-6976.
- [2] Burton T.A., Volterra integral and differential equations, in “Mathematics In Science And Engineering”, 2nd edition, Elsevier, Amsterdam-Boston, 2005.
- [3] Chen P., Hubner W., Spinelli M.A. and Chen B.K., Predominant mode of human immunodeficiency virus transfer between T cells is mediated by sustained env-dependent neutralization-resistant virological synapses, J. Virol., 81 (2007) 12582-12595.
- [4] Culshaw R.V., Ruan S. and Webb G., A mathematical model of cell-to-cell spread of HIV-1 that includes a time delay, J. Math. Biol., 46 (2003) 425-444.
- [5] De Boer R.J. and Perelson A.S., Target cell limited and immune control models of HIV infection: a comparison, J. Theor. Biol., 190 (1998) 201-214.
- [6] Burton T. and Hutson V., Repellers in systems with infinite delay, J. Math. Anal. Appl., 137 (1989) 240-263.
- [7] Del Portillo A., Tripodi J., Najfeld V., Wodarz D., Levy D.N. and Chen B. K., Multiploid Inheritance of HIV-1 during Cell-to-Cell Infection, J. Virol., 85 (2011) 7169-7176.
- [8] Dimitrov D.S., Willey R.L., Sato H., Chang L., Blumenthal R. and Martin M.A., Quantitation of Human Immunodeficiency Virus Type 1 infection kinetics, J. Virol., Vol. 67 No. 4 (1993) 2182-2190.
- [9] Dixit N.M. and Perelson A.S., Multiplicity of Human Immunodeficiency Virus infections in lymphoid tissue, J. Virol., Vol. 78 No. 16 (2004) 8942-8945.
- [10] Hale J. K. and Kato J., Phase space for retarded equations with infinite delay, Funkcial. Ekvac., 21 (1978) 11-41.

- [11] Hale J. K. and Waltman P., Persistence in infinite-dimensional systems, *SIAM J. Math. Anal.*, 20 (1989) 388-395.
- [12] Hale J.K., Verduyn Lunel S.M., Introduction to functional differential equations, Springer-Verlag, NewYork, 1993.
- [13] Hino Y., Murakami S. and Naito T., Functional-differential equations with infinite delay, *Lecture Notes in Mathematics*, Vol. 1473, Springer-Verlag, 1991.
- [14] Hübner W., McNerney G.P., Chen P., Dale B.M., Gordan R.E., Chuang F.Y.S., Li X.D., Asmuth D.M., Huser T. and Chen B.K., Quantitative 3D video microscopy of HIV transfer across T cell virological synapses, *Science*, 323 (2009) 1743-1747.
- [15] Jung A., Maier R., Vartanian J.P., Bocharov G., Jung V., Fischer U., Meese E., Wain-Hobson S. and Meyerhans A., Multiply infected spleen cells in HIV patients, *Nature*, 418 (2002) 144.
- [16] Kajiwara T., Sasaki T. and Takeuchi Y., Construction of Lyapunov functionals for delay differential equations in virology and epidemiology, *Nonlinear Anal. Real World Appl.*, 13 (2012) 1808-1826.
- [17] Kirschner D.E. and Webb G.F., A mathematical model of combined drug therapy of HIV infection, *J. Theor. Med.*, 1 (1997) 25-34.
- [18] Komarova N.L., Anghelina D., Voznesensky I., Trinite B., Levy D.N. and Wodarz D., Relative contribution of free-virus and synaptic transmission to the spread of HIV-1 through target cell populations, *Biology Letters*, 9 (2012) 1049-1055.
- [19] Komarova N.L. Levy D.N. and Wodarz D., Effect of synaptic transmission on viral fitness in HIV infection, *PLoS ONE*, Vol. 7 No. 11 (2012) 1-11.
- [20] Komarova N.L. and Wodarz D., Virus dynamics in the presence of synaptic transmission, *Math. Biosci.*, Vol. 242 No. 2 (2013), 161-71.
- [21] Komarova N.L. Levy D.N. and Wodarz D., Synaptic transmission and the susceptibility of HIV infection to anti-viral drugs, *Scientific Reports*, 3 (2013) 1-8.
- [22] Korobeinikov A., Global properties of basic virus dynamics models, *Bull. Math. Biol.*, 66 (2004) 879-883.
- [23] Kuang Y., Delay differential equations with applications in population biology, Academic Press, San Diego, 1993.

- [24] Martin N. and Sattentau Q., Cell-to-cell HIV-1 spread and its implications for immune evasion, *Curr. Opin. HIV AIDS*, 4 (2009) 143-149.
- [25] Martin N., Welsch S., Jolly C., Briggs J., Vaux D. and Sattentau Q., Virological synapses-mediated spread of Human Immunodeficiency Virus Type 1 between T cells is sensitive to entry inhibition, *J. Virol.*, 84 (2010), 3516-3527.
- [26] McCluskey C.C., Global stability for an SEIR epidemiological model with varying infectivity and infinite delay, *Math. Biosci. Eng.*, Vol 6. No 3 (2009) 603-610.
- [27] McCluskey C.C., Complete global stability for an SIR epidemic model with delay - distributed or discrete, *Nonlinear Anal. Real World Appl.*, 11 (2010) 55-59.
- [28] Mothes W., Sherer N.M., Jin J. and Zhong P., Virus cell-to-cell transmission, *J. Virol.*, 84 (2010) 8360-8368.
- [29] Nelson P.W. and Perelson A.S., Mathematical analysis of delay differential equation models of HIV-1 infection, *Math. Biosci.*, 179 (2002) 73-94.
- [30] Nowak M. and May R., *Virus Dynamics*, Oxford University Press, Cambridge, 2000.
- [31] Perelson A., Neumann A., Markowitz M., Leonard J. and Ho D., HIV-1 dynamics in vivo: virion clearance rate, infected cell life-span, and viral generation time, *Science*, 271 (1996) 1582-1586.
- [32] Perelson A. and Nelson P., Mathematical models of HIV dynamics in vivo, *SIAM Rev.*, 41 (1999) 3-44
- [33] Permanyer M., Ballana E., Ruiz A., Badia R., Riveira-Munoz E., Gonzalo E., Clotet B. and Este J. A., Antiretroviral agents effectively block HIV replication after cell-to-cell transfer, *J. Virol.*, 86 (2012) 8773-8780.
- [34] Röst G. and Wu J., SEIR epidemiological model with varying infectivity and infinite delay, *Math. Biosci.*, Vol 5. No 2 (2008) 389-402.
- [35] Sattentau Q., Avoiding the void: cell-to-cell spread of human viruses, *Nat. Rev. Microbiol.*, 6 (2008) 28-41.
- [36] Sattentau Q., Cell-to-cell spread of retroviruses, *Viruses*, 2 (2010) 1306-1321.
- [37] Sattentau Q., The direct passage of animal viruses between cells, *Current Opinion in Virology*, 1 (2011) 396-402.

- [38] Sherer N.M., Lehmann M.J., Jimenez-Soto L.F., Horensavitz C., Pypaert M. and Mothes W., Retroviruses can establish filopodial bridges for efficient cell-to-cell transmission, *Nat. Cell Biol.*, 9 (2007) 310-315.
- [39] Sigal A., Kim J.T., Balazs A.B., Dekel E., Mayo A., Milo R. and Baltimore D., Cell-to-cell spread of HIV permits ongoing replication despite antiretroviral therapy, *Nature*, 477 (2011) 95-98.
- [40] Thieme H.R., Spectral bound and reproduction number for infinite-dimensional population structure and time heterogeneity, *SIAM J. Appl. Math.*, 70 (2009) 188-211.
- [41] Wang K., Wang W. and Liu X., Global Stability in a viral infection model with lytic and nonlytic immune response, *Computers and Mathematics with Applications*, 51 (2006) 1593-1610.
- [42] Wang K., Wang W., Pang H. and Liu X., Complex dynamic behavior in a viral model with delayed immune response, *Physica D.*, 226 (2007) 197-208.
- [43] Yuan Z. and Zou X., Global threshold dynamics in an HIV virus model with nonlinear infection rate and distributed invasion and production delays, *Math. Biosci. Eng.*, 10 (2013) 483-498.
- [44] Zhu H. and Zou X., Impact of delays in cell infection and virus production on HIV-1 dynamics, *Mathematical Medicine and Biology*, 25 (2008) 99-112.
- [45] Zhu H. and Zou X., Dynamics of a HIV-1 Infection model with cell-mediated immune response and intracellular delay, *Disc. Cont. Dyan. Syst. B.*, 12 (2009) 511-524.

Chapter 4

Modeling cell-to-cell spread of HIV-1 with logistic target cell growth

4.1 Introduction

HIV-1 has two predominant infection modes, the classical cell-free infection and direct cell-to-cell transfer. In the classical mode, viruses released from infected cells travel some distance to find a new target cell to infect. Recently, it was revealed that HIV-1 can be transferred from infected cells to uninfected cells through direct contact via some structures, for example membrane nanotubes or macromolecular adhesive contacts termed virological synapses [5, 6, 7]. During the cell-to-cell transfer, many viral particles can be simultaneously transferred from infected CD4⁺ T cells to uninfected ones.

In the preceding chapter, we incorporated the two modes of viral transmission into a classic model leading to the following model system

$$\begin{aligned}\frac{dT(t)}{dt} &= H - d_T T(t) - \beta_1 T(t)V(t) - \beta_2 T(t)T^*(t), \\ \frac{dT^*(t)}{dt} &= \int_0^\infty [\beta_1 T(t-s)V(t-s) + \beta_2 T(t-s)T^*(t-s)]e^{-ms} f(s)ds - d_{T^*} T^*(t), \\ \frac{dV(t)}{dt} &= \gamma T^*(t) - d_V V(t).\end{aligned}\tag{4.1}$$

Here $T(t)$, $T^*(t)$ and $V(t)$ are the concentrations of susceptible CD4⁺ T cells (target cells), productively infected T cells and free virus particles at time t respectively. A time delay, s , from the time of initial infection until the production of new virions, is considered, and s is assumed to be distributed according to a probability distribution $f(s)$. Target cells are infected by free virus particles and infectious cells at rates $\beta_1 T(t)V(t)$ and $\beta_2 T(t)T^*(t)$ respectively. e^{-ms} represents the survival rate of infected cells during the time delay s . Target cells are recruited

at a constant rate H . Free viruses are released by infected cells at a rate $\gamma T^*(t)$. The loss rate of target cells, productively infected cells and free virus are $d_T T(t)$, $d_{T^*} T^*(t)$ and $d_V V(t)$ respectively. We found that the basic reproduction number was underestimated by some models when only one mode of virus spread was considered. In this model, we have assumed that target T cells have a constant source term and an exponential death rate. This is mainly for the purpose of reducing the difficulty level in analyzing the model, since introduction of delay into the model has already made the model an infinite dimensional system.

It is more realistic to assume that the population of the $CD4^+$ T cells have a logistic growth function. De Boer and Perelson [3] considered the cell-free virus infection with logistic cell growth by model

$$\begin{aligned}\frac{dT(t)}{dt} &= \alpha_T T(t) \left(1 - \frac{T_{tot}}{T_{max}}\right) - (\beta + \gamma) T(t) V(t), \\ \frac{dI(t)}{dt} &= \beta T(t) V(t) - \delta_I I(t), \\ \frac{dV(t)}{dt} &= p I(t) - c V(t),\end{aligned}\tag{4.2}$$

where $T(t)$, $I(t)$ and $V(t)$ represent uninfected target cell counts, productively infected T cell counts and free HIV-1 virus loads at time t respectively. Here, target cells grow at a rate α_T and this growth is limited by a carrying capacity, T_{max} cells. T_{tot} is the total number of T cells, $T_{tot} = T + I$. β is a true infection rate and γ combines all other virus-induced depletion of the $CD4^+$ T cells. δ_I represents the turnover rate of productively infected T cells. Virus particles are produced by productively infected cells at a rate p and cleared at a per capita rate c . In this model, we see that infected cells are produced only by the route that free viruses infect uninfected T cells. Mathematical analysis of this model can be found in [4] when $\gamma = 0$. Although the notation in [4] is different from that in (4.2) and the model is about HBV, the model in [4] have the same properties as model (4.2) mathematically when $\gamma = 0$. It was found that when the basic reproduction number is less than one, the infection cannot establish. When the basic reproduction number is greater than one, the infection can persist and Hopf bifurcation may occur, that is, (4.2) has periodic solutions for some range parameters.

Culshaw *et al.* [1] studied the cell-to-cell spread of HIV-1 by model

$$\begin{aligned}\frac{dC}{dt} &= r_C C(t) \left(1 - \frac{C(t) + I(t)}{C_M}\right) - k_I C(t) I(t), \\ \frac{dI}{dt} &= k'_I \int_{-\infty}^t C(u) I(u) F(t-u) du - \mu_I I(t),\end{aligned}\tag{4.3}$$

where $C(t)$ and $I(t)$ represent the concentration of uninfected target cells and productively infectious cells respectively. Target cells assume logistic growth rate. r_C indicates the effective

reproductive rate of target cells. C_M denotes the effective carrying capacity of the system. Target cells are infected by productively infectious cells at a rate $k_I C(t) I(t)$. k_I/k'_I represents the fraction of infected cells surviving the incubation period. It is assumed here that the cells those productively infectious at time t were infected u time units ago, where u is distributed according to a probability distribution $F(u)$. For the corresponding ODE models, the positive equilibrium is globally stable, while delay models exhibit Hopf bifurcations. We see that in this model, the infection is assumed to spread directly from infected cells to target cells, neglecting cell-free virus infection.

In this chapter, we study the virus dynamics which combines diffusion-limited cell-free virus transmission and cell-to-cell transfer of HIV-1, and the effects of cell-to-cell transfer of HIV-1 on the virus dynamics with *logistic cell growth*. We use the same notation as in model (4.1), and consider the following model

$$\begin{aligned}\frac{dT(t)}{dt} &= rT(t) \left(1 - \frac{T(t) + \alpha T^*(t)}{T_M}\right) - \beta_1 T(t)V(t) - \beta_2 T(t)T^*(t), \\ \frac{dT^*(t)}{dt} &= \beta_1 T(t)V(t) + \beta_2 T(t)T^*(t) - d_{T^*} T^*(t), \\ \frac{dV(t)}{dt} &= \gamma T^*(t) - d_V V(t),\end{aligned}\tag{4.4}$$

where r is target cell growth rate, and this growth is limited by a carrying capacity of target cells, T_M . The constant α represents the limitation of infected cell imposed on the cell growth of target cells, generally $\alpha \geq 1$. In this model, we do not consider any delay effect.

For mathematical convenience, we rescale the model (4.4) by

$$\begin{aligned}u(t) &= \frac{T(t)}{T_M}, \quad w(t) = \frac{T^*(t)}{T_M}, \quad v(t) = \frac{d_{T^*}}{\gamma T_M} V(t), \quad \tilde{t} = d_{T^*} t, \\ \rho_1 &= \frac{\beta_1 \gamma T_M}{d_{T^*}^2}, \quad \rho_2 = \frac{\beta_2 T_M}{d_{T^*}}, \quad \delta = \frac{r}{d_{T^*}}, \quad \mu = \frac{d_V}{d_{T^*}},\end{aligned}$$

then the nondimensionalized model reads

$$\begin{aligned}\frac{du(t)}{dt} &= \delta u(t) [1 - u(t) - \alpha w(t)] - \rho_1 u(t)v(t) - \rho_2 u(t)w(t), \\ \frac{dw(t)}{dt} &= \rho_1 u(t)v(t) + \rho_2 u(t)w(t) - w(t), \\ \frac{dv(t)}{dt} &= w(t) - \mu v(t).\end{aligned}\tag{4.5}$$

The rest of the chapter is organized as follows. Nonnegativity and boundedness of solutions of system (4.5) are given in Section 2. Stability of the infection-free equilibrium is discussed in Section 3. Uniform persistence of the infection is shown in Section 4. Stability of the positive equilibrium and Hopf bifurcation are analyzed in Section 5. Hopf bifurcation is illustrated numerically in Section 6. In Section 7, we give our conclusion and discussion.

4.2 Nonnegativity and boundedness of solutions

Assume initial conditions for system (4.5) are given as follows:

$$u(0) = u_0 > 0, w(0) = w_0 > 0, v(0) = v_0 > 0, \text{ and } u_0 + w_0 \leq 1. \quad (4.6)$$

Since the right hand side functions of (4.5) satisfy Lipschitz condition, there is a unique solution $(u(t), w(t), v(t)) \in C([0, +\infty), \mathbb{R}_+)$ to system (4.5) with the initial condition (4.6).

Theorem 4.2.1 *Let $(u(t), w(t), v(t))$ be a solution of system (4.5) satisfying the initial condition (4.6). Then the solution is positive and bounded: $0 < u(t) \leq 1$, $0 < w(t) \leq 1$, $0 < v(t) < v_0 + \frac{1}{\mu}$, for all $t \geq 0$. Moreover, $u(t) + w(t) \leq 1$, for all $t \geq 0$.*

Proof To prove the positivity of solutions, we suppose by contradiction that t_i , $i = 1, 2, 3$, are the first times when $u(t)$, $w(t)$, $v(t)$ reach zero respectively, and $t_0 = \min\{t_1, t_2, t_3\}$.

First, if $t_0 = t_1$, we assume $t_1 \neq t_2$ and $t_1 \neq t_3$. Then $u(t_1) = 0$, $w(t_1) > 0$, $v(t_1) > 0$, and $u(t), w(t), v(t) > 0$ for all $t \in [0, t_1)$. From the first and second equations in (4.5), we observe that

$$\frac{d}{dt}[u(t) + w(t)] = \delta u(t)[1 - (u(t) + w(t))] - \delta(\alpha - 1)u(t)w(t) - w(t), \quad \forall t \in [0, t_1]. \quad (4.7)$$

It is easy to see that $u(t) + w(t) \leq 1$. In fact, for any $t^* \in [0, t_1]$ such that $u(t^*) + w(t^*) = 1$, we have

$$\frac{d}{dt}[u(t) + w(t)]|_{t=t^*} = -\delta(\alpha - 1)u(t^*)w(t^*) - w(t^*) \leq -w(t^*) < 0. \quad (4.8)$$

This means $u(t) + w(t) \leq 1$, for all $t \in [0, t_1]$. Thus we have $u(t) < 1$ and $w(t) < 1$, for $t \in [0, t_1]$. From the third equation in (4.5), we see that

$$\frac{dv(t)}{dt} \leq 1 - \mu v(t),$$

which means

$$v(t) \leq e^{-\mu t} \left[v(0) + \frac{1}{\mu}(e^{\mu t} - 1) \right] \leq v(0)e^{-\mu t} + \frac{1}{\mu}, \quad t \in [0, t_1]. \quad (4.9)$$

Again from the first equation in (4.5), we have

$$\frac{du(t)}{dt} \geq -[\rho_1 v(t) + (\rho_2 + \delta\alpha)w(t)]u(t), \quad t \in [0, t_1],$$

thus

$$u(t) \geq u(0)e^{-\int_0^t [\rho_1 v(s) + (\rho_2 + \delta\alpha)w(s)] ds}, \quad t \in [0, t_1]. \quad (4.10)$$

We know from (4.9) and (4.10) that

$$u(t_1) \geq u(0)e^{-\int_0^{t_1} [\rho_1(v(0)e^{-\mu s} + \frac{1}{\mu}) + (\rho_2 + \delta\alpha)] ds} = u(0)e^{-[v(0)\rho_1(1 - e^{-\mu t_1}) + (\rho_1 \frac{1}{\mu} + \rho_2 + \delta\alpha)t_1]} > 0,$$

which contradicts with $u(t_1) = 0$.

Secondly, if $t_0 = t_2$, $w(t_2) = 0$, $u(t_2) \geq 0$, $v(t_2) \geq 0$, and $u(t), w(t), v(t) > 0$ for $t \in [0, t_2)$, then from the second equation in (4.5), we have

$$\frac{dw(t)}{dt} \geq -w(t), \quad t \in [0, t_2],$$

thus

$$w(t_2) \geq w(0)e^{-t_2} > 0,$$

which is in contradiction with $w(t_2) = 0$. Notice that this case includes all the cases of $t_2 \neq t_1$ or $t_2 \neq t_3$ or $t_1 = t_2 \neq t_3$ or $t_2 = t_3 \neq t_1$ or $t_1 = t_2 = t_3$.

Thirdly, if $t_0 = t_3$, $v(t_3) = 0$, $u(t_3) \geq 0$, $w(t_3) \geq 0$, and $u(t), w(t), v(t) > 0$ for $t \in [0, t_3)$, then from the third equation in (4.5), we have

$$\frac{dv(t)}{dt} \geq -\mu v(t), \quad t \in [0, t_3],$$

thus

$$v(t_3) \geq v(0)e^{-\mu t_3} > 0,$$

which is in contradiction with $v(t_3) = 0$. This case includes the cases of $t_3 \neq t_1$ or $t_3 \neq t_2$ or $t_3 = t_1 \neq t_2$. So far we have considered all the cases and found a contradiction for each case. Therefore, there is no such t_i , $i = 1, 2, 3$, exist. This means $u(t), w(t), v(t) > 0$, for $t \geq 0$.

With the positivity of the solution $(u(t), w(t), v(t))$, we know that (4.7) (4.8) and (4.9) hold for all $t \geq 0$. Therefore,

$$u(t) + w(t) \leq 1, \quad v(t) \leq v(0) + \frac{1}{\mu}, \quad \forall t \geq 0.$$

This completes the proof. ■

Furthermore, from (4.9), we see that

$$v(t) \leq e^{-\mu t} \left(v(0) - \frac{1}{\mu} \right) + \frac{1}{\mu}.$$

Therefore, if $v(0) \leq \frac{1}{\mu}$, then $v(t) \leq \frac{1}{\mu}$ for all $t \geq 0$.

In fact, we can see from Lemma 4.4.1 and Lemma 4.4.2 shown later, that the set

$$\mathbb{Y} := \left\{ (u, w, v) \in \mathbb{R}^3 \mid u \geq 0, w \geq 0, v \geq 0, u + w \leq 1, v \leq \frac{1}{\mu} \right\},$$

is invariant for the solution semiflow of (4.5).

4.3 Stability of the infection-free equilibrium

For model (4.5), the basic reproduction number is given by

$$\mathcal{R}_0 = \frac{\rho_1 + \mu\rho_2}{\mu} = \mathcal{R}_{01} + \mathcal{R}_{02}, \quad \mathcal{R}_{01} = \frac{\rho_1}{\mu}, \quad \mathcal{R}_{02} = \rho_2.$$

The system (4.5) has three equilibria: the trivial equilibrium $E_0 = (0, 0, 0)$, the infection-free equilibrium $E_1 = (1, 0, 0)$ and the positive equilibrium $\bar{E} = (\bar{u}, \bar{w}, \bar{v})$, where

$$\bar{u} = \frac{\mu}{\rho_1 + \mu\rho_2} = \frac{1}{\mathcal{R}_0}, \quad \bar{w} = \frac{\delta}{\mathcal{R}_0 + \delta\alpha} \left(1 - \frac{1}{\mathcal{R}_0}\right), \quad \bar{v} = \frac{1}{\mu}\bar{w}.$$

We can easily see that for model (4.4), the basic reproduction number is $\mathcal{R}_0 = \mathcal{R}_{01} + \mathcal{R}_{02}$, where

$$\mathcal{R}_{01} = \frac{T_M\beta_1\gamma}{d_{T^*}d_V}, \quad \mathcal{R}_{02} = \frac{T_M\beta_2}{d_{T^*}}.$$

In the following, we consider stability of equilibria for model (4.5).

Theorem 4.3.1 *For system (4.5),*

- (i) *The trivial equilibrium E_0 is always unstable;*
- (ii) *If $\mathcal{R}_0 < 1$, the infection-free equilibrium E_1 is locally asymptotically stable.*
If $\mathcal{R}_0 > 1$, E_1 is unstable.

Proof To discuss local stability, we consider linearized system of (4.5). The Jacobian matrix of (4.5) at E_0 is given by

$$J_0 = \begin{pmatrix} \delta & 0 & 0 \\ 0 & -1 & 0 \\ 0 & 1 & -\mu \end{pmatrix}.$$

We see that J_0 has a positive eigenvalue $\lambda = \delta$. Therefore, E_0 is always unstable.

The Jacobian matrix of (4.5) at E_1 is given by

$$J_1 = \begin{pmatrix} -\delta & -(\delta\alpha + \rho_2) & -\rho_1 \\ 0 & \rho_2 - 1 & \rho_1 \\ 0 & 1 & -\mu \end{pmatrix}.$$

We see that it has an eigenvalue $\lambda_1 = -\delta < 0$, and other eigenvalues are given by eigenvalues of the matrix

$$J_{10} = \begin{pmatrix} \rho_2 - 1 & \rho_1 \\ 1 & -\mu \end{pmatrix},$$

that is, the roots of characteristic equation

$$\lambda^2 + a_1\lambda + a_2 = 0, \quad (4.11)$$

where

$$\begin{aligned} a_1 &= \mu + 1 - \rho_2, \\ a_2 &= \mu(1 - \rho_2) - \rho_1 = \mu(1 - \mathcal{R}_0). \end{aligned}$$

We see that if $\mathcal{R}_0 < 1$, then $a_1 > 0$, $a_2 > 0$, and all eigenvalues have negative real parts. If $\mathcal{R}_0 > 1$, then $a_2 < 0$, and J_{10} has at least one positive eigenvalue. Therefore, E_1 is locally asymptotically stable if $\mathcal{R}_0 < 1$, and unstable if $\mathcal{R}_0 > 1$. ■

Theorem 4.3.2 *If $\mathcal{R}_0 < 1$, the infection-free equilibrium E_1 is globally asymptotically stable.*

Proof We have to prove that $\lim_{t \rightarrow +\infty} (u, w, v) = (1, 0, 0)$. Since $u(t) \leq 1$ for all $t \geq 0$, we have

$$\begin{aligned} \frac{dw(t)}{dt} &\leq \rho_1 v(t) + \rho_2 w(t) - w(t), \\ \frac{dv(t)}{dt} &\leq w(t) - \mu v(t). \end{aligned}$$

For the linear cooperative system

$$\begin{aligned} \frac{d\tilde{w}(t)}{dt} &= \rho_1 \tilde{v}(t) + \rho_2 \tilde{w}(t) - \tilde{w}(t), \\ \frac{d\tilde{v}(t)}{dt} &= \tilde{w}(t) - \mu \tilde{v}(t), \end{aligned} \quad (4.12)$$

there exists a principal eigenvalue λ_0 associated with strictly positive eigenvector ξ_0 . It then follows that the linear system (4.12) admits a solution $(\tilde{w}, \tilde{v}) = e^{\lambda_0 t} \xi_0$. By the comparison principle, it follows that

$$(w, v) \leq e^{\lambda_0 t} \xi_0, \quad \forall t \geq 0.$$

From (4.11), we see that $\lambda_0 < 0$ if $\mathcal{R}_0 < 1$. Therefore, if $\mathcal{R}_0 < 1$, we have

$$\lim_{t \rightarrow +\infty} w(t) = 0, \quad \lim_{t \rightarrow +\infty} v(t) = 0.$$

Then the first equation in (4.5) is asymptotic to the following equation

$$\frac{d\tilde{u}(t)}{dt} = \delta \tilde{u}(t)[1 - \tilde{u}(t)],$$

which is the logistic equation. It is easy to see that $\lim_{t \rightarrow +\infty} \tilde{u}(t) = 1$. By the asymptotic autonomous semiflow theory (Corollary 4.3 in [11]), we have

$$\lim_{t \rightarrow +\infty} u(t) = 1.$$

Thus, if $\mathcal{R}_0 < 1$, then

$$(u, w, v) \rightarrow (1, 0, 0), \quad \text{as } t \rightarrow +\infty.$$

This completes the proof the theorem. ■

4.4 Uniform persistence of infection

Notice that when $u_0 = 0$, the unique solution of (4.5)-(4.6) is given by

$$u(t) = 0, \quad w(t) = w_0 e^{-t}, \quad v(t) = e^{-\mu t} \left[v_0 + w_0 \int_0^t e^{(\mu-1)s} ds \right], \quad \forall t > 0. \quad (4.13)$$

We see that $w(t) \rightarrow 0$ and $v(t) \rightarrow 0$ as $t \rightarrow +\infty$. Therefore, if $u_0 = 0$, the system cannot be persistent. To discuss the persistence of system (4.5), we consider the following solution space:

$$\mathbb{X} := \left\{ (u, w, v) \in \mathbb{R}^3 \mid u > 0, w \geq 0, v \geq 0, u + w \leq 1, v \leq \frac{1}{\mu} \right\},$$

the interior subspace of \mathbb{X} :

$$\mathbb{X}_0 := \{(u, w, v) \in \mathbb{X} \mid w > 0 \text{ and } v > 0\},$$

the boundary of \mathbb{X}_0 :

$$\partial\mathbb{X}_0 := \mathbb{X} \setminus \mathbb{X}_0 = \{(u, w, v) \in \mathbb{X} \mid w = 0 \text{ or } v = 0\},$$

and

$$M_\partial := \{(u_0, w_0, v_0) \in \partial\mathbb{X}_0 \mid \Phi_t(u_0, w_0, v_0) \in \partial\mathbb{X}_0, t \geq 0\},$$

where Φ_t is the solution semiflow defined by (4.5).

Lemma 4.4.1 *The sets \mathbb{X} and \mathbb{X}_0 are positively invariant for the solution semiflow Φ_t defined by (4.5). Moreover,*

$$M_\partial = \{(\hat{u}, 0, 0) \mid 0 < \hat{u} \leq 1\}.$$

Proof When $u_0 > 0$, we consider the different cases of w_0 and v_0 :

(i) If $w_0 = 0$ and $v_0 = 0$, then

$$u(t) = \frac{u_0}{u_0 + [1 - u_0]e^{-\delta t}} > 0, \quad w(t) = 0, \quad v(t) = 0, \quad \forall t \geq 0. \quad (4.14)$$

(ii) If $w_0 = 0$ and $v_0 > 0$, then

$$\frac{d}{dt}w(0) = \rho_1 u(0)v(0) = \rho_1 u_0 v_0 > 0.$$

Thus, for small $\varepsilon > 0$, $w(t) > 0$ for $t \in (0, \varepsilon)$. We assume t_2 to be the first time when $w(t)$ reaches zero other than $t = 0$. By the same argument as the proof of Theorem 4.2.1, we obtain that $u(t) > 0$, $w(t) > 0$ and $v(t) > 0$.

(iii) If $w_0 > 0$ and $v_0 = 0$, then

$$\frac{d}{dt}v(0) = w(0) = w_0 > 0.$$

Like case (ii), it follows that $u(t) > 0$, $w(t) > 0$ and $v(t) > 0$.

(iv) If $w_0 > 0$ and $v_0 > 0$, from Theorem 4.2.1, we have $u(t) > 0$, $w(t) > 0$ and $v(t) > 0$.

In summary, sets \mathbb{X} and \mathbb{X}_0 are positively invariant for the solution semiflow Φ_t defined by (4.5). Moreover,

$$M_\partial = \{(\hat{u}, 0, 0) \mid 0 < \hat{u} \leq 1\}.$$

This completes the proof of the lemma. \blacksquare

Lemma 4.4.2 *If $\mathcal{R}_0 > 1$, there exists an $\eta_0 > 0$ such that the solution $(u(t), w(t), v(t))$ of (4.5) with initial value $(u_0, w_0, v_0) \in \mathbb{X}_0$ satisfies*

$$\limsup_{t \rightarrow \infty} \|(u(t), w(t), v(t)) - (u_1, 0, 0)\| \geq \eta_0,$$

where $u_1 = 1$.

Proof We see that J_{10} is a quasi-positive matrix. By Corollary 4.3.2 in [8], $\lambda_0(u_1) = \max\{\operatorname{Re} \lambda \mid \lambda \in \sigma(J_{10})\}$ is an eigenvalue of J_{10} , called the principle eigenvalue, where $\sigma(J_{10})$ is the set of eigenvalues of matrix J_{10} . From Theorem 4.3.1, we know that if $\mathcal{R}_0 > 1$, then $\lambda_0(u_1) > 0$. By continuity, we have $\lambda_0(u_1 - \eta_0) > 0$, for sufficiently small η_0 . To prove the lemma, we suppose by contradiction that given any $\varepsilon > 0$,

$$\limsup_{t \rightarrow \infty} \|(u(t), w(t), v(t)) - (u_1, 0, 0)\| < \varepsilon,$$

for a solution with some initial value $(u_0, w_0, v_0) \in \mathbb{X}_0$. In particular,

$$\limsup_{t \rightarrow \infty} \|(u(t), w(t), v(t)) - (u_1, 0, 0)\| < \eta_0,$$

for a solution with some initial value $(u_0, w_0, v_0) \in \mathbb{X}_0$. Then for this solution, there exists a $t_0 > 0$ such that $u(t) > u_1 - \eta_0$, $w(t) < \eta_0$, $v(t) < \eta_0$, for $t > t_0$. Thus, from the second equation in (4.5), we have

$$\frac{dw(t)}{dt} \geq \rho_1(u_1 - \eta_0)v(t) + \rho_2(u_1 - \eta_0)w(t) - w(t).$$

It is easy to see that $\lambda_0(u_1 - \eta_0)$ is the principal eigenvalue of the linear cooperative system

$$\begin{aligned} \frac{d\tilde{w}(t)}{dt} &= \rho_1(u_1 - \eta_0)\tilde{v}(t) + \rho_2(u_1 - \eta_0)\tilde{w}(t) - \tilde{w}(t), \\ \frac{d\tilde{v}(t)}{dt} &= \tilde{w}(t) - \mu\tilde{v}(t). \end{aligned} \quad (4.15)$$

Let $(\xi_1, \xi_2)^T$ be the strictly positive eigenvector associated with $\lambda_0(u_1 - \eta_0)$, then $(\tilde{w}, \tilde{v})^T = e^{\lambda_0(u_1 - \eta_0)t}(\xi_1, \xi_2)^T$ is a solution of (4.15). Since $w(t) > 0$, $v(t) > 0$, there exists a $\zeta > 0$, such that $(w(t_0), v(t_0))^T \geq \zeta(\tilde{w}(t_0), \tilde{v}(t_0))^T$. By the comparison principle, we have

$$(w(t), v(t))^T \geq \zeta e^{\lambda_0(u_1 - \eta_0)t}(\xi_1, \xi_2)^T, \forall t \geq t_0.$$

Since $\lambda_0(u_1 - \eta_0) > 0$, it follows that $w(t)$ and $v(t)$ are unbounded. Thus we obtain the contradiction and prove the lemma. ■

Theorem 4.4.3 *For system (4.5), if $\mathcal{R}_0 > 1$, the infection is uniformly persistent with respect to $(\mathbb{X}_0, \partial\mathbb{X}_0)$, in the sense that there exists an $\eta > 0$ such that*

$$\liminf_{t \rightarrow \infty} w(t) \geq \eta, \quad \liminf_{t \rightarrow \infty} v(t) \geq \eta. \quad (4.16)$$

Proof By Lemma 4.4.1, \mathbb{X}_0 is positively invariant for the solution semiflow Φ_t defined by (4.5). Furthermore, Φ_t is compact and point dissipative. By Theorem 1.1.3 in [15], there is a global attractor A for Φ_t .

Let $M = (1, 0, 0)$. From the proof of Lemma 4.4.1, we know that M_θ is the maximal compact invariant set in $\partial\mathbb{X}_0$. From (4.14), we see that $\cup_{x \in M_\theta} \omega(x) = \{M\}$. Lemma 4.4.2 implies that M is an isolated invariant set in \mathbb{X} , and $W^s(M) \cap \mathbb{X}_0 = \emptyset$, where $W^s(M)$ is the stable set of M . Furthermore, there is no cycle in M_θ from M to M .

Define a continuous function $p : \mathbb{X} \rightarrow \mathbb{R}_+$ by

$$p(x) = \min\{w_0, v_0\}, \quad \forall x = (u_0, w_0, v_0) \in \mathbb{X}.$$

Then from Lemma 4.4.1, we see that $p^{-1}(0, \max\{1, 1/\mu\}) \subset \mathbb{X}_0$, and that $p(x) > 0$ for $x \in \mathbb{X}_0$. Moreover, if $p(x) > 0$, then $x \in \mathbb{X}_0$. Thus, p is a generalized distance function for the semiflow $\Phi_t : \mathbb{X} \rightarrow \mathbb{X}$. It follows from Theorem 3 in [9] that there exists an $\eta > 0$ such that

$$\min_{x \in \omega(y)} p(x) > \eta, \quad \forall y \in \mathbb{X}_0.$$

Therefore,

$$\liminf_{t \rightarrow \infty} w(t) \geq \eta, \quad \liminf_{t \rightarrow \infty} v(t) \geq \eta,$$

which completes the proof the theorem. ■

Remark If $\mathcal{R}_0 > 1$, the target cell population $u(t)$ is uniformly weakly persistent in the sense that there exists some $\eta > 0$ such that

$$\limsup_{t \rightarrow \infty} u(t) \geq \eta. \quad (4.17)$$

In fact, if (4.17) is not true, then by the definition $\limsup_{t \rightarrow \infty} u(t) = \lim_{t \rightarrow \infty} \sup_{\tau \geq t} u(\tau)$, for any $\varepsilon > 0$ there exists a $t_1 > 0$ such that $\sup_{\tau \geq t_1} u(\tau) < \varepsilon$, thus $u(t) < \varepsilon$ for $t \geq t_1$. This means $\lim_{t \rightarrow \infty} u(t) = 0$. In this case, the second equation in (4.5) is asymptotic to the following equation

$$\frac{d\tilde{w}(t)}{dt} = -\tilde{w}(t),$$

which has only one equilibrium $\tilde{w} = 0$. By the asymptotic autonomous semiflow theory (Corollary 4.3 in [11]), $w(t) \rightarrow 0$ as $t \rightarrow \infty$. Similarly, from the third equation in (4.5), $v(t) \rightarrow 0$ as $t \rightarrow \infty$. These contradict with (4.16), that is, the uniform persistence of $w(t)$ and $v(t)$.

4.5 Stability of the positive equilibrium \bar{E} and Hopf bifurcation

In this section we consider stability of the positive equilibrium \bar{E} . Noticing that

$$\delta(1 - 2\bar{u} - \alpha\bar{w}) - \rho_1\bar{v} - \rho_2\bar{w} = -\delta\bar{u} = -\frac{\delta}{\mathcal{R}_0},$$

$$\rho_1\bar{v} + \rho_2\bar{w} = \left(\frac{\rho_1}{\mu} + \rho_2\right)\bar{w} = \frac{\delta(\mathcal{R}_0 - 1)}{\mathcal{R}_0 + \delta\alpha},$$

$$\mu(1 - \rho_2\bar{u}) - \rho_1\bar{u} = \mu - (\rho_2\mu + \rho_1)\frac{1}{\mathcal{R}_0} = 0,$$

the Jacobian matrix of (4.5) at \bar{E} is given by

$$\bar{J} = \begin{pmatrix} -\frac{\delta}{\mathcal{R}_0} & -\left(\frac{\delta\alpha}{\mathcal{R}_0} + \rho_2\bar{u}\right) & -\rho_1\bar{u} \\ \rho_1\bar{v} + \rho_2\bar{w} & \rho_2\bar{u} - 1 & \rho_1\bar{u} \\ 0 & 1 & -\mu \end{pmatrix}.$$

The corresponding characteristic equation is

$$\lambda^3 + b_1\lambda^2 + b_2\lambda + b_3 = 0, \quad (4.18)$$

where

$$\begin{aligned} b_1 &= \frac{\delta}{\mathcal{R}_0} + \mu + 1 - \frac{\rho_2}{\mathcal{R}_0} = \frac{\delta}{\mathcal{R}_0} + \mu + \frac{\mathcal{R}_{01}}{\mathcal{R}_0} > 0, \\ b_2 &= \frac{\delta}{\mathcal{R}_0}(1 - \rho_2\bar{u} + \mu) + \mu(1 - \rho_2\bar{u}) - \rho_1\bar{u} + (\rho_1\bar{v} + \rho_2\bar{w})\left(\frac{\delta\alpha}{\mathcal{R}_0} + \rho_2\bar{u}\right) \\ &= \frac{\delta}{\mathcal{R}_0}\left(1 + \mu - \frac{\rho_2}{\mathcal{R}_0}\right) + \frac{\delta(\mathcal{R}_0 - 1)}{\mathcal{R}_0 + \delta\alpha}\left(\frac{\delta\alpha}{\mathcal{R}_0} + \frac{\rho_2}{\mathcal{R}_0}\right) \\ &= \frac{\delta}{\mathcal{R}_0}\left(\mu + \frac{\mathcal{R}_{01}}{\mathcal{R}_0}\right) + \frac{\delta}{\mathcal{R}_0}\frac{\mathcal{R}_{02} + \delta\alpha}{\mathcal{R}_0 + \delta\alpha}(\mathcal{R}_0 - 1) > 0, \\ b_3 &= \frac{\delta}{\mathcal{R}_0}(1 - \rho_2\bar{u})\mu + \rho_1\bar{u}(\rho_1\bar{v} + \rho_2\bar{w}) - \rho_1\bar{u}\frac{\delta}{\mathcal{R}_0} + \mu(\rho_1\bar{v} + \rho_2\bar{w})\left(\frac{\delta\alpha}{\mathcal{R}_0} + \rho_2\bar{u}\right) \\ &= (\rho_1\bar{v} + \rho_2\bar{w})\left[\rho_1\bar{u} + \mu\left(\frac{\delta\alpha}{\mathcal{R}_0} + \rho_2\bar{u}\right)\right] \\ &= \frac{\delta(\mathcal{R}_0 - 1)}{\mathcal{R}_0 + \delta\alpha}\left(\frac{\delta\alpha}{\mathcal{R}_0} + 1\right)\mu \\ &= \frac{\delta\mu}{\mathcal{R}_0}(\mathcal{R}_0 - 1) > 0, \end{aligned}$$

$$\begin{aligned}
& b_1 b_2 - b_3 \\
&= \frac{\delta}{\mathcal{R}_0} \left\{ \left(\frac{\delta}{\mathcal{R}_0} + \mu + \frac{\mathcal{R}_{01}}{\mathcal{R}_0} \right) \left[\left(\mu + \frac{\mathcal{R}_{01}}{\mathcal{R}_0} \right) + \frac{\mathcal{R}_{02} + \delta\alpha}{\mathcal{R}_0 + \delta\alpha} (\mathcal{R}_0 - 1) \right] - \mu (\mathcal{R}_0 - 1) \right\} \\
&= \frac{\delta}{\mathcal{R}_0} \left\{ \left(\frac{\delta}{\mathcal{R}_0} + \frac{\mathcal{R}_{01}}{\mathcal{R}_0} \right) \left[\left(\mu + \frac{\mathcal{R}_{01}}{\mathcal{R}_0} \right) + \frac{\mathcal{R}_{02} + \delta\alpha}{\mathcal{R}_0 + \delta\alpha} (\mathcal{R}_0 - 1) \right] + \mu \left(\mu + \frac{\mathcal{R}_{01}}{\mathcal{R}_0} \right) - \mu \frac{\mathcal{R}_{01}}{\mathcal{R}_0 + \delta\alpha} (\mathcal{R}_0 - 1) \right\} \\
&= \frac{\delta}{\mathcal{R}_0} \left\{ \left(\frac{\delta}{\mathcal{R}_0} + \frac{\mathcal{R}_{01}}{\mathcal{R}_0} \right) \frac{\mathcal{R}_{02} + \delta\alpha}{\mathcal{R}_0 + \delta\alpha} (\mathcal{R}_0 - 1) + \frac{\delta}{\mathcal{R}_0} \left(\mu + \frac{\mathcal{R}_{01}}{\mathcal{R}_0} \right) + \left(\mu + \frac{\mathcal{R}_{01}}{\mathcal{R}_0} \right)^2 - \mu \frac{\mathcal{R}_{01}}{\mathcal{R}_0 + \delta\alpha} (\mathcal{R}_0 - 1) \right\} \\
&= \frac{\delta\mu}{\rho_1 + \mu\rho_2} \left\{ \left(\frac{\delta\mu}{\rho_1 + \mu\rho_2} + \frac{\rho_1}{\rho_1 + \mu\rho_2} \right) \frac{\rho_2 + \delta\alpha}{\rho_1 + \mu\rho_2 + \mu\delta\alpha} (\rho_1 + \mu\rho_2 - \mu) \right. \\
&\quad \left. + \frac{\delta\mu}{\rho_1 + \mu\rho_2} \left(\mu + \frac{\rho_1}{\rho_1 + \mu\rho_2} \right) + \left(\mu + \frac{\rho_1}{\rho_1 + \mu\rho_2} \right)^2 - \frac{\rho_1}{\rho_1 + \mu\rho_2 + \mu\delta\alpha} (\rho_1 + \mu\rho_2 - \mu) \right\}.
\end{aligned}$$

We denote

$$b_1(p)b_2(p) - b_3(p) = G(p)F(p),$$

where

$$\begin{aligned}
p &= (\rho_1, \rho_2, \mu, \delta, \alpha), \\
G(p) &= \frac{\delta\mu}{(\rho_1 + \mu\rho_2)^3 (\rho_1 + \mu\rho_2 + \mu\delta\alpha)}, \\
F(p) &= (\delta\mu + \rho_1)(\rho_1 + \mu\rho_2)(\rho_2 + \delta\alpha)(\rho_1 + \mu\rho_2 - \mu) + \delta\mu[\mu(\rho_1 + \mu\rho_2) + \rho_1][(\rho_1 + \mu\rho_2) + \mu\delta\alpha] \\
&\quad + [\mu(\rho_1 + \mu\rho_2) + \rho_1]^2 [(\rho_1 + \mu\rho_2) + \mu\delta\alpha] - \rho_1(\rho_1 + \mu\rho_2)^2 (\rho_1 + \mu\rho_2 - \mu).
\end{aligned}$$

We see that if $\mathcal{R}_0 > 1$, then $b_i > 0$, $i = 1, 2, 3$. Thus, if $b_1 b_2 - b_3 > 0$ then \bar{E} is locally asymptotically stable by the Routh-Hurwitz criterion, and if $b_1 b_2 - b_3 < 0$, \bar{E} is unstable. Since $G(p) > 0$, the sign of $b_1(p)b_2(p) - b_3(p)$ is determined by the sign of $F(p)$. If there is a $\bar{p} = (\bar{\rho}_1, \bar{\rho}_2, \bar{\mu}, \bar{\delta}, \bar{\alpha})$ such that $F(\bar{p}) = 0$, then there is a Hopf bifurcation at \bar{E} , by Theorem 2 in [14]. In fact, when $p = \bar{p}$, we have $b_3(\bar{p}) = b_1(\bar{p})b_2(\bar{p})$, and further the characteristic equation (4.18) has a negative root $\bar{\lambda}_1 = -b_1(\bar{p})$ and a pair of pure imaginary roots $\bar{\lambda}_{2,3} = \pm i \sqrt{b_2(\bar{p})}$.

First, we consider Hopf bifurcation at \bar{E} choosing ρ_1 as the bifurcation parameter, that is, the parameters $(\rho_2, \mu, \delta, \alpha)$ are fixed at $(\bar{\rho}_2, \bar{\mu}, \bar{\delta}, \bar{\alpha})$ while ρ_1 changes near $\bar{\rho}_1$. Then $F(p)$ is a function of ρ_1 , which can be expressed in the following form

$$\begin{aligned}
& F(\rho_1) \\
&= -\rho_1^4 + (\delta\alpha + \rho_2 + 1 - 3\mu\rho_2 + \mu^2 + 3\mu)\rho_1^3 \\
&\quad + (3\mu^3\rho_2 + \mu^3\delta\alpha + \delta\mu\rho_2 + \delta\mu^2 + 2\rho_2^2\mu + 2\delta\alpha\mu\rho_2 + \delta\mu + \delta^2\mu\alpha + 6\mu^2\rho_2 + 2\mu^2\delta\alpha - 3\rho_2^2\mu^2)\rho_1^2 \\
&\quad + (\delta\alpha\mu^2\rho_2^2 + 2\delta\mu^2\rho_2^2 + \delta^2\mu^3\alpha + 2\delta^2\mu^2\alpha\rho_2 - \rho_2^2\mu^2 + 2\delta\mu^3\rho_2 - \delta\alpha\mu^2\rho_2 + 2\mu^4\rho_2\delta\alpha \\
&\quad + 3\mu^4\rho_2^2 + \rho_2^3\mu^2 + 3\mu^3\rho_2^2 - \mu^3\rho_2^3 + 2\mu^3\rho_2\delta\alpha)\rho_1 \\
&\quad - \delta^2\mu^3\alpha\rho_2 + \mu^5\rho_2^3 + \delta\mu^3\rho_2^3 + b^2\mu^3\alpha\rho_2^2 - \delta\mu^3\rho_2^2 + \delta\mu^4\rho_2^2 + \mu^5\rho_2^2\delta\alpha + \delta^2\mu^4\rho_2\alpha,
\end{aligned}$$

where we omit the bar of $(\bar{\rho}_2, \bar{\mu}, \bar{\delta}, \bar{\alpha})$ for notational convenience. We see that if $\rho_1 = 0$, then $\mathcal{R}_0 = \rho_2 > 1$, and

$$F(0) = \mu^3 \rho_2 (\rho_2 + \delta \alpha) [\delta (\rho_2 - 1) + \mu^2 \rho_2 + \delta \mu] > 0.$$

On the other hand, $\lim_{\rho_1 \rightarrow +\infty} F(\rho_1) = -\infty$. Therefore, $F(\rho_1) = 0$ has at least one positive root.

Proposition 4.5.1 *Assume that parameters $(\rho_2, \mu, \delta, \alpha)$ are fixed. If $\mathcal{R}_0 > 1$ and $F(\rho_1) > 0$, then \bar{E} is locally asymptotically stable. If there exists a critical value $\bar{\rho}_1 > 0$ such that $\mathcal{R}_0 > 1$ and $F(\bar{\rho}_1) = 0$, then a Hopf bifurcation occurs at \bar{E} when ρ_1 passes through the critical value $\bar{\rho}_1$.*

By the similar arguments, we can obtain the following results about different bifurcation parameters.

Proposition 4.5.2 *Assume that parameters $(\rho_1, \mu, \delta, \alpha)$ are fixed. If $\mathcal{R}_0 > 1$ and $F(\rho_2) > 0$, then \bar{E} is locally asymptotically stable. If there exists a critical value $\bar{\rho}_2 > 0$ such that $\mathcal{R}_0 > 1$ and $F(\bar{\rho}_2) = 0$, then a Hopf bifurcation occurs at \bar{E} when ρ_2 passes through the critical value $\bar{\rho}_2$. Here, $F(p)$ is a function of ρ_2 :*

$$\begin{aligned} & F(\rho_2) \\ = & (\rho_1 \mu^2 + \mu^5 + \mu^3 \delta - \mu^3 \rho_1) \rho_2^3 \\ & + (\mu^2 \delta \alpha \rho_1 + \delta^2 \mu^3 \alpha - \rho_1 \mu^2 + 3\mu^3 \rho_1 + 2\rho_1^2 \mu - \mu^3 \delta + \delta \mu^4 + 2\delta \mu^2 \rho_1 + \mu^5 \delta \alpha + 3\mu^4 \rho_1 - 3\mu^2 \rho_1^2) \rho_2^2 \\ & + (2\mu^3 \rho_1 \delta \alpha + \delta \mu \rho_1^2 + 2\rho_1 \delta^2 \mu^2 \alpha + 2\rho_1^2 \mu \delta \alpha + 2\mu^4 \rho_1 \delta \alpha + \delta^2 \mu^4 \alpha - \delta^2 \mu^3 \alpha - \mu^2 \delta \alpha \rho_1 + \rho_1^3 \\ & + 3\mu^3 \rho_1^2 + 6\mu^2 \rho_1^2 - 3\mu \rho_1^3 + 2\delta \mu^3 \rho_1) \rho_2 \\ & + \rho_1^3 + \delta \mu \rho_1^2 + \delta^2 \mu \alpha \rho_1^2 + \mu^2 \rho_1^3 + \mu^3 \rho_1^2 \delta \alpha - \rho_1^4 + \delta^2 \mu^3 \rho_1 \alpha + 2\mu^2 \rho_1^2 \delta \alpha + \delta \mu^2 \rho_1^2 + 3\mu \rho_1^3 + \rho_1^3 \delta \alpha, \end{aligned}$$

where we also omit the bar of $(\bar{\rho}_2, \bar{\mu}, \bar{\delta}, \bar{\alpha})$ for notational convenience.

4.6 Numerical simulation

We choose the baseline parameters in model (4.4) as $r = 0.1$, $T_M = 1000$, $d_{T^*} = 0.4$, $\gamma = 850$ and $d_V = 3$ [2, 10]. Then for model (4.5), we have $\delta = 0.25$, $\mu = 7.5$. We set $\alpha = 1.2$ and use ρ_1 and ρ_2 as bifurcation parameters.

Notice that if $\rho_1 = 0$, then $\mathcal{R}_0 = \rho_2$ and

$$b_1 b_2 - b_3 = \frac{\delta}{\rho_2^2} [\delta (\rho_2 - 1) + \delta \mu + \mu^2 \rho_2].$$

Thus, if $\mathcal{R}_0 = \rho_2 > 1$, $b_1 b_2 - b_3 > 0$. Therefore, \bar{E} is locally asymptotically stable for all $\delta, \alpha, \mu > 0$, $\rho_2 > 1$ and $\rho_1 = 0$. This is the case when there is only cell-to-cell transmission, which is considered by Culshaw *et al.* [1] for $\alpha = 1$.

When $\rho_1 > 0$, the surface $F(\rho_1, \rho_2)$ is shown in Figure 4.1. We see that \bar{E} is also locally asymptotically stable, when ρ_1 and ρ_2 satisfy $\mathcal{R}_0 > 1$, $\rho_1 < \bar{\rho}_1$ and $\rho_2 < \bar{\rho}_2$, where $(\bar{\rho}_1, \bar{\rho}_2)$ is at the intersection curve of the two surface in Figure 4.1, $F(\bar{\rho}_1, \bar{\rho}_2) = 0$.

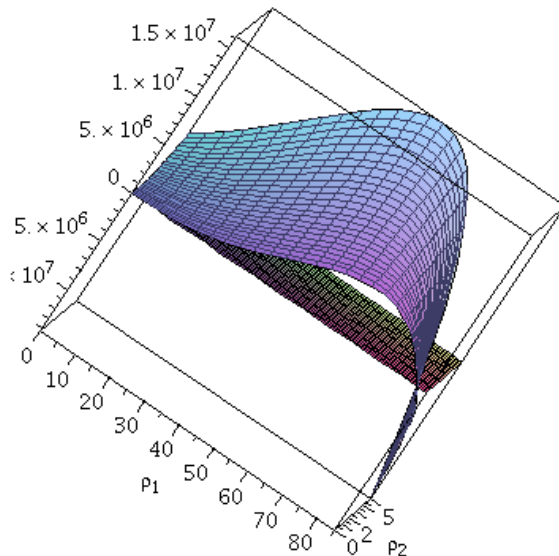


Figure 4.1: The surface of $F(\rho_1, \rho_2)$, when $\delta = 0.2$, $\alpha = 1.2$, $\mu = 10$.

First, we consider ρ_1 as a bifurcation parameter. Assume $\beta_2 = 0.65 \times 10^{-3}$, then $\rho_2 = 1.625$. When the parameters are fixed at $\delta = 0.25$, $\alpha = 1.2$, $\mu = 7.5$ and $\rho_2 = 1.625$, $F(\rho_1) = 0$ has a positive root $\rho_1 = 79.98204093$, a negative root $\rho_1 = -13.50810411$ and a pair of conjugate complex roots $\rho_1 = -10.68071841 \pm 0.2299679133i$. Thus $\bar{\rho}_1 = 79.98204093$ is a critical value for bifurcation. Since $\mathcal{R}_0 \geq \rho_2 > 1$, we see that if $0 \leq \rho_1 < \bar{\rho}_1$, \bar{E} is locally asymptotically stable, while it is unstable if $\rho_1 \geq \bar{\rho}_1$ (see Figure 4.3 and Figure 4.4). When $\rho_1 = \bar{\rho}_1$, there is a Hopf bifurcation, and a family of periodic solutions bifurcate from \bar{E} (see Figure 4.5).

When $\rho_1 = \bar{\rho}_1$, \bar{J} has a pair of pure imaginary eigenvalues $\lambda = \pm 0.4531462285 i$ and a negative real eigenvalue $\lambda = -8.3881137969$. In the following, we determine the bifurcation direction and stability, magnitudes and periods of the bifurcated periodic solutions by applying the normal form theory and Maple program developed by Yu [13] using computer algebra system. First we transform the fixed point to the origin and let $\rho_1 = \bar{\rho}_1 + \varepsilon$, and then transform the Jacobian matrix of system (4.5) evaluated at the trivial equilibrium solution to Jordan canonical form. By the linear transformation

$$\begin{pmatrix} u \\ w \\ v \end{pmatrix} = \begin{pmatrix} \bar{u} \\ \bar{w} \\ \bar{v} \end{pmatrix} + P \begin{pmatrix} x_1 \\ x_2 \\ x_3 \end{pmatrix}, \quad (4.19)$$

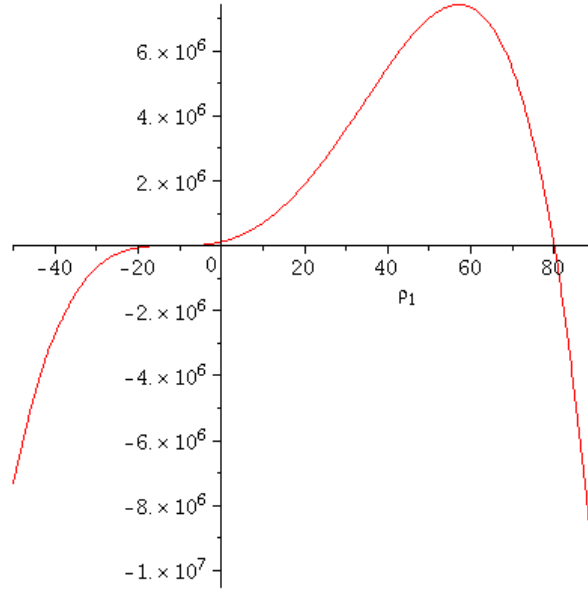


Figure 4.2: The function $F(\rho_1)$ has only positive root $\bar{\rho}_1 = 79.98204093$.

where

$$\begin{pmatrix} \bar{u} \\ \bar{w} \\ \bar{v} \end{pmatrix} = \begin{pmatrix} 0.08137178429 \\ 0.01824228214 \\ 0.002432304285 \end{pmatrix}, \quad P = \begin{pmatrix} 0.9127757680 & 0.0000000000 & 0.4946210560 \\ 0.0025286175 & -0.4048829165 & -0.5771230032 \\ -0.0029139233 & -0.0538083311 & 0.6498300164 \end{pmatrix},$$

system (4.5) is transformed to

$$\frac{dx_i}{d\tau} = F_i(x_1, x_2, x_3; \varepsilon), \quad i = 1, 2, 3, \quad (4.20)$$

where

$$\begin{aligned} F_1 = & 0.4531462284x_2 + \varepsilon(-0.0001967387 - 0.0019711916x_1 + 0.0043523250x_2 \\ & -0.053757844x_3) + \varepsilon(0.0488215521x_1x_2 - 0.5881732311x_1x_3 + 0.0264557501x_3x_2 \\ & +0.0026438705x_1^2 - 0.3194996052x_3^2) + O(\varepsilon) \\ & -0.0206649222x_1^2 - 46.2688096803x_1x_3 + 4.6229780433x_1x_2 \\ & -25.0663848848x_3^2 + 2.5051303527x_3x_2, \end{aligned}$$

$$\begin{aligned} F_2 = & -0.4531462284x_1 + \varepsilon(-0.0004372035 - 0.0043804908x_1 + 0.0096719770x_2 \\ & -0.1194636492x_3) + \varepsilon(0.1084939488x_1x_2 - 1.3070710312x_1x_3 + 0.0587914287x_3x_2 \\ & +0.0058753550x_1^2 - 0.7100096645x_3^2) + O(\varepsilon) \\ & +0.4616677914x_1^2 - 102.6557485267x_1x_3 + 10.0041479776x_1x_2 \\ & -55.7633503054x_3^2 + 5.4211148132x_3x_2, \end{aligned}$$

$$\begin{aligned}
F_3 = & -8.3881137969x_3 + \varepsilon(-0.0000370843 - 0.0003715599x_1 + 0.0008203919x_2 \\
& -0.0101330897x_3) + \varepsilon(0.0092026229x_1x_2 - 0.1108677664x_1x_3 + 0.0049867790x_3x_2 \\
& +0.0004983566x_1^2 - 0.0602241070x_3^2) + O(\varepsilon) \\
& +0.0381351380x_1^2 - 8.7077514501x_1x_3 + 0.8491105307x_1x_2 \\
& -4.7298128146x_3^2 + 0.4601217101x_3x_2.
\end{aligned}$$

It is easy to see that the Jacobian matrix of system (4.20) at $x = (0, 0, 0)$ is in the Jordan canonical form

$$J = \begin{pmatrix} 0 & 0.4531462284 & 0 \\ -0.4531462284 & 0 & 0 \\ 0 & 0 & -8.3881137969 \end{pmatrix}. \quad (4.21)$$

The general normal form can be written in polar coordinates as

$$\begin{aligned}
\frac{dr}{d\tau} &= r(\nu_0\varepsilon + \nu_1r^2) + O(\varepsilon^2r, \varepsilon r^3, r^5), \\
\frac{d\theta}{d\tau} &= \omega_0 + \tau_0\varepsilon + \tau_1r^2 + O(\varepsilon^2, \varepsilon r^2, r^4).
\end{aligned}$$

For system (4.20), $\omega_0 = 0.4531462284$ corresponds to the pair of the pure imaginary eigenvalues. ν_0 and τ_0 can be found from linear analysis. By the theory in [12], we have

$$\begin{aligned}
\nu_0 &= \frac{1}{2} \left(\frac{\partial^2 F_1}{\partial x_1 \partial \varepsilon} + \frac{\partial^2 F_2}{\partial x_2 \partial \varepsilon} \right) \Big|_{\varepsilon=0, x_i=0} \\
&= (0.0048359885 + 0.0542469744x_1 + 0.0293957144x_3) \Big|_{x_i=0} \\
&= 0.0048359885, \\
\tau_0 &= \frac{1}{2} \left(\frac{\partial^2 F_1}{\partial x_2 \partial \varepsilon} - \frac{\partial^2 F_2}{\partial x_1 \partial \varepsilon} \right) \Big|_{\varepsilon=0, x_i=0} \\
&= (0.0021902454 - 0.0542469744x_2 + 0.6535355156x_3 - 0.0058753550x_1) \Big|_{x_i=0} \\
&= 0.0021902454.
\end{aligned}$$

On the other hand, ν_1 and τ_1 are determined by nonlinear analysis. Applying the Maple program developed in [13] to system (4.20), setting $\varepsilon = 0$, we obtain

$$\nu_1 = -0.09674296998, \quad \tau_1 = -2.380920393.$$

Therefore, the normal form of the system (4.20) up to third order is given by

$$\begin{aligned}
\frac{dr}{d\tau} &= r(0.0048359885\varepsilon - 0.09674296998r^2), \\
\frac{d\theta}{d\tau} &= 0.4531462284 + 0.0021902454\varepsilon - 2.380920393r^2.
\end{aligned} \quad (4.22)$$

System (4.25) has equilibrium solutions $\bar{r} = 0$ and $\bar{r}^2 = 0.0499880095\varepsilon$. The solution $\bar{r} = 0$ corresponds to the equilibrium solution \bar{E} of the original system (4.5). Linearization of the equation $dr/d\tau$ indicates that $\bar{r} = 0$ (\bar{E}) is stable for $\varepsilon < 0$, that is $\rho_1 < \bar{\rho}_1$. When ε increases from negative values and crosses zero, a Hopf bifurcation occurs and the amplitude of the periodic solution is given by

$$\bar{r} = 0.2235799845 \sqrt{\varepsilon}, \quad \varepsilon > 0.$$

Since $\nu_1 < 0$, the Hopf bifurcation is supercritical and the bifurcation limit cycle is stable. The amplitude of the bifurcating limit cycle is $\bar{r} = 0.2235799845 \sqrt{\varepsilon}$, and the frequency is

$$\omega = 0.4531462284 - 0.1168272258\varepsilon.$$

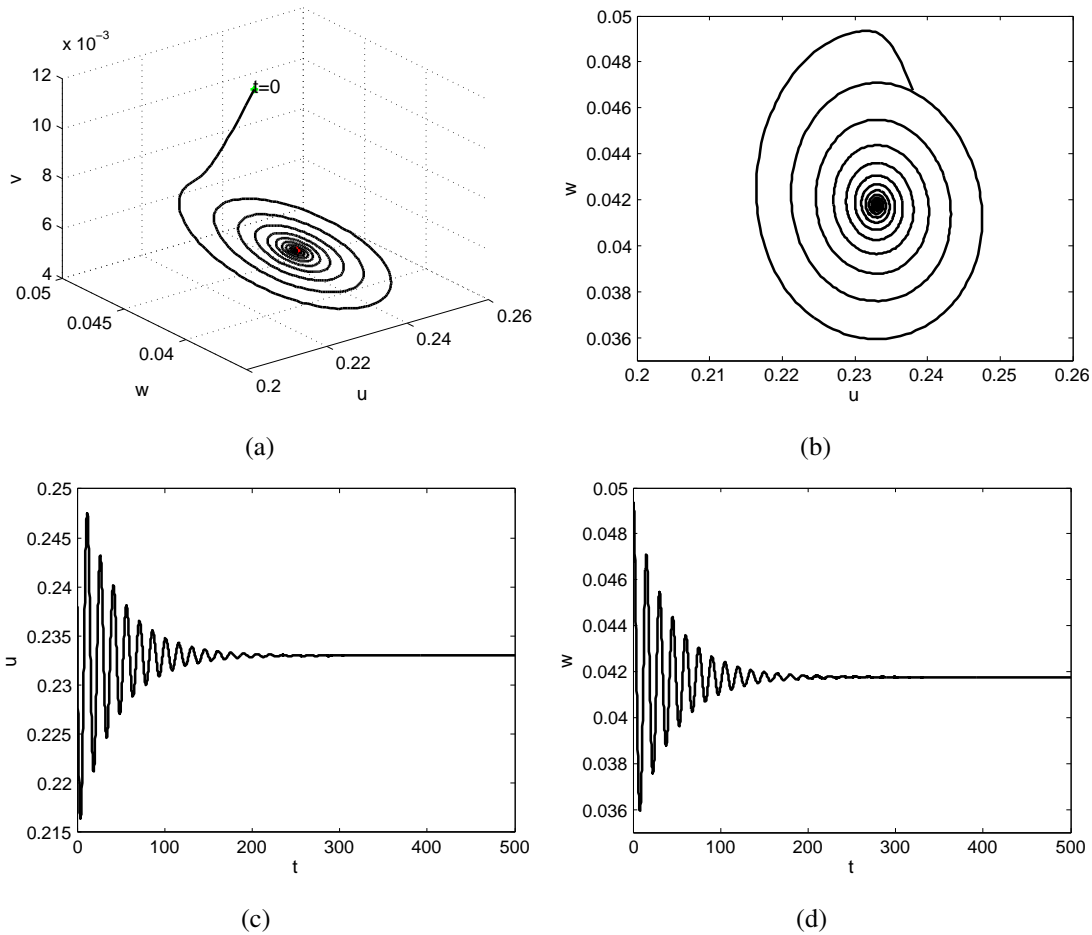


Figure 4.3: Trajectories of system (4.5), when $\rho_1 = 20$. We have $\mathcal{R}_0 = 4.291666666$, and \bar{E} is locally asymptotically stable, where $\bar{E} = (0.233009709, 0.041759907, 0.005567988)$.

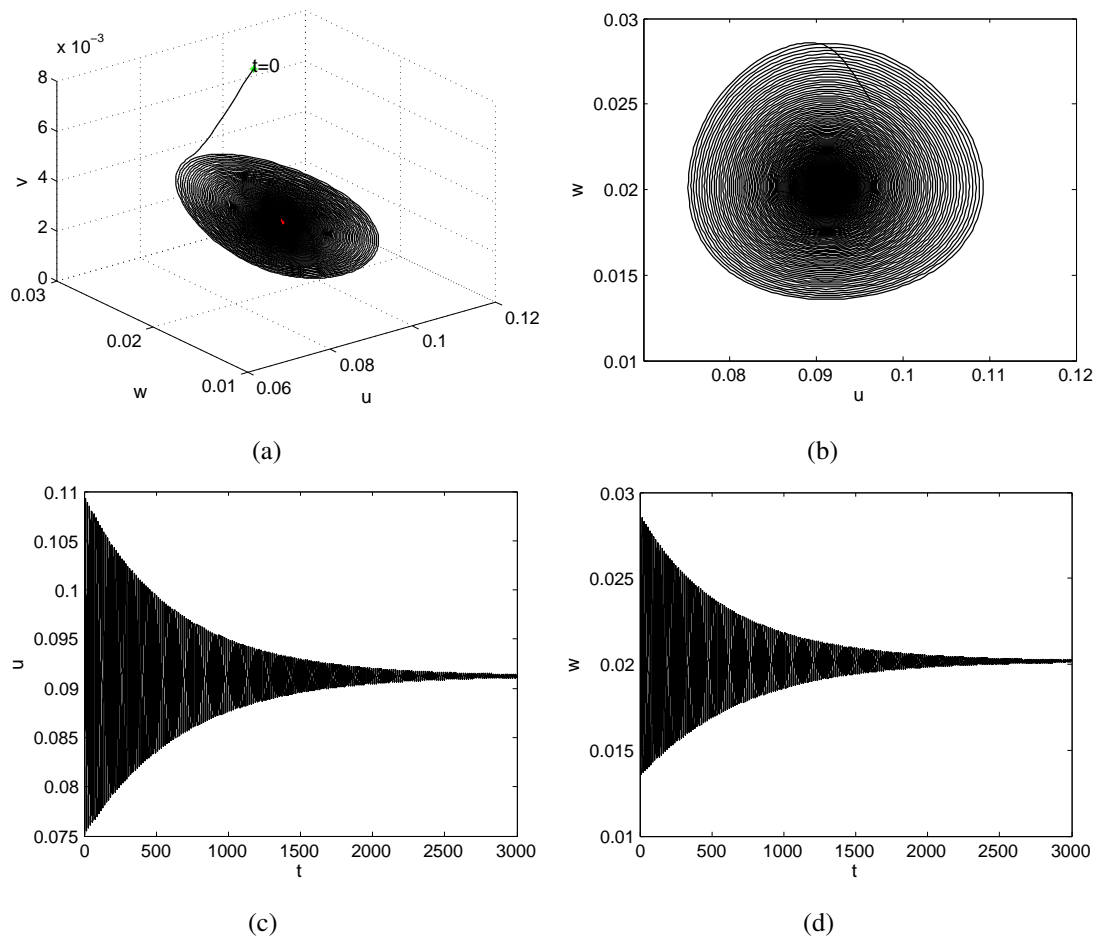


Figure 4.4: Trajectories of system (4.5), when $\rho_1 = 70$. We have $\mathcal{R}_0 = 10.958333333$, and \bar{E} is locally asymptotically stable, where $\bar{E} = (0.091254753, 0.020179391, 0.002690585)$.

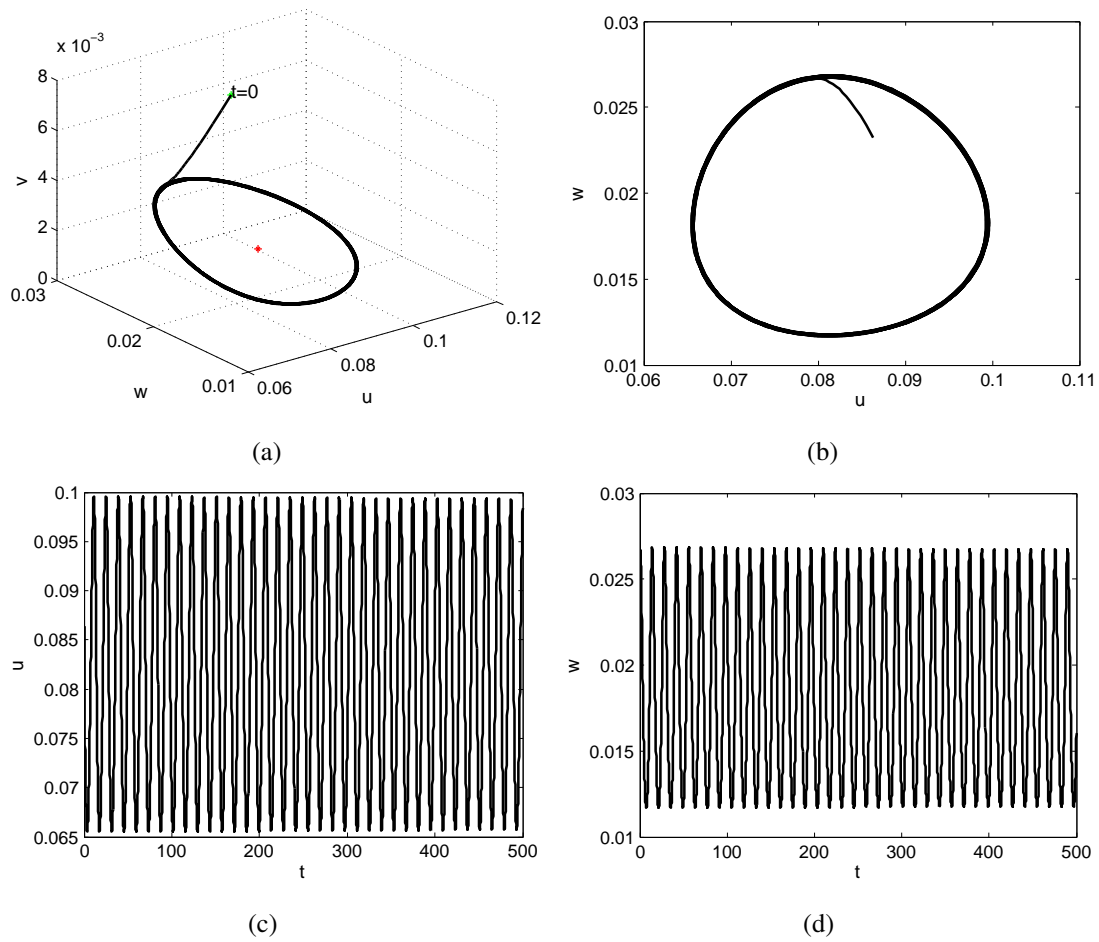


Figure 4.5: Trajectories of system (4.5), when $\rho_1 = 80$. We have $\mathcal{R}_0 = 12.291666667$, and Hopf bifurcation occurs at \bar{E} , and there is a stable limit cycle. Here $\bar{E} = (0.081355932, 0.018239128, 0.002431884)$.

Similarly, if we fix $\delta = 0.25$, $\alpha = 1.2$, $\mu = 7.5$ and $\rho_1 = 70$, $F(\rho_2) = 0$ has only one positive root $\bar{\rho}_2 = 24.06639452$ (see Figure 4.6) and two negative roots $\rho_2 = -9.466977953$ and $\rho_2 = -10.77608331$. Thus $\bar{\rho}_2 = 24.06639452$ is a critical value of bifurcation. When $0 \leq \rho_2 < \bar{\rho}_2$, \bar{E} is locally asymptotically stable (see Figure 4.7), while it is unstable if $\rho_2 \geq \bar{\rho}_2$. When $\rho_2 = \bar{\rho}_2$, there is a Hopf bifurcation, and a family of periodic solutions bifurcates from \bar{E} (see Figure 4.8).

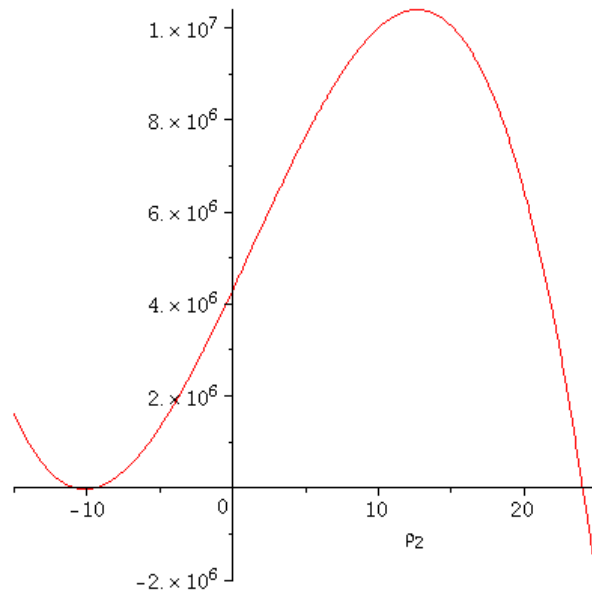


Figure 4.6: The function $F(\rho_2)$ has only one positive root $\bar{\rho}_1 = 24.06639452$.

Let $\rho_2 = \bar{\rho}_2 + \varepsilon$ and the linear transformation (4.19) with

$$\begin{pmatrix} \bar{u} \\ \bar{w} \\ \bar{v} \end{pmatrix} = \begin{pmatrix} 0.0299403637 \\ 0.0071963462 \\ 0.0009595128 \end{pmatrix}, \quad P = \begin{pmatrix} -0.0074850909 & -0.7295387145 & -2.0958254600 \\ 0.2403560052 & -0.2794433946 & 2.0958254600 \\ 0 & 1 & -7.5000000000 \end{pmatrix},$$

then system (4.5) is transformed to

$$\frac{dx_i}{d\tau} = F_i(x_1, x_2, x_3; \varepsilon), \quad i = 1, 2, 3, \quad (4.23)$$

where

$$\begin{aligned} F_1 = & 0.4832999609x_2 + \varepsilon(-0.0002317009 - 0.0069984666x_1 + 0.0138985043x_2 \\ & + 0.0068913568x_3) + \varepsilon(0.2597749886x_1x_3 + 0.1053782781x_3x_2 - 0.0009634203x_1^2 \\ & + 0.0655698598x_3^2 + 0.4178786217x_1x_2) + O(\varepsilon) \\ & - 0.0069840861x_1^2 - 57.1550777084x_1x_3 + 14.0708577570x_1x_2 \\ & - 14.4126015770x_3^2 + 3.5483096890x_3x_2, \end{aligned}$$

$$\begin{aligned}
F_2 &= -0.4832999610x_1 + \varepsilon(-0.0004807986 - 0.0145223983x_1 + 0.0288405483x_2 \\
&\quad + 0.0143001366x_3) + \varepsilon(0.5390546324x_1x_3 + 0.2186686613x_3x_2 - 0.0019991770x_1^2 \\
&\quad + 0.1360628938x_3^2 + 0.8671327754x_1x_2) + O(\varepsilon) \\
&\quad + 0.4526901833x_1^2 - 118.5331112012x_1x_3 + 28.9297201243x_1x_2 \\
&\quad - 29.9198000655x_3^2 + 7.2953339441x_3x_2, \\
F_3 &= -7.7869284856x_3 + \varepsilon(-0.0000303249 - 0.0009159543x_1 + 0.0018190263x_2 \\
&\quad + 0.0009019358x_3) + \varepsilon(0.0339991640x_1x_3 + 0.0137918334x_3x_2 - 0.0001260918x_1^2 \\
&\quad + 0.0085817362x_3^2 + 0.0546916540x_1x_2) + O(\varepsilon) \\
&\quad + 0.0276954677x_1^2 - 7.4762260736x_1x_3 + 1.8251427125x_1x_2 \\
&\quad - 1.8870738072x_3^2 + 0.4602542135x_3x_2.
\end{aligned}$$

It is easy to see that the Jacobian matrix of system (4.23) at $x = (0, 0, 0)$ is in the Jordan canonical form

$$J = \begin{pmatrix} 0 & 0.4832999610 & 0 \\ -0.4832999610 & 0 & 0 \\ 0 & 0 & -7.7869284856 \end{pmatrix}. \quad (4.24)$$

For system (4.23), $\omega_0 = 0.4832999610$ corresponds to the pair of the pure imaginary eigenvalues. ν_0 and τ_0 can be derived from linear analysis similarly to the previous case, we have

$$\begin{aligned}
\nu_0 &= \frac{1}{2} \left(\frac{\partial^2 F_1}{\partial x_1 \partial \varepsilon} + \frac{\partial^2 F_2}{\partial x_2 \partial \varepsilon} \right) \Big|_{\varepsilon=0, x_i=0} \\
&= (0.0144202741 + 0.1093343306x_3 + 0.4335663877x_1) \Big|_{x_i=0} \\
&= 0.0144202741, \\
\tau_0 &= \frac{1}{2} \left(\frac{\partial^2 F_1}{\partial x_2 \partial \varepsilon} - \frac{\partial^2 F_2}{\partial x_1 \partial \varepsilon} \right) \Big|_{\varepsilon=0, x_i=0} \\
&= (0.0072611992 - 0.2695273162x_3 + 0.0019991770x_1 - 0.4335663877x_2) \Big|_{x_i=0} \\
&= 0.0072611992.
\end{aligned}$$

On the other hand, ν_1 and τ_1 are determined by nonlinear analysis. Applying the Maple program developed in [13] to system (4.20) again, setting $\varepsilon = 0$, we obtain

$$\nu_1 = -0.2039007979, \quad \tau_1 = -21.07423997.$$

Therefore, the normal form of the system up to third order is given by

$$\begin{aligned}
\frac{dr}{d\tau} &= r(0.0144202741\varepsilon - 0.2039007979r^2), \\
\frac{d\theta}{d\tau} &= 0.4832999610 + 0.0072611992\varepsilon - 21.07423997r^2.
\end{aligned} \quad (4.25)$$

System (4.25) has equilibrium solutions $\bar{r} = 0$ and $\bar{r}^2 = 0.2039007979\varepsilon$. The solution $\bar{r} = 0$ corresponds to the equilibrium solution \bar{E} of the original system (4.5). Linearization of the equation $dr/d\tau$ indicates that $\bar{r} = 0$ (\bar{E}) is stable for $\varepsilon < 0$, that is $\rho_2 < \bar{\rho}_2$. When ε increases from negative to cross zero, a Hopf bifurcation occurs and the amplitude of the periodic solution is

$$\bar{r} = 0.2659360998 \sqrt{\varepsilon}, \quad \varepsilon > 0.$$

Since $\nu_1 < 0$, the Hopf bifurcation is supercritical and the bifurcation limit cycle is stable. The amplitude of the bifurcating limit cycle is $\bar{r} = 0.2235799845 \sqrt{\varepsilon}$, and the frequency is

$$\omega = 0.4832999610 - 1.4831513940\varepsilon.$$

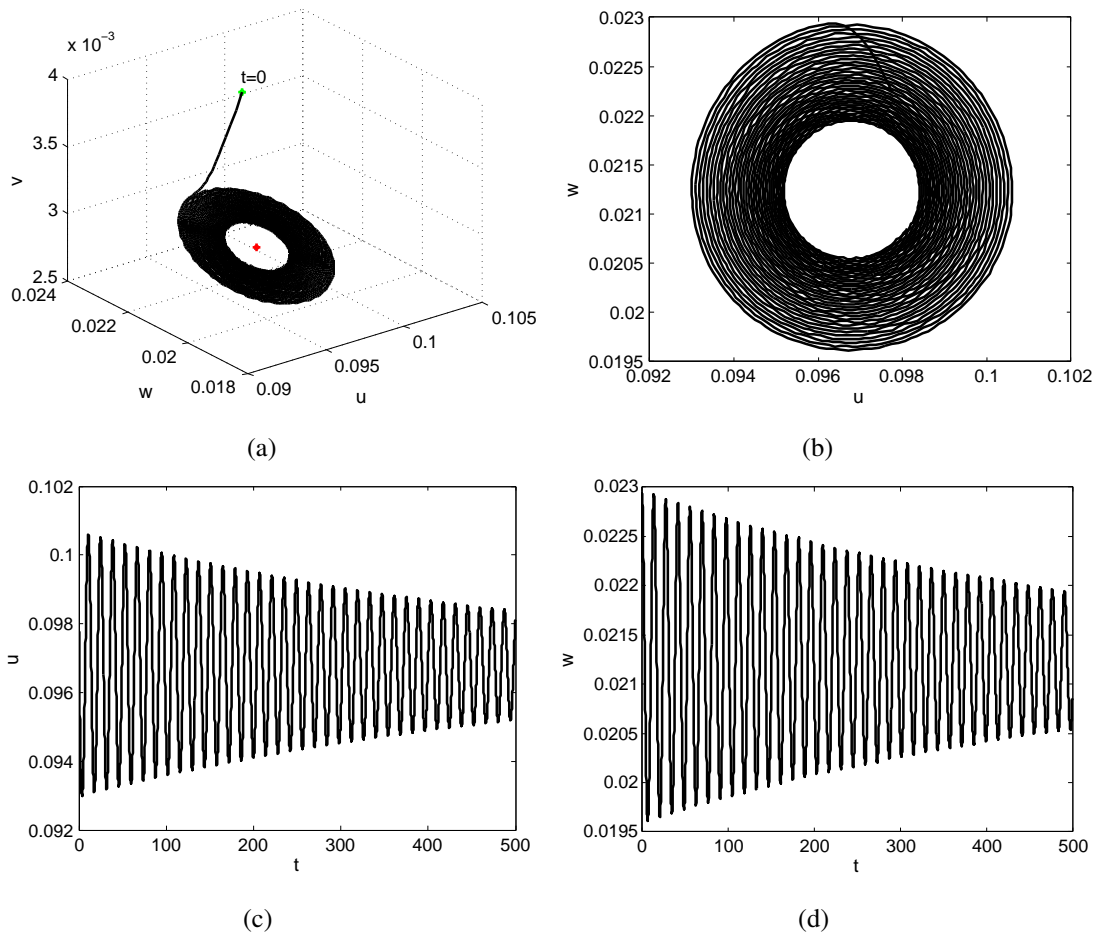


Figure 4.7: Trajectories of system (4.5), when $\rho_2 = 1$. We have $\mathcal{R}_0 = 10.333333333$, and \bar{E} is locally asymptotically stable, where $\bar{E} = (0.096774194, 0.021235716, 0.002831429)$.

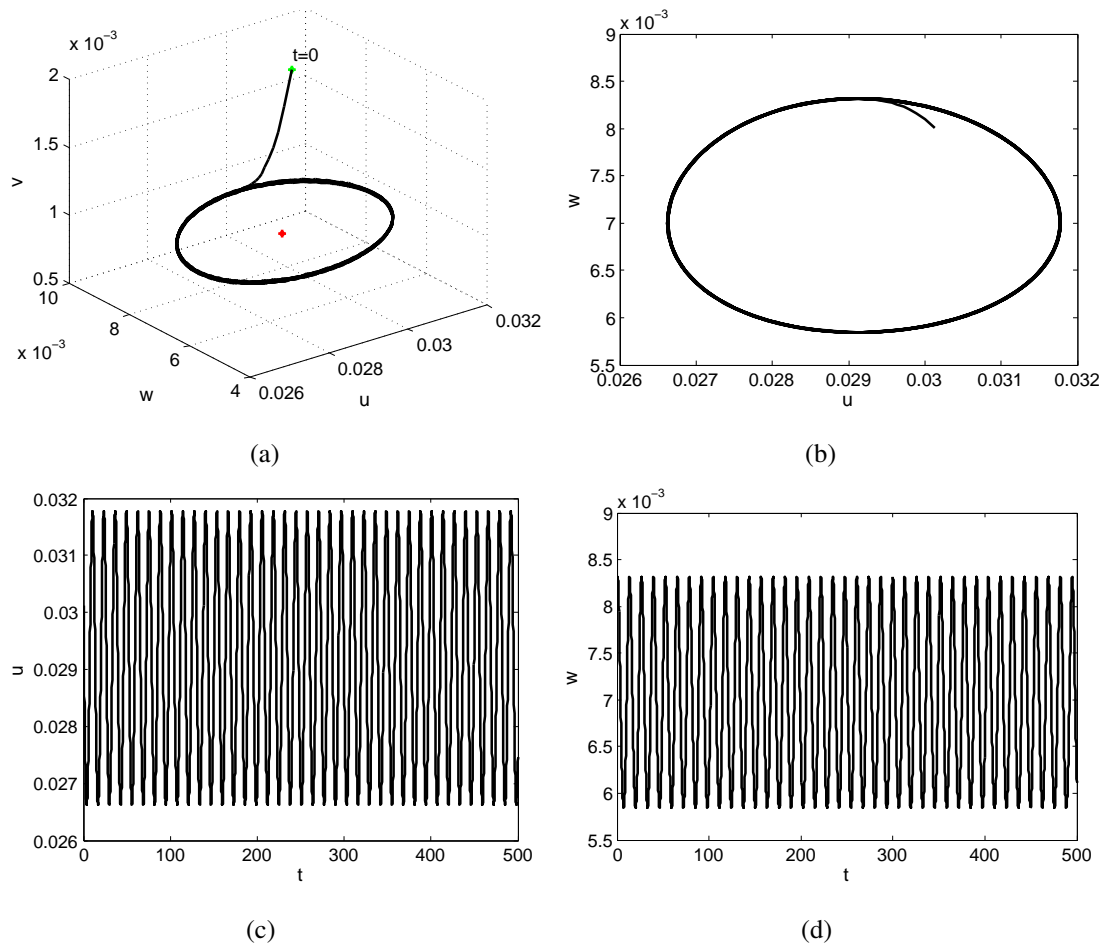


Figure 4.8: Trajectories of system (4.5), when $\rho_2 = 25$. We have $\mathcal{R}_0 = 34.3333333333$, and Hopf bifurcation occurs at \bar{E} , and there is a stable limit cycle. Here $\bar{E} = (0.029126214, 0.007008232, 0, 0009344309783)$.

4.7 Conclusion and discussion

In this chapter, we considered the direct cell-to-cell transfer of HIV-1 in addition to cell-free virus transmission by mathematical modeling. We found that the basic reproduction number \mathcal{R}_0 is larger than that of previous models which just considered cell-free virus spread mode. In fact, \mathcal{R}_0 is the sum of the basic reproduction number determined by cell-free virus infection, \mathcal{R}_{01} , and that determined by cell-to-cell infection, \mathcal{R}_{02} .

When cell-free spread of HIV-1 is only considered, we have $\beta_2 = 0$ in (4.4), and the model (4.4) becomes the model (4.2) with $\gamma = 0$ or the model considered in [4]. We see from the analysis in [4] that the basic reproduction number is $\mathcal{R}_{01} = \frac{T_M \beta_1 \gamma}{d_T^* d_V}$. When $\mathcal{R}_{01} < 1$, the infection cannot establish. When $\mathcal{R}_{01} > 1$, the infection can persist, and for some large β_1 the Hopf bifurcation occurs, that is a family of periodic solutions bifurcates from the positive equilibrium \bar{E} . This property is very similar to the case when cell-to-cell transfer is considered simultaneously. However, the basic reproduction number \mathcal{R}_{01} is only a part of \mathcal{R}_0 , the basic reproduction number of (4.4), that is, the case when both transmission modes exist. On the other hand, we see from Figure 4.1 that the bifurcation critical point $\bar{\rho}_1$ decreases as $\bar{\rho}_2$ increases. Therefore, the bifurcation critical point $\bar{\beta}_1$ decreases as $\bar{\beta}_2$ increases. That means the periodic solutions occur for smaller infection rate of cell-free mode β_1 , when cell-to-cell transfer establishes compared with the case when only cell-free mode is considered.

In contrast, when only cell-to-cell transfer is considered, $\beta_1 = 0$ in (4.4). We know from the analysis in [1] that the basic reproduction number is $\mathcal{R}_{02} = \frac{T_M \beta_2}{d_T^*}$. The infection cannot establish if $\mathcal{R}_{02} < 1$, while it persists if $\mathcal{R}_{02} > 1$. Furthermore, the positive equilibrium \bar{E} is stable if $\mathcal{R}_{02} > 1$, and there are no Hopf bifurcation and periodic solutions. Since \mathcal{R}_{02} is only a part of \mathcal{R}_0 , the basic reproduction number is also underestimated when the cell-to-cell mode is only considered. The dynamical behavior of the system is very different from the case when both infection modes are considered where Hopf bifurcation and periodic solutions occur for some values of infection rates β_1 and β_2 , that is, for some ρ_1 and ρ_2 .

The nonlinear term, that is the logistic growth of target cells, leads to the Hopf bifurcation and periodic solutions of the system for some range of parameter values. With stable periodic solutions, the concentration of infected cells and virus load cannot stabilize at a constant level, but show oscillations. This is important for experimental or clinic estimation of virus load. Due to the periodic oscillation, lower (or higher) virus load detected at a moment does not indicate the same lower (or higher) load for a long time. The oscillations of viral load levels in the plasma are also plausible under the effects of immune responses or delays in the virus infection dynamics [2].

In the model (4.5), we do not consider any delay effects, such as the delay from the time of

initial infection until the production of new virions. Culshaw *et al.* [1] considered this delay for the cell-to-cell infection model and found that there is a Hopf bifurcation for some critical values of the delay time. For the model (4.5), if we consider delay effects, there may be Hopf bifurcations for some delay time. This needs further study.

Bibliography

- [1] Culshaw R.V., Ruan S. and Webb G., A mathematical model of cell-to-cell spread of HIV-1 that includes a time delay, *J. Math. Biol.*, 46 (2003) 425-444.
- [2] Ciupe M.S., Bivort B.L., Bortz D.M. and Nelson P.W., Estimating kinetic parameters from HIV primary infection data through the eyes of three different mathematical models, *Math. Biosci.*, 200 (2006) 1-27.
- [3] De Boer R.J. and Perelson A.S., Target cell limited and immune control models of HIV infection: a comparison, *J. Theor. Biol.*, 190 (1998) 201-214.
- [4] Li J., Wang K. and Yang Y., Dynamical behaviors of an HBV infection model with logistic hepatocyte growth, *Math. Comput. Model.*, 54 (2011) 704-711.
- [5] Sattentau Q., Avoiding the void: cell-to-cell spread of human viruses, *Nat. Rev. Microbiol.*, 6 (2008) 28-41.
- [6] Sattentau Q., Cell-to-cell spread of retroviruses, *Viruses*, 2 (2010) 1306-1321.
- [7] Sattentau Q., The direct passage of animal viruses between cells, *Current Opinion in Virology*, 1 (2011) 396-402.
- [8] Smith H.L., *Monotone dynamical systems*, American Mathematical Society, Providence, RI, 1995.
- [9] Smith H.L. and Zhao X.Q., Robust persistence for semidynamical systems, *Nonlinear Anal.*, 47 (2001) 6169-6179.
- [10] Stafford M., Corey L., Daar E., Ho D. and Perelson A., Modeling plasma virus concentration during primary infection, *J. Theor. Biol.*, 203 (2000) 285-301.
- [11] Thieme H.R., Convergence results and a Poincaré-Bendixson trichotomy for asymptotically autonomous differential equations, *J. Math. Biol.*, 30 (1992) 755-763.

- [12] Yu P. and Huseyin K., A perturbation analysis of interactive static and dynamical bifurcation, *IEEE Trans. Automat. Contr.*, Vol. 33 No. 1 (1988) 28-41.
- [13] Yu P., Computation of normal forms via a perturbation technique, *J. Sound Vib.*, Vol. 211 No. 1 (1998) 19-38.
- [14] Yu P., Closed-form conditions of bifurcation points for general differential equations, *Int. J. Bifurcation Chaos*, Vol. 15 No. 4 (2005) 1467-1483.
- [15] Zhao X.Q., *Dynamical systems in population biology*, Springer-Verlag, New York, 2003.

Chapter 5

Repulsion effect on superinfecting virions by infected cells

5.1 Introduction

Viruses are usually thought to spread across susceptible cells through an iterative process, consisting of attachment to a target cell, entry, replication, and release of new virions, and which then move on to infect other uninfected target cells. According to such an understanding, the spreading speed of virus would be limited by how quickly virus can reproduce in infected cells. However, a recent study published in *Science* [9] reveals that vaccinia virus spreads much faster than previously thought. Using live video microscopy, the authors of [9] found that the vaccinia virus was spreading across one cell fourfold faster than its replication cycle should allow. Indeed, vaccinia virus spreads across one cell every 1.2 hours on average, but in vaccinia viral replication kinetics, new virions are formed only 5 to 6 hours after infection, or in virus-induced cell motility, a cell starts to move 5 to 6 hours after infection.

In seeking an explanation for this phenomenon, a new mechanism was discovered, that is, the repulsion of superinfecting virions by infected cells [9]. Indeed, a peculiar feature of vaccinia infection is the formation of actin tails, which propel virus particles towards other cells late during infection, promoting spread of virus from cell to cell. The authors of [9] observed that an infected cell can produce two important proteins, called A33 and A36, and express them on the cell's outer membrane shortly after infection, which mark the cell as infected. The two proteins are necessary and sufficient to induce formation of actin tails after binding extracellular enveloped vaccinia (EEV) virus. When other cell-free vaccinia viral particles reach the infected cell and come into contact with these proteins, they induce the host cell to form a new actin tail projection, which propels viral particles away and toward other cells that

they can infect. This way, the superinfection is blocked, and the free particles bounce from one cell surface to another until they reach an uninfected cell. This mechanism accelerates virus spread, since virus spreads by surfing from cell to cell, bouncing past the already-infected cells and quickly reaching distant uninfected cells without the need to replicate in each cell on the way.

It is believed that some other viruses may also employ such mechanisms to speed up their spread. For instance, herpes simplex virus (HSV-1), which has replication kinetics similar to vaccinia virus, also spreads faster than predicted by their replication kinetics. Considering this repulsion effect of infected cells on superinfecting virions, we see that the spread rate of viruses should depend on the density of infected cells, and high density of infected cells should promote the spread of viruses. We wish to explore this effect quantitatively by mathematical models.

Mathematical modeling has been shown to be an effective and valuable approach to understand the within host dynamics of virus infection and spread. The dynamics of HIV-1, hepatitis B virus (HBV) and human T cell leukemia type-1 (HTLV-1) infections have been analyzed in detail with the help of mathematical models. Most of these works are based on the assumption that cells and viruses are well mixed, and hence, ignore the mobility of cells and viruses. However, spatial structure is very important for virus dynamics. In the study of evolutionary competitiveness of lytic virus, Komarova [15] considered the spatial dynamics of viral spread by a diffusion model, and found that lytic viruses can be evolutionary competitive due to the mechanism that they exit an infected cell in a large burst such that the antibodies are flooded and a large proportion of virions can escape the immune system and spread to new cells. The efficacy of the flooding depends on the diffusion rate of the antibodies. Wang and Wang [27] developed a reaction diffusion model to simulate the infection and spread of HBV. They assumed that susceptible host cells and infected cells cannot move, while viruses move according to Fickian diffusion. For this model, they discussed existence of traveling wave solutions and minimal wave speed. In a subsequent paper, Gan *et al.* [10] considered the effect of the time delay accounting for the lag from the time of infection to the time when the infected cell becomes productively infectious. Xu and Ma [31] considered the saturation response of the infection rate.

In this chapter, we consider the repulsion effect of infected cells on the spread of virus in the within host environment. Denoting by $T(t, x)$, $T^*(t, x)$ and $V(t, x)$ the concentrations of target cells, infected cells and free virus particles at time t at location x respectively, we consider the following general virus infection dynamic model,

$$\begin{aligned}
\frac{\partial T}{\partial t} &= D_T \Delta T + h(x) - d_T T - \beta(x)TV, \\
\frac{\partial I}{\partial t} &= D_T \Delta I + \beta(x)TV - d_I I, \\
\frac{\partial V}{\partial t} &= \nabla \cdot (D_V(I)\nabla V) + \gamma(x)I - d_V V.
\end{aligned} \tag{5.1}$$

This model system is based on some assumptions. Firstly, the within host environment is spatially heterogenous, that is, the target cell production rate $h(x)$, infection rate $\beta(x)$ and free virus production rate $\gamma(x)$ may depend on the spatial location x . The death rate of target cells, infected cells and viruses are constants, denoted by d_T , d_I and d_V respectively. Secondly, target cells and infected cells can move, following the Fickian diffusion, meaning that the flux of these cells are proportional to their concentration gradient and go from regions of high concentration to regions of low concentration, with the same diffusion rate D_T , that is,

$$\vec{J}_T = -D_T \nabla T, \quad \vec{J}_I = -D_T \nabla I.$$

Notice that the diffusion rate of the cells may be much slower in contrast to the spreading rate of viruses, and is thus often neglected in literature. Thirdly, the flux of free viral particles depends not only on its concentration gradient but also on the concentration of infected cell in the following form

$$\vec{J}_V = D_V(I)(-\nabla V).$$

The repulsion of the superinfecting virions observed in [9] suggests that high concentration of infected cells promotes spread of viruses toward uninfected target cells. Therefore, $D_V(I)$ should be an increasing function of the local concentration of infected cells $I(t, x)$. We assume

$$D_V(I) = D_0 + g(I),$$

where D_0 represents random diffusion rate of free virions, and $g \in \mathbf{C}^2(\mathbb{R}_+, \mathbb{R}_+)$ is an increasing function of I , representing the motility of free virions due to repulsion of superinfecting virions by infected cells. If there is no infected cell, then there is no repulsion effect, meaning that $g(I)$ should satisfy $g(0) = 0$.

The rest of the chapter is organized as follows. In Section 2, we discuss the well-posedness of the model (5.1), derive the basic reproduction number \mathcal{R}_0 of the system (5.1) and calculate \mathcal{R}_0 numerically. For the model (5.1), mathematical proof of stability of steady states is difficult to approach. However, when all the parameters $h(x)$, $\beta(x)$ and $\gamma(x)$ do not depend on space location x , we can establish the linear stability of steady states of system (5.1). In Section 3,

we numerically estimate the spreading rate of virus and discuss the effect of repulsion of superinfecting virions. Section 4 discuss existence of traveling wavefront solutions to the model and their numerical simulations when the diffusion of target cells and infected cells is ignored. Finally, we present conclusions and discussions in Section 5.

5.2 In a bounded domain

In this section, we consider an open bounded domain $\Omega \subset \mathcal{R}^3$ with smooth boundary $\partial\Omega$. Under such a scenario, we examine the dynamics of the model. More precisely, we will investigate the dynamics of the system

$$\begin{aligned} \frac{\partial T}{\partial t} &= D_T \Delta T + h(x) - d_T T - \beta(x)TV, \\ \frac{\partial I}{\partial t} &= D_I \Delta I + \beta(x)TV - d_I I, \quad x \in \Omega, \quad t > 0, \\ \frac{\partial V}{\partial t} &= \nabla \cdot (D_V(I)\nabla V) + \gamma(x)I - d_V V, \end{aligned} \quad (5.2)$$

with zero-flux boundary conditions

$$\frac{\partial T}{\partial \nu} = \frac{\partial I}{\partial \nu} = \frac{\partial V}{\partial \nu} = 0, \quad \forall x \in \partial\Omega, \quad t > 0, \quad (5.3)$$

and initial conditions

$$T(0, x) = T_0(x) > 0, \quad I(0, x) = I_0(x) \geq 0, \quad V(0, x) = V_0(x) \geq 0, \quad \forall x \in \Omega. \quad (5.4)$$

Well-posedness of the model

First, we address the well-posedness of the problem (5.2)-(5.4). As usual, we denote by \mathbb{R}_+^3 the positive cone in \mathbb{R}^3 , i.e.,

$$\mathbb{R}_+^3 = \{w = (T, I, V)^T \in \mathbb{R}^3 \mid T \geq 0, I \geq 0, V \geq 0\}.$$

Let $p > 3$ so that the space $\mathbf{W}^{1,p}(\Omega, \mathbb{R}^3)$ is continuously embedded in the continuous function space $\mathbf{C}(\Omega, \mathbb{R}^3)$ (see, e.g., [1]). Since the unknowns T , I and V are populations, we only need to consider the following solution space

$$\mathbf{X}_+ := \left\{ w \in \mathbf{W}^{1,p}(\Omega, \mathbb{R}^3) \mid w(\bar{\Omega}) \subset \mathbb{R}_+^3 \text{ and } \frac{\partial w}{\partial \nu} = 0 \text{ on } \partial\Omega \right\}.$$

We see that the system (5.2)-(5.3) can be rewritten as the following abstract quasi-linear parabolic system

$$\begin{cases} w_t + \mathcal{A}(w)w = \mathcal{F}(x, w), & x \in \Omega, \quad t > 0, \\ \mathcal{B}w = 0, & x \in \partial\Omega, \quad t > 0 \end{cases} \quad (5.5)$$

where

$$\mathcal{A}(z)w = - \sum_{j,k} \partial_j (a_{jk}(z) \partial_k w), \quad \mathcal{B}w = \frac{\partial w}{\partial \nu},$$

and

$$a_{jk} = a(z) \delta_{jk}, \quad 1 \leq j, k \leq n, \quad a(z) = \begin{pmatrix} D_T & 0 & 0 \\ 0 & D_T & 0 \\ 0 & 0 & D_V(z_3) \end{pmatrix},$$

for $z = (z_1, z_2, z_3) \in \mathbb{R}_+^3$ (here δ_{jk} is the Kronecker delta function), and

$$\mathcal{F}(x, w) = (h(x) - d_T T - \beta(x)TV, \beta(x)TV - d_I I, \gamma(x)I - d_V V)^\top,$$

for $w = (T, I, V)$. It is obvious that $a(z) \in \mathbf{C}^2(\mathbb{R}_+^3, \mathcal{L}(\mathbb{R}_+^3))$, where we identified $\mathcal{L}(\mathbb{R}_+^3)$ with the space of 3×3 real matrices. Since $D_V(I) \geq D_0 > 0$, the eigenvalues of $a(z)$ are positive for each $z \in \mathbb{R}_+^3$. Moreover, the boundary value problem $(\mathcal{A}, \mathcal{B})$ is normally elliptic (see, e.g. [3]).

Theorem 5.2.1 *There exists a constant τ_0 depending on the initial data (T_0, I_0, V_0) such that the system (5.2), with no-flux boundary condition (5.3) and the initial condition (5.4), has a unique maximal classical solution (T, I, V) defined on $[0, \tau_0) \times \Omega$ such that*

$$(T, I, V) \in \mathbf{C}([0, \tau_0), \mathbf{X}) \cap \mathbf{C}^{2,1}((0, \tau_0) \times \bar{\Omega}, \mathbb{R}^3).$$

Moreover, the solution satisfies $T(t, x) \geq 0$, $I(t, x) \geq 0$, $V(t, x) \geq 0$, for all $(t, x) \in [0, \tau_0) \times \Omega$.

Proof As mentioned above, the system (5.5) is normally elliptic and triangular (in fact diagonal). According to Theorem 1 [2] or Theorem 14.4 and Theorem 14.6 [3], (5.5)-(5.4) has a unique classical solution on a maximal interval $[0, \tau_0)$. The non-negativity of the solution follows from Theorem 15.1 [3]. The proof is completed. ■

We can actually show that $\tau_0 = \infty$ in the above theorem, that is, the solution exists globally.

Theorem 5.2.2 *For every initial data (T_0, I_0, V_0) , (5.2)-(5.3)-(5.4) has a unique solution defined on $[0, \infty) \times \Omega$.*

Proof By Theorem 5.2 in [2] and the non-negativeness of the solution confirmed in Theorem 5.2.1, it suffices to prove that the solution (T, I, V) is bounded above by some positive values.

From the T and I equations in (5.2), we see that

$$\begin{aligned} \frac{\partial}{\partial t}(T + I) &= D_T \Delta(T + I) + h(x) - d_T T - d_I I \\ &\leq D_T \Delta(T + I) + \bar{h} - d_m(T + I), \end{aligned}$$

where $\bar{h} = \max_{x \in \Omega} h(x)$ and $d_m = \min\{d_T, d_I\}$. By Lemma 1 in [19], \bar{h}/d_m is the globally attractive steady state for the scalar parabolic equations

$$\begin{aligned} \frac{\partial w(t, x)}{\partial t} &= D_T \Delta w(t, x) + \bar{h} - d_m w(t, x), \quad x \in \Omega, t > 0, \\ \frac{\partial w(t, x)}{\partial \nu} &= 0, \quad x \in \partial\Omega, t > 0. \end{aligned}$$

The parabolic comparison theorem ([25], Theorem 7.3.4) implies that $T + I$ is bounded. This together with the non-negativity of T and I further implies that both $T(t, x)$ and $I(t, x)$ are bounded. We assume $0 \leq T(t, x) \leq T_M$, $0 \leq I(t, x) \leq I_M$.

Let $\bar{\gamma} = \max_{x \in \Omega} \{\gamma(x)\}$, and $V_M = \bar{\gamma} I_M / d_V$. For any given I , define the operator \mathcal{P} by

$$\mathcal{P}V = V_t - \nabla \cdot (D_V(I) \nabla V) - \gamma(x)I + d_V V.$$

For any solution (T, I, V) of the system (5.2)-(5.3)-(5.4), we have $\mathcal{P}V = 0$. On the other hand,

$$\mathcal{P}V_M = d_V V_M - \gamma(x)I \geq d_V V_M - \bar{\gamma} I_M = 0 = PV.$$

On the boundary $\partial\Omega$, we have $\frac{\partial V_M}{\partial \nu} = 0$. Thus $V = V_M$ is an upper solution of the V equation in the system (5.2)-(5.3). By the comparison principle, we obtain that $V(t, x) \leq V_M$. Therefore, the solution (T, I, V) is bounded, and hence, it exists globally. ■

Basic reproduction number

Let $\mathbb{X} := \mathbf{C}(\bar{\Omega}, \mathbb{R}^3)$ be the Banach space of continuous functions with supremum norm $\|\cdot\|_{\mathbb{X}}$. Denote by \mathbb{X}_+ the positive cone of \mathbb{X} , i.e., $\mathbb{X}_+ = \mathbf{C}(\bar{\Omega}, \mathbb{R}_+^3)$. Then \mathbb{X}_+ induces a partial order, making $(\mathbb{X}, \mathbb{X}_+)$ strongly ordered space. Similarly, let $\mathbb{Y} := \mathbf{C}(\bar{\Omega}, \mathbb{R})$ and $\mathbb{Y}_+ := \mathbf{C}(\bar{\Omega}, \mathbb{R}_+)$. Suppose that for each $t \geq 0$, $S_1(t)$ and $S_2(t) : \mathbb{Y} \rightarrow \mathbb{Y}$, are the strongly continuous semigroups associated with $D_T \Delta - d_I$ and $D_0 \Delta - d_V$ subject to homogeneous Neumann boundary conditions respectively, that is,

$$\begin{aligned} [S_1(t)\phi](x) &= e^{-d_I t} \int_{\Omega} \Gamma(x, y, t, D_T) \phi(y) dy, \\ [S_2(t)\phi](x) &= e^{-d_V t} \int_{\Omega} \Gamma(x, y, t, D_0) \phi(y) dy, \end{aligned}$$

for any $\phi_1, \phi_2 \in \mathbb{Y}$, $t \geq 0$, where $\Gamma(x, y, t, D_T)$ and $\Gamma(x, y, t, D_0)$ are the Green functions associated with $D_T \Delta$ and $D_0 \Delta$ subject to homogenous Neumann boundary conditions respectively. It then follows that for each $t > 0$, $S_i(t) : \mathbb{Y} \rightarrow \mathbb{Y}$, $i = 1, 2$, is compact and strongly positive ([25], Corollary 7.2.3). Therefore, $S(t) = (S_1(t), S_2(t))$ is a positive C_0 -semigroup.

Setting $I(t, x) = 0$ and $V(t, x) = 0$ in the T equation in (5.2) leads to

$$\begin{aligned} \frac{\partial T(t, x)}{\partial t} &= D_T \Delta T(t, x) + h(x) - d_T T(t, x), \quad x \in \Omega, t > 0, \\ \frac{\partial T(t, x)}{\partial \nu} &= 0, \quad x \in \partial\Omega, t > 0. \end{aligned} \quad (5.6)$$

From Lemma 1 in [19], we know (5.6) admits a unique positive steady state $\hat{T}(x)$, which is globally attractive in $C(\bar{\Omega}, \mathbb{R})$. This means that the model system (5.2) has a unique infection-free steady state $E_0 = (\hat{T}(x), 0, 0)$.

Linearizing (5.2) at the infection-free steady state E_0 , we obtain the linearized system

$$\begin{aligned} \frac{\partial u_1}{\partial t} &= D_T \Delta u_1 - d_T u_1 - \beta(x) \hat{T}(x) u_3, \\ \frac{\partial u_2}{\partial t} &= D_T \Delta u_2 + \beta(x) \bar{T}(x) u_3 - d_I u_2, \\ \frac{\partial u_3}{\partial t} &= D_0 \Delta u_3 + \gamma(x) u_2 - d_V u_3, \end{aligned} \quad (5.7)$$

subject to the boundary conditions

$$\frac{\partial u_1}{\partial \nu} = \frac{\partial u_2}{\partial \nu} = \frac{\partial u_3}{\partial \nu} = 0, \quad \forall x \in \partial\Omega, t > 0.$$

We see that the equations for u_2 and u_3 , which correspond to the infectious compartments, are decoupled from u_1 , and these two equations constitute a cooperative system. Substituting $u_2(x, t) = e^{\lambda t} \phi_1(x)$ and $u_3(x, t) = e^{\lambda t} \phi_2(x)$ into equations of u_2 and u_3 , we obtain the following eigenvalue problem

$$\begin{aligned} \lambda \phi_1(x) &= D_T \Delta \phi_1(x) + \beta(x) \hat{T}(x) \phi_2(x) - d_I \phi_1(x), \\ \lambda \phi_2(x) &= D_0 \Delta \phi_2 + \gamma(x) \phi_1(x) - d_V \phi_2(x), \\ \frac{\partial \phi_1(x)}{\partial \nu} &= \frac{\partial \phi_2(x)}{\partial \nu} = 0, \quad \forall x \in \partial\Omega, t > 0, \end{aligned} \quad (5.8)$$

where $\phi = (\phi_1, \phi_2) \in \mathbb{Y} \times \mathbb{Y}$.

From Theorem 7.6.1 in [25] we have the following result.

Lemma 5.2.3 *The eigenvalue problem (5.8) has a principal eigenvalue $\lambda_0(D_0, D_T, \hat{T}(x))$ associated with a strictly positive eigenvector.*

This means that λ_0 is a real eigenvalue with algebraic multiplicity one, and $Re(\lambda) < \lambda_0$ for any other eigenvalue λ of (5.8). Furthermore, λ_0 has a corresponding eigenvector $\phi_0(x) = (\phi_{01}, \phi_{02})$ satisfying $\phi_0(x) \gg 0$, and any other nonnegative eigenvector of (5.8) is a positive multiple of $\phi_0(x)$.

Next, as in Wang & Zhao [28] and Guo *et al.* [11], we follow the framework of Thieme [26] to obtain the basic reproduction number of the model (5.2). To this end, we define a positive linear operator by

$$C(\phi)(x) = (C_1(\phi)(x), C_2(\phi)(x)), \quad \forall \phi = (\phi_1, \phi_2) \in \mathbb{Y} \times \mathbb{Y}, \quad x \in \bar{\Omega},$$

where

$$C_1(\phi)(x) = \beta(x)\hat{T}(x)\phi_2(x), \quad C_2(\phi)(x) = \gamma(x)\phi_1(x).$$

Assume that there are no infected cells and free virus initially, that is, the system is near the infection-free steady state; and viruses are introduced at time $t = 0$ and infection occurs immediately. The distribution of initial infected cells and free viruses are assumed to be $(\phi_1(x), \phi_2(x))$ (at time $t = 0$). Then as time evolves, those distributions reach $([S_1(t)\phi_1](x), [S_2(t)\phi_2](x))$ at time t . Thus, the total distribution of new infected cells is

$$\int_0^\infty \beta(x)\hat{T}(x)[S_2(t)\phi_2](x)dt = \left[\int_0^\infty C_1(S(t)\phi)dt \right](x),$$

and the total distribution of new free viruses is

$$\int_0^\infty \gamma(x)[S_1(t)\phi_1](x)dt = \left[\int_0^\infty C_2(S(t)\phi)dt \right](x).$$

Therefore, the next generation operator L is given by

$$L(\phi) := \int_0^\infty C(S(t)\phi)dt = C \left(\int_0^\infty S(t)\phi dt \right).$$

The basic reproduction number of the model (5.2) is defined to be the spectral radius of L , that is,

$$\mathcal{R}_0 := r(L).$$

Using the theory developed by Thieme [26] about spectral bound and basic reproduction number, we then obtain the following Lemma. The proof is very similar to that of Wang and Zhao ([28], Lemma 2.2).

Lemma 5.2.4 $\mathcal{R}_0 - 1$ has the same sign as λ_0 .

When all parameters are location independent (spatially homogeneous), we can actually find an explicit formula for the basic reproduction number \mathcal{R}_0 , as given in the following theorem.

Theorem 5.2.5 Assume that $\beta(x)$, $\gamma(x)$ and $h(x)$ are positive constants so that $\hat{T}(x) = \frac{h}{d_T}$. Then

$$\mathcal{R}_0 = \sqrt{\frac{\beta h \gamma}{d_T d_V d_I}}.$$

Proof Note that L is a compact and positive linear operator. For any $\varepsilon > 0$, we define

$$\begin{aligned} C_\varepsilon(\phi) &= \varepsilon\phi + C(\phi), \quad \forall \phi \in \mathbb{Y} \times \mathbb{Y}, \\ L_\varepsilon(\phi) &= C_\varepsilon\left(\int_0^\infty S(t)\phi dt\right), \quad \forall \phi \in \mathbb{Y} \times \mathbb{Y}. \end{aligned}$$

Then L_ε is strongly positive linear operator. By the Krein-Rutmann theorem, the spectral radius of L_ε , $r(L_\varepsilon) > 0$, is the unique eigenvalue of L_ε with a strongly positive eigenvector. Since $\int_\Omega \Gamma(x, y, a, D_T) dy = 1$ and $\int_\Omega \Gamma(x, y, t, D_0) dy = 1$, $\forall x \in \Omega$, $t > 0$, we have

$$\begin{aligned} C_1\left(\int_0^\infty S(t)\alpha dt\right) &= \int_0^\infty \beta\hat{T}S_2(t)\alpha_2 dt = \frac{\beta\hat{T}}{d_V}\alpha_2, \\ C_2\left(\int_0^\infty S(t)\alpha dt\right) &= \int_0^\infty \gamma S_1(t)\alpha_1 dt = \frac{\gamma}{d_I}\alpha_1, \end{aligned}$$

for any $\alpha := (\alpha_1, \alpha_2) \in \mathbb{R}^2$. Thus

$$L_\varepsilon(\alpha) = M_\varepsilon\alpha, \quad \forall \alpha \in \mathbb{R}^2,$$

where

$$M_\varepsilon = \begin{pmatrix} \varepsilon/d_I & \beta\hat{T}/d_V \\ \gamma/d_I & \varepsilon/d_V \end{pmatrix}.$$

Since M_ε is positive, its spectral radius $r(M_\varepsilon)$ is an eigenvalue with a positive eigenvector in \mathbb{R}^2 . It follows from the uniqueness of the eigenvalue of L_ε with a positive eigenvector that $r(L_\varepsilon) = r(M_\varepsilon)$. Letting $\varepsilon \rightarrow 0^+$, we then obtain

$$\mathcal{R}_0 = r(L) = r(L_0) = r(M_0) = \sqrt{\frac{\beta\hat{T}\gamma}{d_V d_I}} = \sqrt{\frac{\beta h \gamma}{d_T d_V d_I}}.$$

The proof is completed. \blacksquare

Remark Note that, here we define the basic reproduction number as the spectral radius of the next generation operator/matrix [8, 26, 28], which gives the mean number of new infections per infective in any class of infected cell population and virus population, per generation. However, in rest of the thesis, we define the basic reproduction number as the total number of newly infected cells (or viral particles) produced by one infected cell (or virus) during its lifetime, assuming all other target cells are susceptible [13]. By this definition, we have the basic reproduction number

$$\mathcal{R}_0^2 = \frac{\beta h \gamma}{d_T d_V d_I}.$$

The dynamics of the model are always determined by whether \mathcal{R}_0 exceeds 1. Thus, these two definitions of the basic reproduction number will not affect the dynamics of the model mathematically.

For spatial heterogeneous case, that is, if at least one of the model parameters $h(x)$, $\beta(x)$ and $\gamma(x)$ depends on the space location x , we cannot derive an explicit formula for $\mathcal{R}_0 = r(L)$. However, we can compute the spectral radius of the linear operator L numerically by using the orthogonal projection method in computation of eigenvalues for compact linear operators [6]. For the sake of convenience, we consider $\Omega = (0, 1)$, to demonstrate this numerical method. We use Fourier projection [14], where the orthonormal basis is assumed to be $e_k(x) = e^{2k\pi xi}$, $k \in \mathbb{N}$, and then use the Galerkin method. For $\Omega = (0, 1)$, the Green's function associated with $D\Delta$, subject to homogenous Neumann boundary condition, assumes the following explicit form [12]

$$\Gamma(x, y, t, D) = 1 + 2 \sum_{n=1}^{\infty} e^{-Dn^2\pi^2 t} \cos(n\pi x) \cos(n\pi y).$$

For the operator L , the Galerkin matrix is

$$B_n = \begin{pmatrix} 0 & A_n^{(1)} \\ A_n^{(2)} & 0 \end{pmatrix},$$

where

$$A_n^{(1)} = (a_{jk}^{(1)})_{n \times n}, \quad A_n^{(2)} = (a_{jk}^{(2)})_{n \times n}.$$

Here,

$$a_{jk}^{(1)} = \int_0^1 \overline{e_j(x)} \int_0^1 K_1(x, y) e_k(y) dy dx, \quad a_{jk}^{(2)} = \int_0^1 \overline{e_j(x)} \int_0^1 K_2(x, y) e_k(y) dy dx.$$

Then we have

$$\begin{aligned} K_1(x, y) &= \beta(x) \hat{T}(x) \left[\frac{1}{d_V} + 2 \sum_{n=1}^{\infty} \frac{1}{D_0 n^2 \pi^2 + d_V} \cos(n\pi x) \cos(n\pi y) \right], \\ K_2(x, y) &= \gamma \left[\frac{1}{d_I} + 2 \sum_{n=1}^{\infty} \frac{1}{D_T n^2 \pi^2 + d_I} \cos(n\pi x) \cos(n\pi y) \right]. \end{aligned}$$

Figure 5.1 and Figure 5.2 are the plots of the numeric computations of the spectral radius of L with the following baseline parameters

$$h = 10^5, \quad d_T = 0.1, \quad d_I = 0.1, \quad d_V = 5, \quad \gamma = 500, \quad \beta(x) = 5 \times 10^{-10} x^2,$$

showing how the basic reproduction number \mathcal{R}_0 depends on the diffusion rate of infected cells D_T , the basic diffusion rate of free virus D_0 , and virus production rate γ respectively. Note that in the spatially homogeneous case, the diffusion coefficients have no impact on \mathcal{R}_0 .

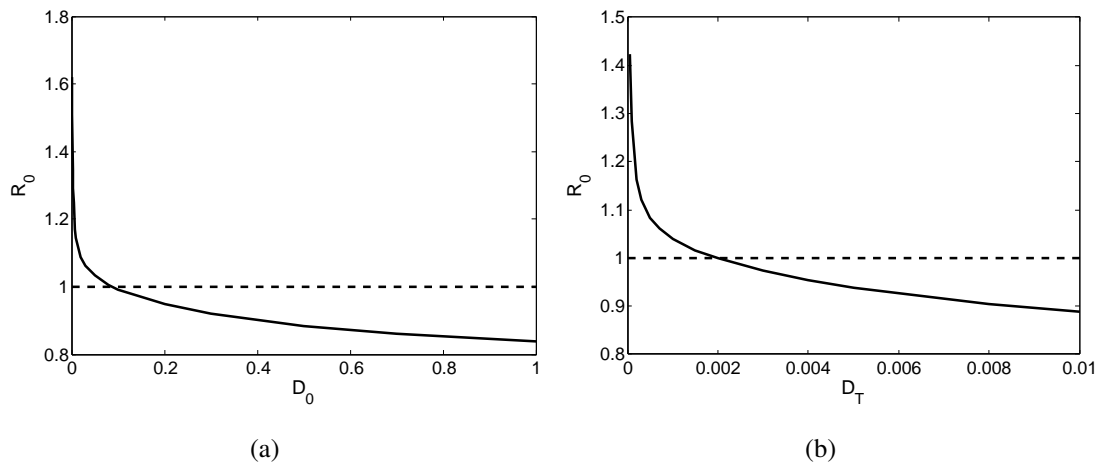


Figure 5.1: The basic reproduction number \mathcal{R}_0 is a decreasing function of D_0 and D_T , where (a) $D_T = 0.00001$, and (b) $D_0 = 0.0001$.

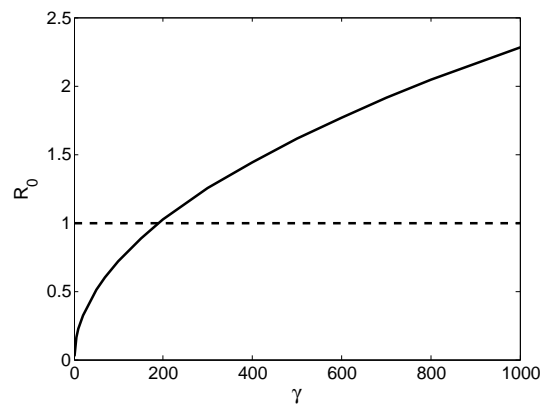


Figure 5.2: The basic reproduction number \mathcal{R}_0 is an increasing function of γ . Here $D_0 = 0.0001$, $D_T = 0.00001$.

Steady states and their linear stability

For the model (5.2)-(5.3)-(5.4), by the biological meaning of the basic reproduction number \mathcal{R}_0 , it is expected that the infection-free steady state $E_0 = (\bar{T}(x), 0, 0)$ is asymptotically stable if $\mathcal{R}_0 < 1$, and there should exist a positive steady state if $\mathcal{R}_0 > 1$. However, it is mathematically difficult to prove these expectations when the model parameters are space dependent. In the rest of the chapter, we only focus on the case when $h(x)$, $\beta(x)$ and $\gamma(x)$ are all positive constants.

In such a spatial homogeneous case, in addition to the infection-free steady state $E_0 = (h/d_T, 0, 0)$, system (5.2) also has the positive steady state $\bar{E} = (\bar{T}, \bar{I}, \bar{V})$ whenever $\mathcal{R}_0 > 1$, where

$$\bar{T} = \frac{h}{d_T \mathcal{R}_0^2}, \quad \bar{I} = \frac{d_T d_V}{\beta \gamma} (\mathcal{R}_0^2 - 1), \quad \bar{V} = \frac{d_T}{\beta} (\mathcal{R}_0^2 - 1).$$

Here, \mathcal{R}_0 is the basic reproduction number of (5.2) with h , γ and β being constants, which has been determined before, that is,

$$\mathcal{R}_0^2 = \frac{\beta h \gamma}{d_T d_V d_I}.$$

Note that E_0 and \bar{E} (if $\mathcal{R}_0 > 1$) are also the steady states in the absence of spatial diffusions, and in such case, it has been shown in [16] that E_0 is globally asymptotically stable if $\mathcal{R}_0 \leq 1$; \bar{E} is globally asymptotically stable if $\mathcal{R}_0 > 1$. For the model (5.2) with diffusions and with no-flux boundary condition, we have the following results on the linear stability of E_0 and \bar{E} .

Theorem 5.2.6 *If $\mathcal{R}_0 < 1$, the infection-free steady state E_0 is linearly stable; if $\mathcal{R}_0 > 1$, the positive steady state \bar{E} is linearly stable.*

Proof Linearizing the system (5.2) at the infection-free steady state $E_0 = (h/d_T, 0, 0)$, we obtain the linear system

$$\frac{\partial}{\partial t} u(t, x) = (D\Delta + A)u(t, x),$$

where

$$D = \begin{pmatrix} D_T & 0 & 0 \\ 0 & D_T & 0 \\ 0 & 0 & D_0 \end{pmatrix}, \quad A = \begin{pmatrix} -d_T & 0 & -\beta h/d_T \\ 0 & -d_I & \beta h/d_T \\ 0 & \gamma & -d_V \end{pmatrix}, \quad u = \begin{pmatrix} u_1 \\ u_2 \\ u_3 \end{pmatrix}.$$

Notice that $\nabla \cdot (D_V(I)\nabla V) = D'_V(I)\nabla I \cdot \nabla V + D_V(I)\Delta V$, $D_V(I) = D_V(\bar{I}) + D'_V(\bar{I})(I - \bar{I}) + \text{h.o.t.}$. The corresponding characteristic polynomial of this linearized system is

$$|\lambda I + Dk^2 - A| = 0, \tag{5.9}$$

where k is the wavenumber, λ is the eigenvalue which determines temporal growth [21]. The steady state E_0 is linearly stable if all eigenvalues have negative real parts.

Substituting the two matrices A and D into (5.9), we obtain

$$\begin{vmatrix} \lambda + D_T k^2 + d_T & 0 & \beta h/d_T \\ 0 & \lambda + D_T k^2 + d_I & -\beta h/d_T \\ 0 & -\gamma & \lambda + D_0 k^2 + d_V \end{vmatrix} = 0.$$

One eigenvalue is $\lambda = -D_T k^2 - d_T < 0$ for all integer $k \geq 0$, and the other eigenvalues are determined by

$$\lambda^2 + a_1(k^2)\lambda + a_2(k^2) = 0,$$

where

$$\begin{aligned} a_1(k^2) &= (D_T + D_0)k^2 + d_I + d_V, \\ a_2(k^2) &= (D_T k^2 + d_I)(D_0 k^2 + d_V) - \gamma\beta h/d_T \\ &= D_T D_0 k^4 + (D_T d_V + D_0 d_I)k^2 + d_I d_V - \gamma\beta h/d_T. \end{aligned}$$

We see that $a_1(k^2) > 0$ for all k , and $a_2(k^2) > 0$, if $d_I d_V - \gamma\beta h/d_T > 0$, that is, if $\mathcal{R}_0 = \frac{\gamma\beta h}{d_I d_V d_T} < 1$. Therefore, if $\mathcal{R}_0 < 1$, the steady state E_0 is linearly stable.

Similarly, linearizing (5.2) at $\bar{E} = (\bar{T}, \bar{I}, \bar{V})$ gives

$$\frac{\partial}{\partial t} u(t, x) = (\bar{D}\Delta + \bar{A})u(t, x),$$

where

$$\bar{D} = \begin{pmatrix} D_T & 0 & 0 \\ 0 & D_T & 0 \\ 0 & 0 & D_V(\bar{I}) \end{pmatrix}, \quad \bar{A} = \begin{pmatrix} -d_T - \beta\bar{V} & 0 & -\beta\bar{T} \\ \beta\bar{V} & -d_I & \beta\bar{T} \\ 0 & \gamma & -d_V \end{pmatrix}, \quad u = \begin{pmatrix} u_1 \\ u_2 \\ u_3 \end{pmatrix}.$$

The corresponding characteristic equation is

$$\begin{vmatrix} \lambda + D_T k^2 + d_T + \beta\bar{V} & 0 & \beta\bar{T} \\ -\beta\bar{V} & \lambda + D_T k^2 + d_I & -\beta\bar{T} \\ 0 & -\gamma & \lambda + D_V(\bar{I})k^2 + d_V \end{vmatrix} = 0,$$

that is,

$$\lambda^3 + b_1(k^2)\lambda^2 + b_2(k^2)\lambda + b_3(k^2) = 0, \tag{5.10}$$

where

$$\begin{aligned}
b_1(k^2) &= (2D_T + D_V(\bar{I}))k^2 + (d_T + d_I + d_V) > 0, \\
b_2(k^2) &= [D_T^2 + 2D_T D_V(\bar{I})]k^4 \\
&\quad + [D_T d_I + D_T(d_T + \beta\bar{V}) + D_T d_V + D_V(\bar{I})(d_T + \beta\bar{V}) + D_T d_V + D_V(\bar{I})d_I]k^2 \\
&\quad + (d_T + \beta\bar{V})d_I + (d_T + \beta\bar{V})d_V > 0, \\
b_3(k^2) &= D_T^2 D_V(\bar{I})k^6 + [D_T^2 d_V + D_T D_V(\bar{I})d_I + D_T D_V(\bar{I})(d_T + \beta\bar{V})]k^4 \\
&\quad + [D_T(d_T + \beta\bar{V})d_V + D_V(\bar{I})(d_T + \beta\bar{V})d_I]k^2 \\
&\quad + \beta\bar{V}d_I d_V > 0.
\end{aligned}$$

$$\begin{aligned}
&b_1(k^2)b_2(k^2) - b_3(k^2) \\
= & (2D_T + D_V(\bar{I}))[D_T^2 + 2D_T D_V(\bar{I})]k^6 \\
& + \{[(2D_T + D_V(\bar{I}))][D_T d_I + (D_T + D_V(\bar{I}))(d_T + \beta\bar{V}) + 2D_T d_V + D_V(\bar{I})d_I] \\
& + [D_T^2 + 2D_T D_V(\bar{I})](d_T + d_I + d_V)\}k^4 + \{(2D_T + D_V(\bar{I}))[(d_T + \beta\bar{V})d_I + (d_T + \beta\bar{V})d_V] \\
& + [D_T d_I + (D_T + D_V(\bar{I}))(d_T + \beta\bar{V}) + 2D_T d_V + D_V(\bar{I})d_I](d_T + d_I + d_V)\}k^2 \\
& + (d_T + d_I + d_V)[(d_T + \beta\bar{V})d_I + (d_T + \beta\bar{V})d_V] \\
& - D_T^2 D_V(\bar{I})k^6 - [D_T^2 d_V + D_T D_V(\bar{I})d_I + D_T D_V(\bar{I})(d_T + \beta\bar{V})]k^4 \\
& - [D_T(d_T + \beta\bar{V})d_V + D_V(\bar{I})(d_T + \beta\bar{V})d_I]k^2 \\
& - \beta\bar{V}d_I d_V \\
\geq & 4D_T^2 D_V(\bar{I})k^6 \\
& + \{2D_T[D_T d_I + D_V(\bar{I})(d_T + \beta\bar{V}) + 2D_T d_V + D_V(\bar{I})d_I] + [D_T^2 + 2D_T D_V(\bar{I})]d_T\}k^4 \\
& + \{D_T[(d_T + \beta\bar{V})d_I + (d_T + \beta\bar{V})d_V] \\
& + [D_T d_I + (D_T + D_V(\bar{I}))(d_T + \beta\bar{V}) + 2D_T d_V + D_V(\bar{I})d_I](d_T + d_I + d_V)\}k^2 \\
& + (d_T + d_I)[(d_T + \beta\bar{V})d_I + (d_T + \beta\bar{V})d_V] \\
> & 0.
\end{aligned}$$

By the Routh-Hurwitz Criteria, we know that all eigenvalues of (5.10) have negative real parts, and therefore, the positive steady state \bar{E} is linearly stable if it exists. ■

5.3 Spreading speed in the case $\Omega = \mathbb{R}$

In the above section, we have seen that in a bounded domain setting, the repulsion effect of infected cells does not change the threshold dynamics characterized by \mathcal{R}_0 . Note that it has

been observed in the experiment [9] that the repulsion effect accelerates the spreading rate of viruses across cells. In this section, we use the model (5.1) to quantitatively investigate the spreading rate of the virus and see how the repulsion effect will affect the spreading speed. Unfortunately, due to the dependence of $D_V(I)$ on I , to the author's knowledge, the existing theories for spreading speed do not apply to (5.1). While a new theory needs to be developed, we will explore this topic numerically here. As in most studies on this topic, we consider the domain $\Omega = \mathbb{R}$ for the spatial variable x , mainly for the convenience in discussing this topic.

To proceed, we choose the following particular function for the diffusion of free virus:

$$D_V(I) = D_0 + \frac{aI}{b+I}. \quad (5.11)$$

Here the repulsion effect is characterized by $g(I) = \frac{aI}{b+I}$, which satisfies $g(0) = 0$ and is an increasing function of I . The parameter a indicates the saturation level and b describes how quickly $g(I)$ increases to its saturation level (see Figure 5.3).

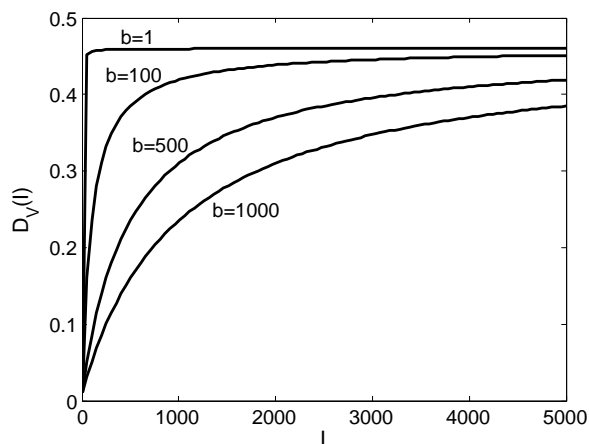


Figure 5.3: The diffusion function of virus $D_V(I) = D_0 + aI/(b+I)$, where we take $D_0 = 0.01$, $a = 0.45$.

The baseline parameter values are taken from [5] as: $h = 10^7$, $\beta = 5 \times 10^{-10}$, $\gamma = 500$, $T = 0.1$, $d_V = 5$, $d_I = 0.1$, $D_0 = 0.0001$ and $b = 1$. In this case, the basic reproduction number is $\mathcal{R}_0 = \sqrt{50}$, and the positive steady state is $(\bar{T}, \bar{I}, \bar{V}) = (0.2 \times 10^7, 9.8 \times 10^7, 9.8 \times 10^9)$. Since our focus is on the repulsion effect, for convenience, here we neglect the mobility of target cells (both infected and uninfected), that is, we assume $D_T = 0$.

We consider different initial distribution functions $T_0(x)$, $I_0(x)$ and $V_0(x)$, and observe, by numerical simulations, the evolution of virus population. First, when the initial distributions

assume

$$T_0(x) = 10^7, \quad I_0(x) = 0, \quad V_0(x) = \begin{cases} 0 & x < 0 \\ 100 & x = 0 \\ 0 & x > 0 \end{cases},$$

meaning that 100 viruses are initially inoculated at the the location $x = 0$. Numerical results are plotted in Figure 5.4(a) for $a = 0$ (no repulsion effect) and $a = 0.45$ (with repulsion effect). From the numerical results, we can estimate the asymptotic spreading speed using the method described by Neubert and Parker [22]. More precisely, the slope of boundaries of inner (outer) triangle region in Figure 5.4(b) is the spreading speed of free virus population in the absence (presence) of repulsion effect.

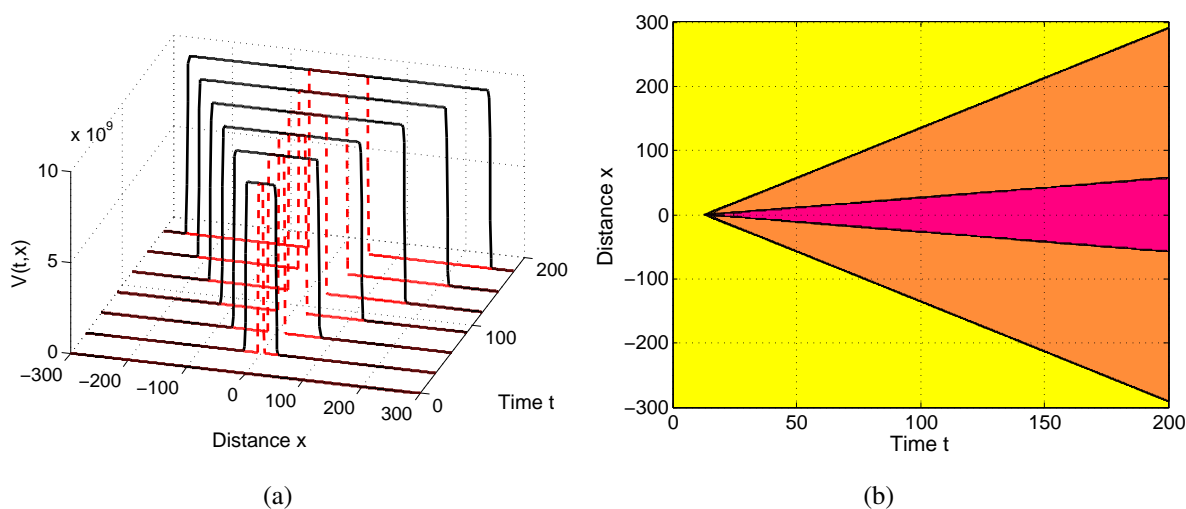


Figure 5.4: (a) The evolution of $V(t, x)$ from the initial distribution $V_0(x)$, where dashed line (red): $a = 0$, solid line (black): $a = 0.45$. (b) The contour of (a).

We see from Figure 5.4(b) that when there is no repulsion effect ($a = 0$), the spreading speed of virus is approximately equal to $c = 0.304$, while in the presence of repulsion effect ($a > 0$), virus spreads more quickly: for $a = 0.45$, the spreading speed is approximately $c = 1.547$, which is more than five times faster than the spreading speed without repulsion effect. This is in close agreement with experimental results observed in Doceul's experiment [9]. Indeed, it was observed [9] that vaccinia virus spreads across one cell every 1.2 hours, but in vaccinia replication kinetics, new virions are formed only 5 to 6 hours after infection. In other words, the vaccinia virus spreads across one cell more quickly than the rate at which it replicates (1.2 hours vs 5-6 hours). As pointed out in [7, 9], and confirmed by our model simulations, such a faster spreading speed is attributed to repulsion effect of superinfecting virions by infected cells.

For different initial distributions, the virus population also spreads at the same speed as $c = 0.304$ for the case without repulsion effect and $c = 1.547$ for the case with repulsion effect. Figure 5.5 gives the numeric simulation results on the evolution of virus population described by the model (5.1) for the following initial distribution,

$$T_0(x) = 10^7, \quad I_0(x) = 0, \quad V_0(x) = \begin{cases} 0 & x \leq -6\pi \\ 50(1 + \cos(x/\pi)) & -6\pi < x \leq 6\pi \\ 0 & x > 6\pi \end{cases} .$$

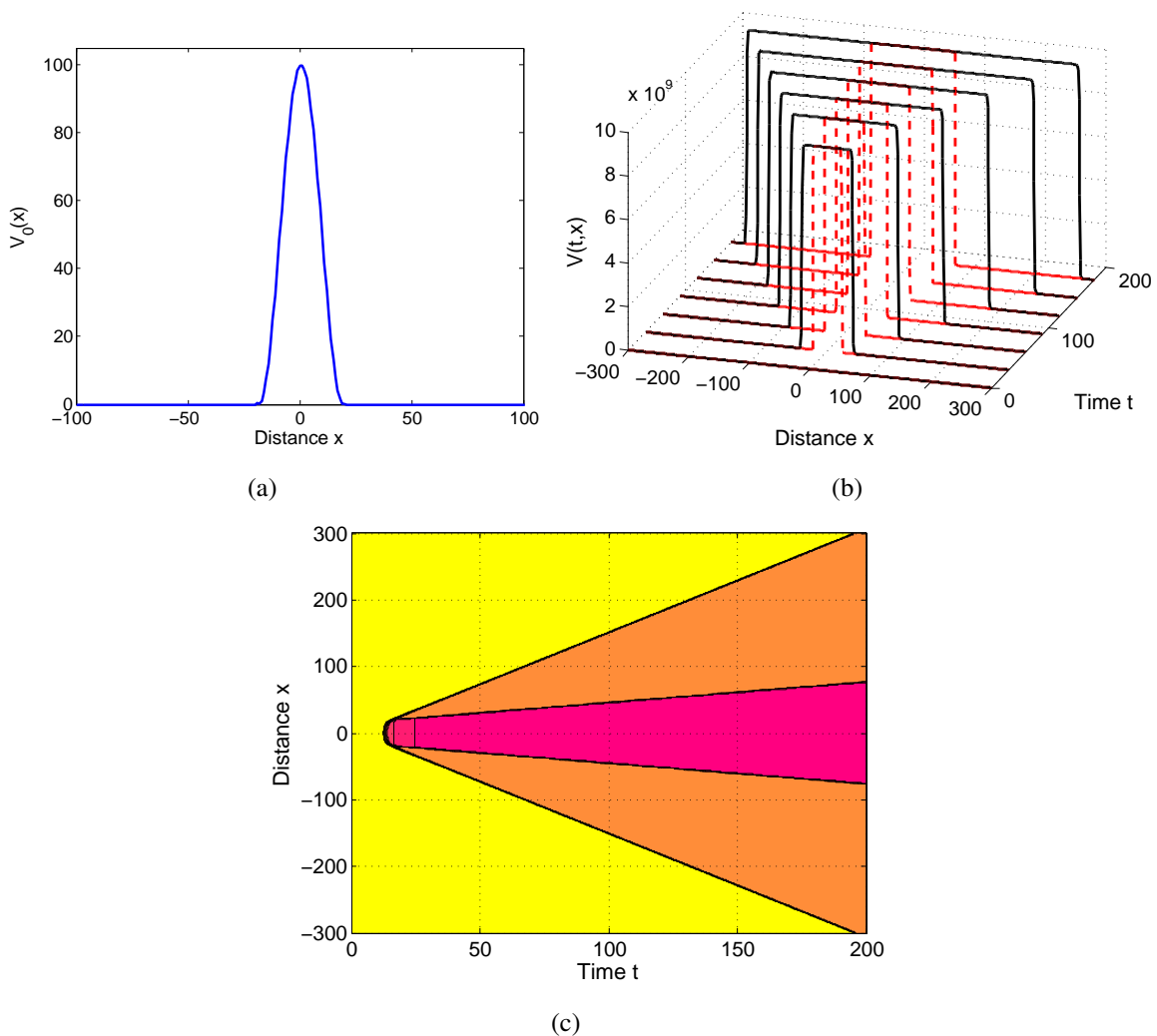


Figure 5.5: (a) The initial distribution $V_0(x)$. (b) The evolution of $V(t, x)$ from the initial distribution, where Dashed line (red): $a = 0$, Solid line (black): $a = 0.45$. (c) The contour of (b).

5.4 Existence of traveling wave solutions in the case $\Omega = \mathbb{R}$

Traveling wavefront solutions are a class of solutions which are in a particular form incorporating the time variable and spatial variable through a moving coordinate. Such a solution describes the spatial transition from one steady state to another. For traveling wavefronts connecting an unstable steady state and a stable steady state, typically there is a minimal wave speed, which is closely related to the spreading speed discussed in the preceding section. Indeed, there have been many works confirming that in many model systems the two speeds coincide (mainly monotone systems), while there are also model systems in which the two speeds are different (see, e.g., [17, 18]).

In this section, we will explore the existence of traveling wavefront connecting the infection free steady state E_0 and the infection steady state \bar{E} , all under the same assumptions/scenario as in the preceding section. That is, we still consider the case $\Omega = \mathbb{R}$ and assume that target cells and infected cells do not move while viral particles diffuse, and consider the following model

$$\begin{aligned}\frac{\partial T}{\partial t} &= h - d_T T - \beta TV, \\ \frac{\partial I}{\partial t} &= \beta TV - d_I I, \\ \frac{\partial V}{\partial t} &= \nabla \cdot (D_V(I)\nabla V) + \gamma I - d_V V.\end{aligned}\tag{5.12}$$

Rescaling the model (5.12) by

$$\begin{aligned}\tilde{t} &= d_T t, \quad \tilde{x} = x, \\ u &= (d_T/h)T, \quad w = (d_T/h)I, \quad v = (\beta/d_T)V, \\ \rho_1 &= d_I/d_T, \quad \rho_2 = \gamma\beta h/d_T^3, \quad \rho_3 = d_V/d_T, \\ D(w) &= D_V(h/d_T w)/d_T,\end{aligned}$$

we obtain (dropping the tildes on t and x)

$$\begin{aligned}\frac{\partial u}{\partial t} &= 1 - u - uv, \\ \frac{\partial w}{\partial t} &= uv - \rho_1 w, \\ \frac{\partial v}{\partial t} &= \nabla \cdot (D(w)\nabla v) + \rho_2 w - \rho_3 v.\end{aligned}\tag{5.13}$$

This rescaled system has two steady states $E_0 = (1, 0, 0)$ and $\bar{E} = (\bar{u}, \bar{w}, \bar{v})$ where

$$\bar{u} = \frac{\rho_1 \rho_3}{\rho_2}, \quad \bar{w} = \frac{\rho_2 - \rho_1 \rho_3}{\rho_1 \rho_2}, \quad \bar{v} = \frac{\rho_2 - \rho_1 \rho_3}{\rho_1 \rho_3}.$$

Obviously, E_0 and \bar{E} are just result of rescaling E_0 and \bar{E} in preceding sections, and \bar{E} is biologically meaningful (positive) iff $\rho_2 > \rho_1\rho_3$ which is equivalent to $\mathcal{R}_0 = \sqrt{\gamma\beta h/d_T d_I d_V} = \sqrt{\rho_2/\rho_1\rho_3} > 1$.

Traveling wave solutions of (5.13) are solutions of the form $\tilde{u}(x, t) = u(x + ct)$, $\tilde{w}(x, t) = w(x + ct)$, $\tilde{v}(x, t) = v(x + ct)$ where $c > 0$ represents the speed of traveling wave solutions. Substituting this solution form into (5.13), we obtain

$$\begin{aligned} cu' &= 1 - u - uv, \\ cw' &= uv - \rho_1 w, \\ cv' &= D'(w)w'v' + D(w)v'' + \rho_2 w - \rho_3 v, \end{aligned} \quad (5.14)$$

where prime denotes differentiation with respect to the wave variable $s = x + ct$.

Letting $z = v'$, system (5.14) is rewritten as

$$\begin{aligned} u' &= \frac{1}{c}(1 - u - uv), \\ w' &= \frac{1}{c}(uv - \rho_1 w), \\ v' &= z, \\ z' &= \frac{1}{D(w)} \left[cz - \frac{1}{c} D'(w)(uv - \rho_1 w)z - \rho_2 w + \rho_3 v \right], \end{aligned} \quad (5.15)$$

which has two steady states $E'_0 = (1, 0, 0, 0)$ and $E'_1 = (\bar{u}, \bar{w}, \bar{v}, 0)$ when $\mathcal{R}_0 > 1$. We consider the existence of solutions of (5.14) satisfying the asymptotic boundary conditions

$$\lim_{s \rightarrow -\infty} (u(s), w(s), v(s), z(s)) = (1, 0, 0, 0), \quad \lim_{s \rightarrow \infty} (u(s), w(s), v(s), z(s)) = (\bar{u}, \bar{w}, \bar{v}, 0), \quad (5.16)$$

which accounts for transition from the infection-free steady state E_0 to the infection steady state \bar{E} .

Behaviors of solutions of (5.15) near E'_0 is typically determined by the linearization of (5.15) at E'_0 . Straightforward calculations give the Jacobian matrix of (5.15) at E'_0 as

$$J_0 = \begin{pmatrix} -1/c & 0 & -1/c & 0 \\ 0 & -\rho_1/c & 1/c & 0 \\ 0 & 0 & 0 & 1 \\ 0 & -\rho_2/D_0 & \rho_3/D_0 & c/D_0 \end{pmatrix}.$$

It has an eigenvalue $\lambda = -1/c$ which is negative for all $c > 0$. So, we only need to consider other eigenvalues which are determined by

$$P(\lambda) := \lambda^3 + a_1\lambda^2 + a_2\lambda + a_3 = 0,$$

where

$$a_1 = \frac{D_0\rho_1 - c^2}{cD_0}, \quad a_2 = -\frac{\rho_1 + \rho_3}{D_0} < 0, \quad a_3 = \frac{\rho_2 - \rho_1\rho_3}{cD_0} > 0.$$

Since $P(0) = a_3 > 0$ and $P(-\infty) = -\infty$, $P(\lambda) = 0$ has a negative root. By the Descartes' rule of signs and by the Routh-Hurwitz criterion, the other two roots of $P(\lambda) = 0$ are either positive and real, or a pair of conjugate complex numbers. In the latter case, the complex eigenvalues imply the oscillations of solutions of (5.15) near E'_0 , implying the w and v will take negative values (making solutions biologically meaningless), and thus (5.15)-(5.16) cannot have positive solutions, meaning that (5.13) cannot have traveling wavefronts connecting E_0 and \bar{E} . Therefore, in order for (5.13) to have traveling wavefronts connecting E_0 and \bar{E} , it is necessary $P(\lambda) = 0$ to have a pair of positive real roots (counting multiplicity).

Note that $P'(\lambda) = 3\left(\lambda^2 + \frac{2a_1}{3}\lambda + \frac{a_2}{3}\right)$ and $P'(\lambda) = 0$ has a unique positive root

$$\lambda^* = \frac{1}{3}\left(-a_1 + \sqrt{a_1^2 - 3a_2}\right).$$

Since $P(0) = a_3 > 0$ and $P'(0) = a_2 < 0$, we conclude that $P(\lambda) = 0$ has two positive real roots if and only if $P(\lambda^*) < 0$. From $P'(\lambda^*) = 0$, we obtain that

$$\lambda^{*2} + \frac{2a_1}{3}\lambda^* + \frac{a_2}{3} = 0, \quad \lambda^{*3} + \frac{2a_1}{3}\lambda^{*2} + \frac{a_2}{3}\lambda^* = 0.$$

Using these equations to simplify the form of $P(\lambda^*)$, we obtain

$$\begin{aligned} P(\lambda^*) &= \frac{a_1}{3}\lambda^{*2} + \frac{2a_2}{3}\lambda^* + a_3 \\ &= \frac{2}{3}\left(a_2 - \frac{a_1^2}{3}\right)\lambda^* + a_3 - \frac{a_1a_2}{9} \\ &= \frac{1}{27}\left[-2\left(a_1^2 - 3a_2\right)^{3/2} + 27a_3 + 2a_1^3 - 9a_1a_2\right]. \end{aligned}$$

It then follows that

$$\begin{aligned} P(\lambda^*) < 0 &\Leftrightarrow 27a_3 + 2a_1^3 - 9a_1a_2 \leq 0, \\ &\text{OR } 27a_3 + 2a_1^3 - 9a_1a_2 > 0 \text{ AND } 4\left(a_1^2 - 3a_2\right)^3 > \left(27a_3 + 2a_1^3 - 9a_1a_2\right)^2; \\ P(\lambda^*) > 0 &\Leftrightarrow 27a_3 + 2a_1^3 - 9a_1a_2 > 0 \text{ AND } 4\left(a_1^2 - 3a_2\right)^3 < \left(27a_3 + 2a_1^3 - 9a_1a_2\right)^2. \end{aligned}$$

Let $Q_1(c) := 27a_3 + 2a_1^3 - 9a_1a_2$, then $Q_1(c) = \frac{1}{D_0^3c^3}\left(d_0c^6 + d_1c^4 + d_2c^2 + d_3\right)$, where $d_0 = -2$, $d_1 = -3D_0(\rho_1 - 3\rho_3)$, $d_2 = 3D_0^2(9\rho_2 - 6\rho_1\rho_3 + \rho_1^2) > 0$ and $d_3 = 2\rho_1^3D_0^3 > 0$. By the Descartes' rule of signs, $\bar{Q}_1(c) := d_0c^6 + d_1c^4 + d_2c^2 + d_3 = 0$ has a unique positive root $c_0^* > 0$. Since $\bar{Q}_1(0) = d_3 > 0$, we see that $\bar{Q}_1(c) > 0$ if $0 < c < c_0^*$, and $\bar{Q}_1(c) < 0$ if $c > c_0^*$. Furthermore, $Q_1(c_0^*) = 0$, $Q_1(c) > 0$ if $0 < c < c_0^*$, and $Q_1(c) < 0$ if $c > c_0^*$.

Let $Q_2(c) := 4(a_1^2 - 3a_2)^3 - (27a_3 + 2a_1^3 - 9a_1a_2)^2$, then $Q_2(c) = \frac{27}{D_0^4 c^4} (b_0 c^6 + b_1 c^4 + b_2 c^2 + b_3)$ where b_i , $i = 0, 1, 2, 3$, are given by

$$\begin{aligned} b_0 &= 4\rho_2 + \rho_1^2 + \rho_3^2 - 2\rho_1\rho_3, \\ b_1 &= D_0(6\rho_2\rho_1 + 2\rho_1^3 - 8\rho_1\rho_3^2 + 4\rho_3^3 + 18\rho_2\rho_3 + 2\rho_1^2\rho_3), \\ b_2 &= D_0^2(8\rho_1^3\rho_3 - 8\rho_1^2\rho_3^2 + \rho_1^4 + 36\rho_2\rho_1\rho_3 - 6\rho_2\rho_1^2 - 27\rho_2^2), \\ b_3 &= 4D_0^3(\rho_1^4\rho_3 - \rho_2\rho_1^3). \end{aligned} \tag{5.17}$$

Note that $b_0 > 0$, $b_1 > 0$, $b_3 < 0$. Again by the Descartes' rule of signs,

$$Q(c) := b_0 c^6 + b_1 c^4 + b_2 c^2 + b_3 = 0, \tag{5.18}$$

has a unique positive root $c^* > 0$. Since $Q(0) = b_3 < 0$, we see that $Q(c) < 0$ if $0 < c < c^*$, and $Q(c) > 0$ if $c > c^*$. Therefore, $Q_2(c^*) = 0$, $Q_2(c) < 0$ if $0 < c < c^*$, and $Q_2(c) > 0$ if $c > c^*$.

Note that $a_1^2(c) - 3a_2 > 0$ for all $c > 0$. Thus, $Q_2(c_0^*) = a_1^2(c_0^*) - 3a_2 > 0$, implying $c^* < c_0^*$. In summary, we have obtained:

$$\begin{aligned} P(\lambda^*) < 0 &\Leftrightarrow Q_2(c) \leq 0, \text{ OR, } Q_2(c) > 0 \text{ AND } Q_1(c) > 0 \\ &\Leftrightarrow c \geq c_0^* \text{ (hence } c > c^*), \text{ OR, } 0 < c < c_0^* \text{ AND } c > c^* \\ &\Leftrightarrow c > c^*; \\ P(\lambda^*) > 0 &\Leftrightarrow Q_2(c) > 0 \text{ AND } Q_1(c) < 0 \\ &\Leftrightarrow 0 < c < c_0^* \text{ AND } c < c^* \\ &\Leftrightarrow 0 < c < c^*. \end{aligned}$$

Thus, for any $c \in (0, c^*)$, system (5.13) has no traveling wavefront solutions with speed c that connects E_0 and \bar{E} .

From the definition of $Q(c)$, we obtain

$$Q(\sqrt{D_0\rho_1}) = D_0^3\rho_1 [4\rho_1(\rho_1 + \rho_3)^3 - 27(\rho_2 - \rho_1\rho_3)^2].$$

It is easy to see that $Q_3(\rho_1) := 4\rho_1(\rho_1 + \rho_3)^3$ is strictly increasing function of ρ_1 , and $Q_3(0) = 0$, $Q_3(+\infty) = +\infty$; $Q_4(\rho_1) := 27(\rho_2 - \rho_1\rho_3)^2$ is strictly decreasing function of ρ_1 when $\rho_2 > \rho_1\rho_3$, and $Q_4(0) = 27\rho_2^2$. Therefore, $Q(\sqrt{D_0\rho_1})$ has a unique positive root ρ_1^* , such that $Q(\sqrt{D_0\rho_1}) < 0$ for $0 < \rho_1 < \rho_1^*$, and $Q(\sqrt{D_0\rho_1}) > 0$ for $\rho_1 > \rho_1^*$. By the property of $Q(c)$, we have $\sqrt{D_0\rho_1} < c^*$ for $0 < \rho_1 < \rho_1^*$; $\sqrt{D_0\rho_1} > c^*$ for $\rho_1 > \rho_1^*$ and $c^* = \sqrt{D_0\rho_1^*}$, where ρ_1 is determined by (5.20). Therefore, we obtain the following information about c^* :

$$\begin{cases} c^* > \sqrt{D_0\rho_1} & \text{if } 0 < \rho_1 < \rho_1^*, \\ c^* = \sqrt{D_0\rho_1} & \text{if } \rho_1 = \rho_1^*, \\ c^* < \sqrt{D_0\rho_1} & \text{if } \rho_1 > \rho_1^*, \end{cases} \tag{5.19}$$

where for given ρ_2 and ρ_3 , ρ_1^* is the unique positive root of the equation

$$\frac{2\sqrt{3}}{9} \sqrt{\rho_1} (\rho_1 + \rho_3)^{3/2} + \rho_1 \rho_3 = \rho_2. \quad (5.20)$$

Although we cannot obtain an explicit formula for c^* , we can numerically calculate it when the model parameters are given. To demonstrate this, we choose the same baseline parameters of (5.12) as those in the preceding section. Then for the rescaled model (5.13), we have $\rho_1 = 1.0$, $\rho_2 = 2500$, $\rho_3 = 50$, $\bar{u} = 0.02$, $\bar{w} = 0.98$, $\bar{v} = 49$. Under the rescaling, the function given in (5.11) is scaled to

$$D(w) = \frac{1}{d_T} \left(D_0 + \frac{ahw}{d_T b + hw} \right).$$

When $D_0 = 0.0001$ for the original system (5.12), that is $D(0) = 0.001$ for the rescaled system (5.13), numerically solving (5.18), we obtain $c^* = 0.2214$ for (5.13). This means that the c^* for original system (5.12) is $c^* = 0.02214$, since the rescaling is $\tilde{t} = d_T t$, $\tilde{x} = x$ and $d_T = 0.1$. Numerically plotting the solutions of (5.18) also shows that c^* is an increasing function of $D(0)$, that is, an increasing function of D_0 (see Figure 5.6).

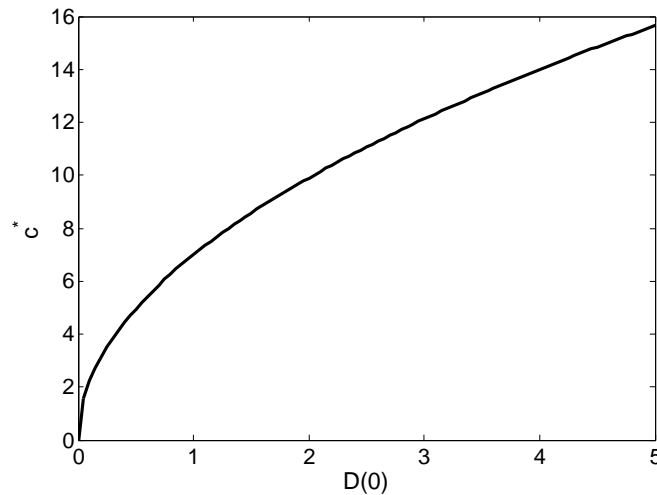


Figure 5.6: Impact of $D(0)$ on c^* .

We have seen that for $c \in (0, c^*)$, there is no traveling wavefront with speed c that connects E_0 and \bar{E} . It is expected that c^* is indeed the minimal wave speed in the sense that for every $c > c^*$, (5.13) actually has traveling wavefront with speed c that connects E_0 and \bar{E} . Unfortunately, we cannot theoretically prove this at the present. In the following, we will explore this numerically. To this end, we use the method developed by Beyn [4]. Firstly, the infinite interval is truncated to a finite interval $[\tau_-, \tau_+]$. Then we consider the boundary-value problem (5.15) and (5.16) on this finite interval with additional projection conditions (see [4],

Section 3) and phase conditions ([4], Section 4). We solve the boundary value problem by BVP solver `bvp4c` in Matlab. The solutions $y(s) = (u(s), w(s), v(s), z(s))$ are split into two segments, $y_1(s) = (u_1, w_1, v_1, z_1)$ on $[0, \tau_+]$, and $y_2(s) = (u_2, w_2, v_2, z_2)$ on $[0, \tau_-]$, and the interval $[\tau_-, \tau_+]$ is projected onto $[-1, 1]$, such that $y_1(s) = y(s\tau_+)$ and $y_2(s) = y(s\tau_-)$. Thus, we need to consider the following 8-dimensional ODE system,

$$y'_1 = \tau_+ f(y_1), \quad y'_2 = \tau_- f(y_2), \quad s \in [0, 1]. \quad (5.21)$$

We see that $y_1(s)$ and $y_2(s)$ should satisfy the boundary condition

$$y_1(0) = y_2(0). \quad (5.22)$$

Let ξ_d be an estimate of the derivative $y'(0)$ and ξ_0 be an estimate of $y(0)$. Then we get the phase condition

$$\xi_d^T (y_1(0) - \xi_0) = 0. \quad (5.23)$$

Let A_- and A_+ be the Jacobian matrix of (5.15) at E'_0 and E'_1 respectively. Let the eigenvectors which span stable subspace of A_{\pm} be columns of $B_{\pm s}$, the eigenvectors which span unstable subspace of A_{\pm} be columns of $B_{\pm u}$, and construct

$$B_{\pm} = (B_{\pm u} B_{\pm s}), \quad B_{\pm}^{-1} = \begin{pmatrix} L_{\pm u} \\ L_{\pm s} \end{pmatrix},$$

where the rows of $L_{\pm s}$ and $L_{\pm u}$ form a basis for the stable and unstable subspaces of A_{\pm}^T respectively. The projection conditions are given by

$$L_{+u}(y_1(1) - E'_0) = 0, \quad L_{+u}(y_2(1) - E'_1) = 0. \quad (5.24)$$

We solve ODE problem (5.21) with boundary conditions (5.22), (5.23) and (5.24), by Matlab, where ξ_d and ξ_0 are chosen to be $\xi_d = ((\bar{u} - 1)/2, \bar{w}/2, \bar{v}/2, 0)$ and $\xi_0 = ((\bar{u} + 1)/2, \bar{w}/2, \bar{v}/2, 0)$. The Jacobian of (5.15) at E'_0 is $A_- = J_0$, and that at E'_1 is

$$A_+ = \begin{pmatrix} -(1 + \bar{v})/c & 0 & -\bar{u}/c & 0 \\ \bar{v}/c & -\rho_1/c & \bar{u}/c & 0 \\ 0 & 0 & 0 & 1 \\ 0 & -\rho_2/D(\bar{w}) & \rho_3/D(\bar{w}) & c/D(\bar{w}) \end{pmatrix}.$$

Setting the parameters as in previous discussions, we can now numerically solve for the traveling wave solutions.

In the absence of repulsion effect, that is $a = 0$, the critical value c^* is obtained by solving the equation (5.18) which is $c^* = 0.2214$. Numerical simulations of the model (5.13) are given

in Figure 5.7 and Figure 5.8. It is seen that for $c < c^*$, $w(s)$ and $v(s)$ go to negative for some values of s , and hence the system (5.13) cannot have traveling wave solution; while for any $c > c^*$, there exists traveling wave solution for (5.13). For example, $c = 0.23$, the wave profiles of $u(s)$ and $w(s)$ are shown in Figure 5.7, $v(s)$ is shown in Figure 5.8(a). For different values of wave speed c , the traveling wave solutions have different wave profiles. Figure 5.8(b) shows the wave profiles of $v(s)$ for $c = 0.23$, $c = 5$ and $c = 10$. In this case, our numerical results show that $c^* = 0.2214$ is indeed that minimal wave speed for system (5.13), and hence, the minimal wave speed for the original system (5.12) should be $c^* = 0.02214$ which is much smaller than the spreading speed $c = 0.304$ established in the preceding section.

In the presence of repulsion effect, that is $a > 0$, solving (5.18) still gives $c^* = 0.2214$ since (5.18) is independent of a . But our simulations show that this critical value is not minimal wave speed in this case. Fixing $a = 0.45$, from the simulation results shown in Figure 5.9, we see that $w(s)$ and $v(s)$ go to negative for some values of s when $c = 5 > c^*$. This means for $c = 5$, there is no traveling wavefront for (5.13). In fact, numerical simulations show that this is also the case for $c \leq 13$. However for $c = 14$, the system (5.13) has traveling wavefront (see Figure 5.10). This implies that the minimal wave speed is between 13 and 14. Obviously, this minimal wave speed is also different from the spreading speed $c = 1.547$ established in the preceding section. From these numerical results, we see that in the presence of repulsion effect, the linearized system will not determine the minimal wave speed for the original system, that is, the minimal wave speed is not linearly deterministic.

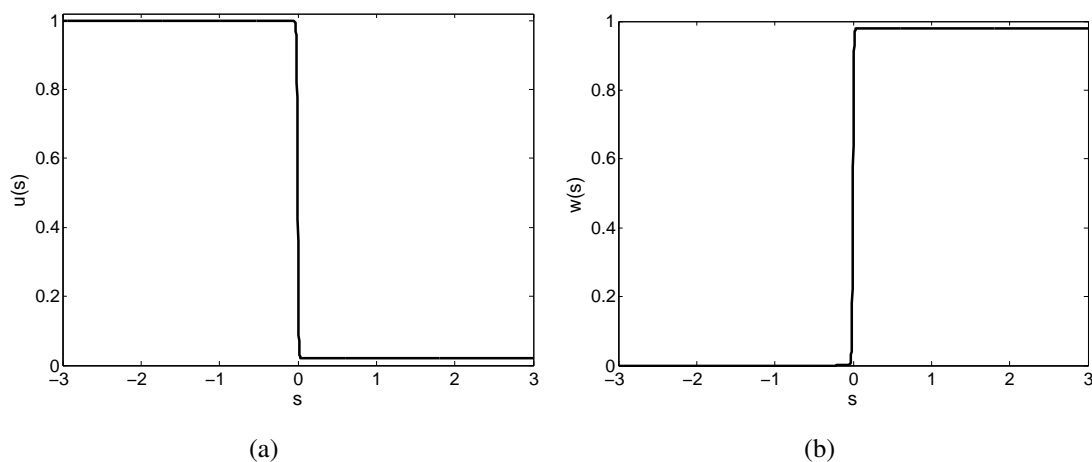


Figure 5.7: Wave profiles when $a = 0$ and $c = 0.23$: (a) profile of $u(s)$; (b) profile of $w(s)$.

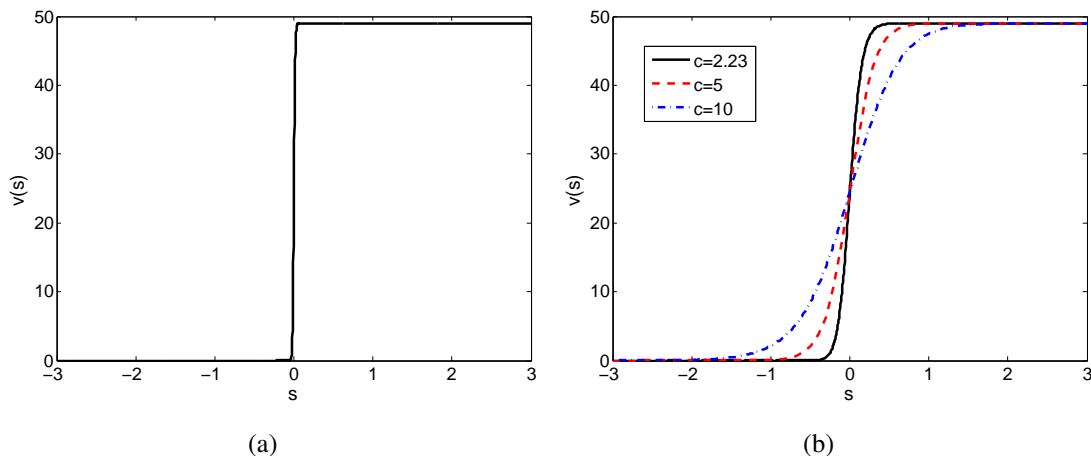


Figure 5.8: Wave profiles of $v(s)$ when $a = 0$: (a) $c = 0.23$; (b) $c = 0.23, 5, 10$.

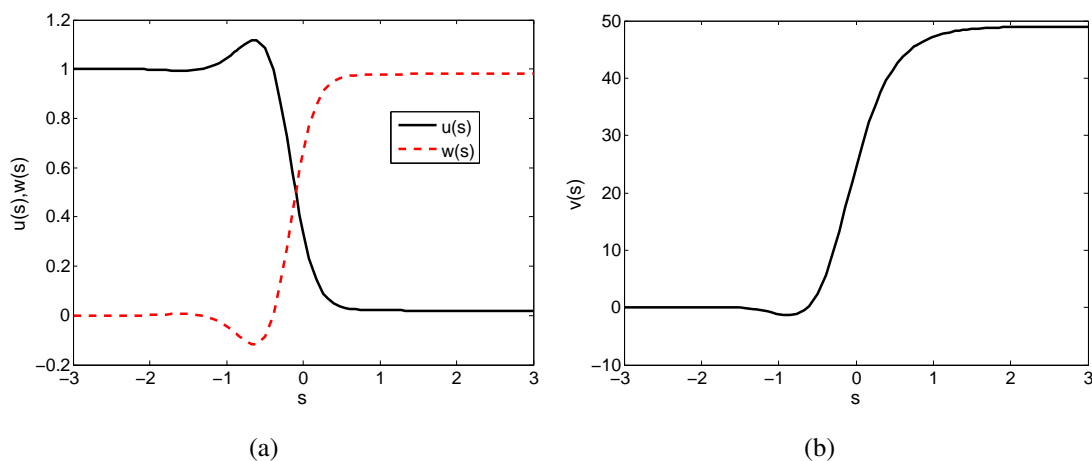


Figure 5.9: For $a = 0.45$, when $c = 5$, there is no traveling wave solution, since $w(s)$ and $v(s)$ go to negative for some s .

5.5 Conclusion and discussion

In this chapter, we propose a general virus infection dynamic model to describe the new mechanism reported in [9] that can speed up the spread of virus within host. This new mechanism is called the repulsion of superinfecting virions by infected cells. Although this mechanism was discovered for vaccinia virus, it was pointed out in [9] that some other viruses may also have this kind of rapid spreading mechanisms. With our general model, we have numerically confirmed the experimental results reported in Doceul *et al.* [9], that is, the repulsion of superinfecting virions ($a > 0$) accelerates the spread of free viral particles. This model has the potential to be used for predicting the spreading speed for other virus with similar repulsion

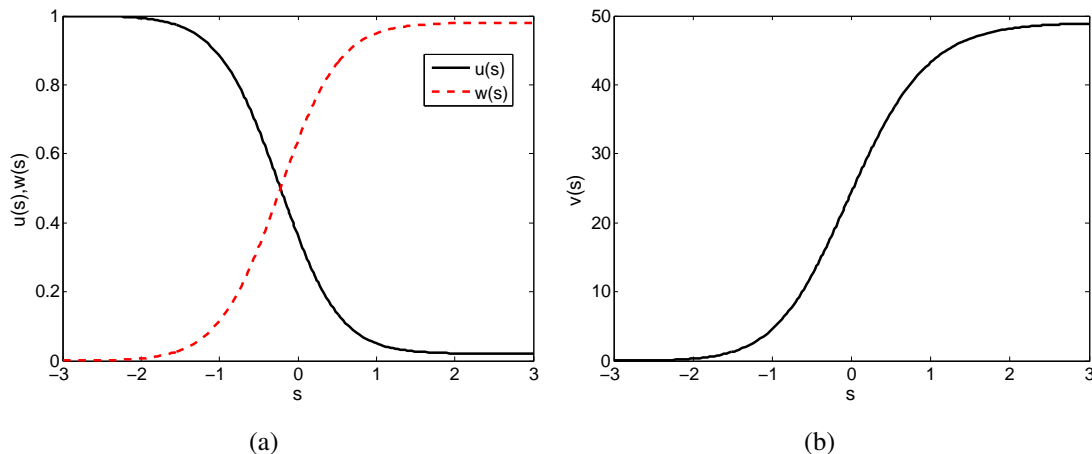


Figure 5.10: For $a = 0.45$, when $c = 14$, there exists a traveling wave solution. (a) The wave profile of $u(s)$ and $w(s)$, (b) The wave profile of $v(s)$.

effect.

In many mathematical and epidemiological models, especially for scalar equation or cooperative systems, the asymptotic spreading speed can be characterized as the slowest speed of traveling wave front solutions connecting an unstable steady state and a stable steady state (see, e.g., [17] and the references therein). Fisher equation is such a model (classical). Such a result is very useful, since the slowest wave speed is more easily to be calculated than the spreading speed.

As far as spreading speed goes, under some conditions, the linear determinacy holds for cooperative systems ([29]), that is, the spreading rate of the full nonlinear model agrees with the spreading rate of the system linearized about the leading edge of the invasion. For example, Lewis *et al.* [18] obtained some parameter ranges for the Lotka-Volterra competition model, for which the spreading speed is linearly determined. They also derived a set of sufficient conditions for linear determinacy in a spatially explicit two-species discrete-time competition model. However, linear determinacy is not always valid, especially for complicated models, such as, competition models and prey-predator models. When linear determinacy does not hold, spread rates may exceed linearly determined predictions. There are also cases that different species in a model system may have different spreading speeds [17, 30]. In our model, the linear determinacy does not hold and the spreading rate is much larger than linearly determined minimal wave speed in the presence of repulsion effect. This may be due to the complexity of the virus dynamic system, which is neither a cooperative system nor a competitive system. In fact, the target cell population and free virus population have a relationship similar to a prey-predator system, while infected cells and free viruses are cooperative. In our model, the minimal wave speed, given by the linearized analysis at infection-free steady state, is only true for the case

when there is no repulsion effect ($a = 0$). If repulsion of superinfecting virions is present, the minimal wave speed would be much higher than the linearly determined wave speed.

Besides the classical route of cell-free virus spread, many viruses can spread through cell-to-cell transmission [23], that is, viruses move between cells without diffusing through the extracellular environment. For instance, HIV-1 and HTLV-1 can spread from cell to cell by virological synapses or cell membrane nanotubes [24]; murine leukemia virus (MLV) can establish filopodial bridges for efficient cell-to-cell transmission [20]; Herpes simplex virus type-1 (HSV-1) can move between fibroblasts by polarized assembly and budding at basolateral intercellular junctions [24]; Vaccinia virus can also spread through cell-to-cell by projection on actin tails [23]. We do not consider this route of spread in this chapter, and leave it for a separate research project.

Bibliography

- [1] Adams R.A., Sobolev spaces, Academic Press, New York, 1975.
- [2] Amann H., Dynamical theory of quasilinear parabolic equations III: Global existence, *Math. Z.*, 202 (1989) 219-250.
- [3] Amann H., Nonhomogeneous linear and quasilinear elliptic and parabolic boundary value problems, in: Schmeisser H.J., Triebel H. (Eds.), *Function spaces, Differential Operators and Nonlinear Analysis*, Teubner Texte Math., 133 (1993) 9-126.
- [4] Beyn W.J., The numerical computation of connecting orbits in dynamical systems, *IMA J. Numer. Anal.*, 9 (1990) 379-405.
- [5] Bonhoeffer S., May R.M., Shaw G.M. and Nowak M.A., Virus dynamics and drug therapy, *Proc. Natl. Acad. Sci. USA*, 94 (1997) 6971.
- [6] Chatelin F., The spectral approximation of linear operators with application to the computation of eigenelements of differential and integral operators, *SIAM Review*, 23 (1981) 495-522.
- [7] Condit R.C., Surf and turf: mechanism of enhanced virus spread during poxvirus infection, *Viruses*, 2 (2010) 1050-1054.
- [8] van den Driessche P., Watmough J., Reproduction numbers and sub-threshold endemic equilibria for compartmental models of disease transmission, *Math. Biosci.*, 180 (2002) 29-48.
- [9] Doceul V., Hollinshead M., van der Linden L. and Smith G.L., Repulsion of superinfecting virions: a mechanism for rapid virus spread, *Science*, 327 (2010) 873-876.
- [10] Gan Q., Xu R. and Yang P., Travelling waves of a hepatitis B virus infection model with spatial diffusion and time delay, *J. Appl. Math.*, 75 (2010) 392-417.

- [11] Guo Z., Wang F.-B. and Zou X., Threshold dynamics of an infective disease model with a fixed latent period and non-local infections, *J. Math. Biol.*, 65 (2012), 1387-1410.
- [12] Haberman R., *Elementary applied partial differential equations: with Fourier series and boundary value problems*, Prentice Hall, New Jersey, 1998.
- [13] Heffernan J.M., Smith R.J. and Wahl L.M., Perspectives on the basic reproductive ratio, *J. R. Soc. Interface*, Vol. 2 No. 4 (2005) 281-293.
- [14] Ikebe Y., The Galerkin method for the numerical solution of Fredholm integral equations of the 2nd kind, *SIAM Review*, 14 (1972) 465-491.
- [15] Komarova N.L., Viral reproductive strategies: how can lytic viruses be evolutionarily competitive?, *J. Theor. Biol.*, 249 (2007) 766-784.
- [16] Korobeinikov A., Global properties of basic virus dynamics models, *Bull. Math. Bio.*, 66 (2004) 879-883.
- [17] Li B., Weinberger H.F. and Lewis M.A., Spreading speeds as slowest wave speeds for cooperative systems, *Math. Biosci.*, 196 (2005) 82-98.
- [18] Lewis M.A., Li B. and Weinberger H.F., Spreading speeds and linear determinacy for two-species competition models, *J. Math. Biol.*, 45 (2002) 219-233.
- [19] Lou Y. and Zhao X.Q., A reaction-diffusion malaria model with incubation period in the vector population, *J. Math. Biol.*, 62 (2011) 543-568.
- [20] Mothes W., Sherer N.M., Jin J. and Zhong P., Virus cell-to-cell transmission, *J. Virol.*, 84 (2010) 8360-8368.
- [21] Murray J.D., *Mathematical biology II: spatial models and biomedical applications*, Springer-Verlag, New York, 2000.
- [22] Neubert M.G. and Parker I.M., Projecting rates of spread for invasive species, *Risk Analysis*, 24 (2004) 817-831.
- [23] Sattentau Q., Avoiding the void: cell-to-cell spread of human viruses, *Nat. Rev. Microbiol.*, 6 (2008) 815-826.
- [24] Sattentau Q., The direct passage of animal viruses between cells, *Curr. Opin. Virol.*, 1 (2011) 396-402.

- [25] Smith H.L., Monotone dynamical systems: an introduction to the theory of competitive and cooperative systems, Amer. Math. Soc. Math. Surveys and Monographs, vol 41, Providence, RI, 1995.
- [26] Thieme H.R., Spectral bound and reproduction number for infinite-dimensional population structure and time heterogeneity, *SIAM J. Appl. Math.*, 70 (2009) 188-211.
- [27] Wang K. and Wang W., Propagation of HBV with spatial dependence, *Math. Biosci.*, 210 (2007) 78-95.
- [28] Wang W. and Zhao X.Q., A nonlocal and time-delayed reaction-diffusion model of Dengue transmission, *SIAM J. Appl. Math.*, 71 (2011) 147-168.
- [29] Weinberger H.F., Lewis M.A. and Li B., Analysis of linear determinacy for spread in cooperative models, *J. Math. Biol.*, 45 (2002) 183-218.
- [30] Weinberger H.F., Lewis M.A. and Li B., Anomalous spreading speeds of cooperative recursion systems, *J. Math. Biol.*, 55 (2007) 207-222.
- [31] Xu R. and Ma Z., An HBV model with diffusion and time delay, *J. Theor. Biol.*, 257 (2009) 499-509.

Chapter 6

A reaction diffusion system modeling HIV-1 infection dynamics with CTL-chemotaxis

6.1 Introduction

Some living organisms or cells, such as somatic cells and lymphocytes, have the ability to detect certain chemicals in their environment and adapt their movement accordingly, moving either toward or away from the chemical stimulus. This phenomenon is called *chemotaxis* or generally *chemosensitive movement*. In the mathematical literature, the term *chemotaxis* is used broadly to describe general chemosensitive movement responses, including chemoattraction (positive chemotaxis) and chemorepulsion (negative chemotaxis). However, in the experimental community, for example, in leukocytes trafficking mechanism, the term *chemotaxis* is defined only as chemoattraction, that is, an active movement of leukocytes toward chemokinetic agents, while chemorepulsion is referred to as *fugetaxis*, describing the active movement of leukocytes away from chemokinetic agents. In this chapter, we use *chemotaxis* as the general chemosensitive movement, either chemoattraction (positive chemotaxis) or chemorepulsion (negative chemotaxis).

Cytotoxic T lymphocytes (CTL), or effector CD8⁺ T cells, play a critical role in host defense against human immunodeficiency virus type 1 (HIV-1) infection. Normally, effector T cells leave lymph nodes and traffic to peripheral sites of infection. However, in HIV-1 infection, the majority of HIV-1 replication occurs in lymphoid tissues. To implement their antiviral activity, CTL must migrate reversely back into infected lymphoid tissues, and remain within them. Thus the recruitment of CTL is very important for the clearance of HIV-1. The move-

ment of lymphocytes between the circulatory system and specific tissues is coordinated by chemokines and their receptors. For example, inflammatory chemokines guide effector T cells to exit lymphoid tissues and home to peripheral sites of infection. HIV-1 infection and replication in the lymphoid tissues changes its the chemotactic and cellular environments. As HIV-1 disease progresses, the homing ability of CTL to infected lymph nodes may be disrupted, due either to reduced lymph node chemokine levels or reduced CTL chemokine receptor expression, and thus affect the cytotoxic effect of CTL in advanced HIV-1 infection [5].

Many viruses encode chemotactically active proteins. For instance, the envelope protein gp120 of HIV-1 has been shown to act as a T-cell chemoattractant via binding to the chemokine receptor and HIV-1 coreceptor CXCR4. However, some studies [4, 13] showed that HIV-specific CTL move toward or away from the CXCR4-binding HIV-1 gp120 in a concentration-dependent manner. The high concentration of CXCR4-binding HIV-1 gp120 repels HIV-specific CTL, while low concentration of gp120 attracts CTL with specific interaction with CXCR4. The repellent activity of HIV-1 gp120 on CTL causes the active movement of HIV-1-specific CTL away from the site of infection, which allows the virus to evade immune recognition and invade immune system.

In this chapter, we study the effect of chemotactic movement of CTL during HIV-1 infection by mathematical modeling. We denote $T(x, t)$, $I(x, t)$ and $E(x, t)$ as the population density of uninfected CD4⁺ T cells, infected CD4⁺ T cells and CTL at location x at time t respectively. Assuming the virus population to be at a quasi-steady state [12], we consider the following model.

$$\begin{aligned}\frac{\partial T}{\partial t} &= D_T \Delta T + h - d_T T - \beta T I, \\ \frac{\partial I}{\partial t} &= D_T \Delta I + \beta T I - d_I I - p I E, \\ \frac{\partial E}{\partial t} &= D_E \Delta E + \nabla \cdot [E \Psi(E, I) \nabla I] + \frac{c E I}{1 + \eta E} - d_E E.\end{aligned}\tag{6.1}$$

Here, we assume that uninfected CD4⁺ T cells are recruited at a constant rate h , infected at a rate $\beta T I$. Infected cells are cleared by CTL at a rate $p I E$. CTL proliferate in response to antigenic stimulation with a rate $c E I$, and the rate of CTL expansion saturates as the number of CTL grows to relatively high numbers. Variable η represents the saturation level. Uninfected CD4⁺ T cells, infected CD4⁺ T cells and CTL are lost at rates $d_T T$, $d_I I$ and $d_E E$ respectively.

In this model, we assume that uninfected and infected CD4⁺ T cells move randomly, with the same diffusion coefficient D_T . In contrast, the diffusion of CTL consists of two parts, the random diffusion and the chemotactic movement. The random diffusion coefficient is assumed to be D_E , that is, the diffusion flux of CTL is proportional to their density gradient $\mathbf{J}_D = -D_E \nabla E$. As mentioned above, the HIV-1 viral protein gp120, binding with the coreceptor

CXCR4, acts as a chemoattractant or chemorepellant for CTL. Thus, the chemotaxis flux \mathbf{J}_C of CTL depends on the their own density, the density of HIV-1 viral protein gp120, and the density gradient of this protein. Here we assume that the density of viral protein gp120 binding to CXCR4 is proportional to the density of infected $CD4^+$ T cells, and the chemotaxis flux of CTL is $\mathbf{J}_C = -E\Psi(E, I)\nabla I$. The derivation of this chemotactic term can be referred from the works of Painter and Hillen [6, 10]. The function $\Psi(E, I)$ represents the chemotactic response, which denotes chemoattraction (chemorepulsion) if it is negative (positive). Note that movement of $CD4^+$ T cells may be very slow comparing with CTL, that is, $D_T \ll D_E$, or they even do not diffuse at all in the lymphoid tissue. Here we assume that $D_T > 0$ but very small compared with D_E for the sake of mathematical consideration.

The rest of the chapter is organized as follows. In section 2 we discuss the well-posedness of the model. Linear stability of the steady states are shown in section 3. The conditions for Turing instability and pattern formation are derived in section 4. Numerical simulation about the stability of positive steady state, steady state bifurcation, Hopf bifurcation and pattern formation are shown in section 5. Finally, we present conclusions and discussions.

6.2 Global existence of solutions

We consider the model (6.1) with the following initial conditions

$$T(0, x) = T_0(x) > 0, \quad I(0, x) = I_0(x) \geq 0, \quad E(0, x) = E_0(x) \geq 0, \quad \forall x \in \Omega, \quad (6.2)$$

and the no-flux boundary conditions,

$$\frac{\partial T}{\partial \nu} = \frac{\partial I}{\partial \nu} = \frac{\partial E}{\partial \nu} = 0, \quad \forall x \in \partial\Omega, \quad t > 0,$$

where Ω is a bounded domain in \mathbb{R}^n with smooth boundary $\partial\Omega$.

We assume that $\Psi(E, I) \in C^2(\mathbb{R}^2, \mathbb{R})$, and there exists a sufficiently large number $E_M > 0$, such that $\Psi(E, I) = 0$, for $E \geq E_M$; $\Psi(E, I) > 0$ (chemorepulsion) or $\Psi(E, I) < 0$ (chemoattraction) for $0 < E < E_M$.

Let $w = (T, I, E)^\top$, and assume \mathbf{G} is a nonempty open subset of \mathbb{R}^3 , such that

$$\mathbf{X}_1 = \{w \in \mathbb{R}^3 \mid T \geq 0, I \geq 0, E \geq 0\} \subset \mathbf{G}.$$

Let $\rho > n$, so that the space $\mathbf{W}^{1,\rho}(\Omega, \mathbb{R}^3)$ is continuously embedded in the continuous function space $\mathbf{C}(\Omega, \mathbb{R}^3)$ [1]. We consider solutions of (6.1) in the following solution space

$$\mathbf{X} := \left\{ w \in \mathbf{W}^{1,\rho}(\Omega, \mathbb{R}^3) \mid w(\bar{\Omega}) \in \mathbf{G}, \frac{\partial w}{\partial \nu} = 0 \text{ on } \partial\Omega \right\}.$$

We see that system (6.1) can be rewritten as following abstract quasilinear parabolic equation

$$\begin{aligned} w_t + \mathcal{A}(w)w &= \mathcal{F}(x, w), \\ \mathcal{B}w &= 0, \end{aligned} \quad (6.3)$$

where

$$\mathcal{A}(z)w = - \sum_{j,k=1}^n \partial_j(a_{jk}(z)\partial_k w), \quad \mathcal{B}w = \frac{\partial w}{\partial \nu},$$

$$a_{jk} = a(z)\delta_{jk}, \quad 1 \leq j, k \leq n, \quad a(z) = \begin{pmatrix} D_T & 0 & 0 \\ 0 & D_T & 0 \\ 0 & z\Psi(z) & D_E \end{pmatrix},$$

for $z \in \mathbf{G}$, (δ_{jk} is the Kronecker delta function), and

$$\mathcal{F}(x, w) = \left(h - d_T T - \beta T I, \beta T I - d_I I - p I E, \frac{c E I}{1 + \eta E} - d_E E \right)^\top.$$

We see that $a(z) \in \mathbf{C}^2(\mathbf{G}, \mathcal{L}(\mathbb{R}^3))$, where we identified $\mathcal{L}(\mathbb{R}^3)$ with the space of real 3×3 matrices. The eigenvalues of $a(z)$ are positive for each $z \in \mathbf{G}$. Moreover, the boundary value problem $(\mathcal{A}, \mathcal{B})$ is normally elliptic [3].

The global existence, boundedness, nonnegativity of solutions of (6.1) are shown in the following two theorems.

Theorem 6.2.1 (i) *There exists a constant τ_0 depending on the initial data (T_0, I_0, E_0) such that the system (6.1), with no-flux boundary condition and initial condition (6.2), has a unique maximal classical solution (T, I, E) defined on $[0, \tau_0) \times \Omega$ such that*

$$(T, I, E) \in \mathbf{C}([0, \tau_0), \mathbf{X}) \cap \mathbf{C}^{2,1}((0, \tau_0) \times \bar{\Omega}, \mathbb{R}^3).$$

(ii) $T(t, x) \geq 0$, $I(t, x) \geq 0$, $E(t, x) \geq 0$, for all $(t, x) \in [0, \tau_0) \times \Omega$.

(iii) *If $(T, I, E)_{([0, \tau_0) \cap [0, \tau])}$ is bounded in $\mathbf{C}(\bar{\Omega}, \mathbb{R}^3)$ and bounded away from the boundary of \mathbf{G} , for every $\tau > 0$, then $\tau_0 \rightarrow +\infty$, namely, the solution is a global classical solution of the system (6.1).*

Proof We see that the system (6.3) is normal elliptic and triangular. According to Theorem 1 [2], or Theorem 14.4 and Theorem 14.6 [3], we obtain (i), the existence of maximal classical solution. From Theorem 15.1 [3], we obtain (ii), the nonnegativity of the solution. We apply Theorem 5.2 [2] to prove (iii), the condition for global existence of a solution. ■

Theorem 6.2.2 *Suppose that (T, I, E) is the solution obtained in Theorem 1, then it is a global solution of the system (6.1).*

Proof In order to prove the global existence of the solution, from the result (iii) of Theorem 1, it remains to prove that the solution (T, I, E) is bounded and bounded away from the boundary of \mathbf{G} . By the definition of \mathbf{G} , it suffices to show that (T, I, E) is bounded below by 0 and also bounded above by some finite data.

From T and I equations of (6.1), we see that

$$\begin{aligned} \frac{\partial}{\partial t}(T + I) &= D_T \Delta(T + I) + h - d_T T - d_I I - pIE \\ &\leq D_T \Delta(T + I) + h - d_m(T + I), \end{aligned}$$

where $d_m = \min\{d_T, d_I\}$. By Lemma 1 in [7], $\frac{h}{d_m}$ is globally attractive in $\mathbf{C}(\bar{\Omega}, \mathbb{R})$ for the scalar parabolic equation

$$\begin{aligned} \frac{\partial w(t, x)}{\partial t} &= D_T \Delta w(t, x) + h - d_m w(t, x), \quad x \in \Omega, \quad t > 0, \\ \frac{\partial w}{\partial \nu} &= 0, \quad x \in \partial\Omega, \quad t > 0. \end{aligned}$$

The parabolic comparison theorem ([11], Theorem 7.3.4) implies that $T + I$ is bounded on $[0, \tau)$. Furthermore, both $T(t, x)$ and $I(t, x)$ are bounded. We assume $0 \leq T(t, x) \leq T_M$, $0 \leq I(t, x) \leq I_M$.

Let $E_M = \frac{c}{\eta d_E} I_M$. We define the operator \mathcal{P} as

$$\mathcal{P}E = E_t - D_E \Delta E - \nabla \cdot (E \Psi(E, I) \nabla I) + \left(d_E E - \frac{cEI}{1 + \eta E} \right).$$

For any solution of the system (6.1), we have $\mathcal{P}E = 0$. However, for $E = E_M$,

$$\mathcal{P}E_M = d_E E_M - \frac{cE_M I}{1 + \eta E_M} \geq d_E E_M - \frac{c}{\eta} I_M = 0.$$

On the boundary $\partial\Omega$, $\frac{\partial E_M}{\partial \nu} = 0$. Therefore, $E = E_M$ is an upper solution of the E equation in system (6.1). By the comparison principle, we obtain that $E(t, x) \leq E_M$. Therefore, the solution (T, I, E) is bounded and bounded away from the boundary of \mathbf{G} . From (iii) of Theorem 1 we see that (T, I, E) is a global solution. ■

6.3 Linear stability analysis

The system (6.1) has three spatially homogeneous steady states.

(i) The infection-free steady state $S_0 = (h/d_T, 0, 0)$ always exists.

(ii) If $\mathcal{R}_0 := \frac{h\beta}{d_I d_T} > 1$, there exists a virus-established steady state $S_1 = (T_1, I_1, 0)$, where

$$T_1 = \frac{d_I}{\beta}, \quad I_1 = \frac{h}{d_I} - \frac{d_T}{\beta}.$$

(iii) If $cI_1 > d_E$, there exists a positive steady state $S^* = (T^*, I^*, E^*)$, where

$$T^* = \frac{1}{2\beta} \left[-\left(\frac{d_T c p}{\beta d_E \eta} + \frac{p}{\eta} - d_I \right) + \sqrt{\left(\frac{d_T c p}{\beta d_E \eta} + \frac{p}{\eta} - d_I \right)^2 + 4h \frac{c p}{d_E \eta}} \right],$$

$$I^* = \frac{h}{\beta T^*} - \frac{d_T}{\beta}, \quad E^* = \frac{1}{p} (\beta T^* - d_I).$$

Note that $cI_1 > d_E$ if and only if $\mathcal{R}_0 > 1 + \frac{\beta d_E}{c d_T}$. If there is no saturation of CTL, that is $\eta = 0$, then the positive steady state turns out to be $S_0^* = (T_0^*, I_0^*, E_0^*)$ where

$$T_0^* = \frac{h c}{d_T c + \beta d_E}, \quad I_0^* = \frac{d_E}{c}, \quad E_0^* = \frac{1}{p} (\beta T_0^* - d_I).$$

We can see that if $cI_1 > d_E$, then

$$I_0^* < I^* < I_1.$$

The formula of T^* is very complicated. But we can show that T^* is an increasing function of p, c, d_I , and a decreasing function of β, η, d_T, d_E . Furthermore, I^* is an increasing function of β, η, d_E , and a decreasing function of p, c, d_T, d_I . E^* is an increasing function of c , and a decreasing function of η, d_E . Here, we take the parameter c as an example to show that as c increases, T^* and E^* increase while I^* decreases.

For $c > 0$, let $f(c) := \frac{d_T c p}{\beta d_E \eta} + \frac{p}{\eta} - d_I$, $g(c) := 4h \frac{c p}{d_E \eta}$, and $\mathcal{F}(c) := -f(c) + \sqrt{f(c)^2 + g(c)}$, then $T^*(c) = \frac{1}{2\beta} \mathcal{F}(c)$, and

$$\mathcal{F}'(c) = -f'(c) + \frac{2f(c)f'(c) + g'(c)}{2\sqrt{f(c)^2 + g(c)}} = \frac{f'(c)}{\sqrt{f(c)^2 + g(c)}} \left[\frac{g'(c)}{2f'(c)} - \mathcal{F}(c) \right].$$

Furthermore,

$$f'(c) = \frac{d_T p}{\beta d_E \eta}, \quad g'(c) = 4h \frac{p}{d_E \eta}, \quad \mathcal{F}'(c) = \frac{2\beta f'(c)}{\sqrt{f(c)^2 + g(c)}} \left[\frac{h}{d_T} - T^* \right] > 0.$$

Therefore,

$$T^{*'}(c) = \frac{1}{2\beta} \mathcal{F}'(c) > 0, \quad I^{*'}(c) = -\frac{h T^{*'}(c)}{\beta T^*(c)^2} < 0, \quad E^{*'}(c) = \frac{\beta}{p} T^{*'}(c) > 0.$$

In a similar way, we can show the dependence of T^* , I^* and E^* on other parameters.

In what follows, we discuss the linear stability of steady states. In the absence of a spatial effect, we know that S_0 is locally asymptotically stable if $\mathcal{R}_0 < 1$; S_1 is locally asymptotically stable if $\mathcal{R}_0 > 1$ and $cI_1 < d_E$; S^* is locally asymptotically stable if $cI_1 > d_E$. In fact, we can see them from the following discussion about the steady states of the system with spatial effect. We consider one-dimensional space.

Let $\hat{S} = (\hat{T}, \hat{I}, \hat{E})$ be a steady state of the system (6.1), then the linearized system of (6.1) at \hat{S} is given by

$$\frac{\partial u}{\partial t} = (D\Delta + A)u, \quad (6.4)$$

where

$$D(\hat{S}) = \begin{pmatrix} D_T & 0 & 0 \\ 0 & D_T & 0 \\ 0 & \hat{\Psi} & D_E \end{pmatrix}, \quad A(\hat{S}) = \begin{pmatrix} -d_T - \beta\hat{I} & -\beta\hat{T} & 0 \\ \beta\hat{I} & \beta\hat{T} - d_I - p\hat{E} & -p\hat{I} \\ 0 & \frac{c\hat{E}}{1+\eta\hat{E}} & \frac{c\hat{I}}{(1+\eta\hat{E})^2} - d_E \end{pmatrix}, \quad u = \begin{pmatrix} u_1 \\ u_2 \\ u_3 \end{pmatrix},$$

and $\hat{\Psi}(\hat{S}) := \hat{E}[\Psi_I(\hat{E}, \hat{I}) + \Psi(\hat{E}, \hat{I})]$. Notice that $\hat{\Psi}(S_0) = 0$, $\hat{\Psi}(S_1) = 0$ and $\Psi^* := \hat{\Psi}(S^*) = E^*[\Psi_I(E^*, I^*) + \Psi(E^*, I^*)]$.

The corresponding characteristic polynomial of the linearized system (6.4) is

$$|\lambda I + Dk^2 - A| = 0, \quad (6.5)$$

where $k \geq 0$, called the wavenumbers or the wave modes, are the eigenvalues of Laplace operator on a finite domain with no-flux boundary conditions. For instance, in one-dimensional domain $[0, L]$, $k^2 = n^2L^2/\pi^2$, or in two-dimensional domain $[0, L_x] \times [0, L_y]$, $k^2 = (n^2/L_x^2 + m^2/L_y^2)\pi^2$, where n and m are integers. λ is the eigenvalue which determines temporal growth. The steady state \hat{S} is linearly stable if $\text{Re}\lambda < 0$, for all eigenvalues λ of (6.5) with all modes k [9].

Theorem 6.3.1 *The infection-free steady state $S_0 = (h/d_T, 0, 0)$ is linearly stable if $\mathcal{R}_0 < 1$, and unstable if $\mathcal{R}_0 > 1$*

Proof For the infection-free steady state $S_0 = (h/d_T, 0, 0)$, we have

$$D(S_0) = \begin{pmatrix} D_T & 0 & 0 \\ 0 & D_T & 0 \\ 0 & 0 & D_E \end{pmatrix}, \quad A(S_0) = \begin{pmatrix} -d_T & -\beta h/d_T & 0 \\ 0 & \beta h/d_T - d_I & 0 \\ 0 & 0 & -d_E \end{pmatrix},$$

and the characteristic equation of the linearized system at S_0 is

$$\begin{vmatrix} \lambda + D_T k^2 + d_T & \beta h/d_T & 0 \\ 0 & \lambda + D_T k^2 - \beta h/d_T + d_I & 0 \\ 0 & 0 & \lambda + D_E k^2 + d_E \end{vmatrix} = 0.$$

It has eigenvalues $\lambda_1 = -D_T k^2 - d_T$, $\lambda_2 = -D_T k^2 + \beta h/d_T - d_I$, $\lambda_3 = -D_E k^2 - d_E$. Note that $\lambda_1 < 0$, $\lambda_3 < 0$, and $\lambda_2 = -D_T k^2 + d_I(\mathcal{R}_0 - 1)$. If $\mathcal{R}_0 < 1$, then $\lambda_2 < 0$ for all k . Therefore, if $\mathcal{R}_0 < 1$, the steady state S_0 is linearly stable. If $\mathcal{R}_0 > 1$, then $\lambda_2 > 0$ for some small modes k , including $k = 0$, which means S_0 is unstable. ■

Theorem 6.3.2 *The virus-established steady state $S_1 = (T_1, I_1, 0)$ is linearly stable if $\mathcal{R}_0 > 1$ and $cI_1 < d_E$. It is unstable if $\mathcal{R}_0 < 1$ or $cI_1 > d_E$.*

Proof For the steady state $S_1 = (T_1, I_1, 0)$, we have

$$D(S_1) = \begin{pmatrix} D_T & 0 & 0 \\ 0 & D_T & 0 \\ 0 & 0 & D_E \end{pmatrix}, \quad A(S_1) = \begin{pmatrix} -d_T - \beta I_1 & -\beta T_1 & 0 \\ \beta I_1 & \beta T_1 - d_I & -pI_1 \\ 0 & 0 & cI_1 - d_E \end{pmatrix}.$$

Noticing that $\beta T_1 = d_I$ and $d_T + \beta I_1 = \frac{h\beta}{d_I}$, the characteristic polynomial of the linearized system at S_1 is given by

$$\begin{vmatrix} \lambda + D_T k^2 + h\beta/d_I & d_I & 0 \\ -h\beta/d_I + d_T & \lambda + D_T k^2 & pI_1 \\ 0 & 0 & \lambda + D_E k^2 - cI_1 + d_E \end{vmatrix} = 0.$$

One eigenvalue is $\lambda_1 = -D_E k^2 + cI_1 - d_E$. We see that if $cI_1 < d_E$, then $\lambda_1 < 0$ for all k . Other eigenvalues are determined by

$$\lambda^2 + a_1(k^2)\lambda + a_2(k^2) = 0, \quad (6.6)$$

where

$$\begin{aligned} a_1(k^2) &= 2D_T k^2 + \frac{h\beta}{d_I}, \\ a_2(k^2) &= D_T^2 k^4 + \frac{D_T h\beta}{d_I} k^2 + \frac{1}{d_I d_T} (\mathcal{R}_0 - 1). \end{aligned}$$

We know that $a_1(k^2) > 0$ and $a_2(k^2) > 0$ if $\mathcal{R}_0 > 1$, thus the roots of (6.6) have negative real parts for all k . Therefore, if $\mathcal{R}_0 > 1$ and $cI_1 < d_E$, the steady state S_1 is linearly stable. In contrast, S_1 is unstable if $\mathcal{R}_0 < 1$ or $cI_1 > d_E$, since if $cI_1 > d_E$, $\lambda_1 > 0$ for some small k including $k = 0$; if $\mathcal{R}_0 < 1$, $a_2 < 0$ for some small k , which implies (6.6) has at least one eigenvalue with positive real part. ■

Theorem 6.3.3 *The positive steady state $S^* = (T^*, I^*, E^*)$ is linearly stable if $b_3(k^2) > 0$ and $b_1(k^2)b_2(k^2) - b_3(k^2) > 0$ for all k , where b_1 , b_2 and b_3 are shown by (6.8), (6.9) and (6.10) respectively.*

Proof For the positive steady state S^* , the characteristic polynomial is given by

$$\begin{vmatrix} \lambda + D_T k^2 + d_T + \beta I^* & \beta T^* & 0 \\ -\beta I^* & \lambda + D_T k^2 & p I^* \\ 0 & \Psi^* k^2 - \frac{c E^*}{1 + \eta E^*} & \lambda + D_E k^2 + d_E - \frac{c I^*}{(1 + \eta E^*)^2} \end{vmatrix} = 0,$$

that is,

$$\lambda^3 + b_1(k^2)\lambda^2 + b_2(k^2)\lambda + b_3(k^2) = 0. \quad (6.7)$$

Here

$$b_1(k^2) = (2D_T + D_E)k^2 + d_T + \beta I^* + d_E \left(1 - \frac{1}{1 + \eta E^*}\right) > 0, \quad (6.8)$$

$$b_2(k^2) = c_1 k^4 + c_2 k^2 + c_3, \quad (6.9)$$

where

$$\begin{aligned} c_1 &= D_T^2 + 2D_T D_E > 0, \\ c_2 &= (D_T + D_E)(d_T + \beta I^*) + 2D_T d_E \left(1 - \frac{1}{1 + \eta E^*}\right) - p I^* \Psi^*, \\ c_3 &= (d_T + \beta I^*)d_E \left(1 - \frac{1}{1 + \eta E^*}\right) + p d_E E^* + \beta^2 T^* I^* > 0; \end{aligned}$$

$$b_3(k^2) = d_1 k^6 + d_2 k^4 + d_3 k^2 + d_4, \quad (6.10)$$

where

$$\begin{aligned} d_1 &= D_T^2 D_E > 0, \\ d_2 &= D_T \left[D_E (d_T + \beta I^*) + D_T d_E \left(1 - \frac{1}{1 + \eta E^*}\right) \right] - D_T p I^* \Psi^*, \\ d_3 &= D_T (d_T + \beta I^*) d_E \left(1 - \frac{1}{1 + \eta E^*}\right) + D_T p d_E E^* + D_E \beta^2 T^* I^* - (d_T + \beta I^*) p I^* \Psi^*, \\ d_4 &= p d_E E^* (d_T + \beta I^*) + \beta^2 T^* I^* d_E \left(1 - \frac{1}{1 + \eta E^*}\right) > 0; \end{aligned}$$

$$b_1(k^2)b_2(k^2) - b_3(k^2) = e_1 k^6 + e_2 k^4 + e_3 k^2 + e_4, \quad (6.11)$$

where

$$\begin{aligned}
e_1 &= 2D_T(D_T + D_E)^2 > 0, \\
e_2 &= (D_T + D_E) \left[(d_T + \beta I^*)(3D_T + D_E) + 4D_T d_E \left(1 - \frac{1}{1 + \eta E^*} \right) \right] - (D_T + D_E) p I^* \Psi^*, \\
e_3 &= 2D_T \beta^2 I^* T^* + (D_T + D_E) \left[p d_E E^* + (d_T + \beta I^*)^2 \right] \\
&\quad + 2 \left[(2D_T + D_E)(d_T + \beta I^*) + D_T d_E \left(1 - \frac{1}{1 + \eta E^*} \right) \right] d_E \left(1 - \frac{1}{1 + \eta E^*} \right) \\
&\quad - d_E \left(1 - \frac{1}{1 + \eta E^*} \right) p I^* \Psi^*, \\
e_4 &= \left[(d_T + \beta I^*)^2 + (d_T + \beta I^*) d_E \left(1 - \frac{1}{1 + \eta E^*} \right) + p d_E E^* \right] d_E \left(1 - \frac{1}{1 + \eta E^*} \right) \\
&\quad + (d_T + \beta I^*) \beta^2 I^* T^* > 0.
\end{aligned}$$

If $b_1(k^2) > 0$, $b_3(k^2) > 0$ and $b_1(k^2)b_2(k^2) - b_3(k^2) > 0$ for all k , then $\text{Re} \lambda < 0$. We see that $b_1(k^2) > 0$ for k . Therefore, if $b_3(k^2) > 0$ and $b_1(k^2)b_2(k^2) - b_3(k^2) > 0$ for all k , then S^* is linearly stable. ■

Note that, in the absence of diffusion, that is, in the spatial homogeneous case ($k = 0$), $b_3(0) = d_4 > 0$ and $b_1(0)b_2(0) - b_3(0) = e_4 > 0$, which implies the positive steady state S^* is linearly stable if it exists, that is if $cI_1 > d_E$. In contrast, under the same condition, the homogeneous steady state S^* can be unstable to small spatial perturbations when diffusion is present, for instance if $b_3(k^2) < 0$ or $b_1(k^2)b_2(k^2) - b_3(k^2) < 0$ for some modes k . This diffusion-driven instability is called Turing instability [9].

6.4 Turing instability and pattern formation

We expect spatial pattern formation when the homogeneous positive steady state S^* is unstable, that is when $b_3(k^2) < 0$ or $b_1(k^2)b_2(k^2) - b_3(k^2) < 0$. In general, if $b_3(k^2) < 0$, a steady state bifurcation occurs from S^* , while there is a Hopf bifurcation from S^* if $b_1(k^2)b_2(k^2) - b_3(k^2) < 0$ for some wave mode k . To clarify these Turing instability conditions, we denote $\phi_d(s) := b_3(s)$ and $\phi_e(s) := b_1(s)b_2(s) - b_3(s)$, that is

$$\phi_d(s) = d_1 s^3 + d_2 s^2 + d_3 s + d_4, \quad \phi_e(s) = e_1 s^3 + e_2 s^2 + e_3 s + e_4,$$

where s is assumed to be $s \in \mathbb{R}$. We see that $\phi_d(s)$ has a negative root, since $d_1 > 0$, $\phi_d(-\infty) = -\infty$ and $\phi_d(0) = d_4 > 0$. If $d_2 \geq 0$ and $d_3 \geq 0$, then $\phi_d(s) > 0$ for $s \geq 0$, and there is no bifurcation. However, if $d_2 < 0$ or $d_3 < 0$, $\phi_d(s)$ has two or no positive roots, by the Descartes'

rule of signs. A steady state bifurcation occurs if $\phi_d(s)$ has two distinct positive roots. The conditions for the existence of two distinct positive roots of $\phi_d(s)$ can be determined by the sign of $\phi_d(s_+^d)$, where s_+^d is one of the roots of $\phi'_d(s) = 3d_1s^2 + 2d_2s + d_3$, say

$$s_{\pm}^d = \frac{1}{3d_1} \left(-d_2 \pm \sqrt{d_2^2 - 3d_1d_3} \right).$$

According to the signs of d_2 and d_3 , we have the following three cases.

(i) If $d_3 < 0$, then $\sqrt{d_2^2 - 3d_1d_3} > |d_2|$, $s_+^d > 0$ and $s_-^d < 0$. In this case, $\phi_d(s)$ has two distinct positive roots, if and only if $\phi_d(s_+^d) < 0$.

(ii) If $d_3 > 0$ and $d_2 < 0$, then for different cases of $d_2^2 - 3d_1d_3$, we have

$$\begin{cases} d_2^2 - 3d_1d_3 > 0 : & \sqrt{d_2^2 - 3d_1d_3} < |d_2|, \quad s_+^d > s_-^d > 0; \\ d_2^2 - 3d_1d_3 = 0 : & s_{\pm}^d = -\frac{d_2}{3d_1} > 0, \quad \phi'_d(s) \geq 0, \quad \text{for } s \in \mathbb{R}; \\ d_2^2 - 3d_1d_3 < 0 : & \phi'_d(s) > 0, \quad \text{for } s \in \mathbb{R}. \end{cases}$$

When $d_2^2 - 3d_1d_3 > 0$, $\phi_d(s)$ has two distinct positive roots, if and only if $\phi_d(s_+^d) < 0$. When $d_2^2 - 3d_1d_3 \leq 0$, $\phi_d(s)$ does not have any positive root, and $\phi_d(s) > 0$ for $s \geq 0$.

(iii) If $d_3 = 0$ and $d_2 < 0$, then $s_+^d > 0$, $s_-^d = 0$, and $\phi_d(s)$ has two distinct positive roots if and only if $\phi_d(s_+^d) < 0$.

In summary, $\phi_d(s)$ has two distinct positive roots if one of the following conditions is satisfied.

(C1) $d_3 < 0$, $\phi_d(s_+^d) < 0$;

(C2) $d_3 \geq 0$, $d_2 < 0$, $d_2^2 - 3d_1d_3 > 0$, $\phi_d(s_+^d) < 0$.

In a similar way, we can determine the conditions for Hopf bifurcation. Defining s_+^e as s_+^d , just changing d_j to e_j ($j=1,2,3$), we have that $\phi_e(s)$ has two distinct positive roots if one of the following conditions is satisfied.

(C3) $e_3 < 0$, $\phi_e(s_+^e) < 0$;

(C4) $e_3 \geq 0$, $e_2 < 0$, $e_2^2 - 3e_1e_3 > 0$, $\phi_e(s_+^e) < 0$.

Turing instability occurs and pattern formation is expected if one of the conditions (C1)-(C4) is satisfied. Here, note that the formula of $\phi_d(s_+^d)$ can be simplified to the following form

$$\phi_d(s_+^d) = \frac{2}{9d_1} \left(3d_1d_3 - d_2^2 \right) s_+^d + \left(d_4 - \frac{d_2d_3}{9d_1} \right),$$

applying the fact that $\phi'_d(s_+^d) = 3d_1s_+^{d2} + 2d_2s_+^d + d_3 = 0$.

We assume $\Psi(E, I) = \chi(I)q(E)$, where the chemotactic sensitivity function $\chi(I)$ is chosen to be a constant χ , and $q(E) = 1 - \frac{E}{E_M}$, the volume-filling effect is considered for CTL to prevent

the blow-up of solutions of the model. Here, E_M is the upper bound of the CTL population E in the model. Then we have

$$\Psi(E, I) = \chi \left(1 - \frac{E}{E_M} \right), \quad (6.12)$$

for chemorepulsion system, and

$$\Psi(E, I) = -\chi \left(1 - \frac{E}{E_M} \right) \quad (6.13)$$

for chemoattraction system. Furthermore, we have

$$\Psi^* = \chi E^* \left(1 - \frac{E^*}{E_M} \right) > 0, \quad (6.14)$$

for chemorepulsion system and

$$\Psi^* = -\chi E^* \left(1 - \frac{E^*}{E_M} \right) < 0, \quad (6.15)$$

for chemoattraction system. For chemoattraction system, since $\Psi^* < 0$, we see from the proof of Theorem 6.3.3 that S^* is linearly stable. However, for chemorepulsion system, Turing instability may occur.

We choose the strength of the chemotactic sensitivity χ as the bifurcation parameter fixing all other parameters. Notice that d_1, d_4, e_1 and e_4 are independent of χ , while $d_2(\chi), d_3(\chi), e_2(\chi)$ and $e_3(\chi)$ are linear strictly decreasing functions of χ , with $d_j(0) > 0, e_j(0) > 0, d_j(+\infty) = -\infty$, and $e_j(+\infty) = -\infty, (j = 1, 2)$. Thus, $d_2^2(\chi) - 3d_1d_3(\chi)$ and $e_2^2(\chi) - 3e_1e_3(\chi)$ are quadratic functions, which tend to positive infinity as $\chi \rightarrow +\infty$. Furthermore, $[\phi_d(s_+^d)](\chi) \rightarrow -\infty, [\phi_e(s_+^e)](\chi) \rightarrow -\infty$, as $\chi \rightarrow +\infty$. Therefore, as χ increases, at least one of the conditions (C1)-(C4) holds. Generally, there exists a critical value χ_c such that there is no pattern formation if $\chi < \chi_c$, while pattern formation can be expected if $\chi > \chi_c$. We can determine this Turing instability threshold value according to the conditions (C1)-(C4).

Let χ_2^d and χ_3^d be the roots of $d_2(\chi) = 0$ and $d_3(\chi) = 0$ respectively, that is, $d_2(\chi_2^d) = 0$ and $d_3(\chi_3^d) = 0$. If $\chi_3^d \leq \chi_2^d$, then at $\chi = \chi_3^d$, we have $d_3 = 0, d_2 \geq 0, s_+^d = 0$ and $\phi_d(s_+^d) = d_4 > 0$. Let χ_1^S be the smallest value that satisfies $\chi_1^S > \chi_3^d, [\phi_d(s_+^d)](\chi_1^S) = 0$, and $[\phi_d(s_+^d)](\chi) < 0$ for $\chi_1^S < \chi < \chi_1^S + \delta_1$, where $\delta_1 > 0$. Then the condition (C1) holds for $\chi_1^S < \chi < \chi_1^S + \delta_1$.

In contrast, if $\chi_2^d < \chi_3^d$, then at $\chi = \chi_2^d$, we have $d_2 = 0, d_3 > 0, d_2^2 - 3d_1d_3 = -3d_1d_3 < 0$. Let χ_4^d be the root of $d_2^2(\chi) - 3d_1d_3(\chi) = 0$ satisfying $\chi_4 > \chi_2$, then $\chi_4^d < \chi_3^d$. At χ_4^d , we have $d_2^2 - 3d_1d_3 = 0, d_3 > 0, d_2 < 0$, and $[\phi_d(s_+^d)](\chi_4^d) = d_4 - \frac{d_2d_3}{9d_1} > 0$. The condition (C2) does not hold for $\chi \leq \chi_4^d$. Let χ_2^S be the smallest value that satisfies $\chi_2^S > \chi_4^d, [\phi_d(s_+^d)](\chi_2^S) = 0$, and $[\phi_d(s_+^d)](\chi) < 0$ for $\chi_2^S < \chi < \chi_2^S + \delta_2$, where $\delta_2 > 0$. In this case, if $\chi_2^S \leq \chi_3^d$, then the condition (C2) holds for $\chi_2^S < \chi < \chi_2^S + \delta_2$, while the condition (C1) holds for $\chi_2^S < \chi < \chi_2^S + \delta_2$ if $\chi_2^S > \chi_3^d$.

The value χ_1^S or χ_2^S gives the threshold for steady state bifurcation. Similarly, we can derive the threshold value χ_1^H or χ_2^H for Hopf bifurcation according to the conditions (C3) and (C4).

From the foregoing analysis, we know that the bifurcation threshold values are determined by the roots of $[\phi_d(s_+^d)](\chi) = 0$ or $[\phi_e(s_+^e)](\chi) = 0$. We assume that $[\phi_d(s_+^d)](\chi_c^S) = 0$ and χ_c^S is the steady state bifurcation threshold value (χ_1^S or χ_2^S), while $[\phi_e(s_+^e)](\chi_c^H) = 0$ and χ_c^H is the Hopf bifurcation threshold value (χ_1^H or χ_2^H). If $\chi_c^S < \chi_c^H$ and $\chi_c^S < \chi$, then $\phi_d(s)$ has two distinct positive solutions s_1^d and s_2^d , the range of unstable modes is $s_1^d < k^2 < s_2^d$. If $\chi_c^H < \chi_c^S$ and $\chi_c^H < \chi$, then $\phi_e(s)$ has two distinct positive solutions s_1^e and s_2^e , the range of unstable modes is $s_1^e < k^2 < s_2^e$. Note that, when we derive the bifurcation thresholds, we assumed s (i.e. k^2) to be continuous. However, with finite spatial domains, there is a discrete set of possible modes k as mentioned above. Therefore, the threshold values χ_c^S and χ_c^H obtained here may be not the exact bifurcation values. χ_c^S and χ_c^H give the lower bound of the bifurcation values. The exact bifurcation values may be somewhat greater than χ_c^S and χ_c^H , depending on the size of the domain and the shapes of $\phi_d(s)$ and $\phi_e(s)$.

In a special case, if the uninfected and infected cells cannot diffuse ($D_T = 0$), we have $d_1 = 0$, $d_2 = 0$ and $e_1 = 0$. Thus $\phi_d(s) = d_3s + d_4$ and $\phi_e(s) = e_2s^2 + e_3s + e_4$. It is easy to see that the Turing instability conditions change to (H1) $d_3 < 0$, or (H2) $e_2 < 0$, or (H3) $e_2 \geq 0$, $e_3 < 0$, $e_3^2 - 4e_2e_4 > 0$. If (H1) holds, a steady state bifurcation occurs, while there is a Hopf bifurcation if any of (H2) and (H3) is satisfied. The threshold value for steady bifurcation is $\chi_c^S = \chi_3^d$, the root of $d_3(\chi) = 0$. From the formulas of e_2 and e_3 , we know that the root χ_2^e of $e_2(\chi) = 0$ is always smaller than the root χ_3^e of $e_3(\chi) = 0$. Thus, the threshold value for Hopf bifurcation is $\chi_c^H = \chi_2^e$, according to the conditions (H2) and (H3).

6.5 Numerical simulation

We choose χ as the bifurcation parameter and other baseline parameters as $H = 10$, $d_T = 0.1$, $d_I = 0.2$, $d_E = 0.1$, $\beta = 0.1$, $p = 0.5$, $c = 0.2$, $\eta = 0.01$ and $E_M = 2000$, then $\mathcal{R}_0 = 50 > 1$, $I_1 - \frac{d_E}{c} = 48.5 > 0$, and $S^* = (64.0197, 0.5620, 12.4039)$. The space is assumed to be one-dimensional and $\Omega = [0, l\pi]$, then $k^2 = n^2/l^2$, where n is an integer and $l = 3$. In what follows, we suppose that k assumes continuous values (i.e. s is continuous), in order to derive the threshold values of χ for bifurcation.

First, we consider $D_T = 0$. Assuming $D_E = 1$, we obtain $\chi_c^S = \chi_3^d = 0.6650$ and $\chi_c^H = \chi_2^e = 0.0451$. Since $\chi_c^H < \chi_c^S$, Hopf bifurcation may occur at $\chi = \chi_c^H = 0.0451$, and pattern forms for $\chi > \chi_c^H$. Figure 6.1 shows the pattern formation of the model when $\chi = 0.5$ and $\chi = 0.6$. We can determine the unstable wave modes from Figure 6.2(c). For $\chi = 0.05$, the zero point of $\phi_e(s) = 0$ is $s_1 = 38.1088$, and $\phi_e(s) < 0$ for $s > s_1$. The minimal unstable mode $k_1 = n_1/l$

is the smallest $k = n/l$ that greater than $\sqrt{s_1} = 6.1732$. Here, we obtain $n_1 = 19$, and pattern forms for modes $k = n/l$, where $n \geq 19$. Similarly, for $\chi = 0.06$, we obtain that the zero point of $\phi_e(s) = 0$ is $s_2 = 12.6025$, and the unstable wave modes are $k = n/l$, where $n \geq 11$.

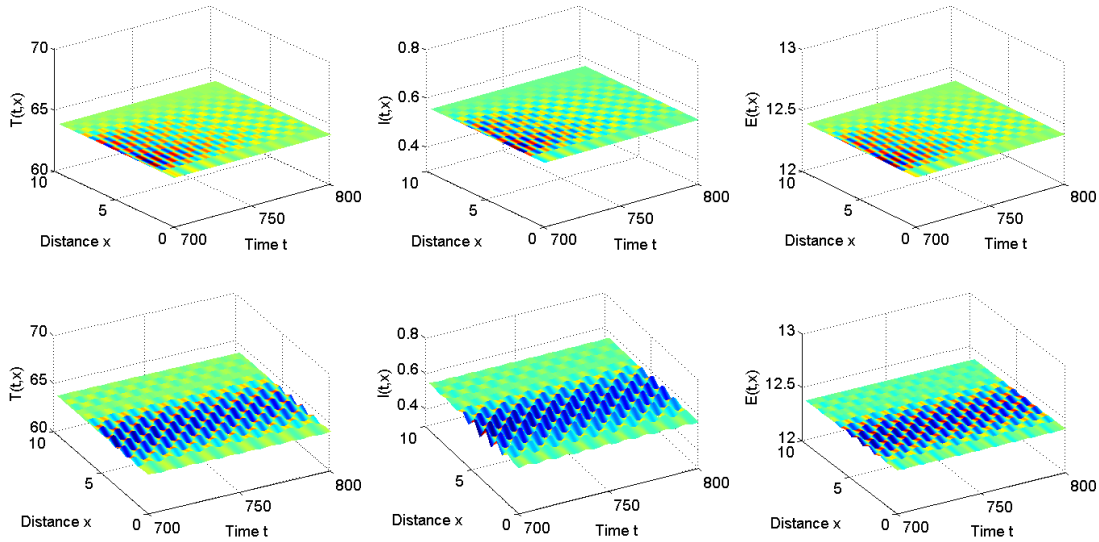


Figure 6.1: Temporal and spatial evolution of $T(x, t)$, $I(x, t)$ and $E(x, t)$. First row: $\chi = 0.05$. Second row: $\chi = 0.06$.

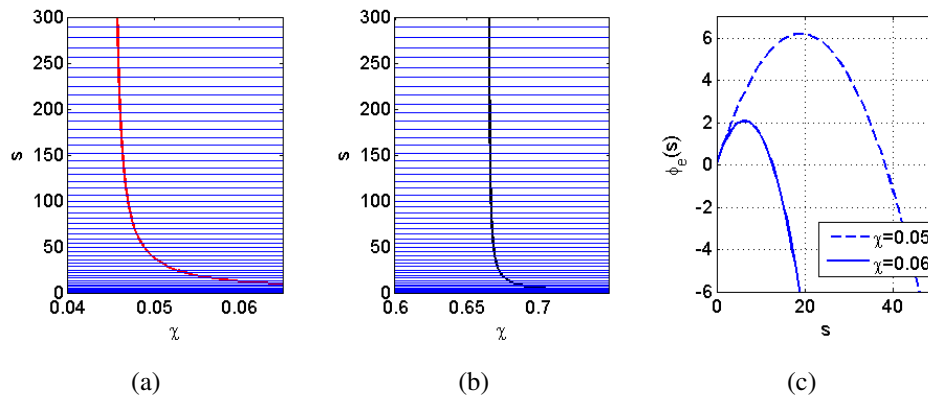


Figure 6.2: (a) Graph of $\phi_e(s, \chi) = e_2(\chi)s^2 + e_3(\chi)s + e_4 = 0$. (b) Graph of $\phi_d(s, \chi) = d_3(\chi)s + d_4 = 0$. The horizontal lines are $s = n^2/l^2$, where $l = 3$, and n is a positive integer, $1 \leq n \leq 51$. (c) Graphs of $\phi_e(s)$ when $\chi = 0.05$ and $\chi = 0.06$.

When $D_T > 0$, we choose another two sets of different diffusion rates of the populations: (I) $D_T = 0.005$, $D_E = 0.1$, and (II) $D_T = 0.1$, $D_E = 0.1$, to show two different bifurcations, say steady state bifurcation and Hopf bifurcation. For the case (I), we see from Figure 6.3(a) that steady state bifurcation may occur for some modes k and some range of χ , and Hopf bifurcation

can also occur for some other modes k and χ . In contrast, for the case (I), Figure 6.3(b) shows that steady state bifurcation may occur for some wave modes k , and Hopf bifurcation cannot occur, since χ satisfying $b_3 = 0$ is always smaller than χ satisfying $b_1 b_2 - b_3 = 0$, for all modes k .

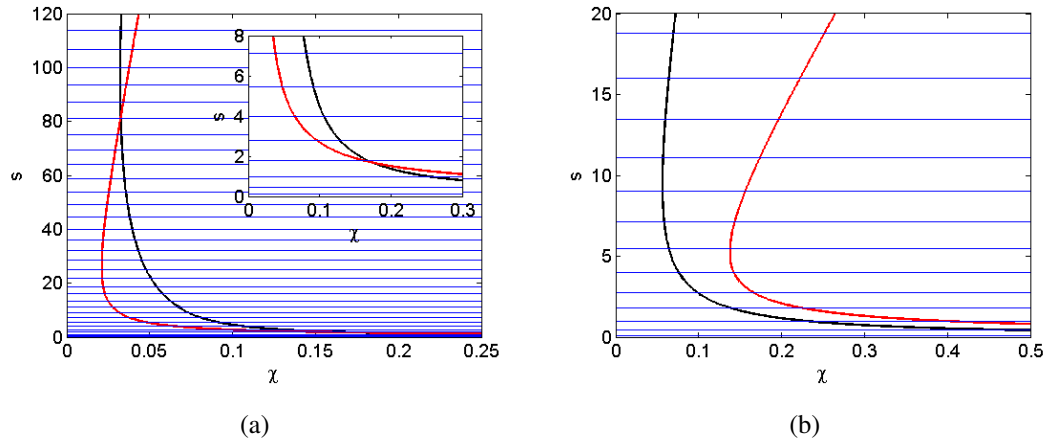


Figure 6.3: Graphs of $\phi_d(s, \chi) = d_1 s^3 + d_2(\chi) s^2 + d_3(\chi) s + d_4 = 0$ (black) and $\phi_e(s, \chi) = e_1 s^3 + e_2(\chi) s^2 + e_3(\chi) s + e_4 = 0$ (red). (a) $D_T = 0.005$, $D_E = 0.1$. (b) $D_T = 0.1$, $D_E = 0.1$. The horizontal lines are $s = n^2/l^2$, where $l = 3$, and n is a positive integer, (a) $1 \leq n \leq 35$, (b) $1 \leq n \leq 13$.

We consider the case when $D_T = 0.005$ and $D_E = 0.1$. The curves of $d_2^2(\chi) - 3d_1 d_3(\chi)$, $\phi_d(\chi)$, $e_2^2(\chi) - 3e_1 e_3(\chi)$ and $\phi_e(\chi)$ are shown in Figure 6.4(a), Figure 6.4(b), Figure 6.4(c) and Figure 6.4(d) respectively. The roots of these functions in the corresponding regions are $\chi_0^d = 0.0288$, $\chi_c^d = 0.0321$, $\chi_0^e = 0.0186$ and $\chi_c^e = 0.0209$ respectively. The functions $d_2(\chi)$, $d_3(\chi)$, $e_2(\chi)$ and $e_3(\chi)$ are linear strictly decreasing functions of χ , and roots of these functions are given by $\chi_2^d = 0.0045$, $\chi_3^d = 0.0722$, $\chi_2^e = 0.0052$ and $\chi_3^e = 1.8747$ respectively.

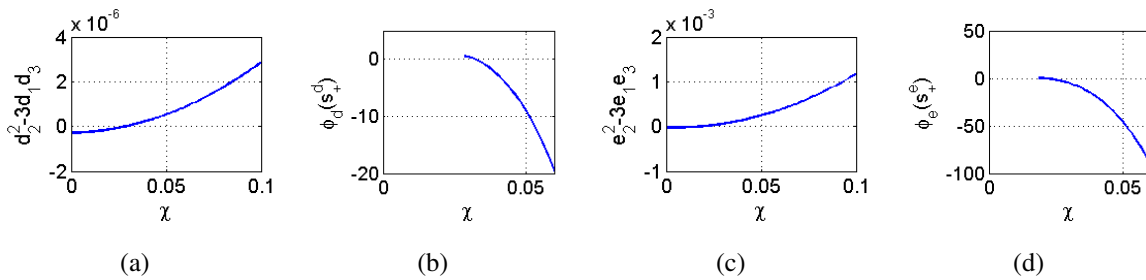


Figure 6.4: (a) $d_2^2(\chi) - 3d_1 d_3(\chi)$. One zero point: $\chi = 0.0288$. (b) $\phi_d(\chi)$. One zero point: $\chi = 0.0321$. (c) $e_2^2(\chi) - 3e_1 e_3(\chi)$. One zero point: $\chi = 0.0186$. (d) $\phi_e(\chi)$. One zero point: $\chi = 0.0209$.

Applying the bifurcation conditions (C1)-(C4), we obtain the bifurcation threshold values $\chi_c^S = \chi_c^d = 0.0321$ and $\chi_c^H = \chi_c^e = 0.0209$. Since $\chi_c^H < \chi_c^S$, Hopf bifurcation may occur at $\chi = \chi_c^H$ and temporal periodic and spatial inhomogeneous pattern forms for $\chi_H^H < \chi < \chi_c^S$. For $\chi > \chi_c^S$, the positive steady state is unstable and spatial heterogeneous pattern forms, which may be not temporal periodic.

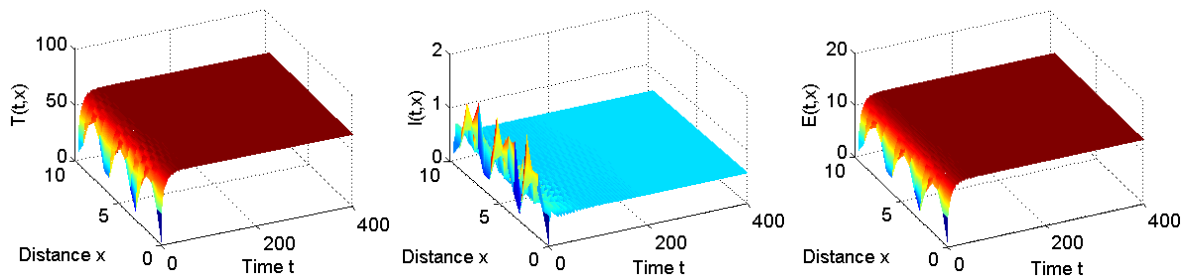


Figure 6.5: Temporal and spatial evolution of $T(x, t)$, $I(x, t)$ and $E(x, t)$. The homogenous positive steady state is stable when $\chi = 0.02 (< \chi_c^H)$.

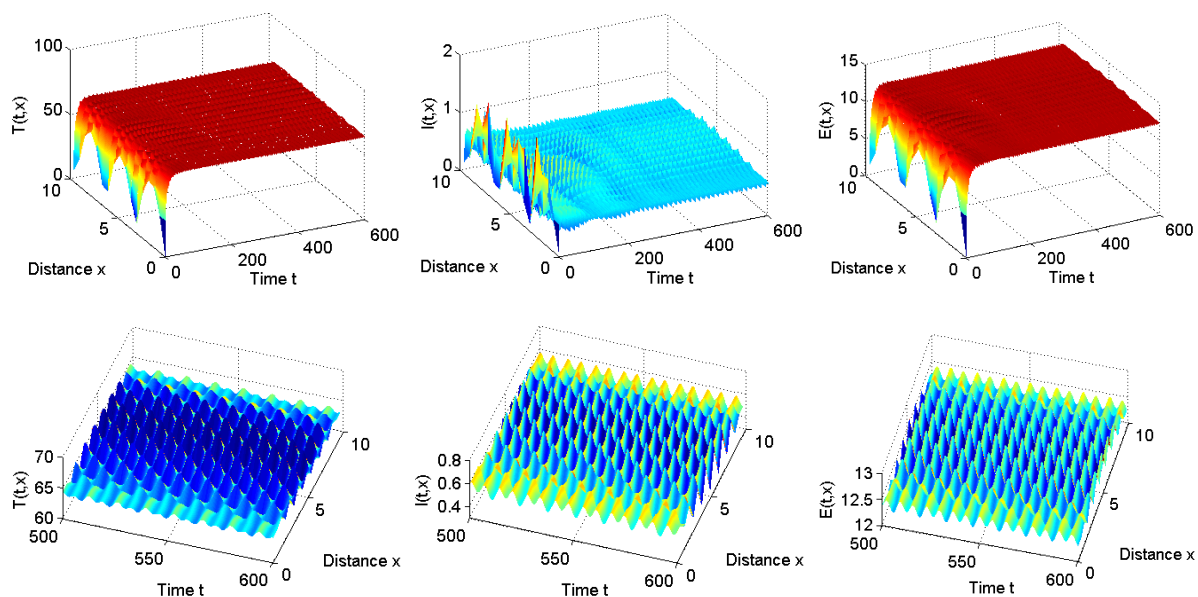


Figure 6.6: Temporal and spatial evolution of $T(x, t)$, $I(x, t)$ and $E(x, t)$. when $\chi = 0.029$ ($\chi_c^H < \chi = 0.029 < \chi_c^S$). The homogeneous positive steady state is unstable, and spatial patterns are formed.

We see from Figure 6.5 that the positive steady state S^* is stable when $\chi = 0.02 < \chi_c^H$. As χ increases so that $\chi > \chi_c^H$ but $\chi < \chi_c^S$, the positive steady state becomes unstable, and Hopf bifurcation occurs. Figure 6.6 shows the temporal and spatial evolution of $T(x, t)$, $I(x, t)$

and $E(x, t)$. From the end part of these time evolution figures (the figures in the second row of Figure 6.6), we see the form of spatial patterns and temporal periodicity of the solutions. Figure 6.7 shows the periodic solutions at space locations $x = 1.5\pi$ and $x = 3\pi$. The amplitudes of the periodic solutions vary in different space locations as shown in Figure 6.7. We see that the amplitudes at $x = 1.5\pi$ are greater than those at $x = 3\pi$ for $T(x, t)$, $I(x, t)$ and $E(x, t)$ respectively. When $\chi = 0.033$ which exceeds the threshold value χ_c^S , the positive steady state also loses its stability and spatial heterogeneous pattern forms, which may be not periodic, as shown in Figure 6.8.

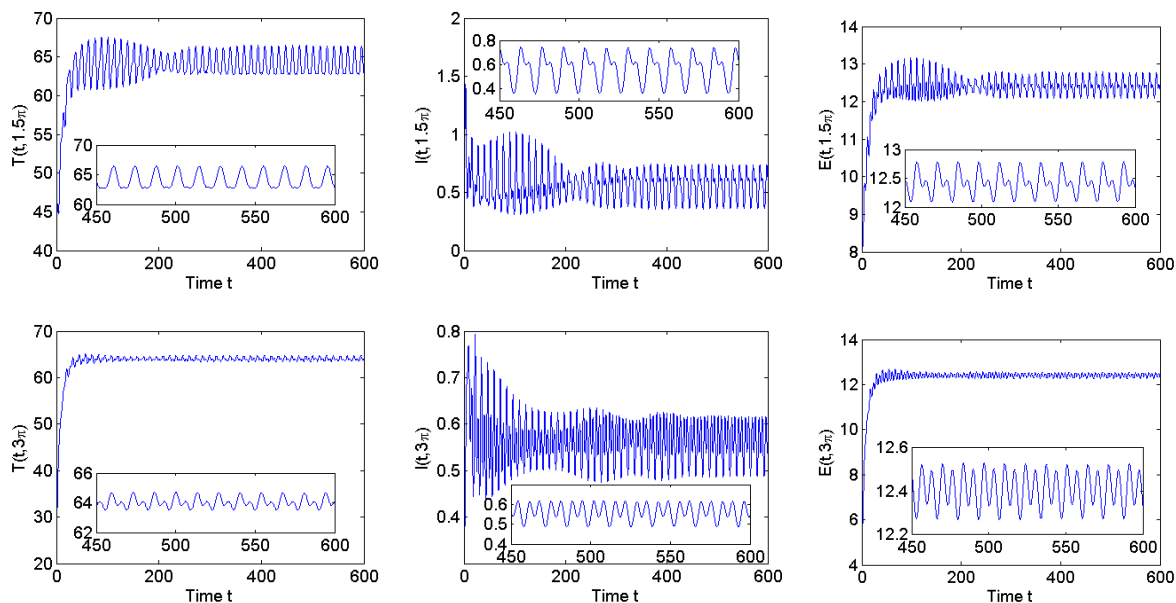


Figure 6.7: Temporal evolution of $T(x, t)$, $I(x, t)$ and $E(x, t)$. First row: $x = 1.5\pi$; Second row: $x = 3\pi$. When $\chi = 0.029$ ($\chi_c^H < \chi = 0.029 < \chi_c^S$), Hopf bifurcation occurs for the system, and there are periodic solutions.

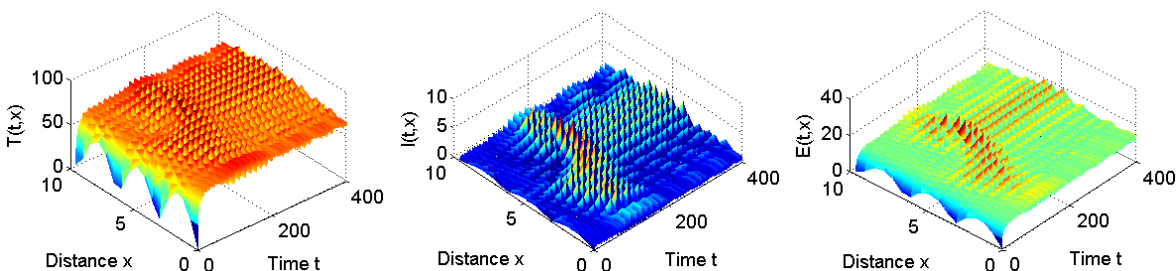


Figure 6.8: Temporal and spatial evolution of $T(x, t)$, $I(x, t)$ and $E(x, t)$. The homogenous positive steady state is unstable and spatial patterns form when $\chi = 0.033$ ($> \chi_c^S$).

For the case when $D_T = 0.1$ and $D_E = 0.1$, Figure 6.9(a) and Figure 6.9(b) show the curves of $d_2^2(\chi) - 3d_1d_3(\chi)$ and $\phi_d(\chi)$ respectively, as Figure 6.9(c) and Figure 6.9(d) show the curves of $e_2^2(\chi) - 3e_1e_3(\chi)$ and $\phi_e(\chi)$ respectively. Roots of these functions in the corresponding regions are $\chi_0^d = 0.0474$, $\chi_c^d = 0.0561$, $\chi_0^e = 0.1187$ and $\chi_c^e = 0.01373$ respectively. The functions $d_2(\chi)$, $d_3(\chi)$, $e_2(\chi)$ and $e_3(\chi)$ are linear strictly decreasing functions of χ , and roots of these functions are given by $\chi_2^d = 0.0048$, $\chi_3^d = 0.1814$, $\chi_2^e = 0.0193$ and $\chi_3^e = 5.2828$ respectively.

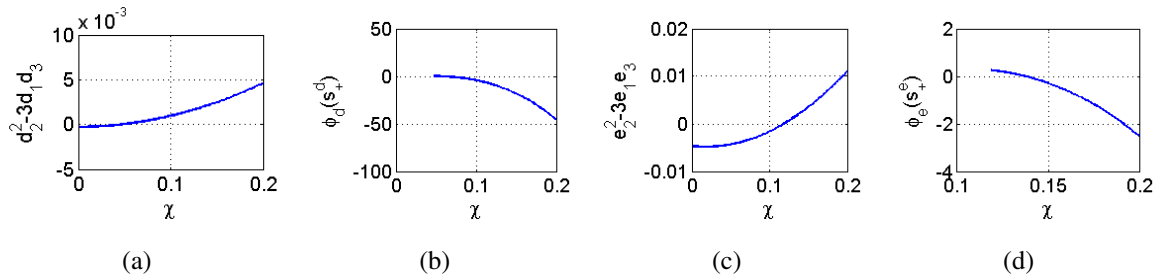


Figure 6.9: (a) $d_2(\chi)^2 - 3d_1d_3(\chi)$. One zero point: $\chi = 0.0474$. (b) $\phi_d(\chi)$. One zero point: $\chi = 0.0561$. (c) $e_2(\chi)^2 - 3e_1e_3(\chi)$. One zero point: $\chi = 0.1187$. (d) $\phi_e(\chi)$. One zero point: $\chi = 0.01373$.

Applying the bifurcation conditions (C1)-(C4), we obtain the bifurcation values $\chi_c^S = \chi_c^d = 0.0561$ and $\chi_c^H = \chi_c^e = 0.1373$. Since $\chi_c^S < \chi_c^H$, we know that steady state bifurcation may occur at $\chi = \chi_c^S$ and spatial pattern forms for $\chi > \chi_c^S$. The positive steady state S^* is stable when χ is less than the steady state bifurcation value χ_c^S . However, when χ exceeds the bifurcation value χ_c^S , the positive steady state loses its stability and spatial inhomogeneous pattern forms, as shown in Figure 6.10, where $\chi = 0.06$. In this case, Hopf bifurcation cannot occur, which can be seen from Figure 6.3(b), showing that $b_3(\chi)$ always reaches zero before $b_1(\chi)b_2(\chi) - b_3(\chi)$ reaching zero for all mode k .

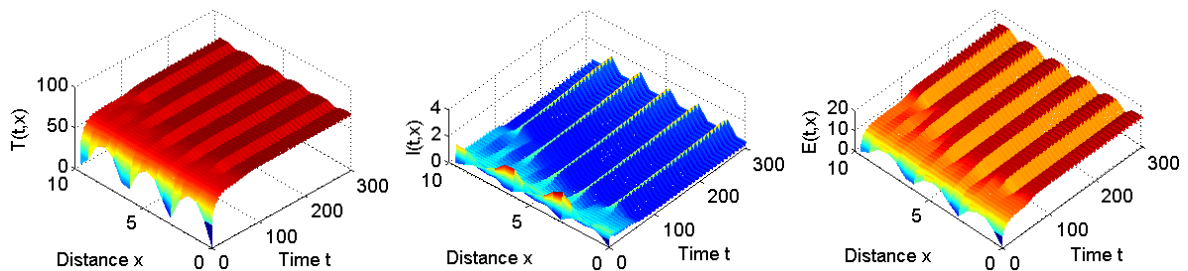


Figure 6.10: Temporal and spatial evolution of $T(x, t)$, $I(x, t)$ and $E(x, t)$. The homogenous positive steady state is unstable and spatial patterns form when $\chi = 0.06 (> \chi_c^S)$.

6.6 Conclusion and discussion

In this chapter, we studied the effect of chemotactic movement, including chemoattraction and chemorepulsion, of CTL on the HIV-1 infection dynamics by a reaction-diffusion-chemotaxis model. In the absence of spatial effect, that is, without random diffusion and chemotactic movement, the homogeneous positive steady state is locally stable. Choosing the typical chemotactic sensitivity function (6.13), we found that chemoattraction movement of CTL also cannot destabilize the homogeneous positive steady state, and there is no heterogeneous pattern formation.

In contrast, chemorepulsion movement of CTL can lead to instability of the homogeneous positive steady state and spatially heterogeneous pattern forms. Using the typical chemotactic sensitivity function (6.12) and choosing the strength of chemotactic sensitivity χ as the bifurcation parameter, we found that Turing instability occurs when χ exceeds some threshold. The bifurcation may be steady state bifurcation or Hopf bifurcation depending on χ and other parameters, such as the diffusion coefficients D_T and D_E . We found Turing instability conditions (C1)-(C4) and bifurcation thresholds for the positive steady state. With a finite domain in one-dimensional space, we demonstrated the stability of positive steady state, steady state bifurcation and Hopf bifurcation for different diffusion coefficients D_T and D_E and chemotactic sensitivities χ .

In order for CTL to successfully control HIV-1 infection, they must home efficiently to infected tissue sites and migrate within the infected tissue to the virus-infected cells. In this chapter, we choose the chemotactic sensitivity functions (6.12) and (6.13) for chemorepulsion and chemoattraction models respectively. For the chemoattraction model with (6.13), the negativity of Ψ^* keeps the positive steady state to be stable. If other chemotactic sensitivity functions are chosen so that Ψ^* is not always negative, then Turing bifurcations may also occur for chemoattraction model. For example, for the Macroscopic form of Lapidus and Schiller (with receptor response law)[8],

$$\chi(I) = -\frac{\rho}{(K + I)^2},$$

we have

$$\Psi^* = -E^* \left(1 - \frac{E^*}{E_M}\right) \frac{\rho}{(K + I^*)^2} \left(1 - \frac{2}{K + I^*}\right),$$

which is positive for some K . For small K , there may be Turing bifurcation and pattern formation.

In our chemorepulsion model, the chemotactic sensitivity is assumed to be constant and positive. However, some experiments [4] demonstrate that gp120 elicits bidirectional T-cell movement in a receptor-mediated, concentration-dependent manner, attracting CD8⁺ lymphocytes and HIV-specific CTL maximally at low concentration of gp120 and repelling the same

cells at a higher concentration of gp120. Therefore, the chemotactic sensitivity function should be negative (chemoattraction) for low concentration of gp120 and positive (chemorepulsion) for high concentration of gp120. Applied to our simplified model, the chemotactic sensitivity function should be negative (chemoattraction) for low level of $I(x, t)$ and positive for high level of $I(x, t)$. Considering this in our model, the analysis would be more difficult mathematically. We will study it for future work.

Bibliography

- [1] Adams R.A., Sobolev spaces, Academic Press, New York, 1975.
- [2] Amann H., Dynamical theory of quasilinear parabolic equations III: Global existence, *Math. Z.*, 202 (1989) 219-250.
- [3] Amann H., Nonhomogeneous linear and quasilinear elliptic and parabolic boundary value problems, in: Schmeisser H.J., Triebel H. (Eds.), *Function spaces, Differential Operators and Nonlinear Analysis*, Teubner Texte Math, 133 (1993) 9-126.
- [4] Brainard D.M. et al., Migration of antigen-specific T cells away from CXCR4-binding Human Immunodeficiency Virus Type 1 gp120, *J. Virol.*, Vol. 78 No. 10 (2004) 5184-5193.
- [5] Brainard D.M. et al., Decreased CXCR3⁺ CD8 T cells in Advanced Human Immunodeficiency Virus infection suggest that a homing defect contributes to cytotoxic T-lymphocyte dysfunction, *J. Virol.*, 81 (2007) 8439-8450.
- [6] Hillen T. and Painter K.J., A user's guide to PDE models for chemotaxis, *J. Math. Biol.*, Vol. 58 No.16 (2009) 183-271.
- [7] Lou Y. and Zhao X.Q., A reaction-diffusion malaria model with incubation period in the vector population, *J. Math. Biol.*, 62 (2011) 543-568.
- [8] Murray J.D., *Mathematical biology I: an introduction*, In: *Interdisciplinary Applied Mathematics*, Vol. 18, Springer New York, 2003.
- [9] Murray J.D., *Mathematical biology II: spatial models and biomedical applications*, In: *Interdisciplinary Applied Mathematics*, Vol. 18, Springer New York, 2003.
- [10] Painter K.J. and Hillen T., Volume-filling and quorum-sensing in models for chemosensitive movement, *Canadian Applied Mathematics Quarterly*, Vol. 10 No. 2 (2002) 501-543.

- [11] Smith H.L., Monotone dynamical systems: an introduction to the theory of competitive and cooperative systems, Amer. Math. Soc. Math. Surveys and Monographs, vol 41, Providence, RI, 1995.
- [12] Wodarz D., Killer cell dynamics: mathematical and computational approaches to immunology, In: Interdisciplinary Applied Mathematics, vol. 32, Springer Berlin, 2007.
- [13] Vianello F., Olszak I.T. and Poznansky M.C., Fugetaxis: active movement of leukocytes away from a chemokinetic agent, J. Mol. Med., 83 (2005) 752-763.

Chapter 7

Conclusion and future work

7.1 Conclusion

In Chapter 2, we proposed and analyzed a mathematical model with distributed delays that describe the competition of budding and lytic virus within a host. Budding virus is featured by a longer release period of new virions, while lytic virus is characterized by a long accumulation period but a shorter release period of new virions. We use the infection age and age structured model to formulate the infected cell population dynamics. We have analyzed the local dynamical behavior of the model. We have considered two concrete forms of functions for the viral production kernel, as a function of the infection age. To study the evolutionary competition of budding and lysis strategies, we assume that the total amount of virions replicated during the lifespan of infected cell is the same for both strains, without considering the release procedure and cell death. Under such a circumstance, the burst size of budding virus is greater than that of lytic virus provided that they have a same death rate. If the budding virus and lytic virus have a same infection rate, budding virus would outcompete the lytic virus, given the same rate of viral production, the infected cell lifespan and neutralizing capacity of the antibodies for budding and lytic viruses. In this case, budding strategy would have evolutionary advantage. If neutralizing capacities of antibodies against budding virus and lytic virus are different, then the lytic virus can survive as long as the reproduction number for lytic virus is very high.

Direct cell-to-cell transfer of HIV-1 is found to be a more potent and efficient means of virus propagation than cell-free virus infection [4]. In Chapter 3, we proposed a mathematical model to consider these two modes of viral infection and spread, in which infection age is also incorporated. By a rigorous analysis of the model, we showed that the model demonstrates a global threshold dynamics, fully described by the basic reproduction number \mathcal{R}_0 , in the sense that the

infection-free equilibrium E_0 is globally asymptotically stable if $\mathcal{R}_0 < 1$, and when $\mathcal{R}_0 > 1$, E_0 yields to a globally asymptotically stable positive equilibrium \bar{E} implying the infection will persist. The formula for the basic reproduction number of our model $\mathcal{R}_0 = \mathcal{R}_{01} + \mathcal{R}_{02}$ reveals that the basic reproduction number of the model that neglects either the cell-to-cell spread or cell-free virus infection is under-evaluated. The formulas for \mathcal{R}_{01} and \mathcal{R}_{02} also reflect the impact of the infection age through the distribution function $f(x)$. In the model of this chapter, we have assumed that target cells $T(t)$ are produced at a constant rate and has a constant death rate. It would be more reasonable to consider density dependent production rate. One possibility is to assume a logistic growth for the healthy cells in the absence of infection. We considered this in Chapter 4 ignoring the delay effect. When cell-free virus spread of HIV-1 is only considered and the basic reproduction number is greater than one, the infection can persist, and for some large infection rate of cell-free mode β_1 , the Hopf bifurcation occurs at the positive equilibrium. This property is similar to the case when cell-to-cell transfer is considered simultaneously. In contrast, when only cell-to-cell transfer is considered, the positive equilibrium \bar{E} is stable and there is no Hopf bifurcation and periodic solutions if the basic reproduction number is greater than one. The basic reproduction number is also underestimated when either cell-to-cell mode or cell-free mode is only considered.

In Chapter 5, we used a general virus infection dynamic model to discuss the rapid virus spread mechanism discovered recently [2], that is the repulsion of superinfecting virions by infected cells. With our general model, numerical estimation of the spreading speed showed that the repulsion of superinfecting virions accelerates the spread of free virus particles, which confirms the result of Doceul *et al.* [2] by mathematical modeling. In our model, the linear determinacy does not hold and the spreading rate is much larger than linearly determined minimal wave speed in the presence of repulsion effect. This may be due to the complexity of the virus dynamic system, which is neither a cooperative nor a competitive system. The minimal wave speed, given by the linearized analysis at infection-free steady state, is only true for the case when there is no repulsion effect. If repulsion of superinfecting virions happens, the minimal wave speed would be much higher than the linearly determined wave speed.

In Chapter 6, we studied the effect of chemotactic movement, including chemoattraction and chemorepulsion, of CTL on the HIV-1 infection dynamics by a reaction diffusion model with chemotaxis. In the absence of spatial effect, that is, without random diffusion and chemotactic movement, the homogeneous positive steady state is locally stable. Choosing the typical chemotactic sensitivity function, we found that chemoattraction movement of CTL also cannot destabilize the homogeneous positive steady state, and there is no heterogeneous pattern

formation. In contrast, chemorepulsion movement of CTL can lead to instability of the homogeneous positive steady state and spatially heterogeneous pattern forms. Using the typical chemotactic sensitivity function and choosing the strength of chemotactic sensitivity χ as the bifurcation parameter, we found that Turing instability occurs when χ exceeds some threshold. The bifurcation may be steady state bifurcation or Hopf bifurcation depending on χ and other parameters, such as the diffusion coefficients.

7.2 Future work

In Chapter 2, we do not consider the diffusion effect of antibodies, instead, we use an ordinary differential equation model with distributed delays accounting for the release strategies. Komarova [3] observed that if the production rate of the virions and the efficacy of the antibodies were the same for a budding and a lytic virus, the lytic virus would always be significantly less efficient in spreading, and thus the lytic strategy would be evolutionary disadvantageous. Lytic virus can be competitive against budding virus if the antibodies are less effective against lytic virions than they are against budding virions. This is because the effect of *antibody flooding* increases the rate of spread of lytic virions. To study this antibody flooding effects, we have to consider the diffusion of viruses and antibody, which is an interesting future work.

In our chemorepulsion model in Chapter 6, the chemotactic sensitivity is assumed to be constant and positive. However, some experiments [1] demonstrate that gp120 elicits bidirectional T-cell movement in a receptor-mediated, concentration-dependent manner, attracting CD8⁺ lymphocytes and HIV-specific CTL maximally at low concentration of gp120 and repelling the same cells at a higher concentration of gp120. Therefore, the chemotactic sensitivity function should be negative (chemoattraction) for low concentration of gp120 and positive (chemorepulsion) for high concentration of gp120. Applied to our simplified model, the chemotactic sensitivity function should be negative (chemoattraction) for low level of $I(x, t)$ and positive for high level of $I(x, t)$. Considering this in our model, the analysis would be more difficult mathematically. We will study it for future work.

Bibliography

- [1] Brainard D.M. et al., Migration of antigen-specific T cells away from CXCR4-binding Human Immunodeficiency Virus Type 1 gp120, *J. Virol.*, Vol. 78 No. 10 (2004) 5184-5193.
- [2] Doceul V., Hollinshead M., van der Linden L. and Smith G.L., Repulsion of superinfecting virions: a mechanism for rapid virus spread. *Science*, 327 (2010) 873-876.
- [3] Komarova, N.L., Viral reproductive strategies: how can lytic viruses be evolutionarily competitive? *J. Theor. Biol.*, 249 (2007) 766-784.
- [4] Sattentau Q., The direct passage of animal viruses between cells, *Current Opinion in Virology*, 1 (2011) 396-402.

Curriculum Vitae

Education

- 2010.5-present Ph.D. candidate, Applied Mathematics,
The University of Western Ontario, Canada,
Supervisor: Professor Xingfu Zou.
- 2007.9-2009.7 Master of Science, Applied Mathematics,
The University of Science & Technology Beijing, China,
Supervisor: Professor Wanbiao Ma.
- 2003.9-2007.7 Bachelor of Science, Information and Computing Science,
Inner Mongolia University, China.

Work experience

- Course Instructor : Calculus II - 1305B, 2013.1 - 2013.4
The University of Western Ontario, Canada
- Teaching Assistant : University of Western Ontario, Canada, 2013.9 - present.
University of Science & Technology Beijing, China, 2007.9 - 2009.7
- Research Assistant : University of Western Ontario, Canada, 2013.5 - present.
University of Science & Technology Beijing, China, 2007.9 - 2009.7

Scholarships and Academic Awards

- 2011 - 2012 Graduate Thesis Research Award
The University of Western Ontario.
- 2005 - 2006 National scholarship
Inner Mongolia University, China.
- 2003 - 2007 Excellent Student Scholarship,
Inner Mongolia University, China.

Publications

- 1) Xiulan Lai and Wanbiao Ma, The impact of T cell activation and differentiation on HIV-1 infection dynamics, *Math. Biol. Eng.*, revised.
- 2) Xiulan Lai and Xingfu Zou, Modeling virus-to-cell and cell-to-cell spread of HIV-1, *SIAM J. Appl. Math.*, revised.
- 3) Xiulan Lai and Xingfu Zou, The dynamics of evolutionary competition between budding and lytic viral release strategies, *Math. Biol. Eng.*, accepted.
- 4) Xiulan Lai and Xingfu Zou, Repulsion effect on superinfecting virions by infected cells, submitted.
- 5) Xiulan Lai and Xingfu Zou, A Reaction diffusion system modeling virus dynamics and CTL response with chemotaxis, in preparation.
- 6) Xiulan Lai and Xingfu Zou, Modeling cell-to-cell spread of HIV-1 with logistic target cell growth, in preparation.
- 7) Liman Dai, Stephen A. Gourley, Graham J. Hickling, Xiulan Lai, Junping Shi, Wendi Wang, Yanyu Xiao, Xingfu Zou, Evaluating the role of white-tailed deer in geographic spread of the blacklegged tick *Ixodes scapularis* in the eastern United States: a diffusion model, in preparation.